Exact solutions to the long-time statistics of nonequilibrium processes

Emil Mallmin

Doctor of Philosophy
The University of Edinburgh
August 2021

Abstract

Nonequilibrium statistical mechanics deals with noisy systems whose dynamics breaks time-reversal symmetry. Stochastic Markov processes form a mathematical framework for a unified theory of nonequilibrium phenomena, particularly at the microscale where fluctuations play a dominant role. The development of both theory and useful applications has been aided by minimal, exactly solvable models, where the logical connection between model feature and behaviour can be ascertained. In this thesis I consider a number of biologically inspired models in relation to two aspects of the long-time statistics of nonequilibrium processes: the attainment of a nonequilibrium steady state, and steady-state fluctuations using dynamical large deviation theory.

For the first topic, I consider two models of particles moving stochastically on a ring under no-crossing interactions. The first is of two lattice *run-and-tumble* particles, each of which moves in a persistent direction interspersed by 'tumble' reorientation events. I extend the previously known steady-state solution to a solution for all time, in the sense of obtaining a diagonalization of the Markov generator of the process. The spectrum exhibits eigenvalue crossings at exceptional points of the tumbling rate, which leads to a singular dependence of the relaxation time to the steady state on this parameter. In the second model of *heterogeneous single-file diffusion*, I solve for the steady state of N driven particles with individual diffusion properties. This reveals an inter-particle ratchet effect by which the particle current is disproportionately affected by slow-diffusing, rather than slow- or fast-driven, particles. The model generalizes to higher dimension without compromising the solution structure, if a key property of quasi-one-dimensionality is maintained. In both models, the relation of key model features to generalized notions of reversibility forms an overarching theme.

For the second topic, I first consider a random walker on a linear lattice and the effect that adding internal states to the walker has on the emergence of singular

behaviour in the fluctuations of either the velocity observable or the time spent at a given site. In particular, I use generalizations of the run-and-tumble particle and probe the trajectories associated with the different fluctuations regimes that this model can exhibit. I show that internal states can either have a drastic influence on the likelihood of a large deviation, or none at all. I then extend the dynamical large deviation formalism for diffusions to the case of reflective boundaries and current-like observables. In particular, this allows the large deviations of the particle current in the heterogeneous single-file diffusion to be obtained analytically. These are found to coincide with those of a single diffusive particle with certain effective parameters, in interesting contrast to comparable studies on the lattice.

In total, this thesis makes contributions to: conceptual aspects of irreversibility; exact solutions to commonly studied nonequilibrium models; the description of mechanisms underlying nonequilibrium phenomena; and to dynamical large deviation methods.

Lay summary

Imagine recording through a microscope the jittery motion of a grain of pollen in a glass of water. If you played that video side-by-side to the same video played in reverse, a viewer would not be able to infer which video corresponded to the actual sequence of events. This is because the grain of pollen is at thermal equilibrium with the water and its randomness is therefore 'time-reversible'. Many noisy systems, in particular those related to the workings of livings cells, are not time-reversible and are called nonequilibrium processes. While physicists have a far-reaching theory for equilibrium processes, the search for general laws that govern nonequilibrium processes is still ongoing.

One of many complementary paths towards an understanding of nonequilibrium processes, is the study of simple mathematical models whose statistics can be calculated exactly. Simple models help clarify key concepts in the theory, develop mathematical tools, and point towards interesting nonequilibrium behaviour that may generalize beyond the particular model studied.

In this thesis I solve the equations that describe the random motion of particles in two such simple models. Both consist of particles moving in one dimension, under the constraint that they cannot pass through each other. In the first model, the way an individual particle moves can be seen as a idealization of the motion of certain bacteria. The second model is inspired by the diffusion of ions through pores in cell membranes. My main contributions with this work lie in describing how time-irreversible aspects of the long-time statistics connect to the basic mathematical ingredients of the models, and in developing mathematical techniques applicable to other models as well.

Declaration

I declare that this thesis was composed by myself, that the work contained herein is my own except where explicitly stated otherwise in the text, and that this work has not been submitted for any other degree or professional qualification except as specified.

Parts of the work contained in this thesis have been published in [1, 2, 4, 5]. Additional work carried out under the PhD studentship but not included in this thesis was published in [3].

(*Emil Mallmin, August 2021*)

[1] E. Mallmin, R. A. Blythe, M. R. Evans. Exact spectral solution of two interacting run-and-tumble particles on a ring lattice. *J. Stat. Mech. Theor. Exper.* 013204 (2019)

[2] E. Mallmin, R. A. Blythe, M. R. Evans. A comparison of dynamical fluctuations of biased diffusion and run-and-tumble dynamics in one dimension. *J. Phys. A: Math. Theor.* **52**, 42 (2019)

[3] F. Cagnetta, E. Mallmin. Efficiency of one-dimensional active transport conditioned on motility. *Phys. Rev. E* **101**, 022130 (2020)

[4] E. Mallmin, R. A. Blythe, M. R. Evans. Inter-particle ratchet effect determines global current of heterogeneous particles diffusing in confinement. *J. Stat. Mech. Theor. Exper.* 013209 (2021)

[5] E. Mallmin, J. du Buisson, H. Touchette. Large deviations of currents in diffusions with reflective boundary. *J. Phys. A: Math. Theor* **54** 295001 (2021)

Acknowledgments

We come to the full possession of our power of drawing inferences, the last of all our faculties; for it is not so much a natural gift as a long and difficult art.

—C. S. Peirce

I am grateful to my supervisors Martin Evans and Richard Blythe for the opportunity to come to Edinburgh. They have given me four precious years in a city I've come to love, to work on topics I find captivating. I thank them for providing excellent academic guidance in many convivial meetings throughout these years.

My fellow student, friend, and collaborator Francesco Cagnetta deserves a special thanks for influencing the direction of my PhD towards dynamical fluctuations. It has likewise been a pleasure collaborating with Johan du Buisson and Hugo Touchette on this topic—I hope we may one day meet in person.

My officemates Michael Chiang and Paul Hush have been a friendly and much appreciated presence in my workdays, until the pandemic forced me to work from home. For four years, Pablo Andrés Martínez has not only been a good flatmate, but a trusted friend with whom I've been able to share my thoughts, big and small.

Without my dear *Ζωή*, living through the pandemic lockdowns would have been a dread. Thanks to her I can look back even on this time with fondness. On her recommendation that the thesis needs more 'actual numbers', I supply some here: $\pi, \sqrt{2}, -5, 42, 17/59, 0.9999987$.

Sist men inte minst vill jag tacka mamma Karin och pappa Mats för allt deras stöd genom livet.

I acknowledge studentship funding via EPSRC grant no. EP/N509644/1.

Contents

Abstract i

Lay summary iii

Declaration iv

Acknowledgments v

Contents vi

List of Figures xii

Introduction 1

I Relaxation to a nonequilibrium steady state **11**

1 Background on nonequilibrium Markov processes 12

1.1 The Markov property in nonequilibrium physics 12

1.1.1 Whence stochasticity and Markovity? 12

1.1.2 Prediction vs. retrodiction 14

1.1.3 The meaning of 'nonequilibrium' 17

1.2 Jump process theory 20

1.2.1 The Master equation and its generator 21

1.2.2 Ergodic relaxation to stationarity 25
1.2.3 Reversibility and detailed balance 28
1.2.4 Characterisation of nonequilibrium steady states 29
1.2.5 Generalized reversibility 31
1.2.6 Activity, dissipation, and entropy 34
1.3 Diffusion processes 35
1.3.1 The diffusive limit 36
1.3.2 Representation as stochastic differential equation 38
1.3.3 Generators of diffusion 39
1.4 Summary of main concepts 40

2 Exceptional points and singular relaxation times for run-and-tumble particles 42

2.1 Background 42
2.1.1 Run-and-tumble particles 42
2.1.2 Interpolating diffusive and ballistic motion 44
2.1.3 Persistence through a spectral lens 45
2.2 N-particle lattice model 47
2.2.1 Master equation 47
2.2.2 Interactions break generalized reversibility 48
2.3 Solution for a single particle 49
2.3.1 Spectrum: band structure and eigenvalue crossings 52
2.3.2 Eigenvectors and the matrix exponential 53
2.3.3 Dynamical exponent and singularity in relaxation time 55
2.3.4 Discussion 56

2.4 Solution for two interacting particles 57

2.4.1 The kernel method and root parametrization 60

2.4.2 Spectrum: band structure and eigenvalue crossings 67

2.4.3 $z_{1,2}$-parametrized eigenvectors 70

2.4.4 Nonequilibrium steady state 71

2.4.5 Relaxation time 72

2.4.6 Discussion 72

Appendices for Chapter 2 74

2.A Asymptotic solution of two-particle spectrum for $\omega > 2$ 74

2.A.1 The middle band 74

2.A.2 The left and right bands 76

2.B Derivation of two-particle eigenvectors 78

3 An inter-particle ratchet effect in heterogeneous single-file diffusion 82

3.1 Background 82

3.1.1 Single-file diffusion 82

3.1.2 The diffusive limit of the ASEP 83

3.1.3 Bethe-ansatz solution of the homogeneous SFD 86

3.1.4 Introducing particle-wise disorder 88

3.2 Heterogeneous single-file diffusion 90

3.2.1 Exact steady-state solution 91

3.2.2 An inter-particle ratchet effect 94

3.2.3 Driven tracers in a passive bath 96

3.2.4 Comparison to a filament ratchet 101

3.3 A quasi-one-dimensional generalization 102

3.3.1 Hard spheres in a d-dimensional tube 102

3.3.2 Solving for the irreversible drift: an inverse FPE solution method 106

3.3.3 The generalized diffusion ratchet effect 109

3.4 Summary and discussion 113

3.5 Epilogue: run-and-tumble particles revisited 113

II Dynamical large deviations **117**

4 Background on dynamical large deviations 118

4.1 Introduction 118

4.1.1 From the statistics of states to the statistics of trajectories .. 118

4.1.2 A motivating example 122

4.1.3 Large deviation basics 124

4.2 Dynamical large deviations from the Level 2.5 perspective 127

4.2.1 Path probabilities for jump processes 127

4.2.2 The Level 2.5 rate function and its meaning 129

4.2.3 Contraction to time-additive dynamical observables 133

4.2.4 The view from ensemble theory 138

4.3 The case of diffusions 141

4.4 Summary of main concepts 144

5 Rare trajectories in multi-state random walks 145

5.1 Background 145

5.1.1 Large deviations in the asymmetric random walk 147

5.1.2 Multi-state random walks 150

5.2 Velocity fluctuations in a multi-state random walk 152

5.2.1 Method of finding the SCGF 152

5.2.2 Velocity fluctuations of the asymmetric RTP 155

5.2.3 A probabilistic quasi-particle 159

5.3 A dynamical phase transition in occupation time 164

5.3.1 Method of finding the SCGF 164

5.3.2 Dynamical phase transition in the ARW 167

5.3.3 Dynamical phase transition in the ARTP 170

5.4 Summary of results 176

Appendices for Chapter 5 178

5.A Marginalization of the N-ARW 178

6 Dynamical large deviations in the presence of boundaries 182

6.1 Background 182

6.1.1 Introducing boundaries 183

6.1.2 Reflected trajectories 186

6.2 Dynamical large deviation theory for reflected diffusions 188

6.2.1 Tilted boundary conditions: argument from duality 188

6.2.2 Tilted boundary conditions: derivation from the diffusive limit 190

6.2.3 General consequences of the tilted boundary conditions 195

6.3 Collective current fluctuations in the heterogeneous single-file diffusion 196

6.3.1 Current fluctuations in the ASEP 196

6.3.2 Exact current large deviations for the heterogeneous SFD .. 197

6.4 Beyond reflection 200

6.5 Summary of results..... 204

Conclusions 206

Bibliography 211

List of Figures

1 Lattice run-and-tumble particles and heterogeneous single-file diffusions as extensions of the (periodic) ASEP. 3

1.1 The trajectory of a jump process 20

1.2 Examples of jump processes 23

1.3 Transient and irreducible components of a transition graph 27

1.4 Anisotropic random walk on the hypercube (illustrated in 2D) . . 36

1.5 Brownian trajectory from the diffusive limit 36

2.1 Persistent random walk 42

2.2 The run-and-tumble motion of E. coli 43

2.3 Solution $\rho(x,t)$ to the telegrapher's equation 44

2.4 Lack of generalized reversibility for interacting RTPs 48

2.5 Spectrum of an RTP on a ring 52

2.6 Single-RTP relaxation times 55

2.7 Spectrum for two RTPs on a ring lattice 69

2.8 Examples of right eigenvectors for two RTPs on a ring lattice . . . 71

2.9 Relaxation times for two interacting RTPs 72

3.1 Illustration of the phase-space boundary for SFD 85

3.2 Crossing of Brownian trajectories 88

3.3 Heterogeneous single-file diffusion in one dimension 90

3.4 Inter-particle ratchet effect 95

3.5 Sketch of driven tracers in a passive medium 98
3.6 Comparison of periodic SFD and the filament ratchet 101
3.7 Tube geometry of the quasi-one-dimensional diffusion 103
3.8 Geometry of collisions in the quasi-one-dimensional-diffusion . . . 105

4.1 From the statistics of states to the statistics of trajectories 120
4.2 Sketch of trajectories satisfying a dynamical constraint 123
4.3 The Legendre-Fenchel transform 126

5.1 Large deviations of velocity for the ARW 147
5.2 Examples of multi-state random walkers 151
5.3 Velocity rate function for the asymmetric RTP 154
5.4 Effective rates for the asymmetric RTP 155
5.5 Spectrum of the asymmetric RTP 159
5.6 The N-level asymmetric random walk 159
5.7 Degenerate RTP as double ARW quasiparticle 161
5.8 Effective rates for the N-ARW conditioned on velocity 162
5.9 Occupation time rate function for the ARW 166
5.10 Effective process for origin occupation time fluctuations in the ARW 168
5.11 Simulated occupation time statistics for the ARW 170
5.12 SCGF and rate function for the occupation-conditioned ARTP . . 171
5.13 Effective rates for the ARTP conditioned on occupation time . . . 173

6.1 Reflection rule for Langevin equations 186
6.2 Planar random walk with a boundary 190
6.3 Effective process for heterogeneous SFD conditioned on the particle current 200
6.4 One-dimensional diffusion with semi-permeable barrier 200

Introduction

The long-time behaviour of nonequilibrium systems

Road traffic, schools of fish, lasers, intracellular processes, climate systems, avalanches, ecological populations, epidemics—all are examples of nonequilibrium systems because they break the assumption of equilibrium physics, that on the relevant temporal or spatial scales a state free of net currents of matter or energy is assumed [6, 7]. While equilibrium physics, through equilibrium statistical mechanics and thermodynamics, comprises coherent theories that span from the microscopic scale to the astronomical, nonequilibrium physics is more often described as a collection of useful mathematical tools and ideas to be tailored to the situation at hand. However, for time-irreversible systems that can be modelled as a certain kind of stochastic process—a nonequilibrium Markov process—there is at least a unifying mathematical framework within which core concepts can be defined with precision; and within which results of some generality can be sought, and, in fact, have been found [8, 9]. In both of these endeavours, the study of minimal models defined by simple stochastic-dynamical rules has been instrumental [10–12]. Such models often take inspiration from the biophysical processes occurring within or between cells, as these are strongly influenced by thermal fluctuations, while also being far from equilibrium in order to maintain life functions. When the rules defining a model are not constrained *a priori* by the need to reproduce time-reversible behaviour at long times, the results can be surprising, such as an abrupt change in dynamical behaviour at a critical value of a model parameter [13], and difficult to predict without solving or simulating the process.

In this thesis, I investigate the long-time behaviour of nonequilibrium Markov processes with the use of analytically tractable minimal models inspired by biophysical examples. A stochastic process is simply a quantity $X(t)$, such as

the position of a particle in space, that evolves in time t according to some stochastic rules [14–16]. The Markov property states that the stochastic rules only depend on the instantaneous value of X, as opposed to on the history (or the future) of the process. This implies that the probability distribution $P(x,t)$ for $X(t) = x$ is evolved in time by a mathematical 'generator' easily defined from kinetic rules with a direct physical meaning. Under commonly assumed conditions, these processes *relax* over some characteristic time scale τ_{rel} towards a unique stationary or 'steady' state where the statistics of $X(t)$—the distribution P and all time-correlations of X—do not change with time. However, the statistics in a steady state may not be invariant with respect to the direction of time: a steady state that contains net, stationary probability currents, and is therefore statistically irreversible, is called a nonequilibrium steady state (a NESS); a process that relaxes towards a NESS is, in the terminology of this thesis, a nonequilibrium process.

I ascribe two meanings to the phrase 'long-time behaviour', which serve to organize this thesis into two parts. The first meaning refers to the description of (nonequilibrium) steady states, their average behaviour, and relaxation characteristics. Often, τ_{rel} is long compared to time scales of individual changes in the value of $X(t)$, and an exact steady state appears only as $t \to \infty$, strictly speaking. In a steady state, while the statistics are time-invariant, $X(t)$ still fluctuates around its typical behaviour in a way consistent with the statistical average. Over any observation time window T, we may observe an atypical behaviour, such as a large deviation of an observable (*i.e.* a function of $X(t)$) from its typical value. The characterization of such events, all of which become rare as $T \gg \tau_{rel}$, is the second meaning of 'long-time'.

In the first part of this thesis, I seek original, exact solutions to two significant variations of a model with a paradigmatic status in the study of NESSs: the ASEP (for 'asymmetric simple exclusion process') [10, 13, 17]. The classic ASEP consists of particles randomly hopping left or right on a one-dimensional lattice under conditions of volume exclusion between particles. Its open-boundary version is the poster-child of a boundary-driven nonequilibrium phase transition [18, 19], where asymmetric injection and extraction of particles at the boundary sites control different regimes of the net particle current (Figure 1a). The periodic case, of more relevance to this thesis, also produces a NESS when the particles are biased in their hopping direction (but no phase transition) and generates a net current that is limited by inter-particle blocking. In addition to being a general

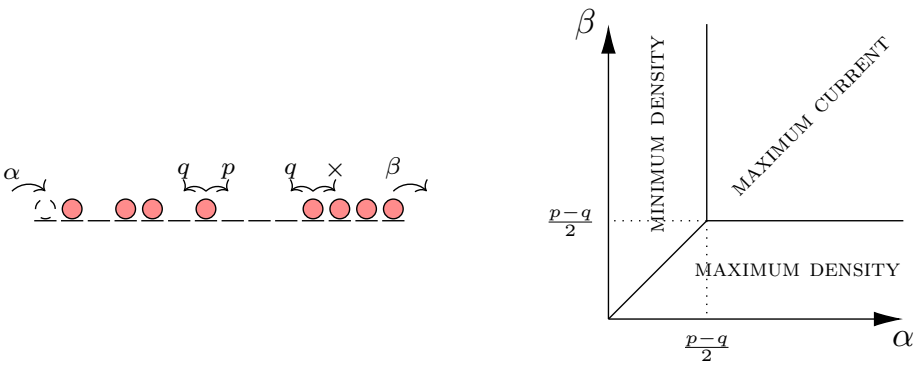

(a) *The open-boundary* ASEP *with its phase diagram. In the periodic case, i.e. on a ring lattice, there is no phase transition.*

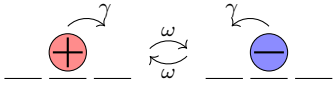

(b) *The lattice run-and-tumble particle alternates between a right-moving and left-moving state.*

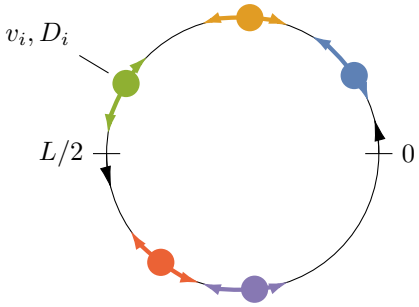

(c) *Heterogeneous single-file diffusion on a continuous ring, with individual drift and diffusivity* v_i, D_i.

Figure 1 *Lattice run-and-tumble particles and heterogeneous single-file diffusions as extensions of the (periodic)* ASEP.

model for understanding the phenomenology of one-dimensional transport, from vehicular traffic to the motion of molecular motors along microtubules inside cells, the ASEP has captured the interest of physicists and mathematicians seeking to understand the subtle symmetries that enable exact solutions to certain many-body problems [17]. By exact solution is usually meant an explicit or implicit analytical representation of the time-dependent distribution $P(x,t)$, or its stationary limit $P^*(x)$, in terms of known functions. In the spirit of previous work on the ASEP and other exactly solvable models, in the models I study, I set out to (i) discover interesting effects that are only possible out of equilibrium; (ii) understand how such effects are logically related to the mathematical features that define the model; (iii) understand when—and then why—the model can be exactly solved.

The first model that I consider has each particle in the periodic ASEP stochastically and independently alternate between an exclusively right-moving state and left-moving state [20] (Figure 1b). This makes each particle an idealized version

of a microswimmer such an E. coli bacterium, whose motion is referred to as 'run-and-tumble' [21]. Such particles fall into a class of nonequilibrium systems called 'self-propelled active particles', characterized by the conversion of energy into motion [22, 23]. Self-propelled active particles interacting with obstacles or other particles display an array of fascinating behaviour due to the phenomenon of jamming. While much progress has been made on the phenomenology of interacting systems of active particles, *e.g.* on 'motility-induced phase separation' that gives a general mechanism for cluster formation even in the absence of attractive forces [24, 25], few exact results have been obtained in scenarios of more then just a single active particle, which sets the challenge.

The second variation on the ASEP that I consider transposes the model to the continuum ring, and lets each particle have unique parameters for their motion (drift and diffusivity) (Figure 1c). The continuum ASEP is commonly called 'single-file-diffusion' (SFD) and has been used to model, for example, the diffusion of particles through pores in minerals or cell membranes [26]. In the *heterogeneous* SFD, the key symmetry of particle-exchange is broken. The typical particle current around the ring can be expected to depend on the whole set of model parameters in some interesting way, to which I apply the considerations (i), (ii), (iii) above.

In the second part of this thesis, I use dynamical large deviation theory (DLDT) [27–29] to explore the trajectories associated with atypical values in observables of nonequilibrium Markov processes. Large deviation theory, in general, concerns the study of 'small' probabilities that decay at an exponential rate with some large parameter [9, 30]. In *dynamical* large deviation theory, that parameter is the large observation time T. At the heart of DLDT is a change in perspective from the view of the statistics of the 'microstates' x that $X(t)$ can attain, to the statistics of trajectories $\omega_T = \{x(t)\}_{t=0}^{T}$ that $X(t)$ generates over the time window T. Remarkably, the mathematical structure of equilibrium statistical mechanics is essentially a 'static' large deviation theory in the particle number N. Therefore, we find in DLDT 'dynamical' generalizations to partition functions, thermodynamic potentials, and phase transitions that is the stuff of equilibrium theory. DLDT is increasingly seen as offering a fundamental structure for systems far from equilibrium [9, 31, 32], and has produced results of celebrated generality. These include 'fluctuation relations' relating the probabilities of events Q (*e.g.* an amount of heat dissipated into a thermal reservoir) to their 'opposites' $-Q$ (the same amount of heat extracted) [33–35], and 'thermodynamic uncertainty

relations' that give universal bounds on the likelihoods of current fluctuations [36, 37].

DLDT also gives practical tools to quantify the structure of rare fluctuations in specific models. I apply these tools to models of one-dimensional random walkers with internal states to explore the conditions under which singularities can develop in the 'dynamical potentials' relating to the velocity observable and the observable of time fraction spent at the origin. In particular, I use a model of an asymmetric run-and-tumble particle, where the asymmetry in hopping can be played out against the asymmetry in direction-reversal to interesting effect. In the last 15 years or so, a construction in DLDT has frequently applied in the physics literature, that allows the character of trajectories associated with a given fluctuation to be described by an 'effective process'. This gives a view onto understanding the mechanism behind fluctuations and is consistently employed in my study of fluctuations in multi-state random walks.

I also consider how to extend the DLDT to study currents in diffusion processes that have reflective boundaries. Many processes in physics and beyond are modelled with reflecting boundaries [38], and extending the theory to be applicable in these cases constitutes a key extension of the basic dynamical large deviation formalism. In particular, the heterogeneous SFD can be mapped to a reflected diffusion, and I study the statistics of its collective particle current. Thus, the second part of the thesis sees us revisiting the models from the first part under a different set of questions.

As a whole, this thesis makes original contributions to exact results in the specific models of run-and-tumble particles and heterogeneous single-file diffusions; to the description of nonequilibrium effects in these models; to development of solution techniques for lattice- and continuum-space processes; and to the theory of dynamical large deviations.

Below we take a tour through the chapters of this thesis, with a more detailed description of the questions asked and answers obtained.

A tour of this thesis

The thesis contains six chapters divided into two parts. Each part begins with a background chapter, to give general context, explain the mathematical

framework, and fix notations. The subsequent two chapters then focus on an original research question related to the general topic of the thesis part, as introduced above. Each of the four original-research chapters contains a background opening section, adapted to the specialized topic of that chapter. The thesis closes with a Conclusions section tying together the different strings spun in the four main chapters.

Part I

Chapter 1:
Background on nonequilibrium Markov processes

I introduce the theory of nonequilibrium Markov processes that forms the mathematical and conceptual backdrop of this entire thesis. Most of the elements presented here can be gleaned from a collection of classic textbooks on nonequilibrium statistical mechanics [6, 7] and applied probability theory [14–16]. However, I have adopted a mode of presentation that I believe is unusual, aiming to give a not-too-technical yet general view of the mathematical structure as such, while organizing the developments around concepts of (ir)reversibility that are of particular interest to physicists.

After a more general opening section inspired by [8], in which I elaborate upon why the Markov property is so central to the structure of nonequilibrium theory, the chapter focuses on jump processes that evolve in continuous time on countable state spaces. Jump processes have a certain primacy, in that processes on continuous state spaces can be constructed as limits of jump processes. Indeed, I introduce diffusions, epitomized by Brownian motion, from this point of view, showcasing a diffusive limit technique that will be employed repeatedly in the following chapters.

Chapter 2:
Exceptional points and singular relaxation times for run-and-tumble particles

Following earlier work [20, 39], I study a minimal model of 'active matter' in the form of run-and-tumble particles (RTPs) on a ring lattice. Each particle hops stochastically in a given direction ('runs') that stochastically reverses ('tumbles') with a rate ω. Volume exclusion prevents a particle from hopping onto an already

occupied site.

Firstly, I use the model to clarify a fundamental point, that it is the combination of persistence and interaction with obstacles (*e.g.* other particles) that cause non-Boltzmann stationary distributions in active systems through the breaking of a *generalized* reversibility property.

The main objective of the chapter is then to derive the exact, time-dependent solution to the model, in the spirit of the periodic ASEP. While the N-particle version of the latter is solved by a 'Bethe ansatz' [17, 40], this technique fails for the RTPs, and a solution must be sought *de novo*. I solve the one- and two-RTP problems exactly for all times using generating function techniques applied to diagonalize the matrix that generates the stochastic evolution of the process.

The main physical result is that the relaxation time of the process to the previously known stationary distribution [39] has a singularity as a function of the tumbling rate ω. This is because at exceptional points ω^* of this parameter, the process generator experiences eigenvalue crossings, only possible due to the breaking of (non-generalized) reversibility.

The ambition to extend the solution to particle number $N > 2$ is thwarted by the considerable complexity of the two-particle solution, which shows that even in minimal models of many-body active matter systems, exact solutions may be a bridge too far.

The results of this chapter have been published in [1].

Chapter 3:
An inter-particle ratchet effect in heterogeneous single-file diffusion

I consider the model of single-file diffusion (SFD) where N particles drift and diffuse on a ring without overtaking. The latter constraint is modelled as reflective boundary conditions of one particle with respect to any other. I treat the case of non-identical particles having constant individual drifts and diffusivities.

While the time-dependent solution of the heterogeneous SFD could not be obtained exactly by any traditional means, I show that the stationary distribution has a simple factorized form similar to the ASEP with particle-wise disorder [41–43]. The steady state of this model is out of equilibrium because there is a net current of particles around the ring. On the continuum as opposed to the

lattice, however, it becomes clear that the diffusivities control the current, which is strongly biased towards the drift of the particles with the lowest diffusivities due to a diffusion-ratchet effect.

The same ratchet effect was found in a non-trivially related model of filament-driven membrane growth [44]. This motivates the objective of the second half of this chapter, which is to generalize the model as far as possible, in order to understand what precisely are the critical features that afford an exactly solvable steady state. By considering instead of a narrow channel, a 'tube' in d dimensions, I show that the condition of 'quasi-one-dimensionality' is key, meaning that no particle is able to overtake *all* others in the tube. This effectively forces a common net velocity of all particles in the long-time limit. In the analysis, the 'irreversible drift' [45] of the process, analysed from a phase-space geometrical point of view, is central. Because the irreversible drift is not zero, the process is out of equilibrium, but with respect to an emergent frame of reference moving at net particle velocity, it appears reversible, which promotes exact solvability.

In the generalized model, there is also a generalized diffusion ratchet effect, where the current is affected by any deviation from triviality of the total diffusion matrix, *e.g.* particle disorder or spatial anisotropy.

The results of this chapter have been published in [4].

Part II

Chapter 4:
Background on dynamical large deviation theory

I present dynamical large deviation theory (DLDT), used to study the long-time deviations from typical behaviour in Markov process, *i.e.* sustained steady-state fluctuations. There are two fundamental questions the theory addresses: how to quantify via 'rate functions' the exponentially decaying probabilities of sustained fluctuations with a large observation time T, and how to characterize the trajectories which give rise to these fluctuations through an 'effective process'.

I first recount some basics of large deviation theory. Then, for jump processes, I derive the 'level 2.5 large deviation principle' which provides the rate function corresponding to the empirical probability density and empirical probability flow

of a Markov process. From this result, I derive the rate functions corresponding to time-averaged observables such as integrated currents, entropy production, and occupation times, by the large-deviation method of contraction, which also furnishes the effective process for these observables. The analogous results for diffusion processes are also presented. This chapter follows entirely the primary literature, in particular [28, 46–48], but gives a self-contained and fully detailed derivation of the contraction-from-level-2.5 approach that aspires to be a useful reference for new entrants to the topic of dynamical large deviations.

Chapter 5:
Rare trajectories of multi-state random walkers

The large deviations of dynamical observables in simple random walks or diffusions have recently been used to investigate under what conditions singularities can develop in rate functions, or in the associated 'scaled cumulant generating function' (SCGF) that is a akin to a 'dynamical' free energy density. I apply the theory of Chapter 4 in exactly deriving the rate functions and effective processes for examples drawn from class of one-dimensional random walkers with internal states.

First, I consider the velocity observable for an asymmetric version of an RTP. By a tuning of the parameters such that the time-scale of tumbles becomes large to that of hopping, one finds a near-flat branch of the rate function separating fluctuation regimes which a smooth cross-over in their associated trajectories as revealed through the effective process. At a different tuning of the parameters, corresponding to a curious giant degeneracy of the process generator's spectrum, the rate function coincides with that of an asymmetric random walk without internal states, but the associated trajectories are qualitatively different. These two examples show that internal states can have either have a drastic influence on the likelihood of a large deviation, or none at all.

Second, I consider for the asymmetric RTP the time spent at the origin, to examine the presence of a dynamical phase transition following [49, 50]. Consistent with previous reasoning about which conditions enable this phenomenon, it appears whenever the particle has a non-zero net velocity, and separates a dynamical phase of trajectories localized around the origin, from one where trajectories spend only part of the time around the origin, and then escape.

The results of this chapter have been published in [2].

Chapter 6:
Dynamical large deviations in the presence of boundaries

I consider how to adapt the dynamical large deviation theory for diffusions to the presence of reflective boundaries. This development is motivated by an interest in understanding what general influence boundaries have on dynamical large deviations, and of allowing dynamical large deviation calculations to be carried out for specific reflected diffusions. In particular, the heterogeneous single-file diffusion from Chapter 3 can be mapped to a reflected diffusion, and the question of how the diffusion-ratchet effect influences current fluctuations is of interest.

Formally, the general problem amounts to deriving boundary conditions for certain 'tilted generators' associated with the given reflected diffusion and dynamical observable of interest. In a previous work [51], the boundary conditions were found for the case of dynamical observables that are of the occupation-time type, using an argument of operator duality. In this chapter we focus instead on current-like observables, to which this argument from duality does not transfer. Instead, I construct a tilted generator for a jump process, such that in the diffusive limit we obtain from it the sought-after boundary conditions. With this main result established, we find as a general consequence that the effective process is also a reflected diffusion.

In applying the new formalism to the heterogeneous N-particle SFD, I find that the fluctuations in the collective particle current are identical to those of just a single particle with certain averaged drift and diffusivity parameters. I give exact expressions for the rate function and the effective process. The latter reveals that sustained current fluctuations arise by all particles modifying their average velocities by the same amount Δv, regardless of the individual parameters of the particle, but Δv itself depends on all particle properties. The results are in interesting contrast with lattice models such as the ASEP, where collective current fluctuations imply not only changes in individual particle velocity but also effective repulsion between particles [52], an effect not surviving the diffusive limit, apparently.

The work in this chapter was done in external collaboration with Johan du Buisson and Hugo Touchette and published in [5].

Part I

Relaxation to a nonequilibrium steady state

Chapter 1

Background on nonequilibrium Markov processes

1.1 The Markov property in nonequilibrium physics

In nonequilibrium statistical mechanics, systems are ubiquitously modelled as time-homogeneous, ergodic Markov processes. Here we introduce these mathematical concepts, and attempt to give an overview of why they provide the appropriate mathematical framework for defining 'nonequilibrium conditions' in a general way. In later sections, we will specialize to jump processes and diffusion processes, which are forms of Markov processes useful is constructing specific models.

1.1.1 Whence stochasticity and Markovity?

To quantitatively model the dynamical behaviour of any kind of system, we assign to it a state $X(t)$ at time t, taking values in some state space $\mathcal{X}$ for times in $\mathcal{T}$. Depending on the situation, time may be modelled discretely or continuously. Likewise, the state space may be a discrete set or some subset of $\mathbb{R}^d$. In physics, there are many reasons why the state $X(t)$ cannot be known with certainty at a given time t, so that $X(t)$ is a random variable, and the sequence over all times constitutes a stochastic process. Consider, for example, the prototypical model of statistical mechanics, with $X(t)$ the $6N$ positions and momenta of an N-particle

fluid in a box:

- Even if the laws of motion are deterministic, $X(t)$ may contain uncertainty due to imperfectly known initial conditions, amplified by deterministic chaos;
- If the particles experience non-elastic collisions with the box walls maintained at some temperature, the external environment constitutes a persistent random influence on $X(t)$;
- If we coarse-grain the box into spatial cells described by the their average particle number and momentum, the dynamics at the level of cells must be described stochastically even if the microscopic dynamics is deterministic.

Regardless of the origin of stochastic behaviour, for many disparate systems, it is often found that the 'right choice' [6] of state variables justifies the assumption of the **Markov property**:

> *Conditioned on the present state, past and future sequences of states are statistically independent.*

Intuitively, this can be thought to reflect a principle of causal closure, in that the state variables encode all proximate influences on their own evolution (whether forward or backward in time) available at that level of description.

To express the Markov property mathematically, let us denote the probability of a sequence of states, ordered in time by $t_N > \ldots > t_0 > \ldots > t_{-M}$, as

$$\begin{aligned} &P_{(M+N+1)}(x_N, t_N; \ldots; x_0, t_0; \ldots; x_{-M}, t_{-M}) := \\ &\quad \mathbb{P}[X(t_N) = x_N, \ldots, X(t_0) = x_0, \ldots, X(t_{-M}) = x_{-M}], \end{aligned} \tag{1.1}$$

where $\mathbb{P}$ is the probability measure of the process. Then the Markov property states that

$$\begin{aligned} &P_{(M+N+1|1)}(x_N, t_N; \ldots; x_0, t_0; \ldots; x_{-M}, t_{-M} \mid x_0, t_0) = \\ &\quad P_{(N|1)}(x_N, t_N; \ldots; x_1, t_1 \mid x_0, t_0) P_{M|1}(x_{-1}, t_{-1}; \ldots; x_{-M}, t_{-M} \mid x_0, t_0). \end{aligned} \tag{1.2}$$

(The subscript on P is used to distinguish functions with different argument

structure.) In particular, if we divide (1.2) by $P_{M|1}$, we obtain

$$P_{(N|M+1)}(x_N, t_N; \ldots; x_1, t_1 \mid x_0, t_0; \ldots; x_{-M}, t_{-M}) = P_{(N|1)}(x_N, t_N; \ldots; x_1, t_1 \mid x_0, t_0), \tag{1.3}$$

often taken as the definition of the Markov property under the slogan that "Markov processes have no memory". This definition is in fact equivalent to (1.2) [8, 15], but obfuscates the **prediction-retrodiction symmetry** of the Markov property.

The Markov property can in some instances be systematically derived for a coarse-grained process, *e.g.* for a colloidal particle in a bath; when a classical phase space is naturally partitioned into regions separated by effective energy barriers, as for suspensions of chemical reactants, or configurational transitions of macromolecules [6, 53]; and more generally by the projection operator method applied to (quantum) Hamiltonians and the separation of 'fast' and 'slow' modes of evolution [7, 54]. In other cases from biophysics and ecology, to economics, and sociology, the Markov property is a reasonable modelling assumption, without which stochastic modelling becomes very difficult, because, as we shall see next, it is central to thinking about processes in terms of initial distributions and dynamical rules.

1.1.2 Prediction vs. retrodiction

A key conceptual and practical consequence of the Markov property is that it allows a process to be defined in terms of an initial distribution and an independently defined evolution operator, that encodes the 'dynamical laws' of the model. This is in contrast to the most general process, which must be defined by the entire set $\{P_{(n)}\}_{n=1}^{\infty}$.

Let us interpret t_0 as the initial time of our process, and define the **initial distribution**

$$\mu(x_0) := P_{(1)}(x_0, t_0). \tag{1.4}$$

We denote the probability distribution at a later time by

$$P_\mu(x, t) := \sum_{x_0 \in \mathcal{X}} P_{(1|1)}(x, t \mid x_0, t_0)\mu(x_0), \quad t > t_0. \tag{1.5}$$

Let us further define the **forward evolution operator** from t to $t' > t$ by

$$U_{t',t}(x', x) := P_{(1|1)}(x', t' \mid x, t). \tag{1.6}$$

Note that if we notationally treat it as a matrix, it satisfies a composition rule with a semi-group structure in the time arguments,

$$U_{t'',t} = U_{t'',t'} U_{t',t}, \quad t'' > t' > t. \tag{1.7}$$

Using the Markov property, we have for $t' > t > t_0$,

$$P_{(2|1)}(x', t'; x, t \mid x_0, t_0) = P_{(1|1)}(x', t' \mid x, t, x_0, t_0) P_{(1|1)}(x, t \mid x_0, t_0) \tag{1.8a}$$

$$= P_{(1|1)}(x', t' \mid x, t) P_{(1|1)}(x, t \mid x_0, t_0). \tag{1.8b}$$

Multiplying by $\mu(x_0)$ and marginalizing over x and x_0, we arrive at the **Chapman-Kolmogorov equation** (CKE)

$$P_\mu(x', t') = \sum_{x \in \mathcal{X}} U_{t',t}(x', x) P_\mu(x, t). \tag{1.9}$$

Thus, we can take the view that the 'physics' of a stochastic system is contained in the operator $U_{t',t}$, separated from the initial condition μ. Furthermore, due to the semi-group property, we have that for an infinitesimal time-step Δt (or the minimal step if time is discrete)

$$U_{t+\Delta t,t} = e^{\Delta t H_t}, \tag{1.10}$$

with H_t an **(infinitesimal) forward generator**, in many ways similar to a quantum Hamiltonian. Beyond Section 1.1 of the thesis, we will focus exclusively on continuous-time Markov processes that are also **time-homogeneous**, meaning that $H_t = H$, and therefore $U_{t',t} =: U_{t'-t} = \exp[(t' - t)H]$. Physically, the interpretation of time-homogeneity is that the dynamical laws themselves are constant in time, *e.g.* because the model contains no time-varying external parameters. In Section 1.2 we will review **jump processes** on countable state spaces, for which H (then to be denoted $\mathbb{W}$) is a transition rate matrix. In Section 1.3 we derive **diffusion processes** that evolve in continuous space, and for which H (then to be denoted $\mathcal{L}^\dagger$) is a differential operator of diffusion type.

The definition of a Markov process as an initial distribution together with an evolution operator forward in time, produces implicitly an evolution operator

backward in time through Bayesian inversion:

$$\bar{U}_{t,t'}(x,x') := P_{(1|1)}(x,t \mid x',t') = U_{t',t}(x',x)\frac{P_\mu(x,t)}{P_\mu(x',t')}. \tag{1.11}$$

It is the operator inverse of $U_{t',t}$ and also has the semi-group property. Due to the prediction-retrodiction symmetry, we could instead have considered a fixed final distribution

$$\nu(x_f) := P_{(1)}(x_f,t_f), \tag{1.12}$$

(with $t_f > t' > t$) and defined probabilities

$$\bar{P}_\nu(x,t) := \sum_{x_f} P(x,t \mid x_f,t_f)\nu(x_f). \tag{1.13}$$

These probabilities would evolve by

$$\bar{P}_\nu(x,t) := \sum_{x'} \bar{U}_{t,t'}(x,x')\bar{P}_\nu(x',t'), \tag{1.14}$$

where $\bar{U}_{t,t'}$ could be defined independently of ν, whereas $U_{t',t}$ would be the dependent quantity via Bayesian inversion. While (1.14) might have been called a **backward Chapman-Kolmogorov equation**, this term is instead reserved for another evolution, that of initial conditions being pushed backward in time,

$$P(x_f,t_f \mid x,t) = \sum_{x'} U^\dagger_{t',t}(x,x')P(x_f,t_f \mid x',t'), \tag{1.15}$$

where $U^\dagger_{t',t}(x,x') = U_{t',t}(x',x)$ is usually called the **backward evolution operator**.

A subtle point raised by Uffink [8], is that by choosing to define a Markov process from the prediction point of view, we inadvertently introduce a certain 'arrow of time' at the statistical level. In particular, if the forward evolution operator is time-homogeneous, this is not necessarily true of the backward evolution operator, *unless* $P_\mu(x,t)$ is time-independent. As we shall see next, this feature of the mathematical theory will allow us two separate the notions of 'nonequilibrium' as relaxation from a special initial condition towards a stationary limit, and as indefinitely maintained conditions of irreversibility.

1.1.3 The meaning of 'nonequilibrium'

Nonequilibrium physics concerns processes that are irreversible in time. For Boltzmann, Gibbs, and their peers, 'nonequilibrium' tended to refer to the transient regime of a thermal system, typically an isolated gas, relaxing towards a macroscopic equilibrium state from some special, nonequilibrium initial condition. Onsager, and later Prigogine, would refocus nonequilibrium physics on dissipative steady states, exemplified by chemically reacting suspensions and convection cells in which stationary currents of mass and heat are indefinitely maintained (on the relevant time-scales). 'Nonequilibrium' then refers to the *physical conditions* under which the system evolves, *e.g.* under external heating or internal chemical activity, rather than the accident of initial distribution. We aim here to present a mathematical definition of a **nonequilibrium process** in this latter sense of 'nonequilibrium' as internal or external conditions of the process that maintain irreversible behaviour indefinitely, regardless of initial conditions. We must first define stationarity and reversibility.

A stochastic process $X^*(t)$ is a **stationary process** if its statistics are time-translation invariant. That is, if for all τ,

$$\mathbb{P}[X^*(t_n+\tau)=x_n,\dots,X^*(t_1+\tau)=x_1]=\mathbb{P}[X^*(t_n)=x_n,\dots,X^*(t_1)=x_1]. \tag{1.16}$$

A stationary process will also be referred to as a **steady state**. Relatedly, a **stationary or steady-state distribution** P^* of a Markov process $X(t)$, is one for which the Chapman-Kolmogorov equation (1.9) is invariant,

$$P^*(x')=\sum_{x\in\mathcal{X}}U_{t',t}(x',x)P^*(x), \tag{1.17}$$

for any t,t'. If $X(t)$ has initial condition $\mu=P^*$, then $X(t)$ will be a stationary process.

One immediately wonders about the existence and uniqueness of stationary distributions for Markov processes, and what limit, if any, a given initial distribution converges to with time:

$$\lim_{t\to\infty}P_\mu(x,t)\stackrel{?}{=}P^*_\mu(x)\stackrel{?}{=}P^*(x). \tag{1.18}$$

Clearly, if the process is not time-homogeneous, one has no reason to expect any stationary distributions to exist; but perhaps a periodic limiting distribution, if the process is periodically driven [55]. A Markov process that convergences from any initial distribution μ to a unique stationary distribution P^* is called **ergodic**, in which case we can say the process itself converges towards a stationary process, $X \to X^*$. A detailed discussion of the pre-conditions for ergodicity is deferred to Section 1.2.2 in the context of jump processes.

If we consider a process $X(t)$ on $\mathcal{T} = [0, +\infty)$, we can over the observation time window $\mathcal{T}^{\text{obs}} = [0, T]$ define the **reverse process**

$$\hat{X}(t) := X(T - t). \tag{1.19}$$

(If the interpretation of $X(t)$ contains coordinates that are momentum-like, then physical time-reversal may entail also conjugating those coordinates; we will discuss such generalized notions of reversed processess in Section 1.2.5.) $X(t)$ is **reversible** if it is statistically indistinguishable from its reverse process, over all observation time windows:

$$\mathbb{P}[X(t_n) = x_N, \ldots, X(t_1) = x_1] = \mathbb{P}[\hat{X}(t_N) = x_N, \ldots, \hat{X}(t_1) = x_1] \tag{1.20}$$

for any $N \geq 1$, $x_n \in \mathcal{X}$, $t_n \in \mathcal{T}^{\text{obs}}$, and for any $T > 0$. For $X(t)$ a Markov process, the reverse process $\hat{X}(t)$ is also Markovian, but with initial distribution

$$\hat{\mu}(x) = P_\mu(x, T), \tag{1.21}$$

and evolution operator

$$\hat{U}_{t',t}(x', x) = U_{T-t,T-t'}(x, x') \frac{P_\mu(x', T - t')}{P_\mu(x, T - t)}. \tag{1.22}$$

A Markov process is hence reversible if

$$\hat{\mu}(x) = \mu(x), \tag{1.23}$$

and

$$\hat{U}_{t',t} = U_{t',t}, \quad t' > t, \tag{1.24}$$

for any $T > 0$. The first conditions implies that $\mu = \hat{\mu} = P^*$ is a stationary distribution, and hence that $X(t)$ is a stationary process. For $X(t)$ being

stationary and time-homogeneous, so that $U_{t',t} = U_{t'-t}$, the second condition can be expressed as the condition of **detailed balance**

$$U_s(x, x')P^*(x') = U_s(x', x)P^*(x). \tag{1.25}$$

Detailed balance expresses that the probability flow from any state x to another state x' is exactly balanced by the reverse flow, over any time scale. When $X(t)$ is interpreted as a physical process, *e.g.* the positions of colloidal particles in a bath, probability flow translates to a physical flow of mass or energy, and detailed balance implies the absence of net, physical currents on any spatial scale captured by the model.

We can then define a **nonequilibrium steady state** (NESS) as a stationary process that is not reversible (*i.e.* is irreversible). In particular, a stationary, time-homogeneous Markov process constitutes a NESS if the condition of detailed balance is violated. For ergodic Markov processes, that converge asymptotically to a unique steady state from any initial distribution, whether that steady state is a NESS or not must be a property of the process generator (*i.e.* of the dynamical rules of the process), because it is independent of the initial distribution. In this instance we can define a **nonequilibrium process** as one whose eventual steady state is a NESS, and, similarly, an **equilibrium process** as one with an equilibrium (reversible) steady state. In the terminology we will adhere to, the non-stationary regime of an equilibrium process will not be referred to as nonequilibrium. Thus we are excluding from consideration the very long-lived states associated with the slow approach to equilibrium in disordered systems [56]. Furthermore, our terminology contrasts with some fields such as ecological population modelling and economic/evolutionary game theory, where (non)equilibrium is synonymous with (non)stationarity, and nonequilibrium steady state means a limit-cycle distribution.

Note that, for non-ergodic processes, it is generally not possible to judge whether the time-reversal non-invariance of state sequences is due to special initial conditions (*i.e.* 'nonequilibrium' in the historic sense of relaxation or transience), or due to some intrinsic quality of the dynamical rules ('nonequilibrium conditions'). This is precisely because there is no unique steady state that isolates only the latter aspect of irreversibility. For non-Markovian processes, there is not necessarily even an evolution operator than can be interpreted as 'dynamical rules' defined independently of the initial distribution. These points emphasize how central the ergodic Markov assumption is to consistently formalize the notion

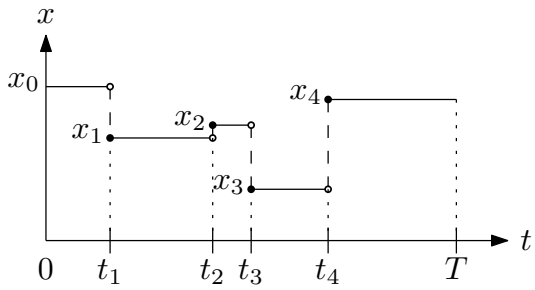

Figure 1.1 *The trajectory of a jump process*

of a nonequilibrium process.

It is important to be mindful that the above definition of a (non)equilibrium process is a purely mathematical one, designed to formalize our physical ideas. Whether a real system is judged in or out of equilibrium by this definition will depend on how it has been modelled, specifically on the spatial and temporal scales that the model faithfully represents. Models of self-propelled, active particles that move by consuming chemical energy are a case in point. Without explicit inclusion of the state of the energy resource in the model description, they undergo nonequilibrium dynamics. If the resource is also included in the description, one may find that the previous model merely represents a short-time, non-stationary regime of what is now an equilibrium process [57]. In a large system of active particles without alignment interactions, the breaking of time-reversal symmetry due to steric interaction at the mesoscopic level may be hidden at the coarse-grained level of clustering dynamics, which can be mapped to an equilibrium model [58].

1.2 Jump process theory

We now consider continuous-time Markov processes on countable state spaces, then known as jump processes[1] (Figure 1.1). Apart from being a form of process with useful applications, it is also fundamental, in that Markov processes in continuous space, whether Lévy flights or drift-diffusions, can be constructed as limits of jump processes [14]. Furthermore, many basic concept of nonequilibrium physics that we shall define—*e.g.* current, activity, entropy production—are most conveniently defined in the jump process language.

[1] Or 'discrete' jump processes, as jump processes with jumps drawn from a continuous range are also possible—but we will not be concerned with the latter.

1.2.1 The Master equation and its generator

We let $X(t)$ be a time-homogeneous Markov process in continuous time on the countable state space $\mathcal{X} \ni x, y, z$, etc. The initial distribution we denote μ, and the probability at a later time $P(x,t) = P_\mu(x,t)$. The time evolution operator (1.6), due to its semi-group structure, has the exponential form

$$U_s(y,x) = (e^{s\mathbb{W}})(y,x), \tag{1.26}$$

with **(forward) generator**

$$\mathbb{W}(y,x) := \lim_{s\to 0} \frac{\mathrm{d}}{\mathrm{d}s} \mathbb{P}[X(s+t) = y \mid X(t) = x] \tag{1.27a}$$

$$= \lim_{s\to 0} \frac{\mathbb{P}[X(s+t) = y \mid X(t) = x] - \delta_{x,y}}{s} \tag{1.27b}$$

For $x \neq y$ we write

$$\mathbb{W}(y,x) = W(y,x), \tag{1.28}$$

which are the **transition rates** *from*[2] x *to* y. By convention we let $W(x,x) = 0$. For $y = x$, we have

$$\mathbb{W}(x,x) = \lim_{s\to 0} \frac{\mathrm{d}}{\mathrm{d}s} \left\{ 1 - \sum_{z\neq x} \mathbb{P}[X(s+t) = z \mid X(t) = x] \right\} \tag{1.29}$$

$$= -\xi(x), \tag{1.30}$$

where we define the **escape rates**

$$\xi(y) := \sum_{z\in\mathcal{X}} W(z,y), \tag{1.31}$$

the probability per unit time of leaving the state y. By construction, $\mathbb{W}$ is column stochastic, meaning that for each column the rows sum to zero,

$$\sum_y \mathbb{W}(y,x) = 0. \tag{1.32}$$

[2]In this thesis, I have settled on $W(y,x)$ for $x \to y$, rather than $W(x,y)$, $W(y \mid x)$ or $W(x \to y)$, as it the form most notationally consistent with $\mathbb{W}$ being a matrix acting on the right. Other conventions were used in some of my publications.

Consider now the Chapman-Kolmogorov equation (1.9),

$$P(y, t+s) = \sum_{x \in \mathcal{X}} U_s(y, x) P(x, t), \tag{1.33}$$

and apply $\lim_{s \to 0} \mathrm{d}/\,\mathrm{d}s$. We then arrive at the **master equation**

$$\partial_t P(y,t) = \sum_x \mathbb{W}(y,x) P(x,t) \tag{1.34a}$$

$$= \sum_y \left[W(y,x) P(x,t) - W(x,y) P(y,t) \right]. \tag{1.34b}$$

The master equation states that the change in probability at a given state is determined by the difference of instantaneous loss and gain terms. We can define

$$J(y, x; t) := W(y, x) P(x, t) - W(x, y) P(y, t), \tag{1.35}$$

and interpret it as the **probability current** across bond $x \to y$ at time t. The probability current is often directly related to a physical current of matter or energy.

In practice, a jump process will be defined by a state space $\mathcal{X}$, a set of transition rates $\{W\}$, and the master equation, to be thought of as a function of the initial distribution μ which often is not thought of as defining the model *per se*. This can be called a kinetic view of model-making [12] because it is centred on implementing dynamical rules that are not necessarily constrained *a priori* by the need to reproduce some imposed distribution (*e.g.* a Boltzmann distribution). Below we consider some examples, as illustrated in Figure 1.2:

(a) A random walk on a graph. $X(t)$ is the position of a particle that moves between the nodes $x \in \mathcal{X}$ of a weighted, directed graph, with edges $(y, x) \in \mathcal{E} \subset \mathcal{X} \times \mathcal{X}$ of weights $w(y, x)$. The particle hops from its current position x to y at a rate proportional to the weight of the edge, hence $W(y, x) = \gamma w(y, x)$, where γ determines the units of time.

This example illustrates the point that any jump process can be thought of as a random walk on some graph.

(b) A run-and-tumble particle. $X(t)$ is the state of a self-propelled particle, which has a position n on a linear lattice and an orientation $\sigma \in \{1, +1\}$

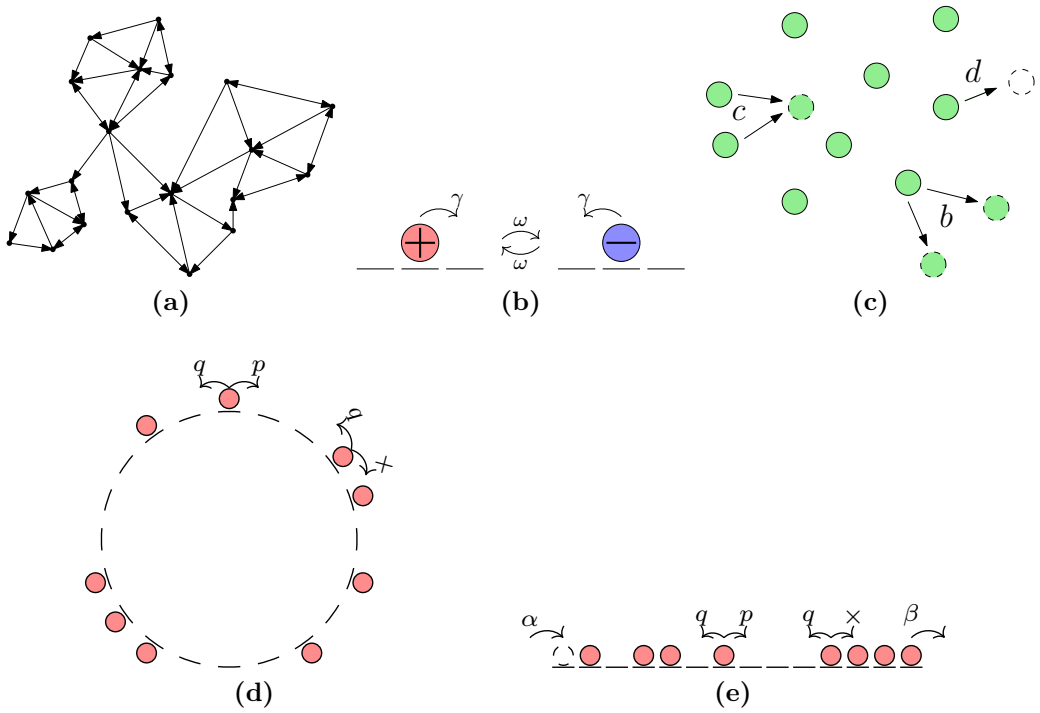

Figure 1.2 *Illustrations of the jump processes described below.*

(=left/right). The particle propels itself one site in the direction of its orientation at a rate γ, and reverses its orientation at a rate ω. The non-zero transition rates are then

$$W((n+\sigma,\sigma),(n,\sigma)) = \gamma, \quad W((n,-\sigma),(n,\sigma)) = \omega. \tag{1.36}$$

This model will be studied in-depth in Chapter 2 were more background on the motivation of this model is also provided.

(c) Birth-death process. $X(t)$ is the number n of individuals of a well-mixed population of a species S. An individual reproduces asexually at a rate b ($S \xrightarrow{b} S+S$) and dies naturally at rate d ($S \xrightarrow{b} \emptyset$). Every individual encounters every other at a rate c, and one of the two dies in competition ($S+S \xrightarrow{c} S$). The rates are then

$$W(n+1,n) = bn, \quad W(n-1,n) = dn + cn(n-1). \tag{1.37}$$

This is an example of an **absorbing process** because $X=0$ is an absorbing state which the process can never leave if attained.

(d) The periodic ASEP. $X(t)$ denotes the positions of N asymmetric random

walkers existing on a lattice ring of L sites. Each walker attempts to hop forward by one site at a rate $p_+ = p$, and backward by one site at a rate $p_- = q$, and only succeeds if the target site is empty—these are **hardcore exclusion interactions**. The states have the structure $x = \{n_1, \ldots, n_N\}$ with n_i the position of particle i. This gives transition rates $W(x', x) = p_\pm$ if x' and x differ only by $n_i' = n_i \pm 1$ with $n_i \pm 1 \neq n_{i\pm1}$, for exactly one index i.

This is the periodic version of the **asymmetric simple exclusion process** (ASEP), a paradigm of the kinetic approach to nonequilibrium theory [10, 12, 17]. In the case $p = q$ the 'asymmetric' is replaced by 'symmetric' (SSEP), and if $p > 0, q = 0$ by 'totally asymmetric' (TASEP).

(e) The open ASEP. Hardcore-excluding asymmetric random walkers hop with rates p and q on a linear lattice of L sites. On the boundary site 1, a particle is injected with rate α if the site is empty; a particle at the boundary site L exits with rate β. Due to non-conservation of particle number, the states x have the structure $\{\tau_1, \ldots, \tau_L\}$, where $\tau_n \in \{0, 1\}$ is the occupancy of site n. The transition rates are written down similarly do (d).

Continuing with the general properties of jump processes: The **waiting-time distribution** $w(\tau \mid x, t)$ is the probability density of waiting a time τ before a jump occurs, given that we find the process in state x at time t. The probability that the particle jumps in a small time-interval $\Delta\tau$ after time τ is the probability of not jumping up to time τ, times the probability of making some jump in the interval $\Delta\tau$:

$$w(\tau \mid x, t)\Delta\tau = \left(1 - \int_0^\tau \mathrm{d}\tau'\, w(\tau' \mid x, t)\right) \times \xi(x)\Delta\tau. \tag{1.38}$$

By differentiation, this equation becomes $\partial_\tau w = -\xi w$ with the solution that waiting times are exponentially distributed with the escape rates as parameter:

$$w(\tau \mid x, t) = \xi(x) e^{-\xi(x)\tau}. \tag{1.39}$$

Jump process trajectories (Figure 1.1) are thus generated by a state-dependent 'Poisson clock' that dictates when to jump, and an embedded discrete-time process dictating where to jump at those times. This we will use in Chapter 4 to write down the jump-process path-probability.

For functions $F : \mathcal{X} \to \mathbb{R}$, we can define an evolution operator $\mathbb{L}$ by

$$(\mathbb{L}F)(x) := \lim_{\mathrm{d}t \to 0} \frac{1}{\mathrm{d}t} \langle F(X(t + \mathrm{d}t)) - F(X(t)) \mid X(t) = x \rangle \tag{1.40a}$$

$$= \partial_t \langle F(X(t)) \rangle_x . \tag{1.40b}$$

It can be checked directly from the definitions that $\mathbb{L} = \mathbb{W}^\top$. This is the **backward generator** of $X(t)$ (often simply called the 'generator' in the mathematical literature). It and the forward generator are duals or adjoints in the sense that

$$\langle F, \mathbb{W}P \rangle = \langle \mathbb{L}F, P \rangle \tag{1.41}$$

with respect to the inner product

$$\langle F, P \rangle := \sum_x F(x)P(x). \tag{1.42}$$

Whether we define a jump process via an initial distribution and a forward *vs.* a backward generator is a matter of taste. Physicist tend to prefer the forward approach, and mathematicians the backwards.

$\mathbb{L}$ is the generator of the **backward master equation** [14, 59] (the infinitesimal form of the backward CKE (1.15)), expressing the evolution of probability as we push the *initial condition* further back in time:

$$\partial_{-t} P(x', t' \mid x, t) := \lim_{\Delta t \to 0} \frac{P(x', t' \mid x, t - \Delta t) - P(x', t' \mid x, t)}{\Delta t} \tag{1.43a}$$

$$= \sum_y \mathbb{L}(x, y) P(x', t' \mid y, t). \tag{1.43b}$$

The backward master equations finds its use in first-passage time calculations [60].

1.2.2 Ergodic relaxation to stationarity

Recall that $X(t)$ is ergodic if there exists a *unique* stationary distribution P^* such that

$$\lim_{t \to \infty} P_\mu(x, t) = P^*(x), \tag{1.44}$$

independent of the initial distribution μ. In particular, such a limit should be a stationary solution of the the master equation (1.34), and therefore satisfy **global balance**:

$$\sum_y [W(y,x)P^*(x) - W(x,y)P^*(y)] = 0. \tag{1.45}$$

To address the question of when ergodicity holds, consider the formal solution to the master equation if $\mathbb{W}$ can be assumed diagonalizable with eigenvalues λ_i and left and right eigenvectors L_i, R_i. Because $\mathbb{W}$ does not need to be symmetric it can have distinct right and left eigenvectors, but they can be chosen to be orthonormal,

$$\sum_x L_i(x)R_j(x) = \delta_{ij}. \tag{1.46}$$

The evolution operator is then

$$U_t(y,x) = (e^{t\mathbb{W}})(y,x) = \sum_i R_i(y)e^{\lambda_i t}L_i(x), \tag{1.47}$$

giving

$$P_\mu(x,t) = \sum_i e^{\lambda_i t}(L_i \cdot \mu)R_i(x). \tag{1.48}$$

Ergodicity is seen to follow if $\mathbb{W}$ has a dominant eigenvalue of $\lambda_0 = \max_i \operatorname{Re}\lambda_i = 0$, which is simple, and corresponds to a left eigenvector $L_0 \equiv 1$ and a right eigenvector $R_0 = P^*$. The 'spectral gap' $\lambda_1 - \lambda_0 = \lambda_1$, *i.e.* the sub-dominant eigenvalue, sets the the time scale of the longest-lived non-stationary mode, *i.e.* the **relaxation time** $\tau_{\text{rel}} = -1/\operatorname{Re}\lambda_1$.

When can $\lambda_0 = 0$ be guaranteed? For finite state spaces, this follows from [15, 61]:

> **The Perron-Frobenius (PF) theorem**. Suppose the square, non-negative, finite-dimensional matrix M is **irreducible**: for each pair (y,x), there is a chain $(y, x_n, \ldots, x_1, x)$, $n \geq 0$, such that $\mathsf{M}(y,x_n)\cdots\mathsf{M}(x_1,x) > 0$. Then M has a 'Perron-Frobenius' eigenvalue r corresponding to a right eigenvector R and a left eigenvector L, such that
>
> (i) r is real, non-negative and simple (*i.e.* has a one-dimensional

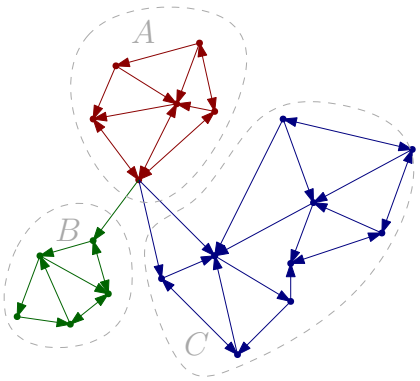

Figure 1.3 *In this state transition graph, the component A is transient, in that once exited into either B or C, A cannot be re-entered. B and C are irreducible components, because within each component any two states are connected by a directed path. The stationary distribution for a jump process on this this graph has the form $P^*(x) = 0$ for $x \in A$ and $P^*(x) = pP^*_B(x) + (1-p)P_C(x)$, $x \in B \cup C$, where $P_{B/C}$ is the unique stationary distribution for each irreducible component treated as a separate system. The factor p depends on the initial distribution (e.g. $p = 1$ if the initial condition is all in B) and the stationary distribution is therefore not unique.*

eigenspace);

(ii) r is the dominant eigenvalue in the sense that $r \geq |\lambda|$ and $r > \operatorname{Re}\lambda$, for any other eigenvalue λ;

(iii) $\min_x \sum_y \mathsf{M}(y,x) \leq r \leq \max_x \sum_y \mathsf{M}(y,x)$ with one equality forcing the other;

(iv) R and L can be chosen to have strictly positive entries. Furthermore, they are the only eigenvectors of any eigenvalue for which this is true.

To apply the PF theorem to continuous-time Markov processes with finite state spaces, we let $\mathsf{M} = \mathbb{W} + \max_y \xi(y) \times \mathbb{1}$, with $\mathbb{1}$ the identity matrix. M then satisfies the conditions of the theorem if $\mathbb{W}$ is irreducible, meaning that there exists some directed path between every pair of states graph of possible state transitions. To understand why this is a necessary property, in particular for property (iv), consider the state transition graph in Figure 1.3 and the explanation in the caption.

The PF eigenvalue r of M is related to the dominant eigenvalue λ_0 of $\mathbb{W}$ as

$$r = \lambda_0 + \max_x \xi(x). \tag{1.49}$$

Part (iii) of the theorem then gives $r = \max_x \xi(x)$ and hence $\lambda_0 = 0$. The eigenvectors L, R are the same for M and $\mathbb{W}$. In particular, R is the unique stationary distribution P^* (once normalized), with strictly positive entries, and L is the vector of ones (following from column-stochasticity).

To extend the PF theorem to infinite matrices, there are some challenges associated with making the state space of the associated jump process infinitely large:

- If there is no upper bound on the escape rates, it is possible for the process to 'explode' and make an infinite number of transitions in a finite time.
- The process may stray infinitely far away from any given state, returning only a finite number of times over arbitrarily long time intervals: such a state is non-recurrent or transient.

Non-explosion, irreducibility, and the existence of a recurrent state are sufficient conditions for ergodicity (see [15] for the rather technical steps involved in proving this statement.) In practice, if we believe a unique stationary distribution ought to exist on physical grounds, and we are able to find a candidate, we will be content to proclaim that as the solution.

1.2.3 Reversibility and detailed balance

Let $X(t)$ be an ergodic Markov process, converging towards the stationary process $X^*(t)$ with stationary distribution $P^*(x)$. To find the generator of the reversed process $\hat{X}^*(t) = X^*(T-t)$, we note that in the stationary, time-homogeneous case (1.22) can be written

$$\hat{U}_s(y,x) = U_s(x,y)\frac{P^*(y)}{P^*(x)}. \tag{1.50}$$

By differentiating, we find

$$\hat{\mathbb{W}}(y,x) = \mathbb{W}(x,y)\frac{P^*(y)}{P^*(x)}. \tag{1.51}$$

The process is reversible if the generators of $X^*(t)$ and $\hat{X}^*(t)$ are identical; $\hat{\mathbb{W}} = \mathbb{W}$. This amounts to a time-instantaneous version of **detailed balance**,

$$W(y,x)P^*(x) = W(x,y)P^*(y). \tag{1.52}$$

This is clearly a special case of global balance (1.45). Eq. (1.52) also follows directly by applying $\lim_{s\to 0} \mathrm{d}/\,\mathrm{d}s$ to the detailed balance relation (1.25).

Given ergodicity, P^* is implicitly determined by the rates, and can even be expressed in terms of them using Kirchhoff's formula [62]. A condition for detailed balance expressed only using the rates ought therefore to exist, and indeed that result is due to Kolmogorov [63]. Denote by $\mathcal{C} = (x_n, \ldots, x_2, x_1, x_n)$ a directed cycle of states in $\mathcal{X}$, and by $\hat{\mathcal{C}}$ the same cycle in reverse sequence. Then detailed balance holds if for all cycles

$$W(\mathcal{C}) = W(\hat{\mathcal{C}}), \tag{1.53}$$

where these quantities are the product of the rates over all transitions in the cycle [64]. Measuring the presence or absence of reversibility in cycles is one direct way of determining whether an experimental system is out of equilibrium at a chosen coarse grained scale [65].

1.2.4 Characterisation of nonequilibrium steady states

We have defined a NESS as a stationary process that violates detailed balance. Therefore, a NESS has a nonvanishing **stationary probability current**

$$J^*(y,x) = W(y,x)P^*(x) - W(x,y)P^*(y) \tag{1.54}$$

across some (or all) bonds (y,x) in its transition graph.

What information is necessary to fully specify a NESS? Unless we also know the rates W defining the model, given just a distribution P^* it is impossible to tell whether the steady state is in equilibrium or not. It has therefore been proposed [10, 64] that a NESS should be characterized by $\{P^*, J^*\}$, the stationary distribution, and the currents across all bonds. This information is sufficient classify the reversibility status of a steady state, because equilibrium steady states are of the form $\{P^*, 0\}$. The remaining degrees of freedom on which two processes can differ while giving the same $\{P^*, J^*\}$ were later dubbed **traffic** [46],

a symmetric counterpart to the current:

$$T^*(x,y) := W(y,x)P^*(x) + W(x,y)P^*(y), \quad x \neq y. \tag{1.55}$$

The traffic measures the steady-state 'activity' across a bond, not distinguishing the direction of transitions. It has turned out to be an important quantity in the study of glassy systems [66], and of fundamental importance in nonequilibrium fluctuation and response theory [67–69].

Inspired by these works I propose that the complementing roles of currents and traffics in the theory is most apparent via a matrix decomposition. First, let us introduce $\Pi := \operatorname{diag} P^*$, that is

$$\Pi(x,y) = P^*(x)\delta_{x,y}. \tag{1.56}$$

Then from (1.51), and using $\mathbb{L} = \mathbb{W}^\top$, we can write the *backward* generator of the reversed process as

$$\hat{\mathbb{L}} = \Pi^{-1}\mathbb{W}\Pi. \tag{1.57}$$

Then define the two matrices

$$\mathbb{J} := \Pi(\hat{\mathbb{L}} - \mathbb{L}), \quad \mathbb{T} := \Pi(\hat{\mathbb{L}} + \mathbb{L}). \tag{1.58}$$

Alternatively, they can be expressed as

$$\mathbb{J} = \mathbb{W}\Pi - (\mathbb{W}\Pi)^\top, \quad \mathbb{T} = \mathbb{W}\Pi + (\mathbb{W}\Pi)^\top. \tag{1.59}$$

Therefore, by construction $\mathbb{J}^\top = -\mathbb{J}$ while $\mathbb{T}^\top = \mathbb{T}$. Furthermore we find that $\mathbb{J}(x,y) = J^*(x,y)$, and in particular $\mathbb{J}(x,x) = 0$; and $\mathbb{T}(x,y) = T^*(x,y)$ for $x \neq y$, and $\mathbb{T}(x,x) = -2\xi(x)P^*(x)$. We can solve for $\mathbb{W}$ as

$$\mathbb{W} = \frac{1}{2}(\mathbb{J} + \mathbb{T})\Pi^{-1}. \tag{1.60}$$

Let $\mathbf{1}$ be the vector of ones. Then from $\mathbf{1}^\top\mathbb{W} = 0$ (column-stochasticity) and $\mathbf{1}^\top\mathbb{J} = 0$ (global balance) follows also $\mathbf{1}^\top\mathbb{T} = 0$, or

$$P^*(x)\xi(x) = \frac{1}{2}\sum_{x:x\neq y} T^*(x,y). \tag{1.61}$$

In particular the average escape rates $\langle \xi \rangle = \sum_{x \neq y} T^*(x, y)$, the total activity in the stationary state [70].

The triplet $\{\Pi, \mathbb{J}, \mathbb{T}\}$ (where the appropriate constraints on the elements of these matrices can be inferred from the above) is thus equivalent to $\mathbb{W}$. Therefore, once we have taken into account all general quantities that may be of potential interest in the NESS—the state distribution, the currents, and the traffics—this amounts to the full detail of the model. The crux is of course that, given $\mathbb{W}$, deriving the stationary distribution P^* explicitly may be incredibly difficult.

Exact solution techniques for steady states form an industry, with notable examples being the matrix-product ansatz pioneered for solving the open ASEP [13], generating function methods, or even direct iteration [71], complemented by approximation techniques, such as continuum limits or large system size expansions [6].

1.2.5 Generalized reversibility

Time-reversal is ultimately a physical concept, and it sometimes involves not only reversing the sequence of states that constitute a trajectory, but also inverting the signs of 'odd' variables such as momentum-like states, or external parameters such as magnetic fields.

Nothing at the level of generality we have hitherto adhered to can be said in the last case involving external parameters [14]. If the rates W_λ depend on the parameter λ, then comparing trajectories under W_λ to the time-reversal of trajectories generated by $W_{-\lambda}$ amounts to comparing trajectories from two processes that can be arbitrarily different. A specific model for the effect of λ is required. In **stochastic thermodynamics** [35] this comes from the criterion of **local detailed balance**: for each λ the W_λ satisfy detailed balance with respect to $P^*_\lambda(x) \propto \exp[-\beta V_\lambda(x)]$ where $V_\lambda(x)$ is an energy function, *e.g.* $V_\lambda(x) = V_0(x) + \lambda M(x)$, if λ is a field and M the 'magnetization' of the state. For 'closed, isolated, physical systems', *i.e.* those completely determined by a Hamiltonian, an 'appropriate' phase-cell coarse-graining leads to a detailed balance relation involving also the reversal of magnetic fields [6].

In contrast, the case of odd state variables can be treated in a more general fashion. We imagine that each state $x \in \mathcal{X}$ has a unique 'dynamically reversed'

[16] state $\theta x \in \mathcal{X}$, such that $\theta(\theta x) = x$. That is, θ is an involution on $\mathcal{X}$. For example, if $x = (p, q)$ contains a momentum p and a position p, then $\theta x = (-p, q)$. For X^* stationary we define its dynamical reversal with respect to θ by

$$\hat{X}^\theta(t) := \theta(X^*(\tau - t)) \tag{1.62}$$

and call X^* **dynamically reversible** with respect to the involution θ if its is statistically indistinguishable from $\hat{X}^\theta$. The stationary distribution of $\hat{X}^\theta(t)$ is $P^*(\theta x)$ and its forward generator

$$\hat{\mathbb{W}}^\theta(y, x) = \mathbb{W}(\theta x, \theta y)\frac{P^*(\theta y)}{P^*(\theta x)}. \tag{1.63}$$

For dynamical reversibility to hold we require that the stationary distributions of $X^*(t)$ and $X^\theta(t)$ coincide,

$$P^*(\theta x) = P^*(x), \tag{1.64}$$

and their forward generators are the same, $\hat{\mathbb{W}}^\theta = \mathbb{W}$, that is

$$\hat{\mathbb{W}}^\theta(y, x)P^*(\theta x) = \mathbb{W}(\theta x, \theta y)P^*(\theta y). \tag{1.65}$$

The off-diagonal elements give (using (1.64))

$$W(\theta y, \theta x)P^*(\theta x) = W(x, y)P^*(y) \tag{1.66}$$

which we recognize as an **extended detailed balance**. The diagonal entries give

$$\xi(\theta x) = \xi(x), \tag{1.67}$$

dynamical reversibility of escape rates.

The matrix decomposition scheme introduced in Section 1.2.4 is readily generalized. Let Θ be the permutation matrix such that $(\Theta F)(x) = F(\theta x)$, that is $\Theta(x, y) = \delta_{x,\theta y}$. It follows that $\Theta = \Theta^{-1} = \Theta^\top$. Then we can write the backward generator of $\hat{X}^\theta(t)$ as

$$\hat{\mathbb{L}}^\theta = (\Pi\Theta)^{-1}\mathbb{W}\Pi\Theta. \tag{1.68}$$

We then define

$$\mathbb{J}^\theta := \Pi(\hat{\mathbb{L}}^\theta - \mathbb{L}), \quad \mathbb{T}^\theta = \Pi(\hat{\mathbb{L}}^\theta + \mathbb{L}) \tag{1.69}$$

If Π and Θ commute, *i.e.* (1.64) holds, then

$$\Theta\mathbb{J}^{\theta\top}\Theta = -\mathbb{J}^\theta, \quad \Theta\mathbb{T}^{\theta\top}\Theta = \mathbb{T}^\theta. \tag{1.70}$$

The elements of these matrices are interpretable as generalized currents and traffics.

What is the significant difference between satisfying reversibility or dynamical reversibility? In the first case, using detailed balance in the form $\mathbb{J} = \mathbb{W}\Pi - \Pi\mathbb{W}^\top \equiv 0$, the matrix

$$\mathbb{V} := \Pi^{-1/2}\mathbb{W}\Pi^{+1/2} = \Pi^{+1/2}\mathbb{W}^\top\Pi^{-1/2} \tag{1.71}$$

is symmetric. $\mathbb{W}$ is thus similar[3] to $\mathbb{V}$, and is therefore called symmetrizable. $\mathbb{W}$ therefore has the same spectrum as $\mathbb{V}$, which is necessarily real.

We may attempt a similar construction in the case of extended detailed balance,

$$\mathbb{V}^\theta := (\Pi\Theta)^{-1/2}\mathbb{W}(\Pi\Theta)^{+1/2} = (\Pi\Theta)^{+1/2}\mathbb{W}^\top(\Pi\Theta)^{-1/2}. \tag{1.72}$$

$\Theta^{\pm 1/2}$ does exist but is in general a complex matrix. For $\mathbb{V}^\theta$ to be Hermitian and thereby guaranteed to have a real spectrum, we need $(\Pi\Theta)^{\pm 1/2}$ to be Hermitian, which is not necessarily the case.[4] Thus, even if a system satisfies extended detailed balance, it can in principle have a complex spectrum, as long as it breaks ordinary detailed balance. This has consequences for the relaxation behaviour, as we will encounter in Chapter 2.

[3] A matrix A is similar to B if $A = P^{-1}BP$ for some P

[4] This question in posed as an exercise in [6, V.6.15]

1.2.6 Activity, dissipation, and entropy

In addition to X being ergodic, suppose that if $W(x,y) > 0$, then also $W(y,x) > 0$. Then we can define [72] **activity parameters**

$$a(y,x) := \sqrt{W(y,x)W(x,y)} \tag{1.73}$$

and **dissipation parameters**

$$q(y,x) := \ln \frac{W(y,x)}{W(x,y)} \tag{1.74}$$

such that

$$W(y,x) = a(y,x)e^{q(y,x)/2}. \tag{1.75}$$

Activity parameters are by definition symmetric, $a(y,x) = a(x,y)$, while dissipation parameters are anti-symmetric, $q(y,x) = -q(y,x)$. If detailed balance pertains

$$q(x,y) = V(x) - V(y), \tag{1.76}$$

with $V(x) = -\ln P^*(x)$. Conversely, whenever the dissipation parameters are all on the form (1.76) for some potential V, detailed balance follows. It is easy to see that $P^*(x)$ is then independent of the activity parameters, and $P^*(x) \propto e^{-V(x)}$. If $X(t)$ represents the the state of a thermal equilibrium system interacting with an environment, then $V(x) = \beta H(x)$, with β the inverse temperature and H an energy function, and we recover the Boltzmann distribution. The dissipation parameter is then the change in energy of the system in one jump divided by temperature, that is the *heat* (taken with sign) ejected into the environment.

In contrast to an equilibrium steady state, a NESS in general *does* depend on activity parameters. One can easily generalize the above decomposition to when a generalized detailed balance pertains.

We can further define the **Shannon-Gibbs entropy** of the process as

$$S(t) := -\sum_x P(x,t) \ln P(x,t) = \langle -\ln P(\cdot,t) \rangle_t \,, \tag{1.77}$$

which is known to be a Lyapunov function for the ergodic process and decreases to

a stationary value [14]. If $X(t)$ represents the state of a thermal system interacting with an environment, we are in equilibrium statistical used to interpret $S(t)$ as the thermodynamic entropy of the *system*. Taking the time derivative,

$$\frac{\mathrm{d}S}{\mathrm{d}t} = \sigma - \phi, \tag{1.78}$$

where the **entropy production rate** σ and **entropy flux** ϕ (to the environment) are defined [73, 74]

$$\sigma(t) := \frac{1}{2}\sum_{x,y} J(y,x;t) \ln \frac{W(y,x)P(x,t)}{W(x,y)P(y,t)}, \tag{1.79}$$

$$\phi(t) := \frac{1}{2}\sum_{x,y} J(y,x;t) q(y,x), \tag{1.80}$$

where J is the non-stationary probability current (1.35). In steady state the change in system entropy is always zero, and entropy production and flux balance. For an equilibrium process, both σ and ϕ vanish identically in the steady state.

Thus, from the initial definition of the jump process in terms of rates, springs a host of derived quantities: time-asymmetric currents, dissipation parameters, the entropy; time-symmetric traffics, activity parameters, and escape rates. There are further generalizations to these quantities at the level of trajectories. Framing the theory in these terms has promoted a fundamental, yet counter-intuitive insight into nonequilibrium physics: the steady state and weak fluctuations (*i.e.* linear response) are completely determined by entropic quantities; nonequilibrium steady-states and fluctuations (both linear and higher order), on the other hand, can depend strongly on what has been termed 'frenetic' quantities, the time-symmetric counterpart to entropy. Because frenetic effects tend to be kinetic and microscopic in origin, this insight has cast doubt on the validity of macroscopic approaches to a far-from-nonequilibrium thermodynamics, which are built around maximum-entropy principles [72, 75, 76].

1.3 Diffusion processes

We give here a brief review of diffusion process in $\mathbb{R}^d$ based on taking the limit of zero lattice spacing for a planar random walk described by a master equation. Not only is this an intuitive way to understand the construction of diffusion processes,

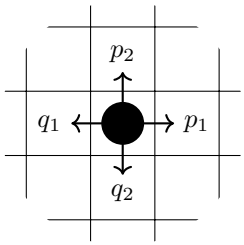

Figure 1.4 *Anisotropic random walk on the hypercube (illustrated in 2D)*

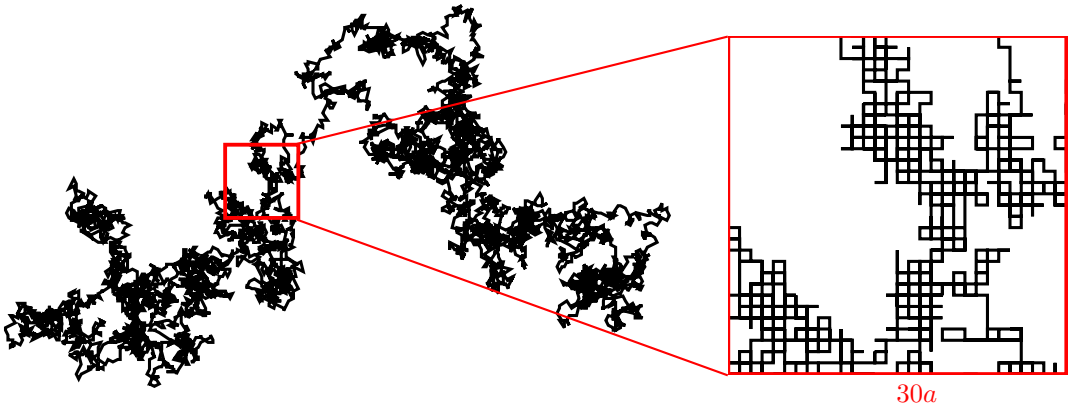

Figure 1.5 *Illustration of how a Brownian trajectory appears as the limit of small lattice spacing for random walk trajectory.*

but it is in itself a useful tool that we will employ in deriving result new results for diffusion processes in later chapters.

1.3.1 The diffusive limit

We consider a Markov jump process $\mathbf{N}(t)$ on a hyper-cubic lattice $\mathscr{L} = \mathbb{Z}^d$, to be thought of as the position of a random walker. As depicted in Figure 1.4, the walker only moves one step $\hat{\boldsymbol{\tau}}_i$ in direction i at a time, according to the rates

$$W(\boldsymbol{n} + \hat{\boldsymbol{\tau}}_i, \boldsymbol{n}) = p_i(\boldsymbol{n}), \tag{1.81a}$$

$$W(\boldsymbol{n} - \hat{\boldsymbol{\tau}}_i, \boldsymbol{n}) = q_i(\boldsymbol{n}). \tag{1.81b}$$

The master equation is thus

$$\begin{aligned}\partial_t P(\boldsymbol{n}, t) = \sum_i \Big\{ &\big[p_i(\boldsymbol{n} - \hat{\boldsymbol{\tau}}_i) P(\boldsymbol{n} - \hat{\boldsymbol{\tau}}_i, t) - p_i(\boldsymbol{n}) P(\boldsymbol{n}, t)\big] \\ &+ \big[q_i(\boldsymbol{n} + \hat{\boldsymbol{\tau}}_i) P(\boldsymbol{n} + \hat{\boldsymbol{\tau}}_i, t) - p_i(\boldsymbol{n}) P(\boldsymbol{n}, t)\big] \Big\}.\end{aligned} \tag{1.82}$$

We now embed the lattice into continuous space via a lattice constant a, $\mathscr{L} \to \mathscr{L}_a \subset \mathbb{R}^d$, so that $\boldsymbol{n} \in \mathscr{L}$ corresponds to $\boldsymbol{x} = a\boldsymbol{n} \in \mathscr{L}_a$. Clearly, as we spatially 'zoom out' on the system by letting a approach 0, the lattice becomes progressively denser in continuous space (Figure 1.5). But we must also view the system over longer time scales, in order to see a discernable displacement over a length scale that is well approximated as continuous. Thus we scale the time parameter from $t \to t_a$ depending on a in some yet-to-be specified way. The hopping rates, whose units are in inverse time, then become a-dependent, and we posit a general series expansion in a for them that also takes into account the lattice's embedding in continuous space:

$$p_i \to p_i^{(a)}(\boldsymbol{n}) = \sum_k a^{-k} \alpha_i^{(k)}(\boldsymbol{x}), \tag{1.83a}$$

$$q_i \to q_i^{(a)}(\boldsymbol{n}) = \sum_k a^{-k} \beta_i^{(k)}(\boldsymbol{x}). \tag{1.83b}$$

We define a probability density ρ_a which for a small enough we shall treat as a continuous function of $\boldsymbol{x}$,

$$\rho_a(\boldsymbol{x}, t_a) := P(\boldsymbol{x}/a, t_a)/a. \tag{1.84}$$

With the above definitions, the density's time evolution, expanded in a, is given by

$$\partial_{t_a} \rho_a = \sum_i \Big\{ -\partial_{x_i} \sum_k a^{1-k} (\alpha_i^{(k)} - \beta_i^{(k)}) + \frac{1}{2} \partial_{x_i}^2 \sum_k a^{2-k} (\alpha_i^{(k)} + \beta_i^{(k)}) \Big\} \rho_a, \tag{1.85}$$

plus higher order terms in a. In order for there to be a sensible limit as $a \to 0$, the sum over k must run no higher than to 2, and we must have $\alpha_i^{(2)} = \beta_i^{(2)}$. Then if we define

$$\alpha_i^{(2)} = \beta_i^{(2)} = D_i \tag{1.86}$$

$$\alpha_i^{(1)} - \beta_i^{(1)} = F_i, \tag{1.87}$$

we obtain the **Fokker-Planck equation** (FPE) for the density of the diffusion process $\mathbf{X}(t)$:

$$\partial_t \rho(\boldsymbol{x}, t) = -\nabla \cdot \boldsymbol{F}(\boldsymbol{x}) \rho(\boldsymbol{x}, t) + \nabla \cdot (\nabla \cdot \mathsf{D}(\boldsymbol{x}) \rho(\boldsymbol{x})). \tag{1.88}$$

with drift vector $\boldsymbol{F}$ and diffusion matrix D. (For t and ρ we drop the previous subscript a rather than put 0.) Because we used a hyper-cubic lattice and only allowed jumps in the orthogonal directions, D is diagonal, but in general it only needs to be symmetric and positive-(semi)definite.

1.3.2 Representation as stochastic differential equation

While the probability density $\rho(\boldsymbol{x}, t)$ evolves smoothly under the FPE, the trajectories that correspond to this process are continuous but nowhere differentiable (as one intuits from Figure 1.5). As any textbook on the subject of stochastic processes will show (*e.g.* [14]), diffusions can be constructed through an Euler scheme,

$$\mathbf{X}(t + \Delta t) = \mathbf{X}(t) + \boldsymbol{F}(\mathbf{X}(t))\Delta t + \mathsf{B}(\mathbf{X}(t))\Delta\mathbf{W}(t), \tag{1.89}$$

whose statistics matches the FPE (1.88) as $\Delta t \to 0$. In the above, B is any matrix such that $\mathsf{D} = (1/2)\mathsf{B}\mathsf{B}^\top$, and $\mathbf{W}(t)$ is the Wiener process whose increments $\Delta\mathbf{W}(t)$ have components $\Delta W_i(t) = \sqrt{\Delta t}\mathcal{N}_i(t)$ where the $\mathcal{N}_i$ are drawn independently from a normal distribution with zero mean and unit variance. Because $\Delta\mathbf{W}(t)/\Delta t = O\left(\Delta t^{-1/2}\right)$, the trajectories or not differentiable. The limit of the above Euler scheme can however be represented as a **stochastic differential equation** (SDE) written

$$\mathrm{d}\mathbf{X}(t) = \boldsymbol{F}(\mathbf{X}(t))\,\mathrm{d}t + \mathsf{B}(\mathbf{X}(t))\,\mathrm{d}\mathbf{W}(t), \tag{1.90}$$

which is easiest thought of as a short-hand for the above Euler scheme, but can be given a rigorous mathematical definition and a 'stochastic calculus'. This SDE is written in the **Ito convention**, meaning that to generate $\mathbf{X}(t + \Delta t)$ we evaluate $\boldsymbol{F}$ and B at the previous step $\mathbf{X}(t)$. If we instead choose the midpoint rule,

$$\mathbf{X}(t+\Delta t) = \mathbf{X}(t)+\boldsymbol{F}\left(\frac{\mathbf{X}(t+\Delta t)+\mathbf{X}(t)}{2}\right)\Delta t+\mathsf{B}\left(\frac{\mathbf{X}(t+\Delta t)+\mathbf{X}(t)}{2}\right)\Delta\mathbf{W}(t), \tag{1.91}$$

known as the **Stratonovich convention**, the discretization scheme corresponds to an FPE

$$\partial_t\rho = -\nabla\cdot\boldsymbol{F}\rho + \nabla\cdot\mathsf{D}\nabla\rho = -\nabla\cdot\boldsymbol{J}, \tag{1.92}$$

with a probability current following the simple expression

$$\boldsymbol{J} = \boldsymbol{F}\rho - \mathsf{D}\nabla\rho. \tag{1.93}$$

When the noise is not multiplicative, meaning that B is a constant matrix, the Ito and Stratonovich conventions are equivalent. In this thesis we will for the most part not deal with multiplicative noise. When we do, we will avoid ambiguity by defining the 'drift' as the $\boldsymbol{F}$ that appears in (1.92).

1.3.3 Generators of diffusion

It is useful to express diffusion processes $\mathbf{X}(t)$ in terms of their forward and backward generators, as we did for jump processes. Matrices (of infinite size) then graduate to differential operators. The FPE can from this point of view be written as

$$\partial_t \rho(\boldsymbol{x}, t) = (\mathcal{L}^\dagger \rho)(\boldsymbol{x}, t), \tag{1.94}$$

where

$$\mathcal{L}^\dagger := -\boldsymbol{F} \cdot \nabla + \nabla \cdot \mathsf{D}\nabla \tag{1.95}$$

is the forward generator or **Fokker-Planck operator**, analogous to $\mathbb{L}^\top = \mathbb{W}$ for a jump process. The inner product analogous to (1.42) is

$$\langle \rho, \phi \rangle := \int_{\mathbb{R}^d} \mathrm{d}\boldsymbol{x}\, \rho(\boldsymbol{x})\phi(\boldsymbol{x}). \tag{1.96}$$

With respect to this inner product, $\mathcal{L}^\dagger$ is adjoint to the backward generator $\mathcal{L}$,

$$\left\langle \mathcal{L}^\dagger \rho, \phi \right\rangle = \langle \rho, \mathcal{L}\phi \rangle\,, \tag{1.97}$$

for any ρ, and ϕ in the respective domains of these operators. Specifically, the paired domains are such that the inner product remains well defined and that ρ and ϕ vanish together with their gradients at infinity. Through integration by parts of the left-hand side of (1.97) using (1.95), one finds

$$\mathcal{L} = \boldsymbol{F} \cdot \nabla + \nabla \cdot \mathsf{D}\nabla. \tag{1.98}$$

The proper definition of the backward generator is as in (1.40), which one shows is equivalent to (1.98).

Reversibility for a diffusion process is defined just as for a jump process. Following (1.57) we find the backward generator of the reversed process to be

$$\hat{\mathcal{L}} = \rho^{*-1}\mathcal{L}\rho^* = \mathcal{L} - \frac{2\boldsymbol{J}^*}{\rho^*} \cdot \nabla, \tag{1.99}$$

where ρ^* is the stationary distribution of the process (assumed to exist and be unique under ergodicity) and $\boldsymbol{J}^*$ the stationary probability current. Reversibility requires $\hat{\mathcal{L}} = \mathcal{L}$, which holds if and only if $\boldsymbol{J}^*(\boldsymbol{x}) \equiv \boldsymbol{0}$. It follows in this case of detailed balance that

$$\rho^*(\boldsymbol{x}) = \frac{1}{Z} e^{-\Phi(\boldsymbol{x})}, \tag{1.100}$$

where

$$\nabla\Phi(\boldsymbol{x}) = -\mathsf{D}^{-1}(\boldsymbol{x})\boldsymbol{F}(\boldsymbol{x}). \tag{1.101}$$

Conversely, if for a given $\boldsymbol{F}$ and D the potential Φ exists, then detailed balance pertains. We will have more to say about the existence of potentials in Section 3.3.2. The ideas of generalized reversibility for jump processes in Section 1.2.5 can be treated similarly for diffusions.

We have here introduced diffusions in unbounded domains. In Section 6.1 we discuss the presence of physical boundaries and how to derive corresponding boundary conditions on the forward and backward generators.

1.4 Summary of main concepts

Time-homogeneous ergodic Markov processes are an appropriate mathematical structure for many noisy nonequilibrium systems. Firstly, they allow processes to be characterized by an initial distribution, and an infinitesimal generator. They contain an inherent 'arrow of time' with regards to statistical uncertainty growing over time, such that initial conditions can relax to steady states. However, whether irreversibility pertains in the steady state is separate to the question of relaxation, and serves to define equilibrium *vs.* nonequilibrium conditions in a model-neutral way.

The setting of continuous time and discrete state space $\mathcal{X}$, leads to jump processes. Their probability $P(x,t)$ evolves in time by the master equation (1.34), involving the forward generator $\mathbb{W}$, defined in terms of the probabilities $W(y,x)\,\mathrm{d}t$ of transitioning from x to y in an infinitesimal time interval $\mathrm{d}t$.

For a jump process, the conditions for ergodicity, *i.e.* relaxation to a unique steady state, are dictated by the Perron-Frobenius theorem. A nonequilibrium steady state by definition is irreversible, which for a jump process means it violates the detailed balance condition (1.52). Generalized forms of reversibility, with respect to a conjugation of variables such as momentum reversal, amount to satisfying conditions (1.64), (1.66), and (1.67). If either reversibility or generalized reversibility pertains, the steady state is of the Boltzmann type, but the latter, in contrast to the former, supports complex spectra of $\mathbb{W}$. Entropy production, dissipation, and other 'physical' quantities can be defined in a general way for jump processes.

The setting of continuous time and continuous trajectories in $\mathbb{R}^d$ leads to diffusion processes. These can be constructed from the diffusive limit applied to a jump process, or via stochastic differential equations. A diffusion process is defined by a drift vector $\boldsymbol{F}$, representing a deterministic force, and a diffusion matrix D, controlling the bias and strength of uncorrelated noise. The evolution of probability is governed by the Fokker-Planck equation (1.94) expressed using the forward generator $\mathcal{L}^\dagger$, which has assumed the Stratonovich convention for the drift. The backward generator $\mathcal{L}$ (1.98) is the dual to $\mathcal{L}^\dagger$ with respect to the inner product (1.97). This aspect of formalism will be relevant in Chapter 6 where we consider how to derive boundary conditions for diffusion processes.

Chapter 2

Exceptional points and singular relaxation times for run-and-tumble particles

2.1 Background

2.1.1 Run-and-tumble particles

The symmetric random walk is the simplest prototype for the motion of a colloidal particle in an environment at thermal equilibrium. By judiciously adding one or a few ingredients that break detailed balance, we discover prototypes for nonequilibrium phenomena. One such alteration is allowing correlations between the directions of subsequent steps of the walk, also known as **persistence**. In the simplest implementation of persistence, a random walker in one dimension is endowed with an 'orientation' $\sigma \in \{-1, +1\}$. It makes jumps of size $\Delta n = \sigma$ at a constant rate γ, and flips its orientation $\sigma \to -\sigma$ at another rate ω (Figure 2.1).

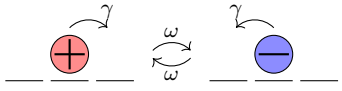

Figure 2.1 *Simple model of a persistent random walk: hopping occurs at rate γ in the direction indicated by the internal state which reverses with rate ω.*

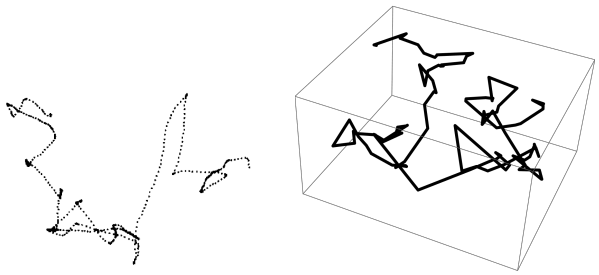

(a) *E. coli path* **(b)** *RTP realization in* $\mathbb{R}^3$

Figure 2.2 *(a) Adapted from [21]: 2D projection of an experimental swim trajectory of a freely suspended E. coli bacterium. (b) A realization of RTP motion in three continuous dimensions. The ith leg of the trajectory is a displacement vector* $\boldsymbol{x}_i = v\tau_i\hat{\boldsymbol{n}}_i$*, where* v *is a constant speed,* τ_i *an exponentially distributed time interval, and* $\hat{\boldsymbol{n}}_i$ *a vector distributed uniformly on the unit sphere.*

Thus the position and orientation taken together satisfy the Markov property, but the position alone does not. Such persistent random walks (PRWs) first appeared in the physics literature around 1920 to model a particle's movement in a turbulent flow (see historical references in [77, 78]). Later examples include the modelling of photon propagation in various media [79, 80], animal movements [81], polymer conformation [82], molecular cargo transport [83].

The most prominent application of the PRW is however in the context of active matter, where it is conventionally referred to as a **run-and-tumble particle** (RTP). The name is inspired by the way certain flagellated bacteria such as *E. coli* move, making 'runs' of a random length before 'tumbling', whereby a new direction is chosen at random (Figure 2.2). The microbiology of this motion came under close study in the 1970s [21] and eventually became a topic of physical modelling in the 90s [84]. Over recent years, the single RTP, either on- or off-lattice, has been studied under almost every condition found in the statistical-mechanics repertoire: confinement [85], potentials [86], thermal noise [87–89], random or inhomogeneous environments [20], resetting [90], and so on. The result often contrasts with that of a passive particle due to jamming, which makes RTPs accumulate around obstacles. Mutually interacting RTPs have therefore been studied as a minimal example of a generic cluster-formation phenomenon for active particles, dubbed motility-induced phase separation [25]: due to interactions, which may be purely repulsive, *e.g.* hardcore exclusion, active particles slow down in regions of higher particle density, which further increases the density and establishes a feedback loop resulting in large clusters. Interacting

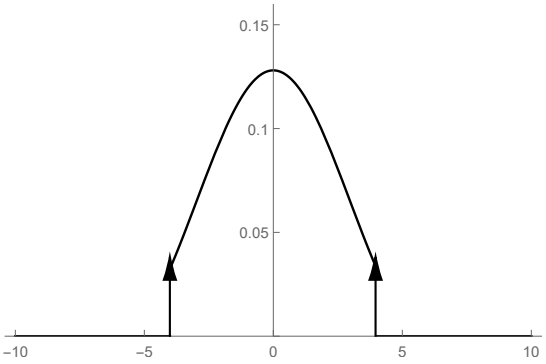

Figure 2.3 *Solution to the telegrapher's equation at $t = 2$ for parameters $v = 1$ and $\omega = 1.5$ with an initial condition localized at $x = 0$ and split evenly between the $+$ and $-$ directions. The arrows represent delta functions that move outward at the speed v coming from realizations that never reverse direction of propagation up to time t. In between these a deformed Gaussian distribution is found coming from realizations that reverse direction many times.*

RTPs have been treated at the level of fluctuating hydrodynamics [20, 24, 91, 92], as well as in on-lattice simulations [93]. Exact results for a microscopic model of interacting volume-excluding RTPs are limited to the steady-state for two particles in one periodic dimension [39, 94].

In this chapter we will consider the complete time-dependent solution to the lattice model of RTPs for a single particle or for two particles interacting through hardcore exclusion [1]. Before we present the motivations and main conclusions of this work, let us dwell on a fundamental characteristic of the RTP: it interpolates between diffusive and ballistic motion.

2.1.2 Interpolating diffusive and ballistic motion

The RTP interpolates between diffusive and ballistic motion. This is perhaps most easily appreciated from the continuum counterpart to the lattice model in Figure 2.1. The master equation of the lattice model is

$$\partial_t P_+(n,t) = \gamma[P_+(n-1,t) - P_+(n,t)] + \omega[P_-(n,t) - P_+(n,t)], \tag{2.1a}$$

$$\partial_t P_-(n,t) = \gamma[P_-(n+1,t) - P_-(n,t)] + \omega[P_+(n,t) - P_-(n,t)]. \tag{2.1b}$$

Applying the continuum limit with lattice spacing $a \to 0$ as in Section 1.3.1, with $n/a \to x$, $P_\sigma(n)/a \to \rho_\sigma(x)$, $\gamma/a \to v$, we find

$$\partial_t \rho_+(x,t) = -v\partial_x \rho_+(x,t) + \omega[\rho_-(x,t) - \rho_+(x,t)], \tag{2.2a}$$

$$\partial_t \rho_-(x,t) = +v\partial_x \rho_-(x,t) + \omega[\rho_+(x,t) - \rho_-(x,t)]. \tag{2.2b}$$

It is useful to consider the sum of and difference between these two equations, which yields equations in the total density $\rho(x,t) = \rho_+(x,t) + \rho_-(x,t)$ and difference $q(x,t) = \rho_+(x,t) - \rho_-(x,t)$. By considering $\partial_t^2 \rho$ one finds by straightforward substitutions that ρ satisfies the **telegrapher's equation** [95]

$$\frac{1}{2\omega}\partial_t^2 \rho(x,t) + \partial_t \rho(x,t) = \frac{v^2}{2\omega}\partial_x^2 \rho(x,t). \tag{2.3}$$

The telegrapher's equation interpolates the diffusion equation and the wave equation: we choose a time scale τ; if $\omega \gg \tau^{-1}$ we can neglect the second-order time derivative in the left-hand side and the equation reduces to the diffusion equation; in the other limit, $\omega \ll \tau^{-1}$, the first-order time-derivative dominates and the equation reduces to the wave equation.

The telegrapher's equation on the infinite line with initial condition $\rho_\sigma(x,0) = \delta(x)/2$ can be be solved in the Laplace domain and then inverted (see [90] for the full expression). In Figure 2.3 the solution at an intermediate time is plotted, showing the combined effects of the ballistic propagation of the probability wave-fronts and the in-between diffusive regime. In particular, we can calculate the mean-squared displacement as [95]

$$\left\langle x^2(t) \right\rangle = \frac{1}{2}\left(\frac{v}{\omega}\right)^2 \left(2\omega t - 1 + e^{-2\omega t}\right), \tag{2.4}$$

from which we see that $\langle x(t)\rangle^2 \simeq (vt)^2$ (ballistic scaling) for $t \ll \omega^{-1}$ and $\langle x^2(t)\rangle \simeq 2Dt$ with $D = v^2/(2\omega)$ (diffusive scaling) for $t \gg \omega^{-1}$.

2.1.3 Persistence through a spectral lens

Let us return to the one-dimensional lattice model in Figure 2.1. In [20, 96] this model was extended to include N RTPs that interact via hardcore exclusion. It is then an 'active' generalization of the simple exclusion process. Paralleling how the single RTP interpolates between diffusive and ballistic motion, the RTP

exclusion process interpolates between the SSEP[1] as $\omega \to \infty$ and the TASEP as $\omega \to 0$ (assuming the particles are aligned at $t = 0$ as the initial orientations get frozen in). On a ring, the SSEP is an equilibrium model since it satisfies detailed balance, whereas the TASEP is a nonequilibrium model, and in a sense strongly so, since no single transition can be reversed in a single event. The RTP exclusion process is therefore of interest as a model whose 'degree' of nonequilibrium is tunable by a continuous parameter. Does its behaviour change smoothly with ω or is there a change in character at some critical, intermediate value?

As special cases of the ASEP, both the SSEP and TASEP are exactly solvable—what about the RTP exclusion process? It is not expected that it will satisfy the Yang-Baxter equations that guarantee the integrability of the former models [17]. Only the NESS for two RTPs has been previously obtained [39] and it reveals a structure reminiscent of the Bethe-ansatz that solves the ASEP but that is distinctly different in that it places an anomalous weight on the jammed particle configuration. It is therefore a worthwhile question to attempt a solution of the two-particle RTP exclusion process in the hope that it reveals a novel Bethe-generalizing pattern that may allow solution of the N-particle model. By solution, we mean a method of diagonalizing the finite-dimensional generator of the model, just as the Bethe-ansatz furnishes the eigenvalues and eigenvectors for the ASEP [10, 17]. However, rather than positing an ansatz for the solution, we must derive the solution *de novo*.

We furthermore expect a spectral decomposition to give a useful view onto the way the process depends on ω. From the fact that $\omega \to \infty$ represents an equilibrium model with a real spectrum, and $\omega \to 0$ a nonequilibrium model with a complex spectrum, there must logically be eigenvalue crossings occurring as ω is varied. Is there any significance attached to those values of ω where eigenvalues cross?

Next, we define explicitly the N-RTP exclusion process on the ring lattice, and analyse it with respect to generalized reversibility. We thereby gain a fundamental understanding of how interactions and persistence conspire to break time symmetry. We then obtain the exact solution to the single RTP problem as a reference case for the much more challenging two-particle problem, treated thereafter.

[1] See example (d) on p.24 for the definition.

2.2 N-particle lattice model

2.2.1 Master equation

We consider a one-dimensional lattice ring of L sites, on which N run-and-tumble particles live on distinct sites. Each RTP has the identical hopping rate γ and tumbling rate ω, and carries out its motion subject to hardcore exclusion: an attempt to hop onto an already occupied site is rejected.

A system configuration is denoted $(\boldsymbol{\sigma}, \boldsymbol{n})$, with a vector of particle orientations $\boldsymbol{\sigma} = (\sigma_1, \ldots, \sigma_N)$, $\sigma_i \in \{-1, +1\}$, and a vector of particle positions $\boldsymbol{n} = \sum_{i=1}^{N} n_i \hat{\boldsymbol{e}}_i = (n_1, \ldots, n_N)$. We denote the probability of a configuration at time t by $P_{\boldsymbol{\sigma}}(\boldsymbol{n}, t)$, leaving the initial condition implicit. To implement the periodicity of the ring, we allow $n_i \in \mathbb{Z}$ while imposing the condition

$$P_{\sigma_1 \ldots \sigma_N}(n_1, \ldots, n_N; t) = P_{\sigma_2 \ldots \sigma_N \sigma_1}(n_2, \ldots, n_N, n_1 + L; t). \tag{2.5}$$

We suppose an initial $\boldsymbol{n}'$ for which $1 \leq n'_1 < n'_2 < \ldots < n'_N \leq L$, and therefore periodicity implies that for $\boldsymbol{n}$ at later times $1 \leq n_1 < n_2 < \ldots < n_N \leq L$ also. However, n_1 does not refer to the position of the same physical particle across time. The first argument corresponds to the particle closest to the right (*i.e.* clockwise) of the reference site 0 implicit in the initial conditions. If given a complete trajectory of the system it is possible to track the individuality of the particles in time, however.

We introduce some notation to express the master equation compactly. Let θ_i be an operator acting on the ith particle by flipping its orientation,

$$\theta_i(\sigma_1, \ldots, \sigma_i, \ldots, \sigma_N) = (\sigma_1, \ldots, -\sigma_i, \ldots, \sigma_N); \tag{2.6}$$

define $I_L(n, m) = \{1 \text{ if } n \not\equiv m \bmod L;\ \text{else } 0\}$ as the indicator function for n and m being distinct lattice sites; and allow the indexing convention $n_{-i} = n_{L-i}$. Then

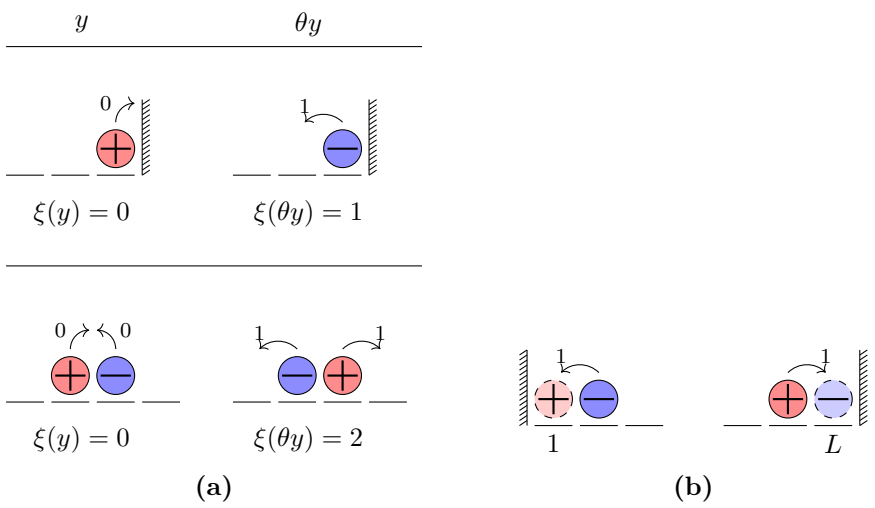

Figure 2.4 *(a) RTPs interacting through hardcore exclusion with a wall (above) or each other (below) lack generalized reversibility because the escape rate ξ is not invariant under orientation reversal. (b) An* RTP *with a modified reflection rule that prevents jamming at the wall does satisfy generalized reversibility.*

$$\partial_t P_{\boldsymbol{\sigma}}(\boldsymbol{n},t) = \gamma \sum_{i=1}^{N} \big[P_{\boldsymbol{\sigma}}(\boldsymbol{n}-\sigma_i \boldsymbol{e}_i,t) I_L(n_i-\sigma_i, n_{i-\sigma_i}) - P_{\boldsymbol{\sigma}}(\boldsymbol{n},t) I_L(n_i+\sigma_i, n_{i+\sigma_i})\big] + \omega \sum_{i=1}^{N} [P_{\theta_i \boldsymbol{\sigma}}(\boldsymbol{n}) - P_{\boldsymbol{\sigma}}(\boldsymbol{n},t)]. \quad (2.7)$$

For convenience we choose units of time such that $\gamma = 1$.

2.2.2 Interactions break generalized reversibility

Clearly, detailed balance is broken in the RTP exclusion process because a particle in the + state may jump $n \to n+1$ (if not obstructed) but never $n+1 \to n$ unless it first reverses its orientation: if y' and y differ by the allowed jump of one particle, then $W(y',y) > 0$ implies $W(y,y') = 0$. Considering just a single RTP on a ring, it does however satisfy a generalized detailed balance with respect to the conjugation of the state $y = (n,\sigma)$ to $\theta y = (n,-\sigma)$. We may in this case think of the orientation as a momentum. This analogy breaks down if the particle is allowed to interact through hardcore exclusion with an obstacle, which could be a hard wall or another particle, because the 'momentum' is not reflected, and instead the particle becomes jammed. The orientation remains an intrinsic property of the particle which affects the probability of leaving a blocked site.

To show that a generalized reversibility under $\theta = \sum_i \theta_i$ does not pertain in the case of interacting RTPs, it is sufficient to disconfirm one of (1.64), (1.66), and (1.67). That (1.67) on the escape rates is not satisfied can be ascertained without the need to solve for the stationary distribution. Comparing $\xi(y)$ and $\xi(\theta y)$ for any configuration y one can deduce that they differ by twice the number of unobstructed nearest-neighbour pairs of particles. It is sufficient however to understand the inequivalence for just two particles, or for a particle and a hard wall, both illustrated in Figure 2.4a.

The above example demonstrates that it is not so much the breaking of detailed balance through self-propulsion that is the critical aspect of active matter, but rather the further lack of generalized reversibility due to interactions. To further argue this point, consider a modified RTP model with reflecting walls at sites 1 and L (Figure 2.4b). Jumping $L-1 \to L$ immediately flips the particle to $-$, and jumping $2 \to 1$ flips it to $+$. Furthermore, the particle cannot flip back until it has left the wall, so that $(-,1)$, $(+,L)$ are no longer accessible configurations. In this case the internal state is more like a momentum that flips due to random collisions in the interior sites, and by elastic collision at the boundary. To implement this scenario, we complement (2.1) with boundary conditions

$$\partial_t P_+(1,t) = P_-(2,t) - P_+(1,t), \tag{2.8a}$$

$$\partial_t P_-(n,t) = P_+(L-1,t) - P_-(L,t). \tag{2.8b}$$

The involution θ now acts trivially on the boundary states as $\theta(+,1) = (+,1)$, $\theta(-,L) = (-,L)$ but flips the orientation in the interior. We see that the flat stationary density solves this master equation. The flat distribution also trivially satisfies invariance under θ, and trivially furnishes generalized detailed balance both in the bulk and at the boundaries. In the bulk the escape rate is $1+\omega$, and on the boundary 1, but in either case it is invariant under θ. Thus generalized reversibility pertains.

2.3 Solution for a single particle

We consider now the case $N = 1$. We can draw on the analysis of the continuum model in Section 2.1.2 to intuit the the behaviour of the lattice model, but the periodicity makes a considerable difference in that there exists a steady state, and a relaxation towards it, and the left and right wavefronts will eventually

meet halfway round the ring.

The master equation (2.7) reduces to

$$\partial_t P_+(n,t) = P_+(n-1,t) - P_+(n,t) + \omega[P_-(n,t) - P_+(n,t)], \tag{2.9a}$$
$$\partial_t P_-(n,t) = P_-(n+1,t) - P_-(n,t) + \omega[P_+(n,t) - P_-(n,t)], \tag{2.9b}$$

with periodicity

$$P_\sigma(n+L,t) = P_\sigma(n,t). \tag{2.10}$$

Our goal is to solve the master equation through a spectral decomposition of the forward generator $\mathbb{W}$.

For convenience we will use the Dirac's bra-ket notation commonly imported into statistical physics from quantum mechanics. We partition the state space $\mathcal{X} = \mathcal{S} \otimes \mathcal{N}$, where $\mathcal{S}$ is the 'spin' or orientation degree of freedom, and $\mathcal{N}$ is physical space, the lattice ring. A natural basis vector for $\mathcal{X}$ is then

$$|\sigma, n\rangle = |\sigma\rangle \otimes |n\rangle \tag{2.11}$$

where $|\sigma\rangle$ is a basis vector of $\mathcal{S}$ and $|n\rangle$ of $\mathcal{N}$. Periodicity suggests the convention $|n+L\rangle = |n\rangle$. The forward generator can then be expressed

$$\begin{aligned}\mathbb{W} = \sum_{n=1}^{L} \Big\{ &|+,n+1\rangle\langle +,n| + |-,n-1\rangle\langle +,n| \\ &+ \omega\Big[|-,n\rangle\langle +,n| + |+,n\rangle\langle -,n|\Big] - (1+\omega)|n\rangle\langle n|\Big\}.\end{aligned} \tag{2.12}$$

If we define

$$|P(t)\rangle := \sum_{n=1}^{L} \sum_{\sigma=\pm} P_\sigma(n,t)|\sigma,n\rangle, \tag{2.13}$$

then the master equation reads

$$\partial_t |P(t)\rangle = \mathbb{W}|P(t)\rangle. \tag{2.14}$$

An alternative basis for $\mathcal{N}$ is the Fourier basis, whose vectors we denote by $|k)$.

It projects onto the spatial basis as

$$(k|n\rangle = \frac{1}{\sqrt{L}} z_k^n, \quad z_k = e^{2\pi i k/L}. \tag{2.15}$$

We have defined 'bras' $(k|$ as complex transposes of 'kets' $|k)$ so that the orthogonality of the Fourier basis holds as $(k|l) = \delta_{k,l}$. We can then express $\mathbb{W}$ in the Fourier basis by the following projection that generates a linear operator on $\mathcal{S}$:

$$\mathbb{S}^{(k,l)} := (k|\mathbb{W}|\ell) \tag{2.16}$$

$$= \big\{ w(k)|+\rangle\langle +| + \omega|+\rangle\langle -| + \omega|-\rangle\langle +| + w(-k)|-\rangle\langle -| \big\}\delta_{k,l} \tag{2.17}$$

where

$$w(k) = z_k - (1+\omega). \tag{2.18}$$

In the Fourier basis, $\mathbb{W}$ is apparently block-diagonal, with each non-zero block $\mathbb{S}^{(k,l)}$ simply a matrix

$$S(k) := \begin{pmatrix} w(k) & \omega \\ \omega & w(-k) \end{pmatrix} \tag{2.19}$$

if we employ the standard representation

$$|+\rangle = \begin{pmatrix} 1 \\ 0 \end{pmatrix}, \quad |-\rangle = \begin{pmatrix} 0 \\ 1 \end{pmatrix}. \tag{2.20}$$

The purpose of this seemingly overcomplicated way of performing a Fourier transform, is to make it clear that the eigenvalues of $\mathbb{W}$ are precisely the eigenvalues of $S(k)$ collected for $k = 1, 2, \ldots, L$. This is now readily appreciated because we have taken $\mathbb{W}$ first as an abstract linear operator on a $2L$-dimensional space, and then found a block-diagonalizing basis. It follows also that $\mathbb{W}$ is diagonalizable if an only if each $S(k)$ is. We now perform the diagonalization of $S(k)$.

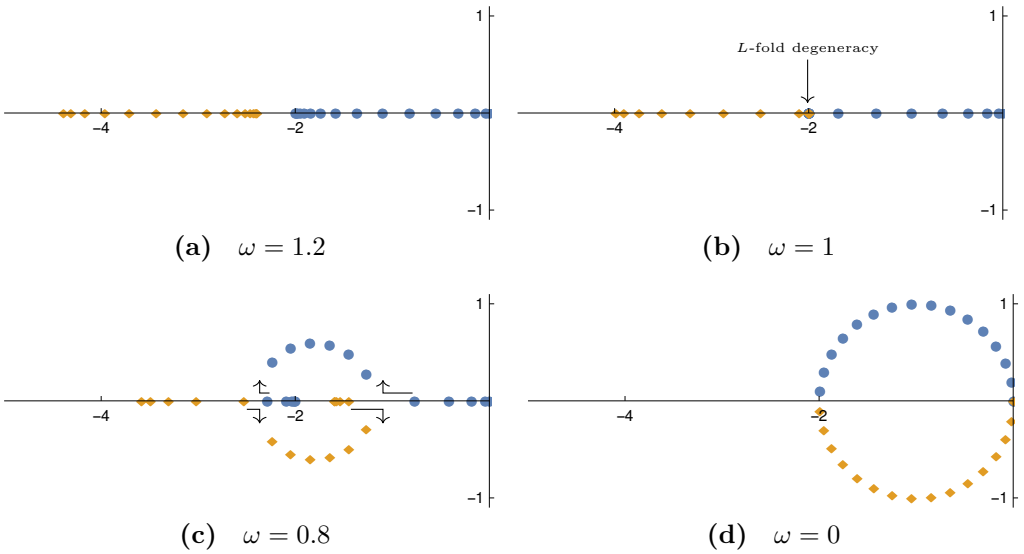

(a) $\omega = 1.2$ **(b)** $\omega = 1$

(c) $\omega = 0.8$ **(d)** $\omega = 0$

Figure 2.5 *One-particle spectrum* (2.21) *in the complex plane for* $L = 31$. *Blue circles: right band* ($s = +1$)*; yellow diamonds: left band* ($s = -1$). *(a) For* $\omega > 1$ *the eigenvalues come in two separate real bands. (b) At* $\omega = 1$ *there is an* L*-fold degeneracy at the eigenvalue* -2. *(c) As* ω *is further decreased, pairs of real eigenvalues cross and separate as complex conjugate pairs. The arrows indicate how the crossing is approached. (d) At* $\omega = 0$ *the spectrum is a unit circle shifted left by* -1.

2.3.1 Spectrum: band structure and eigenvalue crossings

The eigenvalues of $S(k)$ (2.19) are found to be

$$\lambda^{(s)}(k) = -2\sin^2\left(\tfrac{\pi k}{L}\right) - \omega + s\sqrt{\omega^2 - \sin^2\left(\tfrac{2\pi k}{L}\right)}, \tag{2.21}$$

where $s = +1$ indicates the 'right band' and $s = -1$ the 'left band'. By the symmetry $\lambda(k) = \lambda(L-k)$ the spectrum is always doubly degenerate (except possibly for $k = L/2$). This is clearly due to the spatial inversion symmetry of the problem.

We consider now the qualitative changes to the spectrum as ω is varied, as demonstrated in Figure 2.5. For $\omega > 1$, the spectrum is necessarily real, and for large ω

$$\lambda^{(+)}(k) = -2\sin^2\left(\frac{\pi k}{L}\right) + O\left(1/\omega\right), \tag{2.22a}$$

$$\lambda^{(-)}(k) = -2\sin^2\left(\frac{\pi k}{L}\right) - 2\omega + O\left(1/\omega\right). \tag{2.22b}$$

In the symmetric walk limit, $\omega \to \infty$, the left band ($s = -1$) diverges, implying the disappearance of these modes. The remaining eigenvalues are those of the symmetric walker with jump rate $1/2$: the initial jump rate $\gamma = 1$ in the direction of the particle's orientation is now split equally between left and right jumps.

At exactly $\omega = 1$, the eigenvalue -2 becomes L-degenerate (Figure 2.5b) as

$$\lambda^{(s)}(k) = -2 + \cos\left(\frac{2\pi k}{L}\right) + s\left|\cos\left(\frac{2\pi k}{L}\right)\right|. \tag{2.23}$$

This degeneracy comprises the least negative half of the left band ('upper left band') and most negative half of the right band ('lower right band'). Whereas the relaxation times of all modes are in general dependent on the system size L, at $\omega = 1$ half of them are not. The degeneracy allows what we shall call a **macroscopic eigenvalue crossing** of the upper left and lower right bands, because $O(L)$ eigenvalues participate.

For $\omega \leq 1$, at the special values

$$\omega_k := |\sin(2\pi k/L)|, \tag{2.24}$$

the eigenvalue $\lambda^{(-)}(k)$ from the lower (upper) left band and the eigenvalue $\lambda^{(+)}(k)$ of the lower (upper) right band coalesce. For smaller ω, they leave the real line as a complex conjugate pair (Figure 2.5c). Precisely at the crossing, $S(k)$, and hence also $\mathbb{W}$, becomes non-diagonalizable. The consequences for a spectral decomposition of $\mathbb{W}$ in this case are described in Section 2.3.2.

As ω approaches zero (Figure 2.5d),

$$\lambda^{(s)}(k) = -2\sin^2\left(\frac{\pi k}{L}\right) + is\left|\sin\left(\frac{2\pi k}{L}\right)\right|. \tag{2.25}$$

The spectrum is identical to that of the totally asymmetric walker, defined by either $\partial_t P(n) = P(n-1) - P(n)$ or $\partial_t P(n) = P(n+1) - P(n)$, but four-fold degenerate as the two equivalent orientation sectors decouple.

2.3.2 Eigenvectors and the matrix exponential

With the spectrum of $\mathbb{W}$ determined, we turn our attention to finding bases for its eigenspaces. If $|u_s(k)\rangle$ is an eigenvector of $S(k)$ corresponding to the eigenvalue

$\lambda_s(k)$, then

$$|v_s(k)\rangle \propto |u_s(k)\rangle \otimes |k) \tag{2.26}$$

is an eigenvector of $\mathbb{W}$. We have that

$$|u_s(k)\rangle \propto \begin{pmatrix} \omega \\ w(k) - \lambda^{(s)}(k) \end{pmatrix} \tag{2.27}$$

and the two vectors for $s = \pm 1$ for any k are linearly independent *if* ω *is not tuned to* n *special value* (2.24). Assuming no such tuning, $\mathbb{W}$ is diagonalizable, and its matrix exponential as appears in the formal solution (1.48) of the master equation is

$$\exp[\mathbb{W}t] = \sum_{k=1}^{L} \sum_{s=\pm 1} e^{\lambda_s(k)t} |u_s(k)\rangle\langle u_s(k)| \otimes |k)(k| \tag{2.28}$$

Finally,

$$P_\sigma(n,t) = \langle \sigma, n| \exp[\mathbb{W}t]|P(0)\rangle, \tag{2.29}$$

where the only obstacle to a compact result is the need to invert a Fourier transform.

If we do let $\omega = \omega_k$ for some k, then the eigenspace of $S(k)$ has dimension one. Since $\mathbb{W}$ is block-diagonal, its exponential is the block-diagonal of the exponentiated blocks: thus we consider how to calculate $\exp[S(k)]$.

Define $N(k) = S(k) - \lambda(k)\mathbb{1}$. A matrix constructed in this way is in general nilpotent, *i.e.* taken to some power becomes the zero matrix. The smallest such power will be less than or equal to the algebraic multiplicity of that eigenvalue (in fact equal to the 'index' of the eigenvalue, the dimension of the largest Jordan block), which presently is two. We can therefore conclude immediately that $N^2(k) = 0$, which can also be verified from the explicit expression

$$N(k) = \begin{pmatrix} -i\sin\left(\frac{2\pi k}{L}\right) & \omega_k \\ \omega_k & i\sin\left(\frac{2\pi k}{L}\right) \end{pmatrix}. \tag{2.30}$$

The matrix exponential then evaluates to

$$\exp[S(k)t] = \exp[\lambda(k)tI + N(k)t] = e^{\lambda(k)t}(I + N(k)t). \tag{2.31}$$

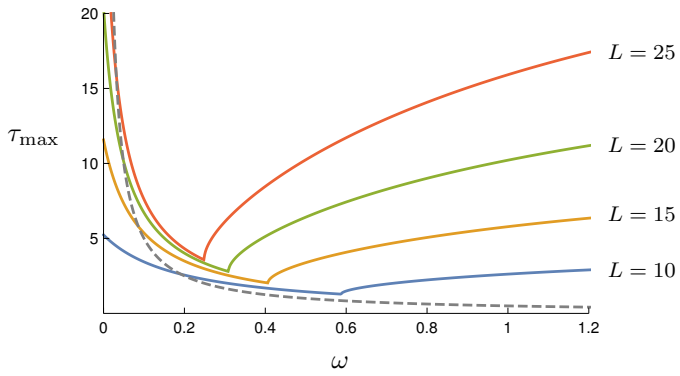

Figure 2.6 *One-particle relaxation times. Coloured lines: longest relaxation time involved in spatial dynamics. The global cusp-shaped minima occur at $\omega = \omega^*(L)$. Dashed line: the tumble mode with relaxation $1/(2\omega)$.*

That is, the dynamical modes which project onto this subspace have exponential decay, modulated by a linear time dependence.

2.3.3 Dynamical exponent and singularity in relaxation time

From (2.21) we determine the spectral gap, *i.e.*, the least negative, non-zero eigenvalue, which sets the longest time-scale $\tau_{\max}$ of relaxation towards the steady state. From this exact result we are particularly interested in the **dynamical exponent** z defined by $\tau_{\max} \sim L^z$. For diffusive systems $z = 2$, for instance.

The relaxation times are for each mode (s, k) given by $\tau_s(k) = -1/\mathrm{Re}\,\lambda^{(s)}(k)$. Clearly $\tau_+(k) \geq \tau_-(k)$, and both $\tau_+(k)$ and $\tau_-(k)$ attain their longest values for small k (or very large k, by symmetry). The two $k = 0$ modes yield the zero eigenvalue corresponding to the steady state and a mode with relaxation time $1/(2\omega)$. The latter is the typical time for an initial distribution localized to one orientation sector to spread into both. We refer to this mode as the 'tumble mode' since it does not contribute to the spatial relaxation dynamics: the corresponding eigenvector of $S(0)$ is $(1, -1)^\top$ which has zero projection onto $\langle +| + \langle -| = (1, 1)$ in

$$P(n,t) = P_+(n,t) + P_-(n,t) = ((\langle +| + \langle -|) \otimes \langle n|)|P(t)\rangle. \tag{2.32}$$

We focus instead on the spatial relaxation, where the longest relaxation time is

given by the $k = 1$ mode of the right band: $\tau_{\max} := \tau_+(1)$. With

$$\omega^*(L) := \omega_1 = \sin(2\pi/L), \tag{2.33}$$

we find

$$1/\tau_{\max} = \begin{cases} 1 + \omega - \sqrt{1-\omega^{*2}} - \sqrt{\omega^2 - \omega^{*2}}, & \omega > \omega^* \\ 1 + \omega - \sqrt{1-\omega^{*2}}, & \omega \leq \omega^*. \end{cases} \tag{2.34}$$

$\tau_{\max}$ is plotted in Figure 2.6. For any L, it is minimized at $\omega = \omega^*$ at which $\tau_{\max}$ has a cusp and is non-analytic. (The shortest possible relaxation of the kth mode similarly occurs at $\omega = \omega_k$.) Since ω^* is in general small,

$$\tau_{\text{opt}} = \tau_{\max}|_{\omega=\omega^*} \approx \frac{1}{\omega^*} \sim L, \tag{2.35}$$

i.e. the dynamical exponent $z = 1$, and not 2 as for the symmetric and totally asymmetric walk limits. It is possible to obtain any dynamical exponent $1 < z < 2$ by choosing $\omega \sim L^{-z}$.

These results are consistent with the work of Diaconis *et al.* [97] on a discrete-time random walk corresponding to the RTP with reflecting walls as in Figure 2.4b. The definition of the model took the tumbling probabilities to be $1/L$ and hopping probabilities $1 - 1/L$, corresponding to the optimum we derived above. Rather than looking at the decay rate of the dominant non-stationary mode as a measure of the relaxation time of the model, they considered the total variational norm

$$||P - P^*||_{\text{TV}} = \frac{1}{2} \sum_{\sigma,n} |P_\sigma(n,t) - P^*_\sigma(n)|, \tag{2.36}$$

which was proven to decay exponentially fast, with rate $1/L$.

2.3.4 Discussion

In summary, we have found a non-analyticity in the relaxation time versus ω at ω^*, that separates a region of strictly exponential relaxation ($\omega > \omega^*$) from one of oscillatory exponential relaxation ($\omega < \omega^*$). At exactly ω^*, the relaxation is exponential modulated by a linear time dependence; *cf.* (2.31). The value $\omega^* = \sin(2\pi/L)$ minimizes the relaxation time and has the optimal system size scaling. The non-analyticity is due to a real-to-complex eigenvalue crossing, such

that the dominant non-zero eigenvalue experiences a branch point at ω^* and there has a non-diagonalizable eigensubspace. Kato [98] introduced the term **exceptional points** for such points in parameter space where eigenvalues of a linear operator coalesce. Exceptional points have been studied in other areas of physics dealing with non-Hermitian matrices, such as open quantum system and multichannel scattering where their effects can be observed experimentally [99].

Finally, to give an intuitive explanation for the presence of an optimum in the relaxation, consider that with respect to the value of ω there is a trade-off between reaching sites far away from the initial one, and diffusing the probability (*cf.* Figure 2.3). In the limit of infinite persistence, we have a ballistic particle, and uncertainty in position comes only from the rate of jumping. At the other end of purely diffusive motion, it takes a long time to reach a site far away from the initial one for the first time. In between there must be an optimum, such that persistence gives a short time to visiting all sites while the particle motion is still sufficiently stochastic to diffuse the initial probability mass. With a tumbling rate $\sim 1/L$, the particle tends to reverse its direction $O(1)$ times per lap around the ring, and within the time of $O(L)$ it takes to make a few laps, it will be hard to predict where the particle is as this depends sensitively on the number of tumbles.

2.4 Solution for two interacting particles

We now consider the case of two RTPs on a ring with hardcore exclusion. We employ a reduced description where we only track the separation $n = n_2 - n_1$ between the particles in addition to their orientations σ_1 and σ_2. The model satisfies the following master equation, which can be derived from (2.7) for $N = 2$, or written down directly from the particle dynamics as

$$\begin{aligned}\partial_t P_{++}(n) = {} & P_{++}(n+1) I_{n\neq L-1} + P_{++}(n-1) I_{n\neq 1} \\ & + \omega \left[P_{+-}(n) + P_{-+}(n)\right] - \left[I_{n\neq 1} + I_{n\neq L-1} + 2\omega\right] P_{++}(n),\end{aligned} \tag{2.37a}$$

$$\begin{aligned}\partial_t P_{+-}(n) = {} & 2P_{+-}(n+1) I_{n\neq L-1} + \omega \left[P_{++}(n) + P_{--}(n)\right] \\ & - 2\left[I_{n\neq 1} + \omega\right] P_{+-}(n),\end{aligned} \tag{2.37b}$$

$$\begin{aligned}\partial_t P_{-+}(n) = {} & 2P_{-+}(n-1) I_{n\neq 1} + \omega \left[P_{++}(n) + P_{--}(n)\right] \\ & - 2\left[I_{n\neq L-1} + \omega\right] P_{-+}(n).\end{aligned} \tag{2.37c}$$

$$\partial_t P_{--}(n) = P_{--}(n+1)I_{n\neq L-1} + P_{--}(n-1)I_{n\neq 1} + \omega\left[P_{+-}(n) + P_{-+}(n)\right] - \left[I_{n\neq L-1} + I_{n\neq 1} + 2\omega\right] P_{--}(n), \tag{2.37d}$$

where $I_Q = \{1 \text{ if } Q \text{ is true; else } 0\}$, and we have suppressed the time argument for brevity. The periodicity constraint (2.5) becomes

$$P_{\sigma_1\sigma_2}(n,t) = P_{\sigma_2\sigma_1}(L-n,t). \tag{2.38}$$

The particle separation argument n is defined as the clockwise measurement from the first particle to the second, as ordered by the indices; (2.38) expresses the arbitrariness of which particle is labelled the 'first'.

We seek a spectral solution to the master equation, obtained by substitution of the elementary solutions

$$P_{\sigma_1\sigma_2}(n,t) \propto e^{\lambda t} u_{\sigma_1\sigma_2}(n) \tag{2.39}$$

into (2.37). That is, we seek the right eigenvector $|u\rangle$ with components $u_{\sigma_1\sigma_2}(n)$ corresponding to the eigenvalue λ of the forward generator $\mathbb{W}$. Because $\mathbb{W}$ is not symmetric, nor even similar to a symmetric matrix as we shall see, the left eigenvectors necessary for projection of the initial condition are not simply the complex transposes $\langle u|$. (This highlights the limitation of the Dirac-notation in dealing with non-Hermitian matrices.) We will however confine our analysis to deriving the right eigenvectors, as the left ones can in principle be obtained by the same method applied to the backward master equation.

In Section 2.4.1 we will solve the spectral problem using a generating function approach, sometimes called the kernel method. To prepare the ground for these calculations we first simplify the problem at hand by exploiting the formal symmetries of (2.37).

First, we note the invariance of this set of equations under $P_{++} \leftrightarrow P_{--}$, as (2.37a) turns into (2.37d) and *vice versa*. Similar to the notation in the one-particle section, let the state space be $\mathcal{X} = \mathcal{S}_1 \otimes \mathcal{S}_2 \otimes \mathcal{N}$ (now $\mathcal{N} = \{1, 2, \ldots L-1\}$) with natural basis vectors $|\sigma_1, \sigma_2, n\rangle$. Let R be a permutation matrix with

$$R|+,+,n\rangle = |-,-,n\rangle, \quad R|-,-,n\rangle = |+,+,n\rangle, \tag{2.40}$$

and that otherwise acts as the identity. Second, we have invariance under $P_{\sigma_1\sigma_2}(n) \leftrightarrow P_{\sigma_1\sigma_2}(L-n)$ with which we associate a matrix S with

$$S|\sigma_1, \sigma_2, n\rangle = |\sigma_2, \sigma_1, L-n\rangle. \tag{2.41}$$

Clearly $R^2 = S^2 = \mathbb{1}$, the unit matrix. Therefore the possible eigenvalues of R and S are $r = \pm 1$ and $s = \pm 1$, respectively. By construction, these matrices commute with $\mathbb{W}$ as they are symmetries of it,

$$\mathbb{W} = R\mathbb{W}R = S\mathbb{W}S. \tag{2.42}$$

Therefore, if $|u\rangle$ is an eigenvector of $\mathbb{W}$ with eigenvalue λ, then so are

$$R|u\rangle, \quad S|u\rangle, \quad \text{and} \quad SR|u\rangle = RS|u\rangle. \tag{2.43}$$

From these we can create the linear combination

$$|u : s, r\rangle := |u\rangle + sS|u\rangle + rR|u\rangle + srSR|u\rangle \tag{2.44}$$

which satisfies

$$\mathbb{W}|u : s, r\rangle = \lambda|u : s, r\rangle, \quad R|u : s, r\rangle = r|u : s, r\rangle, \quad S|u : s, r\rangle = s|u : s, r\rangle. \tag{2.45}$$

We will therefore always choose the eigenvectors $|u\rangle$ of $\mathbb{W}$ such that they are also eigenvectors of R and S, belonging to the 'sector' indexed by the eigenvalue tuple (r, s). Because of the periodicity (2.38), the solution $P_{\sigma_1\sigma_2}(n)$ will only be constructed using eigenvectors in the sectors $(\pm 1, +1)$. We therefore neglect the sectors $(\pm 1, -1)$ from the outset. Of the remaining sectors, we will refer to $(+1, +1)$ as the **symmetric sector** in the sense that its eigenvectors satisfy

$$u_{++}(n) = u_{--}(n), \tag{2.46}$$

and the $(-1, +1)$ as the **antisymmetric sector** because

$$u_{++}(n) = -u_{--}(n). \tag{2.47}$$

2.4.1 The kernel method and root parametrization

We define a vector-valued generating function by

$$\boldsymbol{g}(x) := \sum_{n=1}^{L-1} x^n \boldsymbol{u}(n), \quad \boldsymbol{u}(n) := \begin{pmatrix} u_{++}(n) \\ u_{+-}(n) \\ u_{-+}(n) \end{pmatrix}. \tag{2.48}$$

It is invertible by $\boldsymbol{u}(n) = (1/n!)(\partial_x^n \boldsymbol{g})(0)$. Because either (2.46) or (2.47) holds, it is not necessary to include $u_{--}(n)$ in $\boldsymbol{u}(n)$. We seek first closed equations for the components of $\boldsymbol{g}$. For example, the eigenvalue equation obtained by substituting (2.39) into (2.37b) is

$$\lambda u_{+-}(n) = 2u_{+-}(n+1) I_{n\neq L-1} + \omega\left[u_{++}(n) + u_{--}(n)\right] - 2\left[I_{n\neq 1} + \omega\right] u_{+-}(n). \tag{2.49}$$

We multiply this equation by x^n and sum over n from 1 to $L-1$, evaluating it term by term. We find for the first term in the right-hand side, for instance,

$$\sum_{n=1}^{L-1} x^n u_{+-}(n+1) I_{n\neq L-1} = \sum_{n=2}^{L-1} x^{n-1} u_{+-}(n) = x^{-1} g_{+-}(x) - u_{+-}(1), \tag{2.50}$$

and can similarly express all terms using the components of g and boundary values of u. The end result of proceeding this way with all the equations is

$$(\mu(x) + \nu(x)) g_{++}(x) + \omega(g_{+-}(x) + g_{-+}(x)) = (1-x)(1 - s x^{L-1}) u_{++}(1) \tag{2.51a}$$

$$\nu(x) g_{+-}(x) + \omega \delta_{r,1} g_{++}(1) = (1-x) u_{+-}(1), \tag{2.51b}$$

$$\mu(x) g_{-+}(x) + \omega \delta_{r,1} g_{++}(1) = -s(1-x) x^{L-1} u_{+-}(1), \tag{2.51c}$$

$$(\mu(x) + \nu(x)) g_{++}(x) + r\omega(g_{+-}(x) + g_{-+}(x)) = (1-x)(1 - s x^{L-1}) u_{++}(1). \tag{2.51d}$$

Here we have used $u_{++}(n) = r u_{--}(n)$ and $u_{+-}(n) = s u_{-+}(L-n)$ for $|u\rangle$ in the sector (r, s). Furthermore we have introduced the functions μ, ν and the shifted eigenvalue ζ as

$$\mu(x) := x - \frac{\zeta}{2}, \quad \nu(x) := \frac{1}{x} - \frac{\zeta}{2}, \quad \zeta := \lambda + 2(1+\omega). \tag{2.52}$$

The equations (2.51) can be written in matrix form as

$$H(x,\lambda)\boldsymbol{g}(x) = \boldsymbol{b}(x), \quad \text{for } x \neq 0, \tag{2.53}$$

where $H(x,\lambda) := A(x) - \lambda I$, and $A(x)$ and $\boldsymbol{b}(x)$ will be explicitly given later on, and depend on the sector (r,s). The elements of $A(x)$ are all rational functions of x, and therefore the determinant of $H(x,\lambda)$ is too. We have the two alternative factorizations

$$\det H(x,\lambda) = -\prod_{i=1}^{3}(\lambda - \lambda_i(x)) = \frac{1}{p(x,\lambda)}\prod_{i=1}^{m}(x - z_i(\lambda)). \tag{2.54}$$

The denominator $p(x,\lambda)$ is a polynomial in x with zeroes different from the m zeroes $z_i(\lambda)$ of the numerator. We fix ω, and choose some λ from the actual spectrum (which is finite). Then, $H(x,\lambda)$ will be invertible for all x but those coinciding with some $z_i(\lambda)$, so that

$$\boldsymbol{g}(x) = \frac{p(x,\lambda)}{\prod_{i=1}^{k}(x - z_i(\lambda))} C^{\top}(x,\lambda)\boldsymbol{b}(x), \tag{2.55}$$

where $C^{\top}(x,\lambda)$ is the transposed matrix of cofactors of $H(x,\lambda)$. Since $\boldsymbol{g}(x)$ is by definition continuous, the above expression must hold even in the limits $x \to z_i(\lambda)$ for which $H(x,\lambda)$ is not invertible. For this limit to exist we require that the poles in the denominator be cancelled by zeroes of corresponding order in $C^{\top}\boldsymbol{b}$,

$$C^{\top}(z_i(\lambda),\lambda)\boldsymbol{b}(z_i(\lambda)) = 0, \quad \text{for } i = 1,\ldots,m. \tag{2.56}$$

This constitutes a set of implicit equations in λ that determine in full the spectrum associated with any chosen sector (r,s). With the spectrum in principle determined, choosing any particular eigenvalue λ, the solution (2.55) for the generating function can be inverted to obtain the corresponding eigenfunction.

It will prove advantageous to change basic variables from λ to the set of 'roots' $z_i = z_i(\lambda)$. To close the equations in these variables, additional constraints relating the z_i are derived by eliminating λ between $z_1 = z_1(\lambda)$, $z_2 = z_2(\lambda)$, *etc.* The eigenvectors can also be expressed in terms of these roots. At this point, we separate the analysis for the two relevant sectors, considering first the symmetric sector, which proves to be larger and more complex than the antisymmetric one. We let $\omega > 0$ in both cases, to thereafter treat the singular limit $\omega = 0$ separately.

The symmetric sector

In the sector $(r, s) = (+1, +1)$, the matrix $H(x)$ in (2.53) becomes

$$H(x) = \begin{pmatrix} \mu(x) + \nu(x) & \omega & \omega \\ \omega & \nu(x) & 0 \\ \omega & 0 & \mu(x) \end{pmatrix}. \tag{2.57}$$

Its determinant is

$$\det H(x) = (\mu(x) + \nu(x))(\mu(x)\nu(x) - \omega^2), \tag{2.58}$$

which vanishes for x in the set of roots $\{z_1, \frac{1}{z_1}, z_2, \frac{1}{z_2}\}$, where

$$\mu(z_1) + \nu(z_1) = 0, \quad \mu(z_2)\nu(z_2) = \omega^2. \tag{2.59}$$

From here on we refer only to z_1 and z_2, and not their reciprocals, as 'the roots'. Solving the quadratic equations (2.59) yields

$$z_1 = \frac{\zeta}{2} + \sqrt{\frac{\zeta^2}{4} - 1}, \tag{2.60a}$$

$$z_2 = \frac{\zeta}{4} + \frac{1}{\zeta}\left(1 - \omega^2\right) + \frac{1}{2}\sqrt{\frac{\zeta^2}{4} - 2(1 + \omega^2) + \left(\frac{2(1 - \omega^2)}{\zeta}\right)^2}. \tag{2.60b}$$

(The reciprocals differ by the sign of the square root terms.) It follows that

$$(x - z_1)(x - 1/z_1) = x(\mu(x) + \nu(x)), \tag{2.61a}$$

$$(x - z_2)(x - 1/z_2) = -\frac{2x}{\zeta}(\mu(x)\nu(x) - \omega^2), \tag{2.61b}$$

whence $p(x, \lambda)$ appearing in (2.55) equals $-2x^2/\zeta$.

At this point the eigenvalues are not yet known. Instead of determining the eigenvalues explicitly, we seek tractable and closed equations in z_1 and z_2, whose solutions then produce the eigenvalues through the inversion of (for example) (2.60a),

$$\lambda = z_1 + \frac{1}{z_1} - 2(1 + \omega). \tag{2.62}$$

Since there are two independent variables (z_1 and z_2) we need two equations, which we refer to as **root-parametrized eigenvalue equations**.

The first one is derived by eliminating ζ between the two equations (2.59). Employing the notational shorthand $\bar{z} = 1/z$, the result is

$$(z_1 + \bar{z}_1)\,[2(z_2 + \bar{z}_2) - (z_1 + \bar{z}_1)] = 4(1 - \omega^2). \tag{2.63}$$

Already, it is apparent that $\omega = 1$ is a distinguished value.

The second root equation is derived from the pole cancellation condition (2.56) and is more involved. We require the transposed matrix of cofactors

$$C^\top = \begin{pmatrix} \mu\nu & -\mu\omega & -\nu\omega \\ -\mu\omega & \mu(\mu+\nu) - \omega^2 & \omega^2 \\ -\nu\omega & \omega^2 & \nu(\mu+\nu) - \omega^2 \end{pmatrix} \tag{2.64}$$

and the vector $\boldsymbol{b}(x)$ which we decompose as

$$\boldsymbol{b}(x) = B(x)\tilde{\boldsymbol{u}}, \tag{2.65}$$

where

$$B(x) = (1 - x) \begin{pmatrix} 1 - x^{L-1} & 0 & 0 \\ 0 & 1 & 0 \\ 0 & 0 & -x^{L-1} \end{pmatrix}, \tag{2.66}$$

and

$$\tilde{\boldsymbol{u}} = u_{++}(1) \begin{pmatrix} 1 \\ 0 \\ 0 \end{pmatrix} + u_{+-}(1) \begin{pmatrix} 0 \\ 1 \\ 1 \end{pmatrix}. \tag{2.67}$$

The fact that $\boldsymbol{b}(x)$ depends through $\tilde{\boldsymbol{u}}$ on the components of $(\partial_x \boldsymbol{g})(0)$ implies no additional constraints on $u_{++}(1)$ and $u_{+-}(1)$ over $\tilde{\boldsymbol{u}} \neq 0$ and whatever comes of the pole cancellation condition; the inversion (2.55) is already self-consistent for $(\partial_x \boldsymbol{g})(0)$.

The pole cancellation condition (2.56) gives one equation per component, of which there are three, for each of the four poles $z_1, \frac{1}{z_1}, z_2, \frac{1}{z_2}$. However, due to the reciprocity of the poles, and the relations (2.59), they are not independent. One finds that all the conditions are satisfied if and only if

$$0 = (1 - z_1)[\omega\mu(z_1)(1 - z_1^{L-1})u_{++}(1) + \omega^2(1 + z_1^{L-1})u_{+-}(1)], \tag{2.68a}$$

$$0 = (1-z_2)\mu(z_2)[-\omega(1-z_2^{L-1})u_{++}(1) + (\mu(z_2) - \nu(z_2)z_2^{L-1})u_{+-}(1)]. \tag{2.68b}$$

We think of $u_{++}(1)$ and $u_{+-}(1)$ as constants (for a given λ), so at first sight (2.68a) and (2.68b) may appear to be independent. However, they are not, as becomes clear from writing them in matrix form as

$$\begin{pmatrix} 1-z_1 & 0 \\ 0 & 1-z_2 \end{pmatrix} \begin{pmatrix} \mu(z_1)(1-z_1^{L-1}) & \omega(1+z_1^{L-1}) \\ -\omega(1-z_2^{L-1}) & \mu(z_2) - \nu(z_2)z_2^{L-1} \end{pmatrix} \begin{pmatrix} u_{++}(1) \\ u_{+-}(1) \end{pmatrix} = \begin{pmatrix} 0 \\ 0 \end{pmatrix}. \tag{2.69}$$

We require $\tilde{\boldsymbol{u}} \neq \mathbf{0}$ as otherwise $|u\rangle = 0$ and is not an eigenvector. Therefore, the determinant of the matrix product in (2.69) must vanish. This implies the two possibilities

$$(1-z_1)(1-z_2) = 0 \tag{2.70a}$$

or

$$\mu(z_1)(1-z_1^{L-1})(\mu(z_2) - \nu(z_2)z_2^{L-1}) = -\omega^2(1+z_1^{L-1})(1-z_2^{L-1}), \tag{2.70b}$$

from which we will derive the second root equation.

If (2.70a) is satisfied, then either $z_1 = 1$ or $z_2 = 1$, which creates a double pole in (2.55) because $z_1 = 1/z_1$ or $z_2 = 1/z_2$. The other possibilities of having double poles come from $z_1 = -1$, or $z_2 = -1$, or $z_1 = z_2$, which are in fact possible solutions of (2.70b). In the symmetric sector, only $z_2 = 1$ cancels the double pole by a corresponding double zero in (2.68). We leave the treatment of this special case to the end of this section. $z_1 = 1$ is admissible in the asymmetric sector, treated in the next section. The other cases are inconsistent. There are further special solutions of (2.70) for which a factor on either side of the equality (2.70b) evaluates to zero, *e.g.* $z_1^{L-1} = z_2^{L-1} = 1$. These cases confine both roots to a discrete set of possible values independently of ω. However, the first root equation (2.63) must also be satisfied and it depends explicitly on ω. Therefore, these cases can only be consistent for particular fine-tuned values of ω. We omit the derivation of these values, noting only that they occur for $\omega \leq 2$ and are expected to be the exceptional values for which eigenvalue crossings occur, and to imply non-diagonalizability; compare with the one-particle analysis.

Generic case. Leaving these special cases for now, we continue with the generic case in which (2.70b) is non-trivially satisfied. Then solving for $u^{++}(1)/u^{+-}(1)$

in (2.68a) and (2.68b) we get

$$\frac{u^{++}(1)}{u^{+-}(1)} = -\frac{\omega}{\mu(z_1)}\frac{1+z_1^{L-1}}{1-z_1^{L-1}} = \frac{\mu(z_2)-\nu(z_2)z_2^{L-1}}{\omega(1-z_2^{L-1})}. \tag{2.71}$$

Making judicious use of (2.59) and (2.62), we can rewrite the right equality of (2.71) explicitly in terms of z_1 and z_2, arriving at our second root-parameterized eigenvalue equation (2.72b), stated besides the first, (2.63),

$$(z_1+\bar{z}_1)\left[2(z_2+\bar{z}_2)-(z_1+\bar{z}_1)\right] = 4(1-\omega^2), \tag{2.72a}$$

$$z_2^{L-1} = \frac{2z_2-(z_1+\bar{z}_1)}{2\bar{z}_2-(z_1+\bar{z}_1)}\cdot\frac{(\bar{z}_1-\bar{z}_2)+(z_1-\bar{z}_2)z_1^{L-1}}{(\bar{z}_1-z_2)+(z_1-z_2)z_1^{L-1}}, \tag{2.72b}$$

where, as before, $\bar{z} = 1/z$. The equations (2.72) furnish the exact solution of the spectrum in the symmetric sector (excepting the special cases listed previously). Note that both equations are invariant under either of the transforms $z_1 \to \bar{z}_1$ or $z_2 \to \bar{z}_2$. Hence, if (z_1, z_2) is a solution, then so are $(z_1, \bar{z}_2)$, $(\bar{z}_1, z_2)$, and $(\bar{z}_1, \bar{z}_2)$. Nonetheless, they give the same eigenvalue. Note also that $z_1 = z_2$ remains a spurious solution of (2.72), as explained above, and must be discarded.

Special case $z_2 = 1$. We return now to this case, responsible for two special modes: the steady state and a 'tumble mode' with the L-independent eigenvalue $\lambda = -4\omega$, analogous to the one-particle case. Solving (2.63), the steady state has the real root

$$z_1 = 1 + \omega + \sqrt{\omega(2+\omega)} \tag{2.73}$$

(cf. [39]). The tumble mode has

$$z_1 = 1 - \omega + \sqrt{\omega(\omega-2)}, \tag{2.74}$$

which transitions from the real line to the unit circle for $\omega < 2$. In both cases, in order to ensure $\tilde{\boldsymbol{u}} \neq \mathbf{0}$ we must choose from (2.68a)

$$\frac{u_{++}(1)}{u_{+-}(1)} = \frac{\omega}{\mu(z_1)}\frac{1+z_1^{L-1}}{1-z_1^{L-1}}. \tag{2.75}$$

(This is the left equality of (2.71) and $z_2 = 1$ also solves (2.72b). In practice, we will not need to treat this case separately from the generic one when deriving the eigenvectors or solving (2.72) numerically.) For the tumble mode, (2.75) is undefined for ω such that z_1 is an $(L-1)$-root of 1. Such ω correspond to an

eigenvalue crossing with a mode from the antisymmetric sector, as becomes clear from the next section.

The antisymmetric sector

In this sector, it follows immediately by adding and subtracting (2.51a) and (2.51d) that

$$g_{++}(x) = \frac{x(1-x)(1-x^{L-1})}{(x-z_1)(x-1/z_1)} u_{++}(1), \tag{2.76a}$$

$$g_{+-}(x) = g_{-+}(x) = 0, \tag{2.76b}$$

with z_1 defined by (2.60a) as before. The poles can be cancelled if and only if $z_1^{L-1} = 1$. Letting $\theta_m = m\pi/(L-1)$, $m = 1, 2, \ldots L-1$, the eigenvalues are

$$\lambda_m = -4\sin^2\theta_m - 2\omega. \tag{2.77}$$

For the case of $z_1 = 1$, the eigenvalue is $\lambda = -2\omega$, which we denote as another L-independent tumble mode. The relaxation time of this mode is $1/(2\omega)$, twice that of $1/(4\omega)$ for the tumble mode in the symmetric sector. If the probability distribution has an initial condition with $P_{++}(n,0) = P_{--}(n,0)$ it will not involve the antisymmetric sector, and hence not the slower decaying tumble mode. We may therefore suppose that it is related to the spreading of the probability mass between orientation sectors where both particle move in the same direction (i.e. between the $++$ and $--$ sector). Similarly, the faster tumble mode should be related to relaxation between same-direction and opposite-direction orientation sectors (i.e. between either of $+-/-+$ and either of $++/--$).

The $\omega = 0$ limit

For $\omega = 0$ the orientation sectors are decoupled (*i.e.* the Markov matrix is completely reducible). Now r disappears from the equations (2.51), indicating a double degeneracy of the eigenvalues. Remaining in $s = +1$, $g_{++}(x)$ is identical to (2.76a), whereas

$$g_{+-}(x) = \frac{x(1-x)}{1-\frac{\zeta}{2}x} u_{+-}(1), \quad g_{-+}(x) = \frac{(1-x)x^{L-1}}{\frac{\zeta}{2}-x} u_{+-}(1). \tag{2.78}$$

If $u_{+-}(1)$ is to be non-zero, we must take $\zeta = 2$, *i.e.* $\lambda = 0$, to cancel the poles. Then

$$g_{+-}(x) = xu_{+-}(1), \quad g_{-+}(x) = x^{L-1}u_{+-}(1). \tag{2.79}$$

Clearly, this gives $u_{+-}(n) = \delta_{n,1}u_{+-}(1)$ and $u_{-+}(n) = \delta_{n,L-1}u_{+-}(1)$, which are the jammed steady states of the respective orientation sector. Obviously, for $\lambda = 0$ we will find $u_{++}(n) = u_{++}(1)$. For other eigenvalues, consistency requires $u_{+-}(1) = 0$ and the eigenvalues are associated exclusively with the dynamics of the $++$ (or $--$) orientation sector. These eigenvalues are just (2.77) with $\omega = 0$.

2.4.2 Spectrum: band structure and eigenvalue crossings

We now study the spectrum as a function of ω and L by a combination of numerics and analytical results. For generic parameter values we find $2(L-1)$ eigenvalues, which is half the dimension of the Markov matrix. This is expected since we are restricted to the two $s = +1$ sectors out of four. The picture that emerges is plotted and described in detail in Figure 2.7. For large ω, the spectrum is structured into real bands which interact via eigenvalue crossings as ω tends to zero producing a complicated pattern.

The spectrum is pieced together from the following results. The steady state and the two L-independent tumble modes with $\lambda = -2\omega, -4\omega$ were found analytically in the previous section, as well as the entire antisymmetric sector of eigenvalues (2.77) for arbitrary L and $\omega > 0$. For $\omega = 0$ the formula (2.77) is again applicable but the spectrum is doubly degenerate (except the zero eigenvalue). For the symmetric sector, the eigenvalues are given by solving (2.72) and substituting their solution into (2.62). In general, we do this numerically. While the roots generally fall on or near clear contours in the complex plane, we have omitted plotting the solutions to the roots in favour of plotting the resulting spectrum. For $\omega > 2$ it is possible to obtain an asymptotic analytic solution to the eigenvalue equations, derived in Appendix 2.A. This is facilitated by the numerical observation that in this region the roots form three groups, one with z_1 on the unit circle and z_2 real, and *vice versa* for the other two groups. Using

this as an ansatz we find three real bands of eigenvalues

$$\lambda_m = -4\sin^2\theta_m - \frac{\sin^2 2\theta_m}{\omega} + \frac{2\sin^2 2\theta_m}{L\omega} + \text{h.o.t.}, \qquad m \text{ integer}, \tag{2.80a}$$

$$\lambda_m = -4\sin^2\frac{\theta_m}{2} - 2\omega + \frac{2\sin\theta_m \sin 2\theta_m}{L\omega^2} + \text{h.o.t.}, \qquad m \text{ odd integer}, \tag{2.80b}$$

$$\lambda_m = -4\sin^2\theta_m - 4\omega + \frac{\sin^2 2\theta_m}{\omega} - \frac{2\sin^2 2\theta_m}{L\omega} + \text{h.o.t.}, \quad m \text{ integer}, \tag{2.80c}$$

where $\theta_m = \pi m/(L-1)$ and 'h.o.t' signifies terms with higher order reciprocals of L or ω.

As a side remark: for $L \sim 30$, I have constructed the Markov matrix explicitly on a computer and solved numerically for the spectrum and eigenvectors. Those results are fully consistent with what we obtained by independent means, as presented in this section and the next. The naive numerical approach has the drawback of requiring all eigenvectors to be found and their symmetries determined, in order to select only the eigenvalues belonging to the two relevant symmetry sectors.

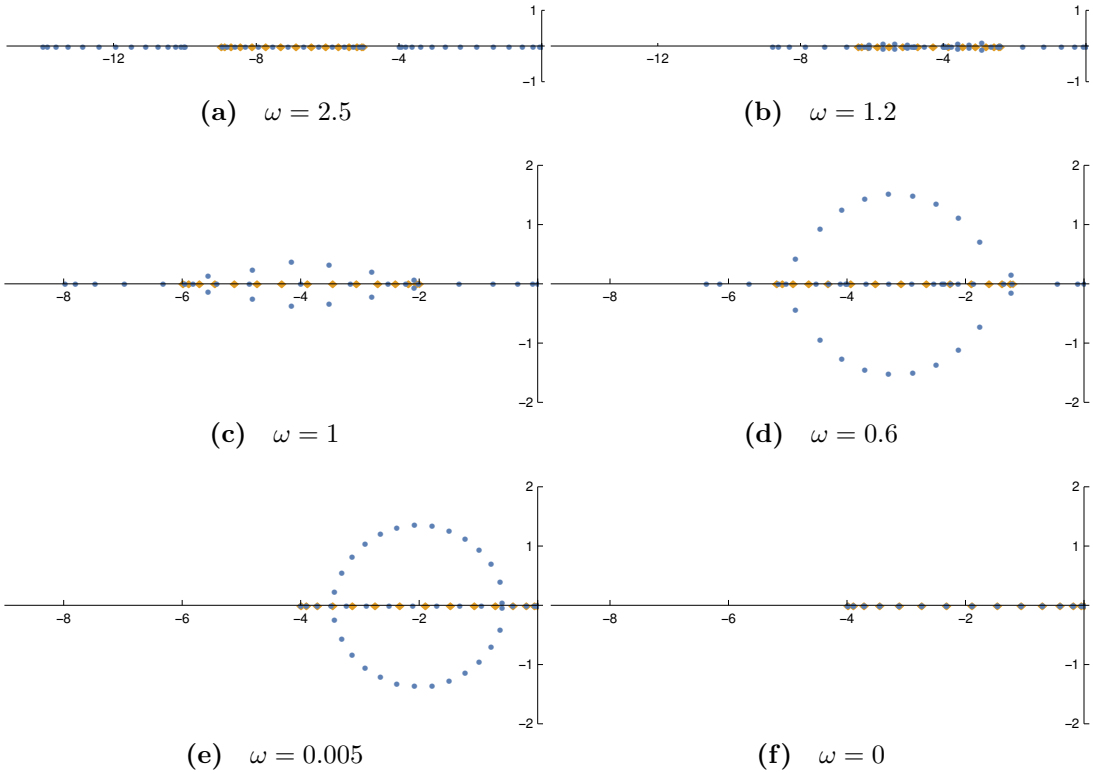

Figure 2.7 *Plot of the two-particle spectrum in the complex plane for $L = 30$. Different L produce the same pattern of eigenvalues. Blue circles: symmetric sector; orange diamonds: antisymmetric sector. (a) The symmetric sector comes in three separate bands for $\omega \geq 2$ where the separation is linear in ω. (b) In the range $2 \geq \omega > 1$ the bands cross, creating small excursions into the complex plane. (c) At exactly $\omega = 1$ there is degeneracy proportional to L at $\lambda = -4$ as a 'macroscopic eigenvalue crossing' takes place, just as in the one-particle case. (d) As the bands continue to cross, pairs of eigenvalues are sent out onto a deformed circle. (e) As ω approaches zero, the circle collapses towards $\lambda = -2$. (f) At $\omega = 0$ the symmetric and antisymmetric sector have the same eigenvalues (except the zero eigenvalue of the steady state which lies in the symmetric sector).*

2.4.3 $z_{1,2}$-parametrized eigenvectors

The generating function expressed in the roots z_1 and z_2 is inverted in Section 2.B to yield the eigenvectors. Here, we state the eigenvectors for any given eigenvalue λ, using (2.60) to define the roots from the shifted eigenvalue $\zeta = \lambda + 2(1+\omega)$.

Take first $\omega > 0$. The eigenvectors in the antisymmetric sector are given by

$$u_{++}(n) = z_1^n + z_1^{L-n} \tag{2.81a}$$
$$u_{+-}(n) = u_{-+}(n) = 0 \tag{2.81b}$$
$$u_{--}(n) = -u_{++}(n). \tag{2.81c}$$

Since in this sector z_1 are $(L-1)$-roots of unity, the non-zero components are essentially Fourier basis functions. The symmetric sector has eigenvectors

$$u_{++}(n) = \nu(z_1)\frac{z_1^n + z_1^{L-n}}{1 - z_1^L} - \omega^2 \frac{z_2^n + z_2^{L-n}}{\mu(z_2) + \nu(z_2) z_2^L}, \tag{2.82a}$$
$$u_{+-}(n) = \omega\left(1 + \tfrac{2}{\zeta - 2}\delta_{n,1}\right)\left[\frac{z_1^n - z_1^{L-n}}{1 - z_1^L} + \frac{\nu(z_2) z_2^n + \mu(z_2) z_2^{L-n}}{\mu(z_2) + \nu(z_2) z_2^L}\right], \tag{2.82b}$$
$$u_{-+}(n) = u_{+-}(L-n), \tag{2.82c}$$
$$u_{--}(n) = u_{++}(n), \tag{2.82d}$$

where $\mu(z) = z - \zeta/2$ and $\nu(z) = \mu(1/z)$. The eigenvectors have two components, one involving z_1 and one z_2. In addition, the opposed orientation components have an 'anomalous weight' on the jammed states $u_{+-}(1)$ and $u_{-+}(L-1)$. A few eigenvectors are shown in Figure 2.8.

For $\omega = 0$, the orientation sectors are decoupled, so the relative scaling of the different orientation components is irrelevant,

$$u_{++}(n) = z_1^n + z_1^{L-n} \tag{2.83a}$$
$$u_{+-}(n) \propto \delta_{\lambda,0}\delta_{n,1} \tag{2.83b}$$
$$u_{-+}(n) \propto u_{+-}(L-n) \tag{2.83c}$$
$$u_{--}(n) \propto u_{++}(n). \tag{2.83d}$$

As a general observation on the basis of the uniqueness of the generating function inversion, a given eigenvalue cannot have distinct eigenvectors from the same sector. At an ω where two eigenvalues with eigenvectors in the same symmetry

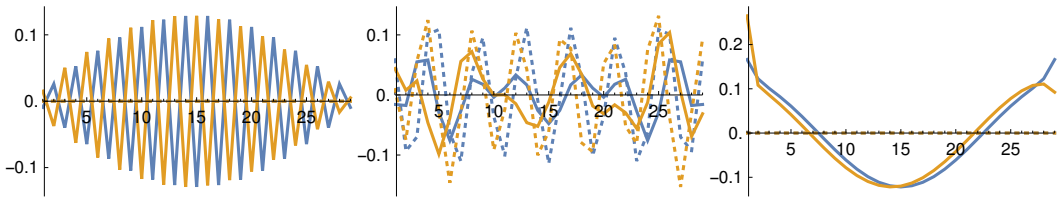

(a) $\lambda = -8.78$ **(b)** $\lambda = -2.92 - i0.0887$ **(c)** $\lambda = -0.0799$

Figure 2.8 *Plot of some normalized eigenvectors for $L = 30$, $\omega = 1.2$ (cf. Figure 2.7b) versus lattice site n. Blue graphs: $u_{++}(n)$. Orange graphs: $u_{+-}(n)$. Full drawn lines show real part, dotted lines show imaginary part. (a) Most negative eigenvalue. (b) An arbitrary complex eigenvalue. (c) The least negative non-zero eigenvalue (spectral gap).*

sector cross, the associated subspace becomes non-diagonalizable, just as in the one-particle case. However, we do not attempt to derive the generalized eigenvectors or projection operators for these cases.

2.4.4 Nonequilibrium steady state

The steady state distribution, $P^*_{\sigma_1\sigma_2}(n)$, has been found and discussed in-depth by Slowman *et al.* [39], but for completeness we state it here in the context of the full spectral solution. The steady state always lies in the symmetric sector (assuming $\omega > 0$ as we do throughout this section); being independent of initial condition, a symmetry argument implies $P^*_{++}(n) = P^*_{--}(n)$. We derived earlier that the roots for the steady state are $z_1 = 1 + \omega + \sqrt{\omega(2+\omega)}$ (2.73) and $z_2 = 1$. The steady state distribution is then

$$P^*_{++}(n) = \frac{1}{Z_L}\left((1+\omega)\frac{z_1^n + z_1^{L-n}}{1 - z_1^L} + \omega\right), \tag{2.84a}$$

$$P^*_{+-}(n) = \frac{1}{Z_L}(\omega + \delta_{n,1})\left(\frac{z_1^n - z_1^{L-n}}{1 - z_1^L} + 1\right), \tag{2.84b}$$

$$P^*_{-+}(n) = P^*_{+-}(L-n), \tag{2.84c}$$

$$P^*_{--}(n) = P^*_{++}(n), \tag{2.84d}$$

where the normalization is

$$Z_L = \sum_{n=1}^{L-1} \sum_{\sigma_1,\sigma_2 \in \{+,-\}} u_{\sigma_1\sigma_2}(n) = 4\left[\omega(L-1) + (1+z_1)\frac{1 - z_1^{L-1}}{1 - z_1^L}\right]. \tag{2.85}$$

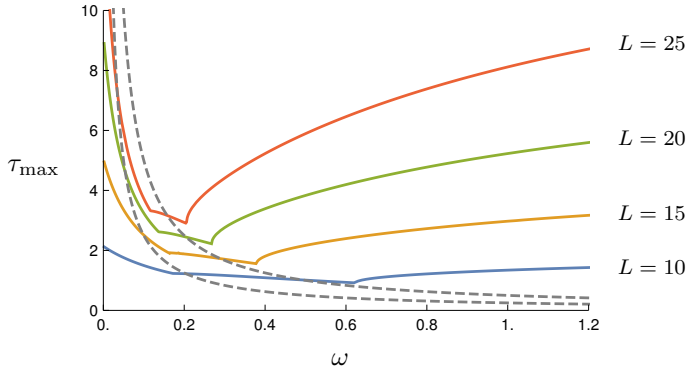

Figure 2.9 *Coloured lines: longest system-size dependent relaxation time. Dashed lines: relaxation times* $1/2\omega$ *and* $1/4\omega$*. Each coloured curve has two minima and cusps (cf. Figure 2.6).*

2.4.5 Relaxation time

The longest relaxation time $\tau_{\max}$, disregarding the tumble modes, is obtained from the numerical solution of the spectrum as a function of ω and plotted in Figure 2.9. While we do not have exact expressions for the values $\omega^*_{1,2}(L)$ at the two cusps, numerics suggests they scale as $\sim 1/L$ (for L larger than about 20), in analogy with the one-particle case. The scaling away from the region between $\omega^*_1(L)$ and $\omega^*_2(L)$ is again $\sim L^2$.

2.4.6 Discussion

We were able to solve the 2-RTP problem, albeit in the relative coordinate. The solution has an intriguing structure given implicitly via the root equations (2.72) that are reminiscent of Bethze equations. However, it is not clear how one would generalize the obtained solution either to two particles in absolute coordinates, or to an ansatz for the 3- or N-particle problem. Whether these problems are amenable to analytical solution remains an open question, but the complexity of even the two-particle case moderates expectations.

Let us nonetheless guess at some features of the N-particle solution. Certainly, the spectrum will be divided into some number of symmetry sectors. We would expect to find branch-point type eigenvalue crossings at exceptional points; these have been proven to exist in the Bethe ansatz solution of the N-particle ASEP [100, 101]. Generalizing our obtained results rather naively, we conjecture that the spectrum consists of a number of real bands for $\omega \gtrsim N$, which cross in

complicated ways for smaller ω. Tumble modes related only to the orientation dynamics will be present, possibly at $\lambda = -2k$, for $k = 1, 2, \ldots, N$. It would be interesting to see if the number of cusps in the relaxation spectrum is related to the number of particles by some simple rule.

After the publication of the material in this chapter ([1], January 2019), Das *et al.* continued this line of inquiry by considering the two-RTP problem on the continuous ring, with the addition of thermal noise ([102], August 2020). The spectrum was found to exhibit a band structure analogous to the lattice case. Somewhat counter-intuitively, on the continuum the addition of thermal noise makes the model *easier* to analyse than without it. This is because hardcore exclusion can then be implemented by certain simple boundary conditions on the probability density, and density delta-spiked due to jamming [39] are smoothed out to exponentials. In the next chapter, we will study a continuum model of N particles that drift and diffuse with individual parameters. While we will study this model in its own right, it does describe as a special case the dynamics of the thermal RTP model for times between tumble events. In an epilogue to the next chapter we will assess the feasibility of obtaining an N-RTP steady state by adopting the continuous, thermal setting.

Appendices for Chapter 2

2.A Asymptotic solution of two-particle spectrum for $\omega > 2$

Here, we solve the polynomial equations (2.72) to order $1/L$, in the regime $\omega > 2$. Guided by the numerical solution, we make the ansatz that either z_1 or z_2 lies on the unit circle. The first assumption produces the middle band, and the second ansatz the left and right bands.

2.A.1 The middle band

Starting with an ansatz for z_1 on the unit circle, we assume it differs from an $(L-1)$-root of negative one by an argument of order $1/L$,

$$z_1 = \exp\left[i\left(\theta - \frac{f(\omega,\theta)}{L} + O\left(L^{-2}\right)\right)\right], \tag{2.86}$$

where $\theta = \theta_m = \pi m/(L-1)$ and m is an odd integer up to $2(L-1)-1$. We rewrite (2.71) as

$$z_2^{L-1} = \frac{\mu(z_2)\mu(z_1) + \omega^2\rho(z_1)}{\nu(z_2)\mu(z_1) + \omega^2\rho(z_1)}, \quad \rho(z_1) := \frac{1+z_1^{L-1}}{1-z_1^{L-1}}, \tag{2.87}$$

which stands in for (2.72b). To leading order, $z_1^{L-1} = -e^{-if}$, so that

$$\rho(z_1) = \frac{1-e^{-if(\omega,\theta)}}{1+e^{-if(\omega,\theta)}} = iT(\omega,\theta), \quad T(\omega,\theta) := \tan[f(\omega,\theta)/2]. \tag{2.88}$$

Using the fact that z_1 is on the unit circle, we rewrite (2.72a) as

$$\bar{z}_2 = -z_2 + \frac{1-\omega^2}{\mathrm{Re}\, z_1} + \mathrm{Re}\, z_1. \tag{2.89}$$

Note that $\mu(x) = x - \mathrm{Re}\, z_1$, so that $\mu(z_1) = i\mathrm{Im}\, z_1$. Then substituting (2.89) and (2.88) into (2.87), one obtains

$$z_2^{L-1} = -\frac{z_2 - \mathrm{Re}\, z_1 + \omega^2 T/\mathrm{Im}\, z_1}{z_2 - 1/\mathrm{Re}\, z_1 - \omega^2\,(T/\mathrm{Im}\, z_1 - 1/\mathrm{Re}\, z_1)}. \tag{2.90}$$

Due to the reciprocal symmetry, we can without loss of generality take $|z_2| < 1$. Then $\lim_{L\to\infty} z_2^{L-1} = 0$, which implies that the numerator in the r.h.s. above vanishes in this limit. Hence

$$\hat{z}_2 := \lim_{L\to\infty} z_2 = \cos\theta - \omega^2 \frac{T(\omega,\theta)}{\sin\theta}. \tag{2.91}$$

We take now the $L \to \infty$ limit of (2.89), and substitute the expression (2.91) for $\hat{z}_2$. Introducing the parameter $\varepsilon = 1/\omega^2$,

$$\left[\cos\theta - \frac{T}{\varepsilon \sin\theta}\right]^{-1} - \frac{T}{\varepsilon \sin\theta} = \frac{\varepsilon - 1}{\varepsilon \cos\theta}. \tag{2.92}$$

Straightforward manipulations lead to the quadratic equation

$$T^2 - [\varepsilon \sin\theta \cos\theta + (1-\varepsilon)\tan\theta]T + \varepsilon \sin^2\theta = 0, \tag{2.93}$$

with solution

$$T(\omega,\theta) = \frac{1}{2}\left[\varepsilon \sin\theta\cos\theta + (1-\varepsilon)\tan\theta\right] \pm \sqrt{\frac{1}{4}\left[\varepsilon \sin\theta\cos\theta + (1-\varepsilon)\tan\theta\right]^2 - \varepsilon \sin^2\theta}. \tag{2.94}$$

The choice of root relates to the reciprocal symmetry of the solutions, and we can without loss of generality take the consistent combination of negative root and $\tan\theta > 0$.

Although $f(\omega,\theta)$ has now been found exactly, the expression is unwieldy. Settling for a truncated Laurent series in ω, a computer algebra package finds for us

$$f(\omega,\theta) = \frac{1}{\omega^2}\left(1 + \frac{1}{\omega^2}\right)\sin 2\theta + O\left(\omega^{-6}\right). \tag{2.95}$$

The corresponding eigenvalue is given by $\lambda = 2\mathrm{Re}\, z_1 - 2(1+\omega)$. Substituting in (2.86) and (2.95), and expanding up to relevant orders,

$$\lambda_m = -4\sin^2\frac{\theta_m}{2} - 2\omega + \frac{2\sin\theta_m \sin 2\theta_m}{L\omega^2} + \text{h.o.t.}, \tag{2.96}$$

where h.o.t. implies terms with higher reciprocal orders of ω or L.

2.A.2 The left and right bands

For values of z_1 that lie on the real axis, the corresponding z_2 lies instead on the unit circle. In particular, there are are two distinct z_2's (with different z_1's) close to every root of positive one. We make the ansatz

$$z_2 = \exp\left[i\left(\varphi - \frac{h(\omega,\varphi)}{L} + O\left(1/L^2\right)\right)\right], \tag{2.97}$$

where $\varphi = \varphi_m = 2\pi m/(L-1)$, $m = 1, 2, \ldots, L-1$. We can then proceed in much the same way as with the previous ansatz, but interchanging the role of z_1 and z_2. First, (2.72b) is written

$$z_1^{L-1} = -\frac{\omega^2 + \mu(z_1)\eta(z_2)}{\omega^2 + \nu(z_1)\eta(z_2)}, \quad \eta(z_2) = \frac{\mu(z_2) - \nu(z_2)z_2^{L-1}}{1 - z_2^L}, \tag{2.98}$$

and (2.72a) is solved

$$z_1 + \bar{z}_1 = 2\left[\mathrm{Re}\, z_2 + q\sqrt{\omega^2 - (\mathrm{Im}\, z_2)^2}\right], \tag{2.99}$$

where $q = \pm 1$ selects between the two solutions. Then, since $\zeta = z_1 + \bar{z}_1$, we have

$$\mu(z_2) = i\mathrm{Im}\, z_2 - q\sqrt{\omega^2 - (\mathrm{Im}\, z_2)^2}, \tag{2.100a}$$
$$\nu(z_2) = -i\mathrm{Im}\, z_2 - q\sqrt{\omega^2 - (\mathrm{Im}\, z_2)^2}. \tag{2.100b}$$

It follows that (to leading order)

$$\eta(z_2) = \frac{i(\mathrm{Im}\, z_2)(1 + z_2^{L-1}) - q\sqrt{\omega^2 - (\mathrm{Im}\, z_2)^2}(1 - z_2^{L-1})}{1 - z_2^{L-1}} \tag{2.101a}$$
$$= i(\mathrm{Im}\, z_2)\frac{1 + z_2^{L-1}}{1 - z_2^{L-1}} - q\sqrt{\omega^2 - (\mathrm{Im}\, z_2)^2} \tag{2.101b}$$

$$= \frac{\operatorname{Im} z_2}{T(\omega,\varphi)} - q\sqrt{\omega^2 - (\operatorname{Im} z_2)^2}, \tag{2.101c}$$

where $T(\omega,\varphi) := \tan[h(\omega,\varphi)/2]$. Without loss of generality we assume $|z_1| < 1$, so that taking the limit $L \to \infty$ of the left equation in (2.98) leads to

$$\mu(\hat{z}_1) = -\frac{\omega^2}{\eta(\hat{z}_2)}. \tag{2.102}$$

This we express using (2.99) and (2.101) as

$$\hat{z}_1 = \cos\varphi + q\sqrt{\omega^2 - \sin^2\varphi} - \frac{\omega^2 T(\omega,\varphi)}{\sin\varphi - q(\sqrt{\omega^2 - \sin^2\varphi})T(\omega,\varphi)}. \tag{2.103}$$

Now, going back to (2.99), we solve for $\hat{z}_1$ to obtain

$$\hat{z}_1 = \cos\varphi + q\sqrt{\omega^2 - \sin^2\varphi} + q'\sqrt{\left(\cos\varphi + q\sqrt{\omega^2 - \sin^2\varphi}\right)^2 - 1}, \tag{2.104}$$

where $q' = \pm 1$ selects the positive or negative root solution. Dividing by ω and taking the limit to infinity, we discover the consistency requirement $q' = -q$. Combining the last two equations,

$$\frac{\omega^2 T(\omega,\varphi)}{\sin\varphi - q\sqrt{\omega^2 - \sin^2\varphi}T(\omega,\varphi)} = q\sqrt{\left(\cos\varphi + \sqrt{\omega^2 - \sin^2\varphi}\right)^2 - 1}. \tag{2.105}$$

After rearranging we find

$$h(\omega,\varphi) = 2\arctan\left[\frac{q\sin\varphi}{\omega^2\left[\left(\cos\varphi + q\sqrt{\omega^2 - \sin^2\varphi}\right)^2 - 1\right]^{-1/2} + \sqrt{\omega^2 - \sin^2\varphi}}\right]. \tag{2.106}$$

This we expand using computer algebra to

$$h(\omega,\varphi) = \frac{q\sin\varphi}{\omega} + \frac{\sin\varphi\cos\varphi}{2\omega^2} - \frac{q\sin\varphi\,(\cos 2\varphi + 5)}{12\omega^3} + O\left(\omega^{-4}\right). \tag{2.107}$$

Once z_2 is known, the eigenvalue is obtained from (2.99) and expanded,

$$\lambda_m = -4\sin^2\frac{\varphi}{2} - 2\omega(1-q) - \frac{q\sin^2\varphi}{\omega} + \frac{2q\sin^2\varphi}{L\omega} + \frac{3\sin\varphi\sin 2\varphi}{2L\omega^2} + \text{h.o.t.} \tag{2.108}$$

2.B Derivation of two-particle eigenvectors

Here we determine the generating function by evaluating the inversion (2.55). We begin with the symmetric sector. Define for convenience

$$J(x) = \mu(x)\nu(x)u_{++}(1) - \omega\mu(x)u_{+-}(1). \tag{2.109}$$

The first component of the generating function can then be expressed

$$g_{++}(x) = -\frac{2x^2(1-x)}{\zeta(x-z_1)(x-\frac{1}{z_1})(x-z_2)(x-\frac{1}{z_2})}[J(x) - x^{L-1}J(1/x)]. \tag{2.110}$$

Since $J(1/x) \sim 1/x$, it follows that $x^2(1-x)J(1/x) \sim x$, and therefore the second term is $\sim x^L$ once the factors in the denominator are expanded in geometric series. It is thus unimportant, since by the definition of $g(x)$ all powers above $L-1$ will eventually cancel out. Hence we write

$$g_{++}(x) = -\frac{2x}{\zeta} \cdot \frac{x(1-x)J(x)}{(x-z_1)(x-\frac{1}{z_1})(x-z_2)(x-\frac{1}{z_2})} + O\left(x^L\right). \tag{2.111}$$

We perform a partial fraction decomposition of the large fraction, possible since the numerator is $\sim x^3$;

$$\begin{aligned} g_{++}(x) = & -\frac{2x}{\zeta}\Bigg\{\frac{z_1(1-z_1)J(z_1)}{(x-z_1)(z_1-\frac{1}{z_1})(z_1-z_2)(z_1-\frac{1}{z_2})} \\ & + \frac{1/z_1(1-1/z_1)J(1/z_1)}{(\frac{1}{z_1}-z_1)(x-\frac{1}{z_1})(\frac{1}{z_1}-z_2)(\frac{1}{z_1}-\frac{1}{z_2})} + \text{perm.}\Bigg\} \\ & + O\left(x^L\right), \end{aligned} \tag{2.112}$$

where 'perm.' implies a repetition of the terms to its left but with z_1 and z_2 permuted. The pole cancellation conditions (2.68) imply succinctly

$$J(z_i) = z_i^{L-1}J(1/z_i), \quad i = 1, 2. \tag{2.113}$$

Using (2.113), together with the algebraic identity

$$(\tfrac{1}{z_1} - z_2)(\tfrac{1}{z_1} - \tfrac{1}{z_2}) = \tfrac{1}{z_1^2}(z_1 - z_2)(z_1 - \tfrac{1}{z_2}), \tag{2.114}$$

the expression (2.111) simplifies to

$$g_{++}(x) = \frac{2(1-z_1)J(1/z_1)}{\zeta(z_1-\frac{1}{z_1})(z_1-z_2)(z_1-\frac{1}{z_2})}\left[\frac{z_1^L x}{z_1-x}+\frac{x}{\frac{1}{z_1}-x}\right]+\text{perm.}+O\left(x^L\right). \tag{2.115}$$

Recognizing the power series

$$\frac{x}{a-x} = \sum_{n=1}^{\infty}(x/a)^n, \tag{2.116}$$

we have found

$$g_{++}(x) = \frac{2(1-z_1)J(1/z_1)}{\zeta(z_1-\frac{1}{z_1})(z_1-z_2)(z_1-\frac{1}{z_2})}\sum_{n=1}^{L-1}[z_1^n+z_1^{L-n}]x^n+\text{perm.}, \tag{2.117}$$

since higher order terms must cancel out. Denote the prefactors by

$$A_1\nu(z_1) := \frac{2(1-z_1)J(1/z_1)}{\zeta(z_1-\frac{1}{z_1})(z_1-z_2)(z_1-\frac{1}{z_2})}, \tag{2.118a}$$

$$-A_2\omega := \frac{2(1-z_2)J(1/z_2)}{\zeta(z_2-\frac{1}{z_2})(z_2-z_1)(z_2-\frac{1}{z_1})}. \tag{2.118b}$$

Then

$$u_{++}(n) = A_1\nu(z_1)(z_1^n+z_1^{L-n})-A_2\omega(z_2^n+z_2^{L-n}). \tag{2.119}$$

To find the second component, $u_{+-}(n)$, we define for convenience the two functions

$$K(x) := \omega\mu(x)u_{++}(1)+\omega^2 u_{+-}(1), \tag{2.120a}$$

$$\begin{aligned} K'(x) &:= \mu(x)(\mu(x)+\nu(x))u_{+-}(1) \\ &= \frac{\mu(x)}{x}(x-z_1)(x-1/z_1)u_{+-}(1). \end{aligned} \tag{2.120b}$$

With these definitions

$$g_{+-}(x) = \frac{2x}{\zeta}\cdot\frac{x(1-x)}{(x-z_1)(x-\frac{1}{z_1})(x-z_2)(x-\frac{1}{z_2})}[K(x)-K'(x)]+O\left(x^L\right). \tag{2.121}$$

The $K(x)$ term can be decomposed into four partial fractions since $K(x)\sim x$,

leaving the numerator $\sim x^3$. The $K'(x)$ term already cancels two of the poles and x in the numerator, after which two partial fractions can be taken. The result is

$$g_{+-}(x) = -\frac{2(1-z_1)}{\zeta(z_1-\frac{1}{z_1})(z_1-z_2)(z_1-\frac{1}{z_2})}\left[\frac{K(1/z_1)x}{1/z_1-x}+\frac{K(z_1)z_1x}{z_1-x}\right]+\text{perm.}$$
$$+\frac{2(1-x)u_{+-}(1)}{\zeta(z_2-\frac{1}{z_2})}\left[\mu(z_2)\frac{x}{z_2-x}-\nu(z_2)\frac{x}{1/z_2-x}\right] \tag{2.122}$$

We make use of the following relations,

$$K(z_1) = \frac{\omega}{\nu(z_1)}z_1^{L-1}J(1/z_1), \tag{2.123a}$$
$$K(1/z_1) = -\frac{\omega}{\nu(z_1)}J(1/z_1), \tag{2.123b}$$
$$K(z_2) = \frac{\mu(z_2)}{\omega}z_2^{L-1}J(z_2)+K'(z_2), \tag{2.123c}$$
$$K(1/z_2) = \frac{\nu(z_2)}{\omega}J(1/z_2)+\frac{\nu(z_2)}{\mu(z_2)}K'(z_2), \tag{2.123d}$$

and the geometric series (2.116), to find

$$g_{+-}(x) = A_1\omega\sum_{n=1}^{\infty}[z_1^n-z_1^{L-n}]x^n+A_2\sum_{n=1}^{\infty}[\nu(z_2)z_2^n+\mu(z_2)z_2^{L-n}]x^n$$
$$-\frac{2(1-z_2)K'(z_2)}{\zeta\mu(z_2)(z_2-\frac{1}{z_2})(z_2-z_1)(z_2-\frac{1}{z_1})}\left[\nu(z_2)\frac{x}{1/z_2-x}+\mu(z_2)\frac{z_2x}{z_2-x}\right]$$
$$+\frac{2(1-x)u_{+-}(1)}{\zeta(z_2-\frac{1}{z_2})}\left[\mu(z_2)\frac{x}{z_2-x}-\nu(z_2)\frac{x}{1/z_2-x}\right]. \tag{2.124}$$

Considering (2.120b), the last two lines almost cancel, leaving only a term $(2/\zeta)xu_{+-}(1)$. We have then found

$$u_{+-}(n) = A_1\omega(z_1^n-z_1^{L-n})+A_2(\nu(z_2)z_2^n+\mu(z_2)z_2^{L-n})+\frac{2}{\zeta}u_{+-}(1)\delta_{n,1}. \tag{2.125}$$

This we can rearrange to

$$u_{+-}(n) = \left(1+\frac{2}{\zeta-2}\delta_{n,1}\right)\left(A_1\omega(z_1^n-z_1^{L-n})+A_2(\nu(z_2)z_2^n+\mu(z_2)z_2^{L-n})\right). \tag{2.126}$$

Finally, we want to choose the arbitrary overall scaling of the eigenvectors such that A_1 and A_2 become simple expressions. The ratio A_1/A_2 is already fixed by $u_{++}(1)/u_{+-}(1)$ which must satisfy (2.71). Rather than attempting to simplify (2.118) directly, we substitute (2.119) and (2.125) into the eigenvalue equation corresponding to (2.37c) for $n = 1$, which reads simply

$$\frac{\zeta}{2}u_{-+}(1) = \omega u_{++}(1). \tag{2.127}$$

After trivial rearrangements, the above equation gives

$$A_1\left[\frac{\zeta}{2}(z_1 - z_1^{L-1}) + \nu(z_1)(z_1 + z_1^{L-1})\right] = A_2\frac{1}{\omega}\Big[\frac{\zeta}{2}(\mu(z_2) + \nu(z_2)z_2^{L-1}) + \omega^2(z_2 + z_2^{L-1})\Big]. \tag{2.128}$$

The bracket on the left-hand side can be written using $\nu(z_1) = -\mu(z_1)$ (2.59) as

$$\left(\frac{\zeta}{2}z_1 + \nu(z_1)z_1\right) - \left(\mu(z_1) + \frac{\zeta}{2}\right)z_1^{L-1}. \tag{2.129}$$

After using the definitions of μ and ν (2.52), the resulting expression is

$$1 - z_1^L. \tag{2.130}$$

For the left-hand-side bracket in (2.128) we use $\omega^2 = \mu(z_2)\nu(z_2)$ (2.59) to express it as

$$\mu(z_2)\left(\frac{\zeta}{2}z_2 + \nu(z_2)z_2\right) + \nu(z_2)\left(\frac{\zeta}{2} + \mu(z_2)\right)z_2^{L-1}. \tag{2.131}$$

After simplifying the above using (2.52), it is clear that we can choose

$$A_1 = \frac{1}{1 - z_1^L}, \quad A_2 = \frac{\omega}{\mu(z_2) + \nu(z_2)z_2^L}. \tag{2.132}$$

This concludes the derivation of eigenvectors for the symmetric sector.

The non-zero eigenvector (2.76a) of the asymmetric sector is obtained by the same method of partial fraction decomposition and geometric series expansion as above.

Chapter 3

An inter-particle ratchet effect in heterogeneous single-file diffusion

3.1 Background

3.1.1 Single-file diffusion

Particles moving in single file under stochastic influences have been considered by modellers from as early as 1955 with the transport of ions through pores in the squid giant axon [103]. Another, more recent, physical realization of particles moving through narrow channels come from diffusion though zeolites, a mineral with parallel pores of sub-microscopic dimensions [104, 105]. Both lattice (the ASEP) and continuum models have been employed in relation to narrow-channel transport, but the continuum version lends itself particularly well to derive the famous result that the mean-square displacement of a tagged particle grows sub-diffusively as $t^{1/2}$, indicating the profound influence crowding can have on the effective speed of transport. This result was first derived by Harris in 1965 [106], with several alternative proofs appearing in later years (see references in [26]).

As is common, we will refer to non-overtaking particle dynamics on the continuum as **single-file diffusion** (SFD), although some authors apply this term also to lattice dynamics. Because SFD is related to the ASEP through the diffusive limit, it is no surprise that advances in solving the ASEP and SFD under various conditions have been made in parallel. For SFD, some highlights include the exact N-

particle solution on the infinite line, and its marginalization to the one-particle distribution [107]; exact solution in a box using the Bethe ansatz [108]; and for time-dependent external forcing [109]. It has been found that, on the infinite line, the $t^{1/2}$ scaling appears only in the finite-density limit, and otherwise a transient regime gives way to diffusive scaling [110]. We shall therefore in this chapter be particularly interested in the case of periodic boundary conditions, which is expected to be analogous to the infinite-line, finite-density scenario in several relevant aspects.

In harmony with the philosophy of Chapter 1, we introduce in this background section the mathematical formulation of SFD via the diffusive limit applied to the ASEP. We then review the exact solution on the ring via the Bethe ansatz. This exercise will illustrate the key role the assumption of identical particles plays in solving the model, and inspire us to pose the question that will drive the further sections of this chapter—what exact results can be derived for non-identical particles?

3.1.2 The diffusive limit of the ASEP

Recall that in the periodic ASEP, each of N particles hops forwards (clockwise) with rate p and backwards (anticlockwise) with rate q, unless the target site is already occupied (hardcore exclusion). For configurations where all particles have at least one empty site ahead and behind them, the system behaves for a short time interval as N non-interacting particles, each of which obeys a master equation

$$\partial_t P_i(n_i, t) = pP_i(n_i - 1, t) - qP_i(n_i + 1, t) - (p + q)P_i(n_i, t), \tag{3.1}$$

with conserved ordering $n_i < n_{i+1}$ (modulo periodicity). The joint probability distribution P_N evolves in this no-collision time interval as $\prod_{i=1}^{N} P_i(n_i)$ does. In the diffusive limit, detailed in Section 1.3.1, we therefore obtain that the continuous probability density ρ_N in a time interval where the particles are far enough apart not to interact evolves as

$$\partial_t \rho_N(\boldsymbol{x}, t) = \sum_{i=1}^{N} \left[-v\partial_{x_i} + D\partial_{x_i}^2\right] \rho_N(\boldsymbol{x}, t), \tag{3.2}$$

with conserved ordering $x_{i+1} > x_i$ and where, for a the lattice constant,

$$v = \lim_{a\to 0} a(p(a) - q(a)), \quad D = \lim_{a\to 0} a^2(p(a) + q(a)). \tag{3.3}$$

Consider now a lattice configuration where all particles are free, except that particle 1 at site $n_1 = n$ is adjacent to particle 2 at site $n_2 = n + 1$. At this configuration, the master equation reads (if we selectively suppress some position arguments for brevity)

$$\begin{aligned}\partial_t P_N(n, n+1, n_3, \ldots, n_N; t) = {} & [pP_N(n-1, n+1) - qP_N(n, n+1)] \\ & + [qP_N(n, n+2) - pP_N(n, n+1)] \\ & + \sum_{i>2}^{N} [pP_N(n, n+1, \ldots, n_i - 1, \ldots) \\ & \quad - qP_N(n, n+1, \ldots, n_i + 1, \ldots)],\end{aligned} \tag{3.4}$$

Expanding in the lattice constant a,

$$\begin{aligned}\partial_t \rho_N(x, x+a, x_3, \ldots, x_N; t) = {} & -ap(a)(\partial_{x_1} - \partial_{x_2})\rho_N(x, x+a) + O(1) \\ & + \sum_{i>2}^{N} [-a(p(a) - q(a))\partial_{x_i} + a^2(p(a) + q(a))\partial_{x_i}^2 \\ & \quad + O(a)]\rho_N(x, x+a).\end{aligned} \tag{3.5}$$

Notice that $ap(a) = D/a + O(1)$, which makes the first term in the right-hand side the one of lowest order, $1/a$. Therefore, multiplying the equation by a and taking $a \to 0$ we find

$$D(\partial_{x_1} - \partial_{x_2})\rho_N(\boldsymbol{x}, t) \mid_{x_1 = x_2} . \tag{3.6}$$

This can be written more suggestively as

$$J_i(\boldsymbol{x}, t) = J_j(\boldsymbol{x}, t) \quad \text{for} \quad x_i = x_j, \tag{3.7}$$

where

$$J_i(\boldsymbol{x}, t) = v\rho_N(\boldsymbol{x}, t) - D\partial_{x_i}\rho_N(\boldsymbol{x}, t) \tag{3.8}$$

is the probability current associated with the motion of particle i, if the other

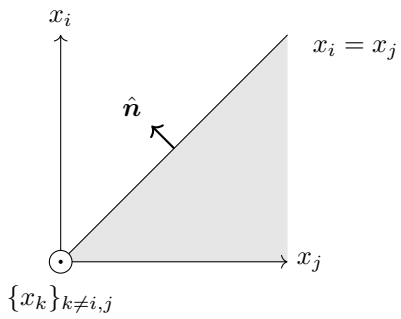

Figure 3.1 *Illustration of the phase-space boundary for SFD*

particles are held fixed. The condition (3.7) states that the probability currents must coincide for any two particles that physically touch. Furthermore, if we interpret the process of N particles in one dimension as one 'super particle' in N dimensions, then the hardcore exclusion constraint between any pair of physical particles becomes an impassable $(N-1)$-dimensional hyperplane for the super particle. At each 'no-crossing' hyperplane $x_i = x_j$ with normal

$$\hat{\boldsymbol{n}} = \frac{1}{\sqrt{2}}(\hat{\boldsymbol{e}}_i - \hat{\boldsymbol{e}}_j), \tag{3.9}$$

there is a reflective boundary condition

$$\hat{\boldsymbol{n}} \cdot \boldsymbol{J}(\boldsymbol{x}, t)|_{x_i = x_j} = 0, \tag{3.10}$$

stating that the total probability current normal to the boundary is at all times zero. The geometry of the situation is illustrated in Figure 3.1.

Just as particles in the ASEP can block each other, but cannot not push, so reflective boundary conditions do not model transfer of momentum. There are subtleties in interpreting exactly how trajectories of reflected diffusions behave at the boundary due to the non-differentiability of Brownian motion; we will discuss this later in Section 6.1.2. Another thing to note is that in the diffusive limit our particles have become point-like, but that this is not essential. An SFD with finite-sized particles is trivially mapped to a system of point-like particles, because the dynamics only depends on the separation between particles, whether measured centre-to-centre for point-like particles, or edge-to-edge for finite-sized particles.

3.1.3 Bethe-ansatz solution of the homogeneous SFD

As noted in Chapter 1, one route to solving the ASEP is via the coordinate Bethe ansatz [17, 111]. But as Elliott Lieb states [112, p.5]: "*In some sense the 'natural' setting for Bethe's ansatz is the continuum (line segment) rather than the lattice because some of the technicalities involved simplify there.*" Let us review how it solves the homogeneous SFD.

The first step in the ansatz is to note that the free FPE (3.2) has elementary solutions $e^{-\lambda(\boldsymbol{k})t}e^{\boldsymbol{k}\cdot\boldsymbol{x}}$ where

$$\lambda(\boldsymbol{k}) = v\mathbf{1}\cdot\boldsymbol{k} - Dk^2, \quad \mathbf{1} = (1,1,\ldots,1)^\top. \tag{3.11}$$

We see that $\lambda(\boldsymbol{k}) = \lambda(\boldsymbol{k}')$ if $\boldsymbol{k}$ and $\boldsymbol{k}'$ only differ by a permutation of their elements. Hence we can take the elementary solutions as $e^{-\lambda(\boldsymbol{k})t}\psi_{\boldsymbol{k}}(\boldsymbol{x})$ where the spatial function is a linear combination of all ways to distribute the N 'momenta' k_j over the N particles:

$$\psi_{\boldsymbol{k}}(\boldsymbol{x}) := \sum_{s\in S_N} A_s e^{\sum_j k_{s_j}x_j} = \sum_{s\in S_N} A_s \prod_j z_{s_j}^{x_j}, \tag{3.12}$$

with $z_i := e^{k_j}$, and S_N the set of permutations on the N-tuple $(1,\ldots,N)$. The central idea of the Bethe ansatz is to suppose that $e^{-\lambda(\boldsymbol{k})t}\psi_{\boldsymbol{k}}(\boldsymbol{x})$ solves not just the free FPE but also the periodicity and the no-crossing boundary conditions through a consistent choice of amplitudes $A_s = A_s(\boldsymbol{k})$ and 'Bethe roots' z_i.

Substituting the Bethe ansatz into the periodicity condition

$$\rho_N(\boldsymbol{x}) = \rho_N(\boldsymbol{x} + L\mathbf{1}), \tag{3.13}$$

with L the ring circumference, one finds that in order to be consistent for all relevant $\boldsymbol{x}$ one must have

$$\frac{A_{cos}}{A_s} = e^{k_{s_N}}, \tag{3.14}$$

where c is the 'cycle' permutation operator that shifts all elements to the right by one:

$$c\circ s = c\circ(s_1,s_2,\ldots,s_N) = (s_N,s_1,\ldots,s_{N-1}). \tag{3.15}$$

In particular, by iterating (3.14) one concludes

$$e^{\sum_j k_j} = 1. \tag{3.16}$$

To satisfy the reflective boundary conditions (3.10) we must have

$$A_s = A_{\tau_{i,i-1}\circ s}, \tag{3.17}$$

where $\tau_{i,i-1}$ swaps the two indicated elements:

$$\tau_{i,i-1} \circ (s_1, s_2, \dots, s_{i-1}, s_i, \dots s_N) = (s_1, s_2, \dots, s_i, s_{i-1}, \dots s_N). \tag{3.18}$$

Applying this relation repeatedly, we realize that $A_s = A$, a constant that may be put to unity. Going back to (3.14) this gives

$$k_j = 2\pi i m_j, \quad m_j \in \mathbb{Z}. \tag{3.19}$$

The general solution is then

$$\rho_N(\boldsymbol{x}, t) = \sum_{m_1=-\infty}^{\infty} \cdots \sum_{m_N=-\infty}^{\infty} c_{m_1 \dots m_N} e^{-[4\pi^2 D \sum_j m_j^2 + 2\pi i v \sum_j m_j]t} \sum_{s \in S_N} e^{2\pi i \sum_j m_{s_j} x_j}, \tag{3.20}$$

where the $c_{\boldsymbol{m}}$ are to be determined form the initial conditions. In particular, let us suppose a localized initial condition

$$\rho_N(\boldsymbol{x}, 0) = \delta(\boldsymbol{x} - \boldsymbol{y}). \tag{3.21}$$

Using the Fourier representation of the delta function we have $c_{\boldsymbol{m}} = e^{-2\pi i \boldsymbol{m}\cdot\boldsymbol{y}}$ and therefore

$$\begin{aligned} \rho_N(\boldsymbol{x}, t|\boldsymbol{y}, 0) &= \sum_{s \in S_N} \prod_{j=1}^{N} \sum_{m_j=-\infty}^{\infty} e^{-[4\pi^2 D m_j^2 + 2\pi i v m_j]t} e^{2\pi i m_j (x_{s_j} - y_j)} \\ &= \sum_{s \in S_N} \prod_{j=1}^{N} \rho_1(x_{s_j}, t|y_j, 0). \end{aligned} \tag{3.22}$$

In the last line we have identified $\rho_1(x, t|y, 0)$ as the solution to the one-particle problem on the ring, starting from position y. Note that while ρ_1 is normalized over $x \in [0, L]$, ρ_N is normalized over all $\boldsymbol{x} \in [0, L]^N$ subject to the constraint

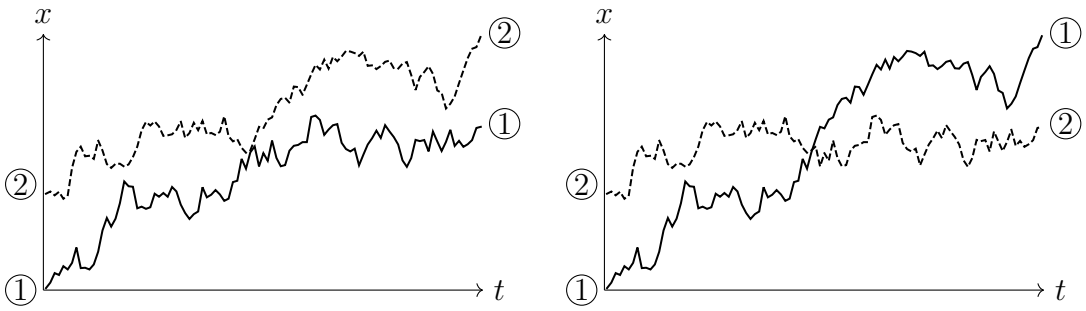

(a) *Reflecting trajectories* **(b)** *Crossing trajectories*

Figure 3.2 *Two non-interacting identical Brownian particles cannot be distinguished at a point of crossing. The left and right scenario therefore have identical probability.*

that $\boldsymbol{x}$ must represent the same particle ordering as $\boldsymbol{y}$.

That the N-particle distribution can be thus constructed from the one-particle distribution follows from the particle-exchange symmetry stemming from the assumption of identical particles: non-crossing trajectories of reflecting particles can be mapped to crossing trajectories of non-interacting particles, as shown in Figure 3.2. This argument was used by Harris in 1965 [106] in his original treatment of single-file diffusion of identical Brownian particles, where the position of the ith particle can be constructed as

$$X_i(t) = i\text{th-max}\{\tilde{X}_1, \ldots, \tilde{X}_N\}, \tag{3.23}$$

for $\{\tilde{X}_j\}_{j=1}^N$ a set of non-interacting Brownian motions.

Next we consider how the solution structure (3.22) breaks down due to the lack of particle-exchange symmetry for a heterogeneous system.

3.1.4 Introducing particle-wise disorder

It is natural to want to consider a SFD system where the particles are not all identical. For instance, a membrane pore may be permeable to several types of ion or molecule. Alternatively, being interested in the behaviour of a tracer particle, one may suppose it is different than all other particles, for example by being selectively driven by an external field. To cover all cases, one ideally would like a solution to the problem with full particle-wise disorder. Therefore, let each particle i diffuse with its individual diffusion coefficient D_i, and with drift

v_i. For the moment, we do not consider space-dependent or particle-separation dependent parameters, although these generalizations are of obvious interest.

The FPE now reads

$$\partial_t \rho_N(\boldsymbol{x}, t) = -\boldsymbol{v} \cdot \nabla \rho_N(\boldsymbol{x}, t) + \nabla \cdot \mathsf{D} \nabla \rho_N(\boldsymbol{x}, t), \tag{3.24}$$

where we have defined $\boldsymbol{v} := (v_1, \ldots, v_N)^\top$ and $\mathsf{D} := \mathrm{diag}\{D_1, \ldots, D_N\}$. The no-crossing boundary conditions amount to

$$(v_i - v_j)\rho_N(\boldsymbol{x}, t)|_{x_i = x_j} = (D_i \partial_{x_i} - D_j \partial_{x_j})\rho_N(\boldsymbol{x}, t)|_{x_i = x_j}. \tag{3.25}$$

The attempt to solve this problem by the Bethe ansatz fails already in the first step: the proposed eigenvalue $\lambda(\boldsymbol{k}) = \boldsymbol{v} \cdot \boldsymbol{k} - \boldsymbol{k} \cdot \mathsf{D}\boldsymbol{k}$ has in general no exchange symmetries for the components of $\boldsymbol{k}$. Then, we cannot build basis functions with enough undetermined coefficients to allow us to solve all the no-crossing boundary conditions.

A second attempt to generalize from the solution of the identical-particles case is to posit again a 'permanantal' (determinant without sign changes [109]) structure for the density. Indeed, this form is more general than the Bethe ansatz, because it solves the identical-particle problem with individual drift $F(x_i, t)$ [109]. We thus posit

$$\rho_N(\boldsymbol{x}, t \mid \boldsymbol{y}, 0) = \frac{1}{Z_N} \sum_s \prod_i \rho_1^{(i)}(x_i, t \mid y_{s_i}, 0), \tag{3.26}$$

where the superscript i on the one-particle density indicates that this function uses the parameters v_i, D_i. (3.26) satisfies the FPE (3.24), but not necessarily the boundary conditions (3.25). Curiously, the ansatz works on the infinite line for arbitrary N if the diffusivities but not the drifts are disordered, as one checks by substitution. However, the normalization constant for the infinite-line solution depends non-trivially and non-symmetrically on the D_i's and cannot be computed analytically for N larger that just a few particles [113]. On the ring the ansatz fails for arbitrary N unless particles are identical.

Having thus moderated our hopes that deriving an exact time-dependent solution is a tractable problem for the fully disordered case on the ring, we focus instead on the lesser challenge of obtaining the exact steady-state distribution and current. Indeed, for the periodic ASEP or TASEP with disordered hopping rates, the

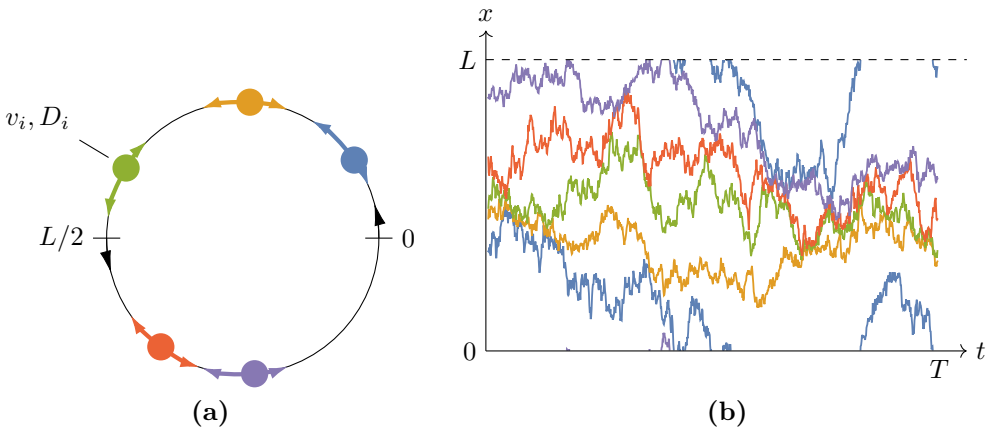

Figure 3.3 *(a) Illustration of heterogeneous single-file diffusion on a ring. (b) Space-time plot of a typical realization. Due to hardcore exclusion, i.e. reflection, the particles' paths do not cross.*

nonequilibrium steady state was derived in the late 90s by a mapping to a zero-range process with site-wise disorder [41–43]. It was then found in the TASEP (no backward hopping) that if the individual forward hopping rates p_i were drawn independently from a power-law $f(p) \sim (p - c)^\gamma$ with support in $[c, 1]$, then platoon-formation—$O(N)$ queue-formation behind the slowest particle—occurs above a critical density of walkers if $\gamma > 0$, in a way mathematically analogous to Bose-Einstein condensation. For the disordered ASEP where hopping occurs in both directions, however, although the steady-state was found analytically, drawing physical consequences from it was difficult due to its complicated dependence on the model parameters [41, 43]. We find in the next section that on the continuum, where some algebraic complexity is reduced, the steady state solution shows that it is the least diffusive particle, not the slowest one, that 'enslaves' the others.

3.2 Heterogeneous single-file diffusion

We reiterate the definition of the model: N particles exist on a ring, each one i moving with constant intrinsic drift velocity v_i and diffusing with diffusivity D_i, unable to overtake any other particle. All together, the positions, velocities and diffusivities are $\boldsymbol{x} = (x_1, \ldots, x_N)^\top$, $\boldsymbol{v} = (v_1, \ldots, v_N)^\top$, and $\mathsf{D} = \mathrm{diag}\{D_1, \ldots, D_N\}$. The probability density (dropping now the N subscript)

is given by the set of equations

$$\begin{cases} \partial_t \rho(\boldsymbol{x},t) + \nabla \cdot \boldsymbol{J}(\boldsymbol{x},t) = 0, & \text{Fokker-Planck equation} \quad (3.27a) \\ \boldsymbol{J}(\boldsymbol{x},t) = \boldsymbol{v}\rho(\boldsymbol{x},t) - \mathsf{D}\nabla\rho(\boldsymbol{x},t), & \text{probability current} \quad (3.27b) \\ \rho(\boldsymbol{x},t) = \rho(\boldsymbol{x} + L\mathbf{1},t), & \text{periodicity} \quad (3.27c) \\ J_i(\boldsymbol{x},t)|_{x_i=x_j} = J_j(\boldsymbol{x},t)|_{x_i=x_j} \quad \forall i,j, & \text{no-crossing b.c.} \quad (3.27d) \\ \rho(\boldsymbol{x},0) = \delta(\boldsymbol{x} - \boldsymbol{x}_0). & \text{initial condition} \quad (3.27e) \end{cases}$$

3.2.1 Exact steady-state solution

The steady-state density $\rho^*(\boldsymbol{x})$ is solved for by an exponential ansatz, similar to how a factorized ansatz solves the lattice version of the model:

$$\rho^*(\boldsymbol{x}) = \frac{1}{Z} e^{\boldsymbol{k}\cdot\boldsymbol{x}} \Theta(\boldsymbol{x}), \tag{3.28}$$

where Θ represents the constraint that particles must appear in the same order on the ring as they do in the initial configuration $\boldsymbol{x}_0$. Assuming without loss of generality that the ordering of particles is $1, 2, 3, \ldots$ (periodically),

$$\Theta(\boldsymbol{x}) = \sum_{j=1}^{N} \theta(x_j - x_{j-1}) \cdots \theta(x_2 - x_1)\theta(x_1 - x_N) \cdots \theta(x_{j+2} - x_{j+1}), \tag{3.29}$$

where θ is Heaviside's step function. The stationary probability current under this ansatz is

$$\boldsymbol{J}^*(\boldsymbol{x}) = (\boldsymbol{v} - D\boldsymbol{k})\rho(\boldsymbol{x}). \tag{3.30}$$

The no-crossing boundary condition (3.27d) requires that

$$v_i - D_i k_i = v_j - D_j k_j, \tag{3.31}$$

which must hence equal some constant, $\bar{v}$, say, independently of the particle index. Therefore

$$k_i = \frac{v_i - \bar{v}}{D_i}. \tag{3.32}$$

The constant $\bar{v}$, which will turn out to be the particles' common net velocity, is determined from the periodicity condition (3.27c), which requires $\sum_i k_i = 0$, and

therefore

$$\bar{v} = \sum_{i=1}^{N} \left(\frac{D_i^{-1}}{\sum_j D_j^{-1}} \right) v_i. \tag{3.33}$$

One can check that (3.28) with (3.32) and (3.33) also satisfies the stationarity condition, $\nabla \cdot \boldsymbol{J}^*(\boldsymbol{x}) = 0$.

It is useful to introduce the effective diffusivity $\overline{D}$ via

$$\frac{1}{\overline{D}} := \sum_{i=1}^{N} \frac{1}{D_i}. \tag{3.34}$$

We can then express (3.33) more suggestively as

$$\frac{\bar{v}}{\overline{D}} = \sum_{i=1}^{N} \frac{v_i}{D_i}. \tag{3.35}$$

$\overline{D}$ also features in the prefactor of the $(t \to \infty)$ mean-square displacement of unbiased random walkers with heterogeneous diffusivities [114, 115].

To prove that $\bar{v}$ is indeed the common net velocity, note that for each particle i it is given by integrating the ith component $J_i^*(\boldsymbol{x})$ of the probability current over phase space, and presently

$$J_i(\boldsymbol{x}) = \bar{v}\rho(\boldsymbol{x}). \tag{3.36}$$

The best strategy to determine the normalization constant of (3.28) is to change variables to the 'gaps' y_i between a particle i and its clockwise neighbour particle $i+1$ (with $N+i$ equivalent to i),

$$y_i := x_{i+1} - x_i. \tag{3.37}$$

The following notational convention is useful:

$$y_{i:j} = y_i + y_{i+1} + y_{i+2} + \ldots + y_j = \begin{cases} \sum_{l=i}^{j} y_l, & i \leq j \\ 0, & i > j \end{cases}. \tag{3.38}$$

We then go from absolute coordinates x_i to gap coordinates via

$$x_i = x_1 + y_{1:i-1}. \tag{3.39}$$

This allows us to rewrite

$$\boldsymbol{k}\cdot\boldsymbol{x} = x_1 \underbrace{\sum_{i=1}^{N} k_i}_{=0} + \sum_{i=1}^{N} k_i y_{1:i-1} = \sum_{i=1}^{N} k_{i+1:N}\, y_i, \tag{3.40}$$

where the last equality follows from writing out the sums in the previous step term by term and summing up the coefficient for each y_i before summing over i. For our convenience, let us define

$$w_i := k_{i+1:N} = -k_{1:i}. \tag{3.41}$$

Then the exact stationary probability distribution may be expressed as

$$\rho^*(\boldsymbol{x}) = \rho_1^*(x_1) \times \rho_{\text{gaps}}^*(\boldsymbol{y}(\boldsymbol{x})) = \frac{1}{L} \times \frac{1}{Z_N(\boldsymbol{w}; L)} \exp[\boldsymbol{w}\cdot\boldsymbol{y}]\delta\left(\sum_{i=1}^{N} y_i - L\right), \tag{3.42}$$

a product of the flat one-particle distribution $(1/L)$ and the gap distribution. Note that the gap distribution factorises into weights $\mathrm{e}^{w_i y_i}$ for each gap, but the gaps are still correlated due to the global constraint that they sum to L, as implied by the delta function. The partition function Z_N is defined

$$Z_N(\boldsymbol{w}; L) := \left(\prod_{i=1}^{N} \int_0^\infty dy_i\, e^{w_i y_i}\right) \delta\left(L - y_{1:N}\right). \tag{3.43}$$

To solve the integrals, we decouple them by applying a Laplace transform on the ring circumference,

$$\begin{aligned}
\tilde{Z}_N(\boldsymbol{w}; s) &:= \int_0^\infty \mathrm{d}L\, e^{-sL} Z_N(\boldsymbol{w}; L) && \text{(3.44a)}\\
&= \int_0^\infty \mathrm{d}y_1 \cdots \mathrm{d}y_N\, e^{\boldsymbol{w}\cdot\boldsymbol{y}} \int_0^\infty \mathrm{d}L\, e^{-sL} \delta(y_i - L) && \text{(3.44b)}\\
&= \prod_{i=1}^{N} \int_0^\infty \mathrm{d}y_i\, e^{(w_i - s)y_i} && \text{(3.44c)}\\
&= \prod_{i=1}^{N} \frac{1}{s - w_i}, && \text{(3.44d)}
\end{aligned}$$

where we have chosen the real part of s larger than any w_i. We perform a partial fraction decomposition

$$\prod_{i=1}^{N} \frac{1}{s - w_i} = \sum_{i=1}^{N} \frac{a_i}{s - w_i}, \tag{3.45}$$

where we can determine that

$$a_i = \prod_{j=1 \neq i}^{N} \frac{1}{w_i - w_j} \tag{3.46}$$

using Heaviside's cover-up method. Inverting the Laplace transform term by term we find the final closed form

$$Z_N(\boldsymbol{w}; L) = \sum_{i=1}^{N} e^{w_i L} \prod_{j=1 \neq i}^{N} \frac{1}{w_i - w_j}. \tag{3.47}$$

3.2.2 An inter-particle ratchet effect

We now study how the distribution of particle properties affects the common net velocity. We can write (3.33) as a weighted sum

$$\bar{v} = \sum_i \alpha_i v_i, \tag{3.48}$$

$$\alpha_i := \frac{\overline{D}}{D_i} = \frac{D_i^{-1}}{\sum_j D_j^{-1}} \geq 0, \quad \sum_i \alpha_i = 1. \tag{3.49}$$

Now consider the D_i to be i.i.d. random variables. The α_i are then *dependent* but still identically distributed, which together with their conservation law implies $[\alpha_i]_D = 1/N$, where $[\cdot]_D$ denotes averaging over the diffusivity disorder. Hence

$$[\bar{v}]_D = \frac{1}{N} \sum_{i=1}^{N} v_i, \tag{3.50}$$

the right-hand side of which is the sample mean over velocities, independently of the diffusivity distribution chosen. In particular, this is the same as for particles with identical diffusivity. If also the v_i are considered i.i.d. random variables, with a well-defined mean u, then

$$[\bar{v}]_{D,v} = u. \tag{3.51}$$

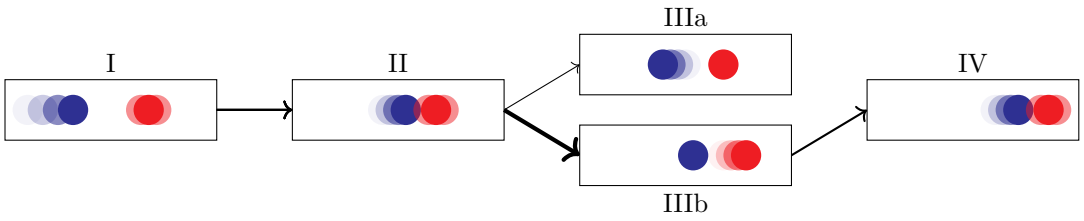

Figure 3.4 *In this illustration of the inter-particle ratchet effect, the blue particle ('shepherd') has positive drift and small diffusivity; the red particle ('sheep') has zero drift and higher diffusivity. I→II: the shepherd catches up with the sheep. II→III: a fluctuation creates a separation, which is more likely the sheep meandering forward (IIIb) than the shepherd backward (IIIa). IIIb→IV: shepherd again catches up. Through rectification, the sheep gets a non-zero net velocity.*

However, the *typical* current $\bar{v}_{\text{typ}}$ may be very different from u, meaning that the current is not self-averaging over the disorder, assuming there is some spread in individual velocities (if all $v_i = u$ then $\bar{v} = u$ independently of the diffusivities). Now, (3.48) is a sum of i.i.d. random variables $R_i = \alpha_i v_i$. It is well known that if the distribution of R has a power-law tail $\sim R^{-(a+1)}$ with $0 < a < 1$, then the sum will be dominated by one particular i, say i^* [18]. The physical significance of this is that particle i^* dictates the current. To illustrate a situation where self-averaging does not occur, assume finite support for the velocity distribution, and consider $\text{Prob}(1/D_i) \sim (D_i)^{a+1}$, $0 < a < 1$, for D_i small, for example by drawing D_i from the appropriate Gamma distribution. Then α_{i^*} will be of order one and $\bar{v} \approx v_{i^*}$. For instance, if the v_i are $\pm|v|$ with equal chance, then the typical current will be either $\approx \pm|v|$, which is different from $[\bar{v}]_{D,v} = 0$.

Turning now to the distribution of particle gaps, ideally one would like to average the exact gap distribution (3.42) over various disorder distributions. However, due to the complexity of *e.g.* the partition function (3.43), this is forbiddingly difficult. Instead, we make progress by assuming a simple case where particle one, say, is dominating, so that $\bar{v} \approx v_1$, whereas the other $N-1$ particles can approximately be treated as having identical parameters v and D. Then

$$\bar{v} = \alpha v_1 + (1-\alpha)v, \quad \alpha = \frac{1}{1 + (N-1)\frac{D_1}{D}}, \tag{3.52}$$

and for the non-dominant particles

$$k_i = \frac{v - \bar{v}}{D} = \frac{v - v_1}{D + (N-1)D_1} =: -k, \tag{3.53}$$

whereas

$$k_1 = (N-1)k \tag{3.54}$$

due to the conservation law $\sum_i k_i = 0$.

We seek the particle density $\nu(x)$ a clockwise distance from the dominant particle one. It is possible, but arduous, to perform the necessary marginalization over the joint position distribution. Fortunately, the exact result can be obtained by the following heuristic argument. We replace the dominant particle with a hard wall moving at fixed velocity $\bar{v}$. A single (v, D)–particle trapped between two hard walls moving at velocity $\bar{v}$ would have spatial distribution $\propto \exp[-((v-\bar{v})/D)x] = \exp[-kx]$, where x is the position relative to the left wall. By the reflection-symmetry of Brownian trajectories [107], identical particles in single file behave as a set of non-interacting particles (as discussed in Section 3.1.3). We therefore expect the density

$$\nu^*(x) = (N-1)\frac{ke^{-kx}}{1-e^{kL}}, \tag{3.55}$$

which can be proved exactly from (3.42) (see the calculations in Section 3.2.3). Without loss of generality we assume $v_1 > v$ so that $1/k > 0$ gives the characteristic length scale over which particles are clustered ahead of particle one. It is thus apparent that when diffusion enters the picture, a 'shepherd' particle that is both fast and has low diffusivity can force 'sheep' particles ahead of it to speed up through a ratchet effect: if a gap opens up between the shepherd and the sheep, it is most likely to be because a sheep diffuses forward than the shepherd diffusing backward. The shepherd is then quick to close the gap. This is illustrated in Figure 3.4. Similarly, a stubborn 'donkey' particle with speed $v_1 < v$ and low diffusion will slow down the faster 'horse carriages' behind it if the horses are more diffusive.

3.2.3 Driven tracers in a passive bath

A typical question in statistical mechanics is to determine the response of an interacting particle system when a force is applied to it. For an equilibrium system experiencing a small perturbation, classical linear response theory governs the outcome. Out of equilibrium, an array of intriguing response phenomena are possible. For example, in the case of a single driven particle, a tracer, which

can overtake the surrounding passive particles with some rate, this parameter separates phases in the tracer current [116], and can enable absolute negative mobility [117].

We investigate the physics of a system of non-overtaking, unbiased, identical particles with diffusivity D, where a subset of particles, tracers, are subjected to an additional force which gives them a constant drift v. This is essentially a two-species SFD, a special case of the fully heterogeneous model whose steady state we have solved. Using (3.57) we can obtain the marginal distribution of the tracers. What, effectively, is the interaction between the tracers as mediated by the interstitial 'bath particles'?

For the heterogeneous SFD it turns out to be possible to explicitly marginalize the stationary distribution over any subset of particles. Select a subset of M particles, with index $\tau_1, \dots, \tau_M$, and let z_i be the gap between particle τ_i and τ_{i+1}. Using the colon summation notation (3.38),

$$z_i = y_{\tau_i:\tau_{i+1}-1}, \tag{3.56}$$

with y_i the gap between particle i and $i+1$, as before. Then

$$\rho^*_{\{\tau\}}(z_1, \dots, z_M) = \left\langle \prod_{i=1}^{M} \delta\left(y_{\tau_i:\tau_{i+1}-1} - z_i\right) \right\rangle \tag{3.57a}$$

$$= \frac{1}{Z_N(w_1, \dots, w_N; L)} \left(\prod_{i=1}^{N} \int_0^L dy_i \, e^{w_i y_i} \right) \delta\left(L - y_{1:N}\right) \prod_{i=1}^{M} \delta\left(y_{\tau_i:\tau_{i+1}-1} - z_i\right) \tag{3.57b}$$

$$= \delta\left(L - z_{1:M}\right) \frac{\prod_{i=1}^{M} Z_{\tau_{i+1}-\tau_i}(w_{\tau_i}, \dots, w_{\tau_{i+1}-1}; z_i)}{Z_N(w_1, \dots, w_N; L)}. \tag{3.57c}$$

For the last step, we note that the product of delta functions decouples the integrals into 'blocks' $[\tau_1, \tau_1 + 1 \dots \tau_2 - 1]$ $[\tau_2, \dots] \cdots [\tau_M, \dots, N]$, each of which by definition recovers a partition function (3.43) for the appropriate arguments.

Let particle τ_n be the nth tracer, in front of which there are b_n bath particles until the next tracer, as shown in Figure 3.5. The total number of tracers is N_T and the bath particles number $N_B = b_{1:N_T} = N - N_T$. Recall the definitions $w_i = k_{i+1:N}$ (3.41) and $k_i = (v_i - \bar{v})/D_i$ (3.32). For a two-species setup (T- and

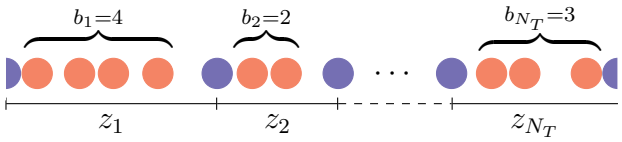

Figure 3.5 *Sketch of driven tracers in a passive medium. Blue balls are tracers and red balls are passive bath particles. The distance between a tracer i and the next is z_i, and there is a number b_i of bath particles in between.*

B-particles), k_i is either

$$k_B =: -k \quad \text{or} \quad k_T = (N_B/N_T)k. \tag{3.58}$$

Since k is the only continuous parameter on which the distribution depends, the assumptions that all particles have diffusivity D, and that $v_T > 0$ whereas $v_B = 0$, imply no loss of generality. Then

$$k = \bar{v}/D = f_T v_T/D > 0, \tag{3.59}$$

where $f_T = N_T/N$ is the fraction of tracers. We need to calculate partition functions of the form

$$Z_{b_n+1}(w_{\tau_n}, \ldots, w_{\tau_n+b_n}; z_n) = \sum_{i=0}^{b_n} \exp[w_{\tau_n+i}\, z_n] \prod_{j=0\neq i}^{b_n} \frac{1}{w_{\tau_n+i} - w_{\tau_n+j}}. \tag{3.60}$$

To this end we write the weight factor in the exponential as

$$\begin{aligned} w_{\tau_n+i} = k_{\tau_n+i+1:N} &= k_{\tau_n+i+1:\tau_{n+1}-1} + k_{\tau_{n+1}:N} \\ &= (-k)(b_n - i) \ + (-k)g_n. \end{aligned} \tag{3.61}$$

By definition, $-kg_n := (N_T - n)k_T + b_{n+1:N_T}k_B$, which, using the expressions for k_T and k_B (3.58), can be written more meaningfully as

$$g_n = \bar{b}n - b_{1:n} = \sum_{m=1}^{n} (\bar{b} - b_m), \tag{3.62}$$

where $\bar{b} = N_B/N_T$ is the average number of consecutive bath particles. Next, the difference of weight factors in the product in (3.60) can be written

$$w_{\tau_n+i} - w_{\tau_n+j} = (-k)(j - i). \tag{3.63}$$

Hence

$$\prod_{j=0\neq i}^{b_n} \frac{1}{w_{\tau_n+i} - w_{\tau_n+j}} = \frac{1}{k^{b_n}} \frac{(-1)^{b_n-i}}{i!(b_n-i)!}. \tag{3.64}$$

Putting these results together,

$$Z_{b_n+1} = \frac{e^{-kg_nz_n}}{k^{b_n}b_n!} \sum_{i=0}^{b_n} (-1)^{b_n-i} e^{-k(b_n-i)z_n} \binom{b_n}{i} \tag{3.65a}$$

$$= \frac{e^{-kg_nz_n}}{b_n!} \left(\frac{1-e^{-kz_n}}{k}\right)^{b_n}. \tag{3.65b}$$

Finally, the tracer gap distribution comes out as

$$\rho^*_{\{\tau\}}(z_1, \ldots, z_{N_T}) = \delta\left(L - \sum_{n=1}^{N_T} z_n\right) \frac{1}{Z_N} \prod_{n=1}^{N_T} \frac{e^{-kg_nz_n}}{b_n!} \left(\frac{1-e^{-kz_n}}{k}\right)^{b_n}. \tag{3.66}$$

If we compare this marginalized distribution to the original distribution (3.42), we see that the structure of a factorization over the particle labels, with a global conservation constraint, is retained, but the functional form of the weight factor is different (*viz.* Z_{b_n+1} *vs.* $\exp[w_n y_n]$). Let us try to interpret the augmented structure of the weight factor.

To understand the origin of the exponential $\exp[-kg_nz_n]$ in the weight factor, we reverse-engineer the SFD of N_T driven particles that in the absence of any intermediate bath particles would result in the distribution

$$\rho^{*\text{no-bath}}(z_1, \ldots, z_{N_T}) = \delta\left(L - \sum_{n=1}^{N_T} z_n\right) \frac{1}{Z^{\text{no-bath}}_{N_T}} \prod_{n=1}^{N_T} e^{-kg_nz_n}. \tag{3.67}$$

Comparing the exponential constant $-kg_n$ with w_n in (3.42) for fixed diffusivity D, we deduce that the effective velocity of the nth tracer in the no-bath model must be

$$u_n = u^{\text{ref}} - \bar{v}b_n = u^{\text{ref}} - [b_n/(1+\bar{b})]v_T, \tag{3.68}$$

where u^{ref} is a reference velocity that cannot be inferred from the stationary distribution alone, but which is not important for our purposes. Thus, a tracer with fewer bath particles ahead of it in the the tracer-and-bath SFD, would in the no-bath mock have a larger (signed) effective velocity u_n. As a result, it

disproportionally compresses the space to its neighbours in the positive direction. This effect grows with the parameter k. For instance, taking $N_T = 2$, if $b_1 > b_2$, then typically z_1 will be large, as tracer two with fewer bath particles in front of it succeeds in compressing the relatively fewer bath particles in front of it until it gets close to tracer one. On the other hand, if all $b_n = N_B/N_T$ there is no heterogeneity and all $g_n = 0$. As one then expects from symmetry, typically all $z_n \approx L/N_T$, and the remaining factor $(1 - e^{-kz_n})^{b_n}/(k^{b_n} b_n!)$ of Z_{b_n+1} determines the distribution $\rho^*_{\{\tau\}}$.

To interpret this remaining factor, consider a single bath particle trapped in a box $[0, L]$ whose boundaries move forward at velocity $\bar{v}$. Its position with respect to the left box boundary would be distributed with cumulative density $q_B(x) \propto 1 - \exp[-kx]$. The probability of finding b_n indistinguishable particles crammed into $[0, z_n]$ would be

$$q_B^{b_n}(z_n)/b_n! \ , \tag{3.69}$$

as we make use of the reflection principle discussed in Section 3.1.3. This is precisely the second factor in the gap size weight Z_{b_n+1}.

Putting the pieces together, we conclude that the full gap distribution (3.66) may be viewed as a product of two subsystems, each of which factorises: one describing a system of tracers without bath particles with heterogeneous effective velocities, and one representing a system of bath particles distributed in boxes, the space between a pair of tracers. The weight for a single gap size z_n is then the product of the weight for gap size z_n in the tracer subsystem multiplied by the probability that b_n bath particles occupy space less than z_n in the bath subsystem. However, these subsystems are correlated through the conservation of space and the global current established cooperatively by all particles.

We close this section by making a comparison to a closely related lattice model [118]. There, symmetric random walkers (bath particles) and totally asymmetric walkers (tracers) move under hardcore exclusion on lattice in continuous time. Ref. [118] considered the ring geometry, for both one and several tracers. For a single driven tracer, an exponentially decaying pile-up of bath particles was found ahead of it: compare (3.55) with $v = 0$, $D > 0$ for the bath particles and $v_1 > 0$, $D_1 = 0$ for the tracer. For a system with several tracers, a cooperation effect was described where the system current grows with the density of tracers, in a way dependent on the tracers' relative placement in between symmetric particles. In

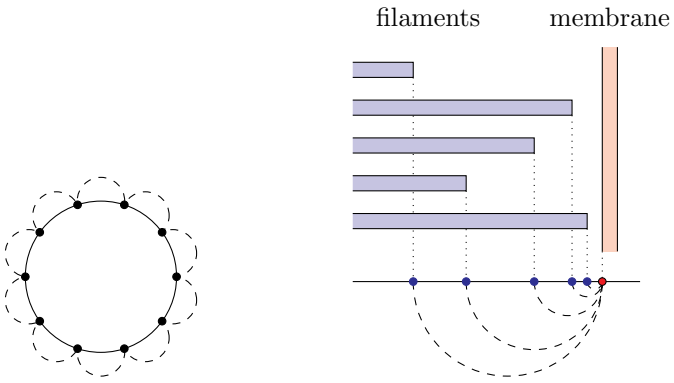

(a) *Periodic SFD* **(b)** *Filament ratchet*

Figure 3.6 *(a) In SFD no particle can cross its neighbour. (b) In the N-filament ratchet, we put the absolute length x_i of the N filaments as mutually non-interacting particles on the real line. Each filament however cannot cross through the membrane, represented as particle $N+1$.*

our present continuum model, according to (3.48) the common net velocity will be

$$\bar{v} = f_T v_T, \tag{3.70}$$

independent of the placement of the tracers. It should be observed, however, that our model is the continuum limit of the lattice model with a non-totally asymmetric walker as the tracer, which in the limit makes an important difference, as otherwise the tracers move deterministically and ratchet the bath particles with one hundred percent efficiency, giving $\bar{v} = v_T$. The conclusion is that there are interesting effects in the lattice models, relating to finite size and fluctuations in totally asymmetric movement, that do not survive the continuum limit.

3.2.4 Comparison to a filament ratchet

A recent paper by Wood et al. [44] introduced a model for membrane growth, where a number of filaments grow by polymerization and extend a membrane in the growth direction through a ratchet effect (Figure 3.6b). A central result of that work was the solution for the net velocity $\bar{v}_{\mathrm{M}}$ of the membrane, when the N filaments have constant nominal growth rates $v_{\mathrm{F},i}$ with a diffusivity $D_{\mathrm{F},i}$, whereas

the membrane has a nominal velocity $-v_{\mathrm{M}}$ and diffusivity D_{M}:

$$\bar{v}_{\mathrm{M}} = \frac{-v_{\mathrm{M}} D_{\mathrm{M}}^{-1} + \sum_{i=1}^{N} v_{\mathrm{F},i}^{(i)} D_{\mathrm{F},i}^{-1}}{D_{\mathrm{M}}^{-1} + \sum_{i=1}^{N} D_{\mathrm{F},i}^{-1}}. \tag{3.71}$$

This expression is formally identical to (3.33) derived for single-file diffusion. What explains this correspondence?

Figure 3.6 shows how to map the Brownian many-filament ratchet to a particle problem directly comparable to SFD, but not equivalent to it. The absolute positions of the membrane and each filament correspond to the positions of particles on an infinite line. In either figure panel, two particles that cannot cross one another are connected by a dashed line. For the periodic domain shown on the left, it is intuitively clear that if the 'graph of mutual exclusions' (dots and dashed lines in Figure 3.6) includes all particles—whether any given two particles are directly connected—then they are geometrically constrained to have a common net velocity. This is true also for the infinite line, with the caveat that the model parameters must allow the particles to cluster rather than disperse in the long-time limit.

While the mapping of the filament ratchet to a particle problem similar to SFD convinces us that the two models will behave similarly, it does not make the quantitative agreement of the net velocity formulas immediately obvious. That this formula applies to all the models with a connected graph of mutual exclusions follows from making the ansatz $J_i^*(\boldsymbol{x}) = \bar{v}_i \rho^*(\boldsymbol{x})$. Then the no-crossing condition $J_i = J_j$ on the boundary immediately implies $\bar{v}_i = \bar{v}_j$, so that all particles in the graph of mutual exclusion must have the same $\bar{v}$.

In the next section we shall attempt to generalize as far as possible the SFD model while retaining the property that makes its steady state exactly solvable. The key, as it turns out, is the property that no particle is able to overtake all others.

3.3 A quasi-one-dimensional generalization

3.3.1 Hard spheres in a d-dimensional tube

As a generalization of the heterogeneous SFD, we consider spherical particles in a d-dimensional tube which has one periodic axial direction $\hat{\boldsymbol{r}}$ (although an

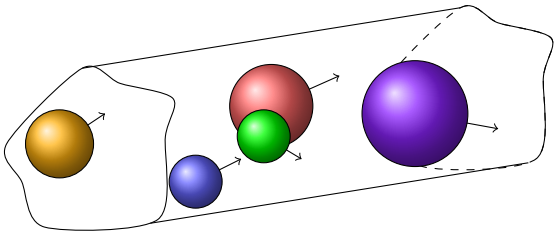

Figure 3.7 *Tube geometry: constant cross section and periodic or infinite axial direction. Illustrated here for dimension $d = 3$.*

infinite tube can be treated as well [4]), and a cross section that is constant along the tube, but otherwise of arbitrary shape, as illustrated in Figure 3.7. As before, the particles interact mutually by volume exclusion, but now also with the boundary of the tube. Based on the insights of Section 3.2.4, we make the critical assumption that no particle is able to overtake all others, a property we will refer to as **quasi-one-dimensionality**.

The motion of the particles is overdamped, so that the system is fully described by the spatial coordinates $\mathbf{Q}^{(i)}(t)$ in d dimensions for the particles $i = 1, \ldots, N$. We organize these into

$$\mathbf{X}(t) := \begin{pmatrix} \mathbf{Q}^{(1)}(t) \\ \vdots \\ \mathbf{Q}^{(N)}(t) \end{pmatrix} = \sum_{i=1}^{N} \hat{\boldsymbol{e}}_i \otimes \mathbf{Q}^{(i)}(t), \tag{3.72}$$

where $\hat{\boldsymbol{e}}_i$ is a standard basis vector of $\mathbb{R}^N$ and $\otimes$ is the Kronecker product. $\mathbf{X}(t)$ is thus an $(N \times d)$-dimensional diffusion process evolving in a state space $\Gamma \subset \mathbb{R}^{d \times N}$ representing all possible configurations of the particles inside the tube geometry. We first construct the phase space Γ and then define the stochastic dynamics.

The tube is a space $\mathcal{Q} \subset \mathbb{R}^d$ within which there is a unique axial direction $\hat{\boldsymbol{r}}$ that is unbounded whereas all other directions are bounded. The boundary $\partial\mathcal{Q}$ is axially constant, meaning that a boundary normal $\hat{\boldsymbol{n}}$ is always orthogonal to $\hat{\boldsymbol{r}}$. Each particle $i \in \{1, 2, \ldots, N\}$ inherits a copy $\mathcal{Q}^{(i)}$ of $\mathcal{Q}$, so $\Gamma \subset \mathcal{Q}^{(1)} \times \cdots \times \mathcal{Q}^{(N)}$. The inclusion is strict because we have yet to exclude phase space points forbidden due to physical volume exclusion. The components of $\boldsymbol{x} \in \Gamma$ are organized like (3.72) as

$$\boldsymbol{x} = \sum_{i=1}^{N} \hat{\boldsymbol{e}}_i \otimes \boldsymbol{q}^{(i)}, \tag{3.73}$$

with $\boldsymbol{q}^{(i)} \in \mathcal{Q}^{(i)}$. The part of the phase space boundary $\partial\Gamma$ arising from particle i touching the tube walls at $\boldsymbol{q} \in \partial\mathcal{Q}$ is

$$B_i(\boldsymbol{q}) := \{\boldsymbol{x} \in \Gamma : ||\boldsymbol{q}^{(i)} - \boldsymbol{q}|| = r_i\}, \tag{3.74}$$

where r_i is the radius specific to particle i. We compute the boundary normal by applying the gradient operator

$$\nabla := \nabla_{\boldsymbol{x}} = \sum_{i=1}^{N} \hat{\boldsymbol{e}}_i \otimes \nabla_{\boldsymbol{q}^{(i)}} \tag{3.75}$$

to the locus $||\boldsymbol{q}^{(i)} - \boldsymbol{q}|| = r_i$. The result is

$$\hat{\boldsymbol{n}}(\boldsymbol{x}) = \hat{\boldsymbol{e}}_i \otimes \delta\hat{\boldsymbol{q}}(\boldsymbol{x}), \quad \boldsymbol{x} \in B_i(\boldsymbol{q}), \tag{3.76}$$

with $\delta\hat{\boldsymbol{q}} = (\boldsymbol{q}^{(i)} - \boldsymbol{q})/r_i$ as illustrated in Figure 3.8a. Note that $\delta\hat{\boldsymbol{q}} \cdot \hat{\boldsymbol{r}} = 0$.

For mutual volume exclusion between particles we consider an 'interaction graph' G where a node represents a particle, and an edge between two particles signifies that they mutually exclude volume. For example, as per Figure 3.6, SFD on a ring has the complete graph, and the filament ratchet a star graph. If $(i, j) \in G$, then we must introduce a boundary surface

$$B_{ij} := \{\boldsymbol{x} \in \Gamma : ||\boldsymbol{q}^{(i)} - \boldsymbol{q}^{(j)}|| = r_i + r_j\}. \tag{3.77}$$

Its normal is

$$\hat{\boldsymbol{n}}(\boldsymbol{x}) = \frac{1}{\sqrt{2}}(\hat{\boldsymbol{e}}_i - \hat{\boldsymbol{e}}_j) \otimes \delta\hat{\boldsymbol{q}}(\boldsymbol{x}), \quad \boldsymbol{x} \in B_{ij}, \tag{3.78}$$

where $\delta\hat{\boldsymbol{q}} \propto \boldsymbol{q}^{(i)} - \boldsymbol{q}^{(j)}$, illustrated in Figure 3.8b.

The full phase space boundary is then

$$\partial\Gamma = \left(\bigcup_{i,\boldsymbol{q}\in\partial Q} B_i(\boldsymbol{q})\right) \bigcup \left(\bigcup_{(i,j)\in G} B_{ij}\right). \tag{3.79}$$

Γ is the restriction of $\mathbb{R}^{d\times N}$ that lies inside or on this boundary. If the geometry of the tube and particles is such that a certain ordering of particles is logically preserved, e.g. as is necessarily the case for SFD ($d = 1$ and G the complete graph) then the process is confined to the sector $\Gamma_{\boldsymbol{x}_0} \subset \Gamma$ containing the initial

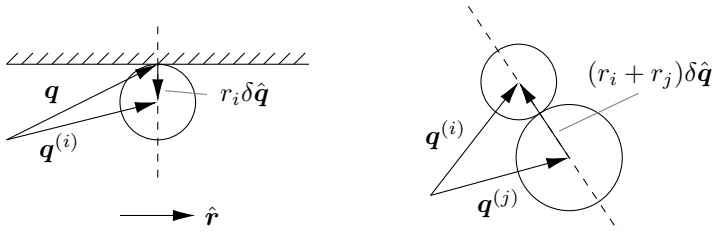

(a) *Particle–boundary* **(b)** *Particle–particle*

Figure 3.8 *Direction of incidence $\delta\hat{\boldsymbol{q}}$ for collision between particle i and a wall or between particle i and particle j.*

condition $\boldsymbol{x}_0$.

We now define the dynamics of the diffusion $\mathbf{X}(t)$ through the Fokker-Planck equation (1.92) and additional boundary conditions. The FPE reads

$$\partial_t \rho(\boldsymbol{x}, t) + \nabla \cdot \boldsymbol{J}(\boldsymbol{x}, t) = 0, \quad \boldsymbol{x} \in \Gamma \setminus \partial\Gamma, \tag{3.80}$$

using the probability current

$$\boldsymbol{J}(\boldsymbol{x}, t) = \boldsymbol{v}(\boldsymbol{x})\rho(\boldsymbol{x}, t) - \mathsf{D}(\boldsymbol{x})\nabla\rho(\boldsymbol{x}, t). \tag{3.81}$$

The above matches the Stratonovich rather than Ito SDE with drift $\boldsymbol{v}$ if D depends on $\boldsymbol{x}$ (see Section 1.3.2). On the phase space boundary $\partial\Gamma$ the process is reflected, meaning that the probability flow through boundaries must vanish:

$$\boldsymbol{J}(\boldsymbol{x}, t) \cdot \hat{\boldsymbol{n}}(\boldsymbol{x}) = 0, \quad \boldsymbol{x} \in \partial\Gamma. \tag{3.82}$$

The remaining conditions differ depending on whether the tube is periodic or infinite. In the following we will suppose periodicity (details on the infinite tube can be found in my publication [3]). Thus we require invariance under translating the whole system by one axial period L,

$$\rho(\boldsymbol{x} + L\boldsymbol{\tau}, t) = \rho(\boldsymbol{x}, t), \tag{3.83}$$

where we have defined the global translation vector

$$\boldsymbol{\tau} := \sum_{i=1}^{N} \hat{\boldsymbol{\tau}}^{(i)} = \mathbf{1} \otimes \hat{\boldsymbol{r}}, \tag{3.84}$$

constructed from the vectors

$$\hat{\boldsymbol{\tau}}^{(i)} := \hat{\boldsymbol{e}}_i \otimes \hat{\boldsymbol{r}} \tag{3.85}$$

that move particle i forward axially a unit distance, keeping all else constant. By assuming more strongly translation invariance of the model parameters, *i.e.* axial homogeneity of the tube,

$$\boldsymbol{v}(\boldsymbol{x} + r\boldsymbol{\tau}) = \boldsymbol{v}(\boldsymbol{x}), \quad \mathsf{D}(\boldsymbol{x} + r\boldsymbol{\tau}) = \mathsf{D}(\boldsymbol{x}), \quad r \in \mathbb{R}, \tag{3.86}$$

we obtain (3.83) automatically.

It is in relation to periodicity that the quasi-one-dimensionality supposition comes into play. Had we not assumed this property, then there would exist some possible trajectory $\omega_T = \{\boldsymbol{x}(s)\}_{s=0}^{T}$, where $\boldsymbol{x}(T) = \boldsymbol{x}(0) + L\hat{\boldsymbol{\tau}}^{(i)}$, that is, where particle i has made one net circulation of the tube, while the other particles have not. Then $\boldsymbol{x}(0)$ and $\boldsymbol{x}(T)$ are physically the same due to tube periodicity and therefore we would need to impose,

$$\rho(\boldsymbol{x} + L\hat{\boldsymbol{\tau}}^{(i)}, t) = \rho(\boldsymbol{x}, t). \tag{3.87}$$

However, if no such trajectory exists for particle i, *i.e.* it is prevented by other particles from circling the tube by itself, then there is no logical reason to impose (3.87). We will see that the absence of (3.87) as a necessary constraint is key to the solvability of the model.

3.3.2 Solving for the irreversible drift: an inverse FPE solution method

There exist certain 'potential conditions' [45, 119, 120] which make the steady state of a diffusion process solvable in terms of an explicit integral—*i.e.* the process is integrable. In this section we derive these conditions in an unconventional way, tailored to the presence of a phase space boundary.

A steady-state density $\rho^*(\boldsymbol{x})$ for the process $\mathbf{X}(t)$ in its original coordinates exists, as guaranteed by the boundedness of the phase space of the periodic tube. Let us define the function $\boldsymbol{u}(\boldsymbol{x})$ by

$$\boldsymbol{J}^*(\boldsymbol{x}) = \boldsymbol{u}(\boldsymbol{x})\rho^*(\boldsymbol{x}). \tag{3.88}$$

Assuming $\rho^*(\boldsymbol{x}) > 0$ for all $\boldsymbol{x}$, this definition is unambiguous. We take the components of $\mathbf{X}(t)$ to be even under time reversal. Then $\boldsymbol{u}(\boldsymbol{x})$ is called the **irreversible drift** [45] for reasons to become clear. Eliminating $\boldsymbol{J}^*$ for $\boldsymbol{u}$ in the stationary versions of (3.80), (3.81), and (3.82) the result is

$$\begin{cases} \nabla \cdot \boldsymbol{u}(\boldsymbol{x}) + \boldsymbol{u}(\boldsymbol{x}) \cdot \nabla \ln \rho^*(\boldsymbol{x}) = 0, & \boldsymbol{x} \in \Gamma \setminus \partial\Gamma, \quad (3.89a) \\ \nabla \ln \rho^*(\boldsymbol{x}) = \mathsf{D}^{-1}(\boldsymbol{x})[\boldsymbol{v}(\boldsymbol{x}) - \boldsymbol{u}(\boldsymbol{x})], & \boldsymbol{x} \in \Gamma \setminus \partial\Gamma, \quad (3.89b) \\ \boldsymbol{u}(\boldsymbol{x}) \cdot \hat{\boldsymbol{n}}(\boldsymbol{x}) = 0, & \boldsymbol{x} \in \partial\Gamma. \quad (3.89c) \end{cases}$$

By combining (3.89a) and (3.89b) we can view (3.89) as a closed equation for $\boldsymbol{u}(\boldsymbol{x})$,

$$\begin{cases} \nabla \cdot \boldsymbol{u}(\boldsymbol{x}) + \boldsymbol{u}(\boldsymbol{x}) \cdot \mathsf{D}^{-1}(\boldsymbol{x})[\boldsymbol{v}(\boldsymbol{x}) - \boldsymbol{u}(\boldsymbol{x})] = 0, & \boldsymbol{x} \in \Gamma \setminus \partial\Gamma, \quad (3.90a) \\ \boldsymbol{u}(\boldsymbol{x}) \cdot \hat{\boldsymbol{n}}(\boldsymbol{x}) = 0, & \boldsymbol{x} \in \partial\Gamma, \quad (3.90b) \end{cases}$$

together with the definition of a potential $\Phi_{\boldsymbol{u}}(\boldsymbol{x})$ by

$$\nabla \Phi_{\boldsymbol{u}}(\boldsymbol{x}) = -\mathsf{D}^{-1}(\boldsymbol{x})[\boldsymbol{v}(\boldsymbol{x}) - \boldsymbol{u}(\boldsymbol{x})]. \quad (3.91)$$

This potential generates the probability density through

$$\rho^*(\boldsymbol{x}) = \frac{e^{-\Phi_{\boldsymbol{u}}(\boldsymbol{x})}}{Z}, \quad (3.92)$$

following the path-independent integration

$$\Phi_{\boldsymbol{u}}(\boldsymbol{x}) - \Phi_{\boldsymbol{u}}(\boldsymbol{c}) = \int_{\boldsymbol{c}}^{\boldsymbol{x}} d\boldsymbol{y} \cdot \nabla \Phi_{\boldsymbol{u}}(\boldsymbol{y}). \quad (3.93)$$

The assumed existence and uniqueness of the steady state has two important consequences: For given $\boldsymbol{v}(\boldsymbol{x})$ and $\mathsf{D}(\boldsymbol{x})$, the problem (3.90) (together with any additional boundary conditions, like periodicity) has a unique solution $\boldsymbol{u}(\boldsymbol{x})$ that makes (3.91) integrable.

But we can turn the logic around. Instead of fixing $\boldsymbol{v}(\boldsymbol{x})$ and $\mathsf{D}(\boldsymbol{x})$, which implies a specific $\boldsymbol{u}(\boldsymbol{x})$, we assume that $\boldsymbol{u}(\boldsymbol{x})$ is of a certain form, which imposes restrictions on which $\boldsymbol{v}(\boldsymbol{x})$ and $\mathsf{D}(\boldsymbol{x})$ are consistent with this form. The constraints on $\boldsymbol{v}(\boldsymbol{x})$ and $\mathsf{D}(\boldsymbol{x})$ are that they must solve (3.90) for the given $\boldsymbol{u}(\boldsymbol{x})$ while also making (3.91) integrable. For example, $\boldsymbol{u} = \boldsymbol{0}$ is always a trivial solution of (3.90). Equation (3.91) then states the well-known integrability conditions for a detailed-balanced system, as stated in Section 1.3.3.

Observe that given a process $\mathbf{X}(t)$ with drift vector $\boldsymbol{v}(\boldsymbol{x})$ and diffusion $\mathsf{D}(\boldsymbol{x})$ leading to irreversible drift $\boldsymbol{u}(\boldsymbol{x})$, we can always define a new process $\mathbf{X}'(t)$ with the same steady state density but satisfying detailed balance: take this process to have $\boldsymbol{v}'(\boldsymbol{x}) := \boldsymbol{v}(\boldsymbol{x}) - \boldsymbol{u}(\boldsymbol{x})$ and $\mathsf{D}'(\boldsymbol{x}) := \mathsf{D}(\boldsymbol{x})$. The trivial solution $\boldsymbol{u}' = \mathbf{0}$ is then the most general one because it assumes no new integrability conditions on $\boldsymbol{v}'(\boldsymbol{x})$ and $\mathsf{D}'(\boldsymbol{x})$ in order to solve for $\Phi'_{\boldsymbol{u}'}(\boldsymbol{x})$ ($= \Phi_{\boldsymbol{u}}(\boldsymbol{x})$). This shows that the irreversible drift $\boldsymbol{u}(\boldsymbol{x})$ is the part of the drift without which detailed balance holds, but the density remains the same, hence its name.

To make progress with the tube problem, consider the following ansatz for the solution $\boldsymbol{u}(\boldsymbol{x})$:

(i) The direction $\hat{\boldsymbol{u}}$ is constant

(ii) The magnitude $u(\boldsymbol{x}) \not\equiv 0$ is invariant in the $\hat{\boldsymbol{u}}$-direction,

$$u(\boldsymbol{x}) = u(\boldsymbol{x} + s\hat{\boldsymbol{u}}) \quad \text{for all } s \in \mathbb{R}. \tag{3.94}$$

The condition (i) is motivated by the observation that there may exist such a *constant* direction that solves all the reflective boundary conditions. We make the ansatz

$$\hat{\boldsymbol{u}} \propto \sum_i \hat{u}_i \hat{\boldsymbol{\tau}}^{(i)} \tag{3.95}$$

(recall (3.85)). Then $\hat{\boldsymbol{u}} \cdot \hat{\boldsymbol{n}} = 0$ for the normal (3.76) of particle-wall boundary, and holds as well for the normal (3.78) of the particle$_i$-particle$_j$ boundary if

$$\hat{u}_i = \hat{u}_j. \tag{3.96}$$

Let us assume that all particles are connected in the graph of mutual exclusions, but not necessarily that the graph is complete. Then it follows that $\hat{\boldsymbol{u}} = \hat{\boldsymbol{\tau}}$.

The condition (ii) has the effect that $\nabla \cdot \boldsymbol{u}(\boldsymbol{x}) = \hat{\boldsymbol{u}} \cdot \nabla u(\boldsymbol{x}) = 0$. Then $u(\boldsymbol{x})$ can be solved for algebraically from (3.90a) as

$$u(\boldsymbol{x}) = \frac{\hat{\boldsymbol{u}}^\top \mathsf{D}^{-1}(\boldsymbol{x}) \boldsymbol{v}(\boldsymbol{x})}{\hat{\boldsymbol{u}}^\top \mathsf{D}^{-1}(\boldsymbol{x}) \hat{\boldsymbol{u}}}. \tag{3.97}$$

For condition (ii) to hold, we would generically require

$$\boldsymbol{v}(\boldsymbol{x} + s\hat{\boldsymbol{u}}) = \boldsymbol{v}(\boldsymbol{x}), \quad \mathsf{D}(\boldsymbol{x} + s\hat{\boldsymbol{u}}) = \mathsf{D}(\boldsymbol{x}), \quad \text{for all } s \in \mathbb{R}. \tag{3.98}$$

Since $\hat{\boldsymbol{u}} = \hat{\boldsymbol{\tau}}$, the above simply states translation invariance which was already assumed.

With this trial solution, we have

$$\nabla\Phi_{\boldsymbol{u}}(\boldsymbol{x}) = -\mathsf{H}(\boldsymbol{x})\boldsymbol{v}(\boldsymbol{x}), \quad \mathsf{H}(\boldsymbol{x}) = \mathsf{D}^{-1}(\boldsymbol{x}) - \frac{\mathsf{D}^{-1}(\boldsymbol{x})\hat{\boldsymbol{u}} \otimes \hat{\boldsymbol{u}}^{\top}\mathsf{D}^{-1}(\boldsymbol{x})}{\hat{\boldsymbol{u}}^{\top}\mathsf{D}^{-1}(\boldsymbol{x})\hat{\boldsymbol{u}}}. \tag{3.99}$$

The matrix $\mathsf{H}(\boldsymbol{x})$ is symmetric and $\mathsf{H}(\boldsymbol{x})\hat{\boldsymbol{u}} = \boldsymbol{0}$. We have implicitly assumed that this potential exists, which may be difficult to satisfy but for $\boldsymbol{v}, \mathsf{D}$ chosen constant or with a rather artificial $\boldsymbol{x}$-dependence.

If the system is *not* quasi-one-dimensional, then we must also satisfy (3.87). For instance, with constant model parameters, we will find $\rho^*(\boldsymbol{x}) \propto \exp[\boldsymbol{v}^{\top}\mathsf{H}\boldsymbol{x}]$. The condition is then that

$$\boldsymbol{v}^{\top}\mathsf{H}\boldsymbol{\tau}^{(i)} = 0, \tag{3.100}$$

for every particle i that is able to overtake every other particle. Generically, these constraints cannot be accommodated because they overdetermine the components of the irreversible drift. Logically, assumptions (i) or (ii) on $\boldsymbol{u}$ will be violated. Then, we cannot solve (3.89) by algebraic means. A trivial case where (3.100) can in fact be solved, is when the particles have the same drift $\boldsymbol{v} = v\hat{\boldsymbol{u}}$ which is then only in the axial direction. Then we have a flat steady state. As seen directly from (3.89), a flat density $\rho^* = 1/|\Gamma|$ with current $\boldsymbol{v}(\boldsymbol{x})/|\Gamma|$ occurs whenever $\boldsymbol{v}(\boldsymbol{x}) \cdot \hat{\boldsymbol{n}}(\boldsymbol{x}) = 0$ and $\nabla \cdot \boldsymbol{v}(\boldsymbol{x}) = 0$, *i.e.* when $\boldsymbol{u}(\boldsymbol{x}) = \boldsymbol{v}(\boldsymbol{x})$.

3.3.3 The generalized diffusion ratchet effect

We now seek the expression for the net velocity $\bar{v}_i$ of particle i in the axial direction of the tube. Consider first the net number $\bar{n}_i(r)$ of crossings per unit time of particle i at a cross-section of the tube at axial distance r. We define the hypersurface $S_r^{(i)}$ in Γ given by $\boldsymbol{q}^{(i)} \cdot \hat{\boldsymbol{r}} = r$ and whose normal is $\hat{\boldsymbol{n}} = \nabla(\boldsymbol{q}^{(i)} \cdot \hat{\boldsymbol{r}}) = \hat{\boldsymbol{\tau}}^{(i)}$. It corresponds to all configurations where the ith particle is a distance r down the tube. Then $\bar{n}_i(r)$ is given by integrating the probability flow across $S_r^{(i)}$, *i.e.* by integrating $\boldsymbol{J}^*(\boldsymbol{x}) \cdot \hat{\boldsymbol{n}}$ over all $\boldsymbol{x} \in S_r^{(i)}$:

$$\bar{n}_i(r) = \int_{S_r^{(i)}} d\boldsymbol{x}\, \hat{\boldsymbol{\tau}}^{(i)} \cdot \boldsymbol{J}^*(\boldsymbol{x}) \tag{3.101a}$$

$$= \int_\Gamma d\boldsymbol{x}\, \delta(\boldsymbol{q}^{(i)} \cdot \hat{\boldsymbol{r}} - r) \hat{\boldsymbol{\tau}}^{(i)} \cdot \boldsymbol{J}^*(\boldsymbol{x}). \tag{3.101b}$$

The net velocity is given by the ring circumference times the net number of circulations per unit time, hence

$$\bar{v}_i = L \times \frac{1}{L} \int_0^L dr\, \bar{n}_i(r) \tag{3.102a}$$

$$= \int_\Gamma d\boldsymbol{x}\, \hat{\boldsymbol{\tau}}^{(i)} \cdot \boldsymbol{J}^*(\boldsymbol{x}) \tag{3.102b}$$

$$= \left\langle \hat{\boldsymbol{\tau}}^{(i)} \cdot \boldsymbol{u}(\boldsymbol{x}) \right\rangle. \tag{3.102c}$$

When, as we found before, $\boldsymbol{u} = u\hat{\boldsymbol{\tau}}$, all $\bar{v}_i = \bar{v}$ are identical, with the final result

$$\bar{v} = \frac{\boldsymbol{\tau}^\top \mathsf{D}^{-1} \boldsymbol{v}}{\boldsymbol{\tau}^\top \mathsf{D}^{-1} \boldsymbol{\tau}}. \tag{3.103}$$

This case has a special interpretation because it represents the situation where a change of variables $\mathbf{X}(t) \to \mathbf{X}'(t) = \mathbf{X}(t) - \boldsymbol{u}t$ into a moving frame brings about detailed balance relative to it.

In the simple case where all particles diffuse (i) independently, (ii) identically, and (iii) isotropically, the common net velocity is simply

$$\bar{v} = \hat{\boldsymbol{r}} \cdot \frac{1}{N} \sum_i \boldsymbol{v}^{(i)}, \tag{3.104}$$

as for unconfined, non-interacting particles. Whenever any of these three conditions is violated, there is a non-trivial dependence of the common net velocity on the diffusion matrix. It is difficult to think of a scenario in which the diffusion of the particles is correlated, so let us therefore focus on conditions (ii) or (iii).

Particle disorder

As we did for the one-dimensional SFD, let us consider N particles with constant, individual drift vectors $\boldsymbol{v}^{(i)}$ and diffusion matrices $\mathsf{D}^{(i)}$. Then

$$\boldsymbol{v} := \sum_{i=1}^N \hat{\boldsymbol{e}}_i \otimes \boldsymbol{v}^{(i)} \tag{3.105}$$

and

$$\mathsf{D} := \sum_{i=1}^{N} \hat{\boldsymbol{e}}_i \hat{\boldsymbol{e}}_i^{\top} \otimes \mathsf{D}^{(i)}. \tag{3.106}$$

The common net velocity evaluates via (3.103) to

$$\bar{v} = \frac{\sum_{i=1}^{N} \hat{\boldsymbol{r}}^{\top} (\mathsf{D}^{(i)})^{-1} \boldsymbol{v}^{(i)}}{\sum_{i=1}^{N} \hat{\boldsymbol{r}}^{\top} (\mathsf{D}^{(i)})^{-1} \hat{\boldsymbol{r}}}. \tag{3.107}$$

Assuming no spatial noise correlation or anisotropy, the individual diffusion matrices further reduce to

$$\mathsf{D}^{(i)} = D_i \mathbb{1}_d, \tag{3.108}$$

where $\mathbb{1}_d$ is the $d \times d$ identity matrix. One can then see that the component of $\boldsymbol{v}^{(i)}$ that is orthogonal to the axial direction $\hat{\boldsymbol{r}}$ will not matter, so let us assume $\boldsymbol{v}^{(i)} = v_i \hat{\boldsymbol{r}}$. Then

$$\bar{v} = \sum_i \alpha_i v_i, \quad \alpha_i = \frac{1/D_i}{\sum_j 1/D_j}, \tag{3.109}$$

which is identical to the one dimensional result (3.48).

Spatial anisotropy and correlations

To isolate the effect of spatial anisotropy and correlation, we consider for simplicity just a single particle in a two-dimensional tube. We let the axial direction be x from 0 to L (periodic) and the vertical direction y from $-H$ to H. Assuming nothing but axial translation invariance we write

$$\boldsymbol{v}(y) = \begin{pmatrix} v_1(y) \\ v_2(y) \end{pmatrix}, \quad \mathsf{D}(y) = \begin{pmatrix} D_1(y) & C(y) \\ C(y) & D_2(y) \end{pmatrix}. \tag{3.110}$$

We suppose that the direction of the irreversible drift is $\hat{\boldsymbol{\tau}} = (1, 0)^{\top}$, which turns out to be exactly true. Then $\mathbb{H}$ in (3.99) is

$$\mathsf{H}(y) = \begin{pmatrix} 0 & 0 \\ 0 & 1/D_2(y) \end{pmatrix}, \tag{3.111}$$

and

$$\nabla\Phi(x,y) = -\begin{pmatrix} 0 \\ v_2(y)/D_2(y) \end{pmatrix}. \tag{3.112}$$

Clearly this potential always exists, because the problem has been reduced to one bounded dimension. From (3.97)

$$u(y) = v_1(y) - \frac{C(y)}{D_2(y)} v_2(y). \tag{3.113}$$

Putting this into (3.102)

$$\bar{v} = \langle v_1 \rangle - \int_0^L dx \int_{-H}^H dy\, C(y) \frac{v_2(y)}{D_2(y)} \frac{e^{-\Phi(y)}}{Z} \tag{3.114a}$$

$$= \langle v_1 \rangle - \int_0^L dx \int_{-H}^H dy\, C(y) \frac{d}{dy} \frac{e^{-\Phi(y)}}{Z} \tag{3.114b}$$

$$= \langle v_1 \rangle - \int_{-H}^H dy\, r(y) \frac{d}{dy} \rho_2(y). \tag{3.114c}$$

Here $\rho_2(y)$ is the probability that the particle is at a height y. After integration by parts,

$$\bar{v} = \langle v_1 \rangle - [C(H)\rho_2(H) - C(-H)\rho_2(-H)] + \langle C' \rangle\,. \tag{3.115}$$

There are thus three distinct components to the axial current. The first comes from the axial drift, but depends implicitly on the vertical drift and diffusion via $\rho_2(y)$. It is independent of C, however; the strength of the noise component which drives the particles in both directions. The remaining components only exist for $C \neq 0$. Furthermore, they depend on a broken symmetry about the tube midline $y = 0$: in the presence of the symmetries

$$v_2(y) = v_2(-y), \quad D_2(y) = D_2(-y), \quad C(y) = C(-y), \tag{3.116}$$

we find simply $\bar{v} = \langle v_1 \rangle$. The term in square brackets in (3.115) relates directly to what transpires at the boundaries. The last term depends on how C varies in the bulk and not at all on reflection at the boundary: we could have a process with zero probability of reaching the boundary and still observe this term.

3.4 Summary and discussion

We began by studying the heterogeneous SFD, a disordered one-dimensional model. To understand something deeper about what makes the steady state of this model solvable we generalized it to higher dimensions. The key property was quasi-one-dimensionality, which constrains particles to have the same net velocity in the long-time limit. Associated with this is an irreversible drift that coincides with a unique direction in phase space that encounters no boundaries. We derived the conditions on the model parameters (drift and diffusivity) for which the solution follows this form. In the case of spatially independent parameters, on which we have mostly focussed, we saw that relative to a frame of reference that moves at the common net velocity of particles, the system satisfies detailed balance. This explains the simple form of the solution. It is more than an 'equilibrium system on wheels', however, as the velocity of the metaphorical cart arises non-trivially from microscopic interactions between the particles.

The main practical result of this chapter is the description of the diffusion ratchet effect. Many ratchet effects in nonequilibrium physics have been previously revealed. Iconic studies of a single particle ratcheted by an asymmetric potential [121, 122] have been complemented by descriptions of inherently many-body ratchet phenomena, *e.g.* collectively induced asymmetric ratchet potentials in magnetic vortices in superconducting films [123], density-dependent current reversals [124, 125], and active matter motion rectified by asymmetric obstacles [126]. What makes the present inter-particle ratchet effect an interesting addition to this list is that it can arise in a static, structureless environment, only due to heterogeneity in particle properties and the simplest of particle interaction, hardcore exclusion.

3.5 Epilogue: run-and-tumble particles revisited

To close off this chapter, and part of the thesis, let us reconnect with the RTPs of the previous chapter. Consider the heterogeneous SFD where $\boldsymbol{v} = v\boldsymbol{\sigma}$, $\sigma_i \in \{+1, -1\}$, and $\mathsf{D} = D\mathbb{1}$. This describes the spatial behaviour of a thermal N-RTP while in the 'orientation sector' $\boldsymbol{\sigma}$. Can its stationary distribution can be found by an ansatz inspired by the SFD solution? We now know that an approximate

solution in the limit of low tumbling rate is

$$\rho^*_{\boldsymbol{\sigma}}(\boldsymbol{x}) \approx \frac{1}{2^N}\rho^{*\mathrm{SFD}}(\boldsymbol{x})|_{\boldsymbol{v}=v\boldsymbol{\sigma}}, \tag{3.117}$$

as the relaxation time within each orientation sector is much faster than the typical jump times between sectors. For arbitrary tumbling rates, we cannot expect to construct the solution directly from $\rho^{*\mathrm{SFD}}$, however. Below we sketch an approach to a solution based on generalizing the exponential ansatz for the SFD steady state in a way suggested by the 2-particle solution method in [102]. Unfortunately, in the end we shall see that determining whether this ansatz produces the right functional form is in itself very difficult.

The forward generator of the full thermal N-RTP process, *i.e.* including tumbling, is the 'matrix-differential operator' $\mathcal{W}$ with elements

$$\mathcal{W}_{\boldsymbol{\sigma}',\boldsymbol{\sigma}}(\nabla) = \delta_{\boldsymbol{\sigma}',\boldsymbol{\sigma}}\mathcal{L}^\dagger_{\boldsymbol{\sigma}}(\nabla) + \mathbb{T}_{\boldsymbol{\sigma}',\boldsymbol{\sigma}}, \tag{3.118}$$

where

$$\mathcal{L}^\dagger_{\boldsymbol{\sigma}}(\nabla) = -v\boldsymbol{\sigma}\cdot\nabla + \nabla\cdot\mathsf{D}\nabla \tag{3.119}$$

is the FP generator of the SFD corresponding to orientation sector $\boldsymbol{\sigma}$, and $\mathbb{T}$ is the 'tumble matrix' with elements,

$$\mathbb{T}_{\boldsymbol{\sigma}',\boldsymbol{\sigma}} = \omega\sum_{i=1}^{N}(\delta_{\boldsymbol{\sigma}',\theta_i\boldsymbol{\sigma}} - \delta_{\boldsymbol{\sigma}',\boldsymbol{\sigma}}), \tag{3.120}$$

where θ_i is the orientation-flip operator on particle i. Writing ∇ as a vector argument of $\mathcal{W}$ and $\mathcal{L}$ will soon prove its utility. Within each orientation sector we impose the no-crossing boundary conditions of the SFD, namely

$$v(\sigma_i - \sigma_j)\rho^*_{\boldsymbol{\sigma}}(\boldsymbol{x})|_{x_i=x_j} = D(\partial_{x_i} - \partial_{x_j})\rho^*_{\boldsymbol{\sigma}}(\boldsymbol{x})|_{x_i=x_j}. \tag{3.121}$$

Using Dirac notation for the orientation space, we write the steady state density as $|\rho^*(\boldsymbol{x})\rangle$. The stationary condition is

$$\mathcal{W}(\nabla)|\rho^*(\boldsymbol{x})\rangle = 0, \tag{3.122}$$

for all $\boldsymbol{x}$. Furthermore we have the periodicity constraint, which we can extend

to a general translation invariance for the steady state as

$$|\rho^*(\boldsymbol{x} + r\mathbf{1})\rangle = |\rho^*(\boldsymbol{x})\rangle, \quad r \in \mathbb{R}. \tag{3.123}$$

Generalizing the exponential ansatz used for the SFD steady state, consider functions of the form

$$|\phi_{\boldsymbol{k}}(\boldsymbol{x})\rangle := e^{\boldsymbol{k}\cdot\boldsymbol{x}}|A(\boldsymbol{k})\rangle \tag{3.124}$$

for which

$$\mathcal{W}(\nabla)|\phi_{\boldsymbol{k}}(\boldsymbol{x})\rangle = e^{\boldsymbol{k}\cdot\boldsymbol{x}}\mathcal{W}(\boldsymbol{k})|A(\boldsymbol{k})\rangle. \tag{3.125}$$

If we choose $|A(\boldsymbol{k})\rangle = |A_i(\boldsymbol{k})\rangle$, one of a number of vector in the nullspace of $\mathcal{W}(\boldsymbol{k})$ indexed by i, *i.e.*

$$\mathcal{W}(\boldsymbol{k})|A_i(\boldsymbol{k})\rangle = 0, \tag{3.126}$$

then $|\phi_{\boldsymbol{k}}(\boldsymbol{x})\rangle$ satisfies stationarity. We then build an ansatz

$$|\rho^*(\boldsymbol{x})\rangle = \sum_{\boldsymbol{k}\in\mathcal{K}}\sum_i c_i(\boldsymbol{k})|\phi_{\boldsymbol{k},i}(\boldsymbol{x})\rangle = \sum_{\boldsymbol{k}\in\mathcal{K}} e^{\boldsymbol{k}\cdot\boldsymbol{x}}\sum_i c_i(\boldsymbol{k})|A_i(\boldsymbol{k})\rangle, \tag{3.127}$$

where $\mathcal{K}$ is some set of $\boldsymbol{k}$'s that we must choose appropriately—this is the critical aspect of the approach. If the set $\mathcal{K}$ is diverse enough, there is some hope that the ansatz contains enough coefficients $c_i(\boldsymbol{k})$ that they can be consistently chosen so as to satisfy the no-crossing conditions (3.121).

Possible values of $\boldsymbol{k}$ are constrained in several other ways. For (3.125) to have a non-trivial solution, we must require

$$\det \mathcal{W}(\boldsymbol{k}) = 0. \tag{3.128}$$

Symmetries of $\mathcal{W}(\boldsymbol{k})$ can also be exploited, *e.g.* $\mathcal{W}_{\boldsymbol{\sigma}',\boldsymbol{\sigma}}(\boldsymbol{k}) = \mathcal{W}_{-\boldsymbol{\sigma}',-\boldsymbol{\sigma}}(-\boldsymbol{k})$, so that

$$\det \mathcal{W}(-\boldsymbol{k}) = 0. \tag{3.129}$$

Thus if $\boldsymbol{k} \in \mathcal{K}$, then $-\boldsymbol{k} \in \mathcal{K}$. To satisfy the translation invariance we must also

have

$$\mathbf{1} \cdot \boldsymbol{k} = 0. \tag{3.130}$$

To make progress, a further ansatz that limits the set $\mathcal{K}$ is required. We may suppose a particular structural form of $\boldsymbol{k}$'s, *e.g.* $\boldsymbol{k} = k(\hat{\boldsymbol{e}}_i - \hat{\boldsymbol{e}}_j)$, or $\boldsymbol{k} = k\boldsymbol{\sigma}$ for some spin vector $\boldsymbol{\sigma}$, and then apply all symmetries of the generator repeatedly to this basic form until the set closes.

For the 2-RTP problem we can without loss of generality put $\boldsymbol{k} = k(+1, -1)$, and a small number of possible k follow from (3.128). These are indeed enough to produce the legitimate stationary distribution [102]. I have attempted the three-body problem, with one ansatz that's analytically tractable, $\boldsymbol{k} = k(\hat{\boldsymbol{e}}_i - \hat{\boldsymbol{e}}_j)$. There is no option but to painstakingly enumerate the set $\mathcal{K}$ based on this ansatz, and to find explicitly all the corresponding $|A\phi_{\boldsymbol{k},i}\rangle$, and then attempt solving for the $c_i(\boldsymbol{k})$'s via the no-crossing conditions. Going through with this, I find no consistent solution. A more complicated structure for $\boldsymbol{k}$ that mixes all three particle coordinates would be next to try, but probably also unmanageable, algebraically.

An exact N-RTP steady state remains elusive, whether on the lattice or continuum.

Part II

Dynamical large deviations

Chapter 4

Background on dynamical large deviations

4.1 Introduction

4.1.1 From the statistics of states to the statistics of trajectories

Equilibrium statistical mechanics centres on the interplay between statistical ensembles, *i.e.* between different probability distributions over microstates of an N-particle dynamical system. Let us recall some key features:

- There is a microcanonical ensemble, where every microstate x has the identical energy per particle $E(x)/N = \varepsilon$:

$$P^{\text{micro}}(x) \propto P^{\text{prior}}(x)\delta(E(x)/N - \varepsilon) \tag{4.1}$$

  In particular, Boltzmann's postulate of equal a priori probabilities states that the prior distribution is uniform if there are no additional conservation laws beside particle number and energy.

- Einstein's theory of microcanonical fluctuations [9] holds that for a macroscopic observable M, the likelihood of observing at a given time a value m,

different from the typical m^*, is

$$P^{\text{micro}}(M = m) \approx e^{N[s_B(m) - s_B(m^*)]}, \tag{4.2}$$

where $S_B(m) = N s_B(m) = \ln \Omega(m)$ is the *extensive* macroscopic Boltzmann entropy associated with counting the number $\Omega(m)$ of microstates compatible with $M = m$.

- There is a canonical ensemble of fixed *mean* energy per particle $\bar{\varepsilon}$ controlled by an inverse temperature $\beta = 1/k_B T$:

$$P^{\text{cano}}(x) = \frac{1}{Z} e^{-\beta N \varepsilon(x)}. \tag{4.3}$$

The partition function

$$Z = \sum_x e^{-\beta N \varepsilon} \tag{4.4}$$

defines the free energy density via

$$f = -(N\beta)^{-1} \ln Z. \tag{4.5}$$

for which we can systematically derive the cumulants of the energy in the canonical ensemble, through

$$\langle \varepsilon \rangle = \partial_\beta (\beta f), \tag{4.6a}$$

$$\langle N(\varepsilon - \bar{\varepsilon}) \rangle = -\partial_\beta^2 (\beta f), \tag{4.6b}$$

and so on for higher cumulants.

- The canonical distribution can be derived by Jaynes' MaxEnt principle of maximizing the Gibbs entropy $S_G(E) = -k_B \sum_x P(x) \ln P(x)$ under the constraint $\langle \epsilon \rangle = \bar{\varepsilon}$. The temperature enters as a Lagrange multiplier that is tuned to $1/T = (\mathrm{d}S_G/\,\mathrm{d}E)(N\bar{\varepsilon})$ to furnish $\bar{\varepsilon}$.

- The variance of fluctuations in the canonical ensemble typically scales as $N^{-1/2}$. Unless close to a thermodynamic phase transition, in the thermodynamic limit $N \gg 1$, the microcanonical and canonical ensembles are equivalent. In particular, one can derive the equivalence by showing that the Boltzmann and Gibbs entropies converge in this limit. The basis

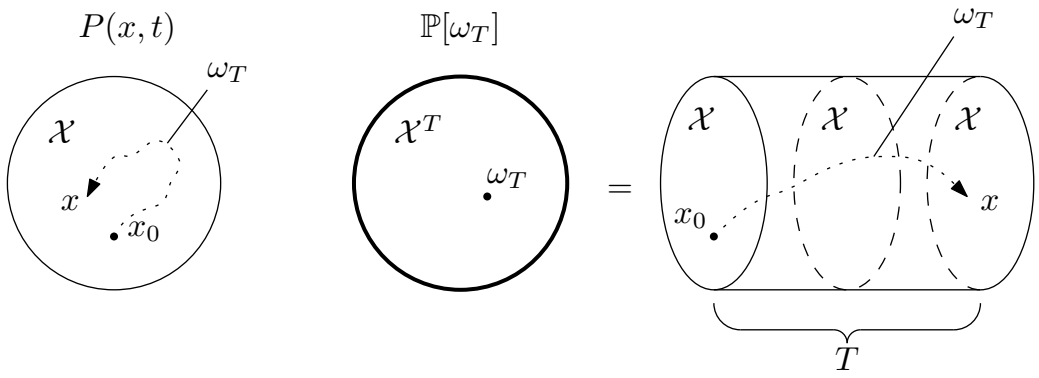

Figure 4.1 *Sketch of the conceptual leap from the statistics of microstates x, with time-dependent distributions $P(x,t)$, to the statistics of trajectories ω_T of a given duration T, with a path-distribution $\mathbb{P}[\omega_T]$.*

for the deviation is Stirling's formula

$$N! \approx N^N e^{-N} \tag{4.7}$$

applied to to combinatorial expression Ω.

- Equilibrium phase transitions are associated with non-convexity of entropy *vs.* energy, and of non-analyticity of free energy density *vs.* temperature.

These properties are all unified by the mathematical **theory of large deviations**: the study of small probabilities that are exponentially rare with some large parameter [9, 30] (*cf.* (4.1) and (4.3) *vs.* N). While physicists have implicitly been using large deviation methods since the days of Boltzmann, its development as a rigorous mathematical discipline began in the 1930s in the study of extensions of the central limit theorem by Cramér, with major contributions in the 70s by Donsker and Varadhan to the modern formulation of the subject, and in the context of Markov processes [127–129], and by Fredlin and Wentzell for noise-perturbed dynamical systems [130] (see [9, 30] for further historical references). In equilibrium statistical physics, the large deviation framework was developed and popularized by Ellis [131] and others. It seems, however, that the biggest impact of large deviation theory on the mainstream of statistical physics has been in recent decades in relation to nonequilibrium Markov processes. By applying these mathematical tools in that context, one rediscovers rather wholesale the mathematical structure of equilibrium statistical mechanics, but with some novel features.

The conceptual leap required to apply large deviation theory to nonequilibrium

processes, is to go from the statistics of microstates to the statistics of microscopic trajectories in phase space (Figure 4.1). A trajectory view of (stochastic) dynamics has been pursued from a variety of perspectives: by Feynman and Kac in their development of path integrals for quantum mechanics and Brownian motion [132, 133]; in the 'thermodynamic formalism' of Ruelle for chaotic dynamical systems [134–136]; by Jaynes in an extension of his MaxEnt principle to MaxCal ('maximum caliber'), where a path-wise entropy is maximized with constraints [137–139]; in stochastic thermodynamics where heat and work are defined at the trajectory level [34, 35, 140].

To apply large deviation theory to trajectory ensembles, one must identify a large parameter. This can be the reciprocal of a small noise amplitude ϵ (*e.g.* inverse carrying capacity in a biological population process, or $\hbar$ in the semi-classical limit), the number N of independent copies of a process; or the observation time T of a single process. In particular, the large deviations from typical behaviour in Markov processes in the limit of long observation times is what we shall refer to as **dynamical large deviation theory** (DLDT). By 'long' we mean observation times longer than any relevant relaxation time scale of the process. For quantities such as the occupation time of a state, the current across a reference point, or the total entropy production, or a particle-density profile, sustained deviations from their typical values for long times should therefore be thought of as **steady-state fluctuations**.

The interest in microscopic, kinetic approaches to NESSs growing from the late 80s, has incentivized the development of dynamical large deviation theory to deal with steady-state fluctuations, because classical fluctuation results, such as the Onsager reciprocity relations and fluctuation-dissipation theorems, are based on a symmetry between the response to a small external perturbation from equilibrium and the statistics of spontanesouly generated equilibrium fluctuations, and do not extend to strongly nonequilibrium processes [141]. A seminal result on nonequilibrium fluctuations coming from DLDT is the Gallavotti-Cohen symmetry [142–144] that underlies the asymptotic fluctuation theorem, relating the probability of observing over long time an entropy production rate σ to observing $-\sigma$. Soon after, this result could be refined and generalized to a host of finite-time fluctuation relations [33–35, 140, 145]. These do not necessarily use large deviation theory, but follow from the trajectory-view also underlying DLDT of comparing a dynamical event, *e.g.* the generation of an amount $T\sigma$ of entropy, between the original process, and some auxiliary process. In DLDT,

the latter is a process that makes $T\sigma$ typical in the long-time limit, whereas in stochastic thermodynamics is it the time-reversed process. More recently, much attention has been given to 'thermodynamic uncertainty relations' derived by large deviation techniques [36, 146, 147]. These relations bound the long-time fluctuations of currents, and give universal trade-offs between accuracy and dissipation for nanoscale processes.

DLDT has thus been pivotal in uncovering universal results for nonequilibrium Markov processes, but it is just as much a practical tool for understanding sustained steady-state fluctuations in specific models. Firstly, it provides methods to calculate rates of exponential decay in likelihood of sustained fluctuations with long observation times, in particular via the spectral approach of Donsker and Varadhan. Secondly, it provides the construction of an effective process that adds 'control forces' to the original dynamics, such that a chosen fluctuation is made typical. The trajectories responsible for a fluctuation can in this way be probed. The effective process construction is relatively recent, although it has precedents in the study of Brownian bridges, absorbing processes conditioned on non-extinction, and quasi-potentials in Freidlin-Wentzell theory [28]. It has been applied to currents in the ASEP [52, 148] and zero-range process [149, 150], activity in models of kinetically constrained glasses [66, 151], Ising model [27], and birth-death processes [152–154], and occupation times in simple diffusion processes [29, 49, 50]. The techniques underlying the effective process are central to reweighting methods for sampling rare events [155–157]. The effective process is also the result of a long-time MaxCal principle, used to infer nonequilibrium microscopic dynamics from macroscopic dynamical constraints, as brought to the fore by R.M.L Evans in application to sheared fluids [158–160].

The purpose of this chapter is to derive in some detail the DLDT that will be put to use in specific models in subsequent chapters. We first look at a simple example to fix ideas, and then develop the formalism based on the modern literature.

4.1.2 A motivating example

Consider the simplest of diffusion processes:

$$dX(t) = \sqrt{2D}dW(t). \tag{4.8}$$

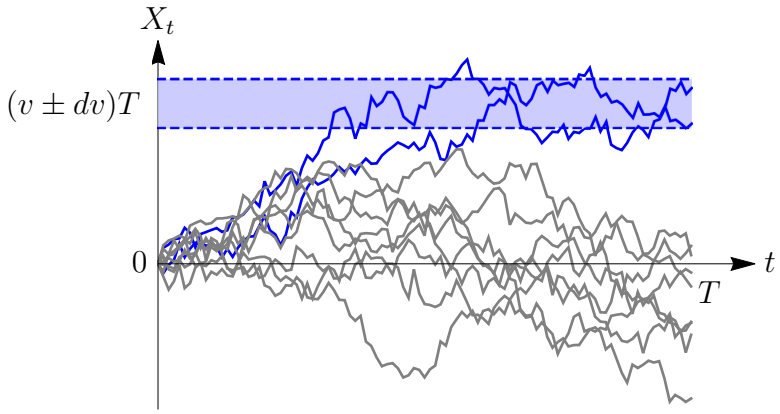

Figure 4.2 *Trajectories of duration T for a symmetric random walker in one dimension. Trajectories that satisfy $V_T \in v \pm \mathrm{d}v$ are highlighted in blue, and constitute (a few realizations of) the constrained trajectory sub-ensemble.*

Let us ask for the probability that we observe a non-typical value v of the net drift defined as

$$V_T = \frac{X_T - X_0}{T} \tag{4.9}$$

over a long observation time T. In this simple case we know the exact answer $P_T(v) := \mathbb{P}[V_T = v]$ for any v:

$$P_T(v) = \left(\frac{T}{4\pi D}\right)^{1/2} e^{-\frac{v^2 T}{4D}} = \exp[-TI(v) + o(T)]. \tag{4.10}$$

This probability exhibits an exponential scaling form with T. The quadratic function $I(v) = v^2/4D$ reflects the fact that V_T is a sum of independent increments drawn from a Gaussian distribution. In countless other examples, the same exponential scaling form is found for some observable like V_T, but the corresponding I may be only be locally quadratic around its minimum, with its tails then quantifying the large deviations from the the predictions of the central limit theorem. The so-called **rate function** I is thus a quantity of central concern in describing rare fluctuations.

We may furthermore want to know what the trajectories ω_T of duration T look like that realize any particular value v for V_T. Their likelihoods are given by the conditioned path probability distribution $\mathbb{P}[\{X(t)\}_{t=0}^{T} = \omega_T \mid V_T = v]$. Conceptually, this corresponds to the subset of possible trajectories that satisfy the constraint (Figure 4.2). Consider applying a drift field of strength v to the

original process to obtain a new process

$$\mathrm{d}\hat{X}(t) = v\,\mathrm{d}t + \sqrt{2D}\,\mathrm{d}W(t). \tag{4.11}$$

The typical trajectories of $\hat{X}(t)$ achieve a net velocity v, and we may suspect that in the limit of long times, these are precisely the trajectories of the constrained path ensemble.

After presenting in this chapter the tools that formalize and prove this intuition, we shall return to the velocity fluctuations of the biased diffusion in Section 5.1.1 as a simple example of the application of the theory. In the following, we give first a general introduction to large deviation theory, and then take the approach of Chapter 1 of deriving fundamental theory for jump processes (Section 4.2), and subsequently transposing the results to diffusion processes (Section 4.3).

4.1.3 Large deviation basics

Suppose we have a random variable A_T depending on a 'large' parameter T. In subsequent sections we will have observation time of a process in mind for T, but T could alternatively be a physical system size, or the reciprocal of a small model parameter. For simplicity we will think of A_T as taking scalar values, but the ideas introduced below are easily extended to more complicated objects, like vector- or function-valued random variables. In many relevant cases, A_T satisfies a **large deviation principle** defined by the scaling form

$$P_T(a) := \mathbb{P}[A_T = a] = e^{-TI(a)+o(T)}. \tag{4.12}$$

The **rate function**[1] $I(a)$ quantifies how rapidly a fluctuation a becomes improbable as the parameter T increases. $I(a)$ is necessarily a semi-positive function, and its zeroes correspond to those values of a which are typical as $T \to \infty$, in the sense that $P_T(a)$ concentrates on these values in the limit.

The rate function is intimately related to the **scaled cumulant generating function**, or SCGF, defined by

$$\Lambda(s) := \lim_{T\to\infty} \frac{1}{T} \ln \left\langle e^{sTA_T} \right\rangle. \tag{4.13}$$

[1] As often done in physics, we bypass the rigorous mathematical treatment of defining upper and lower rate functions and proving convergence to a shared limit [30].

It generates the long-time cumulants of A_T through

$$\Lambda'(0) = \lim_{T\to\infty} \langle A_T \rangle \,, \tag{4.14a}$$

$$\Lambda''(0) = \lim_{T\to\infty} T[\langle A_T^2 \rangle - \langle A_T \rangle^2], \tag{4.14b}$$

and so on. To relate the SCGF and rate function, we insert the large deviation principle (4.12) into the expectation in (4.13),

$$\Lambda(s) = \lim_{T\to\infty} \frac{1}{T} \ln \int \mathrm{d}a \, e^{[sa - I(a)]T + o(T)}. \tag{4.15a}$$

In the limit of large T the integral is sharply peaked around the maximum value of its integrand and can be evaluated by the saddle-point method,

$$\int \mathrm{d}a \, e^{[sa - I(a)]T + o(T)} = \exp\left[\max_a \{sa - I(a)\}T + o(T)\right]. \tag{4.16}$$

Hence we find that

$$\Lambda(s) = \max_a \{sa - I(a)\}. \tag{4.17}$$

This is the form of a **Legendre-Fenchel** (LF) transform from I to Λ [9, 161] (see Figure 4.3). Such a transform always produces a convex function. If I is known to be convex, the transform is its own self-inverse, so that

$$I(a) = \max_s \{sa - \Lambda(s)\} = s^*(a)a - \Lambda(s^*(a)), \tag{4.18}$$

where $s^*(a) = I'(a)$ is the maximizer. If we have no *a priori* guarantee that I will exist and be convex, we may consult the **Gärtner-Ellis theorem**, which in its simplified form states that if $\Lambda(s)$ exists and is continuously differentiable in s, then the large deviation principle for A_T exists and the rate function is given by (4.18) [9]. In the event the rate function is not convex, (4.18) gives the convex envelope of the rate function.

Suppose that $A_T = A(B_T)$, a function of a different random variable B_T that satisfies a large deviation principle with known rate function $J(b)$. Then the door is open to deriving the large deviation elements, *viz.* SCGF and rate function, for A_T from $J(b)$. Using the large deviation principle for B_T in the definition of the

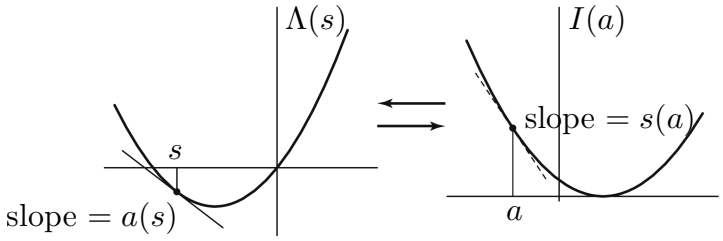

(a) *If $I(a)$ has slope $s(a)$ at a, its* LF *transform $\Lambda(s)$ has slope a at $s(a)$. For convex function the transform is self-inverse.*

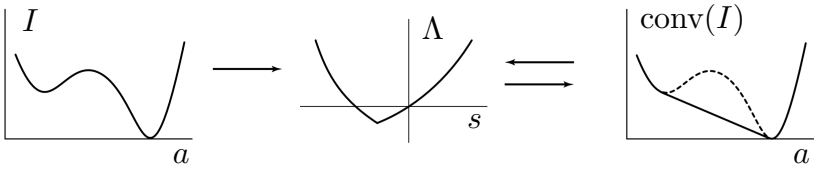

(b) *If $I(a)$ is not locally convex in some range $a \in [a_0, a_1]$, then the* LF *transform has a singularity with slopes a_0 and a_1 from each side. The* LF *transform is then not self-inverse but yields the convex envelope.*

Figure 4.3 *The Legendre-Fenchel transform between* SCGF *and rate function. Adapted from [9].*

SCGF $\Lambda(s)$ of A_T,

$$\Lambda(s) = \lim_{T\to\infty} \frac{1}{T} \ln \int \mathrm{d}b\, e^{[sA(b)-J(b)]T+o(T)}, \tag{4.19}$$

which upon saddle-point evaluation of the integral gives the **Laplace principle**

$$\Lambda(s) = \max_b \{sA(b) - J(b)\} = sA(b^\dagger(s)) - J(b^\dagger(s)), \tag{4.20}$$

where $b^\dagger(s)$ is the maximizer. The rate function $I(a)$ can also be given a variational form with respect to $J(b)$. Consider

$$\mathbb{P}[A_T = a] = \int_{\{b:A(b)=a\}} \mathrm{d}b\, \mathbb{P}[B_T = b]. \tag{4.21}$$

Inserting the respective large deviation principles and evaluating the integrals using the saddle-point method we obtain the **contraction principle**

$$I(a) = \min_b \{J(b) : A(b) = a\} = J(b^*(a)), \tag{4.22}$$

where $b^*(a)$ is the minimizer. We can perform the constrained minimization (4.22) using a Lagrange multiplier that with foresight we call s. Then we first

find the b that *minimizes* $J(b) - sA(b)$, which must be $b^\dagger(s)$ that according to (4.20) *maximizes* $sA(b) - J(b)$. Then we must tune the Lagrange parameter s to satisfy the constraint $A(b^\dagger(s)) = a$. Assume a *unique* value $s^\dagger(a)$ accomplishes this. Then

$$I(a) = J(b^\dagger(s^\dagger(a))) \tag{4.23a}$$
$$= s^\dagger(a)a - \Lambda(s^\dagger(a)). \tag{4.23b}$$

Comparing with (4.18) and (4.22) we conclude that the optimizers are related by

$$s^\dagger(a) = s^*(a), \quad b^\dagger(s^\dagger(a)) = b^*(a). \tag{4.24}$$

If the function A is not bijective, we can consider A_T to be a variable at a lower 'level' than B_T. That is, the large deviations of lower-level random variables can be obtained from a higher-level random variable through contraction.

4.2 Dynamical large deviations from the Level 2.5 perspective

4.2.1 Path probabilities for jump processes

We let $X(t)$ be an ergodic jump process on some countable state space $\mathcal{X} \ni x, y, z, \ldots$, as in Chapter 1. Consider for this process a particular realization, path, or trajectory, from time $t = 0$ to T that we shall denote $\omega_T = \{x(t)_{t=0}^T\}$. The trajectory is sufficiently described by the jump times t_i and the states $x_i = x(t_i)$ jumped to at those times, for $i = 1, \ldots, N$, where the number of jumps N may differ between trajectories. We use the convection that $t_0 := 0$, x_0 is the initial state, and $t_{N+1} := T$ (*i.e.* $T - t_N$ represents the final time interval in which no jump occurs, at least with probability one).

As a basis for developing dynamical large deviation theory, we construct a path-probability measure, which, with some abuse of notation, we will write as $\mathbb{P}[\omega_T]\mathcal{D}[\omega_T] := \mathbb{P}[\{X(t)\}_{t=0}^T \in \mathcal{C}(\omega_T)]$ where $\mathcal{C}(\omega_T)$ is a small 'cylinder set' of

trajectories surrounding ω_T in the space of trajectories. In this notation

$$\int \mathcal{D}[\omega_T]\mathbb{P}[\omega_T] = 1, \tag{4.25}$$

i.e. we formally represent summing over all possible trajectories by $\int \mathcal{D}[\omega_T]$ and will handle $\mathbb{P}[\omega_T]$ like a probability density.

Jump processes are composites of a Poisson clock for jump times, and a discrete-time Markov chain for the state transitions. Separating these aspects, we first recall the waiting time distribution (1.39), that gives waiting a time $\Delta t_i = t_{i+1} - t_i$ for the next jump after x_i was entered the density

$$\rho_{\text{clock}}(\Delta t_i \mid x_i) = \xi(x_i) e^{-\Delta t_i \xi(x_i)}. \tag{4.26}$$

For the last interval, $\Delta t_N = T - t_N$, we instead require the probability of not leaving x_N which is

$$P_{\text{no-jump}}(\Delta t_N \mid x_N) = e^{-\Delta t_N \xi(x_N)}. \tag{4.27}$$

Next, given that a jump from x_i occurs at time t_{i+1}, the probability that the target state will be x_{i+1} comes from normalizing the corresponding transition rate,

$$P_{\text{chain}}(x_{i+1} \mid x_i) = \frac{W(x_{i+1}, x_i)}{\sum_y W(y, x_i)} = \frac{W(x_{i+1}, x_i)}{\xi(x_i)}. \tag{4.28}$$

Combining the probabilities (or densities) of the these elementary events, and letting the initial distribution be μ,

$$\mathbb{P}[\omega_T] = P_{\text{no-jump}}(\Delta t_N \mid x_N) \left(\prod_{i=0}^{N-1} \rho_{\text{clock}}(\Delta t_i) P_{\text{chain}}(x_{i+1} \mid x_i) \right) \mu(x_0) \tag{4.29a}$$

$$= \mu(x_0) e^{-\int_0^T \mathrm{d}t\, \xi(\omega_T(\tau))} \prod_{\substack{0<t<T \\ \omega_T(t^-) \neq \omega_T(t^+)}} W(\omega_T(t^+), \omega_T(t^-)). \tag{4.29b}$$

This expression allows an alternative derivation of detailed balance to the generator approach we gave in Section 1.2.3. We let ω_T be a realization of the stationary process, *i.e.* the initial distribution $\mu = P^*$. Then reversibility is equivalent to requiring that for any trajectory ω_T, and reversed trajectory $\hat{\omega}_T := \{X(T-t)\}_{t=0}^T$, their weights are identical: $\mathbb{P}[\omega_T] = \mathbb{P}[\hat{\omega}_T]$. Using (4.29b)

this amounts to

$$\frac{P^*(x_0)}{P^*(x_N)} = \frac{W(x_N, x_{N-1}) \cdots W(x_1, x_0)}{W(x_0, x_1) \dots W(x_{N-1}, x_N)}, \tag{4.30}$$

which, since true for any set of x_i's, is equivalent to detailed balance (1.52).

4.2.2 The Level 2.5 rate function and its meaning

Donsker and Varadhan in their seminal works identified three levels of observables for dynamical large deviations of Markov processes, related by contraction [127–129, 162]. The highest, level 3, consists of the long-time statistics of trajectories; level 2, the time fraction spent in each state; level 1, time-averaged observables of the process. It was later realized, *e.g.* [46], that to study fluctuations of currents and entropy productions—of particular interest in nonequilibrium processes—a level in between 2 and 3 was necessary, hence named 2.5 (see [48] for historical references). The objects of study for the level 2.5 theory are the **empirical density** P_T^e and the **empirical flow** C_T^e, defined

$$P_T^e(x) = P_T^e(x; X) := \frac{1}{T} \int_0^T \delta_{X(t),x}, \tag{4.31}$$

$$C_T^e(y, x) = C_T^e(y, x; X) := \frac{1}{T} \sum_{\substack{0<t<T \\ X(t^-)\neq X(t^+)}} \delta_{X(t^+),y}\, \delta_{X(t^-),x}. \tag{4.32}$$

The empirical density counts the fraction of time spent in a given state and the empirical flow counts the number of transitions per unit time across a bond. Due to ergodicity of the process, in the long-time limit

$$P_T^e(x) \to P^*(x), \tag{4.33}$$

$$C_T^e(y, x) \to W(y, x) P^*(x). \tag{4.34}$$

The level 2.5 large deviation principle then expresses the exponential decay of likelihood in observing an empirical density and flow, $\hat{P}, \hat{C}$, different than the typical ones, P^*, C^*:

$$P_T^{2.5}[\hat{P}, \hat{C}] := \mathbb{P}[P_T^e = \hat{P}, C_T^e = \hat{C}] \asymp e^{-TI[\hat{P},\hat{C}]}. \tag{4.35}$$

Remarkably, an explicit expression for the rate function $I[\hat{P}, \hat{C}]$ is known, which

makes contraction not only possible in principle but also in practice. For example, one can derive variational representations for the rate of the empirical current J_T^e and traffic T_T^e [46],

$$J_T^e(y,x) := C_T^e(y,x) - C_T^e(x,y), \quad T_T^e = C_T^e(y,x) + C_T^e(x,y). \tag{4.36}$$

As we will see below, the functions $\hat{P}, \hat{C}$ must be consistent with being the stationary density and flow of some process with path-measure $\hat{\mathbb{P}}$, so that

$$\sum_x \hat{P}(x) = 1, \tag{4.37a}$$

$$\sum_y [\hat{C}(y,x) - \hat{C}(x,y)] = 0. \tag{4.37b}$$

This also follows directly from considering that

$$\sum_x P_T^e(x) = 1, \tag{4.38}$$

and that

$$\sum_y J_T^e(y,x) = \frac{1}{T} \sum_y \sum_{\substack{0<t<T \\ X(t^-)\neq X(t^+)}} \left[\delta_{X(t^+),y}\, \delta_{X(t^-),x} - \delta_{X(t^+),x}\, \delta_{X(t^-),y}\right] \tag{4.39a}$$

$$= \frac{1}{T} \sum_{i=1}^{N} \left[\delta_{X(t_{i-1}),x} - \delta_{X(t_i),x}\right] \tag{4.39b}$$

$$= \frac{1}{T}(\delta_{X(0),x} - \delta_{X(T),x}) \tag{4.39c}$$

$$\overset{T\to\infty}{\to} 0, \tag{4.39d}$$

where t_i are the jump times with $t_0 = 0$ and $t_N = T$.

We now derive the level 2.5 rate function and interpret it, following [46, 47]. In the next section, we explicitly perform the contraction to level 1 observables, in order to motivate the formalism that will be put to practical use in Chapters 5 and 6. As before, we let $\mathbb{P}$ be the path-distribution of the process X, and we also let $\mathbb{Q}$ be the path-probability of some different process $Y(t)$, such that $\mathbb{P}$ and $\mathbb{Q}$ are absolutely continuous with respect to each other, *i.e.* that they have the same set of zero-probability trajectories. Then we can perform the **exponential**

change of measure [30] from the $\mathbb{P}$ to $\mathbb{Q}$[2],

$$\mathbb{P}[\omega_T]\mathcal{D}[\omega_T] = \exp\left\{-\ln\frac{\mathbb{Q}[\omega_T]}{\mathbb{P}[\omega_T]}\right\}\mathbb{Q}[\omega_T]\mathcal{D}[\omega_T], \tag{4.40}$$

Let us further say that $Y(t)$ is also a jump process with the initial distribution μ, but with transition rates K and escape rates η. Then using first (4.29b), and thereafter the definitions (4.31) and (4.32), we find

$$\ln\frac{\mathbb{Q}[\omega_T]}{\mathbb{P}[\omega_T]} = \int_0^T \mathrm{d}s[\xi(x_s) - \eta(x_s)] + \sum_{\substack{0<s<t \\ x_{s^-}\neq x_{s^+}}} \ln\frac{K(x_{s^+}, x_{s^-})}{W(x_{s^+}, x_{s^-})} \tag{4.41a}$$

$$= T\left\{\sum_x P_T^e(x;\omega_T)[\xi(x) - \eta(x)] + \sum_{x,y} C_T^e(y,x;\omega_T)\ln\frac{K(y,x)}{W(y,x)}\right\} \tag{4.41b}$$

$$=: T\, I_{W,K}[P_T^e(\,\cdot\,;\omega_T), C_T^e(\,\cdot\,,\,\cdot\,;\omega_T)]. \tag{4.41c}$$

(We will henceforth let context imply when P_T^e and C_T^e are functions of ω_T rather than of X.) Importantly, $I_{W,K}$ only depends on the trajectory ω_T via the level 2.5 empirical observables.

We now seek $P_T^{2.5}[\hat{P}, \hat{C}]$ defined in (4.35) by marginalizing (4.40). In the following

$$\delta[P_T^e - \hat{P}] = \prod_x \delta(P_T^e(x) - \hat{P}(x)), \tag{4.42}$$

$$\delta[C_T^e - \hat{C}] = \prod_{x\neq y} \delta(C_T^e(y,x) - \hat{C}(y,x)). \tag{4.43}$$

Then

$$P_T^{2.5}[\hat{P}, \hat{C}] = \left\langle \delta[C^e - \hat{C}]\delta[P_T^e - \hat{P}]\right\rangle_{\mathbb{P}} \tag{4.44a}$$

$$= \int \mathcal{D}[\omega_T]\delta[C_T^e - \hat{C}]\delta[P_T^e - \hat{P}]e^{-TI_K[P_T^e, C_T^e]}\mathbb{Q}[\omega_T] \tag{4.44b}$$

$$= e^{-TI_{W,K}[\hat{P},\hat{C}]}Q_T^{2.5}[\hat{P}, \hat{C}]. \tag{4.44c}$$

Now, if we choose the rates K according to

$$K(y,x) = \hat{W}(y,x) := \frac{\hat{C}(y,x)}{\hat{P}(x)}. \tag{4.45}$$

[2]In the simplified, non-rigorous style we use, this relation is transparently tautologous, but in strict definition, the ratio of the two measures is a Radon-Nikodym derivative defined by measure-theoretic concepts.

then the the long-time averages of $P^e(x;Y)$ and $C^e(y,x;Y)$ will be $\hat{P}$ and $\hat{C}$. For this choice of K, let us denote $\mathbb{Q}|_{K=\hat{W}} =: \hat{\mathbb{P}}$. Then $I_{W,\hat{W}} =: I$ is simply

$$I[\hat{P},\hat{C}] = \sum_{x,y} \left\{ W(y,x)\hat{P}(x) - \hat{C}(y,x) + \hat{C}(y,x) \ln \frac{\hat{C}(y,x)}{W(y,x)\hat{P}(x)} \right\}, \quad (4.46)$$

where we have just expanded out the escape rates. We then arrive at the *exact* relation

$$\mathbb{P}[\hat{P},\hat{C}] = e^{-TI[\hat{P},\hat{C}]}\hat{\mathbb{P}}[\hat{P},\hat{C}]. \quad (4.47)$$

To establish the large deviation principle (4.35), all we need to note is that, as T becomes large, $T^{-1}\ln\hat{\mathbb{P}}[\hat{P},\hat{C}] \to 0$, since the probability concentrates around the long-time values $\hat{P},\hat{C}$.

Let us introduce the information-theoretic relative entropy between two distributions as

$$S_T[\mathbb{Q} \mid \mathbb{P}] := \int \mathcal{D}[\omega_T]\, \mathbb{Q}[\omega_T] \ln \frac{\mathbb{Q}[\omega_T]}{\mathbb{P}[\omega_T]} \quad (4.48a)$$

$$= T I_{W,K}[\langle P^e \rangle_{\mathbb{Q}}, \langle C^e \rangle_{\mathbb{Q}}]. \quad (4.48b)$$

The relative entropy is non-negative, and zero if and only if the two distributions are identical on all positive-measure sets [163]. It is often viewed as a pseudo-distance between distributions, but is neither symmetric nor satisfies the triangle inequality as required of a true distance metric. In the long-time limit $\langle P^e \rangle_{\mathbb{Q}}$, converges to the stationary density of Y, *etc.* Thus, in particular, we have for $\mathbb{Q} = \hat{\mathbb{P}}$,

$$\lim_{T\to\infty} \frac{1}{T} S_T[\hat{\mathbb{P}} \mid \mathbb{P}] = I[\hat{P},\hat{C}]. \quad (4.49)$$

One then realizes that applying the contraction principle to this level 2.5 rate function, *i.e.* to optimize it with constraints, amounts in an information-theoretic sense to finding the Markov process 'closest' to the original process given those constraints.

4.2.3 Contraction to time-additive dynamical observables

The rate function $I(a)$ of any variable $A_T = A[P_T^e, C_T^e]$ can now be obtained according to the contraction principle (4.22) by minimizing the level 2.5 rate function $I[\hat{P}, \hat{C}]$ under constraints. Of particular interest are level 1 dynamical observables, which are weighted averages of the empirical density and/or flow. The most general form for this kind of observable is $A_T = A_T^{\text{occ}} + A_T^{\text{flow}}$ consisting of an 'occupation-like' and a 'flow-like' component given by

$$A_T^{\text{occ}} = \sum_x f(x) P_T^e(x) = \frac{1}{T} \int_0^T \mathrm{d}t\, f(X(t)), \tag{4.50a}$$

$$A_T^{\text{flow}} = \sum_{x,y} g(y,x) C_T^e(y,x) = \frac{1}{T} \sum_{\substack{0<t<T \\ X(t^-)\neq X(t^+)}} g(X(t^+), X(t^-)). \tag{4.50b}$$

In practice, however, we are usually concerned with A_T having only one of these components and not the other. We give some examples of commonly studied dynamical observables:

- **Occupation time**. The fraction of time spent in a given subset $\mathcal{R} \subset \mathcal{X}$ is given by A_T^{occ} with $f(x) = I_{\mathcal{R}}(x)$ (the indicator function for $\mathcal{R}$). Occupation time statistics, whether in a large deviation limit or not, feature heavily in physical and mathematical applications. Some recent large-deviation studies include time spent at a given location or interval for simple 1D processes such as biased diffusions and Ornstein-Uhlenbeck processes [29, 49, 50, 164], and special configurations related to clustering in interacting many-body system [165, 166].

- **Total activity**. By taking A_T^{flow} with $g \equiv 1$ we are counting the total number of state transitions (per time), or, equivalently, the integrated traffic. This observable has, for example, been studied in kinetically constrained models of glassy systems to show that they generically exhibit a dynamical phase coexistence of active and inactive trajectories [66, 151].

- **Entropy production.** Consider a process that can be interpreted as interacting with a thermal environment. Then A_T^{flow} with $g(y,x) = \ln[W(y,x)/W(x,y)] = q(y,x)$ gives us an observable ϕ_T^e that, from the definitions relating to thermal physics in Section 1.2.6, we interpret as the

change in environmental entropy per unit time,

$$\phi_T^e = \frac{S_{\text{env}}(T) - S_{\text{env}}(0)}{T}. \tag{4.51}$$

For long times, we expect the system entropy to be sub-extensive in time (but see for a discussion of caveats [35, Sect. 1.8.1]), so that we can equate ϕ_T^e with the the empirical entropy production rate σ_e^T. This quantity satisfies the **Gallavotti-Cohen symmetry** of the rate function (first discovered for deterministic chaotic systems [142] and later proved for stochastic dynamics [143, 144]),

$$\Lambda(s) = \Lambda(-s-1). \tag{4.52}$$

(We will derive this later on.) By LF transform follows the asymptotic fluctuation relation

$$I(\sigma) = I(-\sigma) - \sigma. \tag{4.53}$$

A recent direction of research has been to consider entropy production in many-body active systems, where atypically high entropy production rates (due to the 'active work') correspond to phases of spontaneously coordinated motion [3, 167–170].

Applying the Laplace and contraction principles, (4.20) and (4.22), in the level 2.5 context,

$$\Lambda(s) = \max_{\hat{P},\hat{C}} \{sA[\hat{P},\hat{C}] - I[\hat{P},\hat{C}]\} \tag{4.54a}$$

$$= sA[\hat{P}_s^*, \hat{C}_s^*] - I[\hat{P}_s^*, \hat{C}_s^*] \tag{4.54b}$$

where $\hat{P}_s^*, \hat{C}_s^*$ are the maximizers, and

$$I(a) = \min_{\hat{P},\hat{C}} \{I[\hat{P},\hat{C}] : A[\hat{P},\hat{C}] = a\} \tag{4.55a}$$

$$= I[\hat{P}_{s^*(a)}^*, \hat{C}_{s^*(a)}^*], \tag{4.55b}$$

where $s^*(a)$ is such that $A[\hat{P}_{s^*(a)}^*, \hat{C}_{s^*(a)}^*] = a$. We recall that I is given by (4.46)

and A via (4.50) as

$$A[\hat{P},\hat{C}] = \sum_x f(x)\hat{P}(x) + \sum_{x,y} g(y,x)\hat{C}(y,x). \tag{4.56}$$

Let us start by finding $\hat{P}_s^*, \hat{C}_s^*$ through the maximization in (4.54), or equivalently, the constrained minimization in (4.55) with undetermined Lagrange multiplier s. There are the additional consistency constraints (4.37) that we also implement with Lagrange multipliers. We then set out to minimize

$$\begin{aligned}\mathcal{I}[\hat{P},\hat{C}] := I[\hat{P},\hat{C}] - sA[\hat{P},\hat{C}] + \Lambda_s \sum_x \hat{P}(x) \\ - \sum_x V_s(x) \sum_y \left[\hat{C}(y,x) - \hat{C}(x,y)\right],\end{aligned} \tag{4.57}$$

where we have introduced the parameters $-\Lambda_s$ and $\{V_s(x)\}_{x\in\mathcal{X}}$. The symbol for the first parameter has been chosen with the foreknowledge that we shall eventually find $\Lambda(s) = \Lambda_s$, which is not assumed *a priori*, however. Setting the variations of $\mathcal{I}$ to zero:

$$0 \equiv \frac{\delta\mathcal{I}}{\delta\hat{P}(x)} = \sum_y \left[W(y,x) - \frac{\hat{C}(y,x)}{\hat{P}(x)}\right] + \Lambda_s - sf(x), \tag{4.58a}$$

$$0 \equiv \frac{\delta\mathcal{I}}{\delta\hat{C}(y,x)} = \ln\frac{\hat{C}(y,x)}{W(y,x)\hat{P}(x)} - V_s(x) + V_s(y) - sg(y,x). \tag{4.58b}$$

From (4.58b) we find

$$\frac{\hat{C}(y,x)}{\hat{P}(x)} = \hat{W}_s(y,x) := W(y,x)e^{sg(y,x)}e^{-[V_s(y)-V_s(x)]}. \tag{4.59}$$

Define

$$R_s(x) := e^{-V_s(x)}. \tag{4.60}$$

Then by substituting (4.59) into (4.58a) and rearranging, we have

$$\Lambda_s R_s(x) = \sum_y W(y,x)[e^{sg(y,x)}R_s(y) - R_s(x)] + sf(x)R_s(x). \tag{4.61}$$

This relation is compactly expressed

$$\Lambda_s R_s = \widetilde{\mathbb{L}}_s R_s, \tag{4.62}$$

where the matrix

$$\widetilde{\mathbb{L}}_s(y,x) := \mathbb{L}(y,x)e^{sg(x,y)} + sf(x)\delta_{x,y} \tag{4.63}$$

is referred to as the **tilted (backward) generator** with respect to the observable A_T. (Recall from Section 1.2.1 that $\mathbb{L} = \mathbb{W}^\top$ is the (backward) generator of the process.) We adorn it with a tilde as a mnemonic aid. In contrast to $\mathbb{L}$, for $s \neq 0$, $\widetilde{\mathbb{L}}_s$ is generally not row-stochastic. It is therefore not the generator of a probability-conserving Markov process. It is instead an example of a **Metzler matrix**: it is real with non-negative off-diagonal elements, and arbitrary diagonal entries. The Perron-Frobenius (PF) theorem (Section 1.2.2) can be applied to Metzler matrices, because adding to them some constant times the identity matrix makes them non-negative. In particular, since $\mathbb{L}$ has been assumed to satisfy the conditions of the PF theorem, so too will $\widetilde{\mathbb{L}}_s$. Then, because R_s through its definition (4.60) is strictly positive:

> *Λ_s and R_s must be the Perron-Frobenius (i.e. dominant) spectral elements.*

They are thus *uniquely* determined by (4.62) as there is no question over which eigenvalue and eigenvector the equation solves for.

Remark: for the entropy flux observable $g(y,x) = \ln[W(y,x)/W(x,y)]$, when all such rate ratios exist, one finds $\widetilde{\mathbb{L}}_s = \widetilde{\mathbb{L}}_{-1-s}$ from which follows the Gallavotti-Cohen symmetry $\Lambda_s = \Lambda_{-1-s}$.

There is also a dominant left eigenvalue equation to pair with (4.62), namely

$$\Lambda_s L_s^\top = L_s^\top \widetilde{\mathbb{L}}_s, \tag{4.64}$$

or equivalently

$$\Lambda_s L_s = \widetilde{\mathbb{W}}_s L_s, \tag{4.65}$$

where

$$\widetilde{\mathbb{W}}_s(y,x) = \widetilde{\mathbb{L}}_s^\top(y,x) = W(y,x)e^{sg(y,x)} - [\xi(x) - sf(x)]\delta_{x,y} \tag{4.66}$$

is the **tilted (forward) generator**. By the PF theorem, L_s is also a strictly

positive vector. We will impose the normalization

$$\sum_x L_s(x) = 1, \tag{4.67a}$$

$$\sum_x L(x)_s R_s(x) = 1. \tag{4.67b}$$

Next, we check that this solution for the Lagrange multipliers is consistent with the constraints (4.37) they were introduced to satisfy. We let $\hat{\mathbb{W}}_s$ be the rate matrix corresponding to the rates $\hat{W}_s$ of (4.59). We then require

$$0 = \sum_x [\hat{C}(y,x) - \hat{C}(x,y)] = \sum_x \hat{\mathbb{W}}_s(y,x)\hat{P}(x). \tag{4.68}$$

Thus $\hat{P} = \hat{P}_s^*$, the stationary distribution of the process with rate matrix $\hat{\mathbb{W}}_s$, and $\hat{C}(y,x) = \hat{W}_s(y,x)P_s^*(x)$. From previous definitions we can check the veracity of the relation

$$\hat{\mathbb{W}}_s(y,x) = R_s(y)\widetilde{\mathbb{W}}_s(y,x)R_s^{-1}(x) - \delta_{x,y}\Lambda_s. \tag{4.69}$$

This form is known as a **generalized Doob transform** [28], which turns a Metzler matrix into a stochastic matrix. The stationary distribution of $\hat{\mathbb{W}}_s$ is by substitution verified to be

$$\hat{P}_s^*(x) = L_s(x)R_s(x), \tag{4.70}$$

given the choice of normalization (4.67b).

Substituting $\hat{P}_s^*$ and $\hat{C}_s^*$ back into the level 2.5 rate function, and using (4.58)

$$I[\hat{P}_s^*, \hat{C}_s^*] = \sum_x \left[sf(x) - \Lambda_s\right] P_s^*(x) + \sum_{x,y} \hat{C}_s^*(y,x)\left[V_s(x) - V_s(y) + sg(y,x)\right] \tag{4.71a}$$

$$= s\left[\sum_x f(x)\hat{P}_s^*(x) + \sum_{x,y} g(y,x)\hat{C}_s^*(y,x)\right] - \Lambda_s \sum_x \hat{P}_s^*(x) + \sum_x V(x) \sum_y \left[\hat{C}_s^*(y,x) - \hat{C}_s^*(x,y)\right] \tag{4.71b}$$

$$= sA[\hat{P}_s^*, \hat{C}_s^*] - \Lambda_s. \tag{4.71c}$$

We then have from (4.54), as advertised,

$$\Lambda(s) = \Lambda_s. \tag{4.72}$$

From (4.55),

$$I(a) = as^*(a) - \Lambda_{s^*(a)}, \tag{4.73}$$

supposing a unique $s^*(a)$ exists, which is to say that the SCGF is smooth and strictly convex.

Motivated by (4.49), (4.55) tells us that $\hat{\mathbb{W}}_{s^*(a)}$ is the forward generator of the Markov process closest to the original processes constrained on achieving $A_T = a$ in the long-time limit. We shall refer to it as the **effective process**, in the literature also called the 'auxiliary' or 'driven' process. As we have noted, we shall interpret its typical behaviour as representing how the fluctuation a arises in the original process. Looking at the the effective rates (4.59), we see that there are two effects in play: there is an added **effective potential** V_s to the dynamics, and, if the observable has a flow-like component, an additional **nonequilibrium force** sg that is in general not a potential difference. If the original process is a many-body lattice process, for instance, then V_s represent effective interactions between particles that *a priori* may be arbitrarily complex.

But how can we be sure that the constrained trajectory ensemble is (in some relevant approximate sense) described by this closest Markov process, rather than some very different non-Markovian process? This requires an analysis of ensemble equivalence that we review in the following, based on [28, 171, 172].

4.2.4 The view from ensemble theory

Two path ensembles $\mathbb{P}, \mathbb{Q}$, whether Markovian or not, are said to be **asymptotically equivalent** [28, 172], written

$$\mathbb{P} \asymp \mathbb{Q}, \tag{4.74}$$

if for 'almost all' paths ω_T,

$$\lim_{T\to\infty} \frac{1}{T} \ln \frac{\mathbb{P}[\omega_T]}{\mathbb{Q}[\omega_T]} = 0. \tag{4.75}$$

Asymptotic equivalence means that the *typical* properties of both processes are the same. Once can check that the relation $\asymp$ is transitive, symmetric, and reflexive.

A series of different dynamical ensembles are introduced, with the intention of showing that (under certain conditions) they are asymptotically equivalent.

- **Microcanonical ensemble**. This is the original process under the hard constraint $A_T = a$,

$$\mathbb{P}_a^{\text{micro}}[\omega_T] := \frac{\mathbb{P}[\omega_T]\delta(A(\omega_T) - a)}{P_T(a)}. \tag{4.76}$$

  It gives the exact answer to the question of which trajectories cause a certain fluctuation. It is not Markovian, because each trajectory has to anticipate a precise value of A_T.

- **Tilted ensemble**. Sometimes called the s-ensemble, or penalized ensemble, this is the path measure of the non-conservative process with forward generator $\widetilde{\mathbb{W}}_s$ (4.63),

$$\widetilde{\mathbb{P}}_s[\omega_T] := e^{sTA_T(\omega_T)}\mathbb{P}[\omega_T]. \tag{4.77}$$

- **Canonical ensemble**. This normalized ensemble replaces the hard constraint on A_T with a soft constraint,

$$\mathbb{P}_s^{\text{cano}}[\omega_T] := \frac{e^{sA_T(\omega_T)T}\mathbb{P}[\omega_T]}{\langle e^{sTA_T}\rangle_{\mathbb{P}}}. \tag{4.78}$$

  For finite T it is *not* necessarily Markovian. Our expectation from the equilibrium statistical mechanics context, is that in the $T \to \infty$ limit the canonical and microcanonical ensembles are interchangeable, once the 'temperature' $-s^{-1}$ is appropriately tuned.

  Note that that we can define a **dynamical partition function**,

$$Z_T(s) := \left\langle e^{sTA_T}\right\rangle_{\mathbb{P}}, \tag{4.79}$$

  so that the SCGF is akin to a 'dynamical free-energy density´,

$$\Lambda(s) = \lim_{T\to\infty} \frac{1}{T} \ln Z_T(s). \tag{4.80}$$

- **Effective process ensemble**. This is the Markovian path ensemble for the process with forward generator $\hat{\mathbb{W}}_s$ (4.69),

$$\hat{\mathbb{P}}_s[\omega_T] = e^{TI[P_s^*(\omega_T), C_s^*(\omega_T)]}\mathbb{P}[\omega_T]. \tag{4.81}$$

It can then been proven based on asymptotic spectral representations of the process generators involved that [28]

$$\mathbb{P}_s^{\text{cano}} \asymp e^{\Lambda(s)T}\widetilde{\mathbb{P}}_s \asymp \hat{\mathbb{P}}_s. \tag{4.82}$$

Finally, the microcanonical and canonical ensembles are asymptotically equivalent,

$$\mathbb{P}_a^{\text{micro}} \asymp \mathbb{P}_s^{\text{cano}}, \tag{4.83}$$

given that $s = I'(a)$, for points a where $I(a)$ is locally smooth and convex, or any $s \in [I'(a^-), I'(a^+)]$ when $I(a)$ is convex but has a kink at a. In the latter cases the effective process is not unique. For a where the rate function is not locally convex, the microcanonical–canonical ensemble equivalence breaks down. Non-convexity of I, we recall, arises when $\Lambda(s)$ has a non-analyticity. At such point we experience a **dynamical phase transition** (DPT), which is formally (but not physically) equivalent to an equilibrium phase transition, given the interpretation of the SCGF as a (dynamical) free energy density. On either side of a DPT the dynamical trajectories of the system are qualitatively different, and at the phase transition point there is dynamical phase coexistence.

Finally, there is a subtlety in that the asymptotic equivalence relation is only sensitive to the behaviour of the processes in the 'interior time' $[0, T)$ as T is pushed to infinity. Thus, if the fluctuations in A_T arise from a 'jump' at the end of the observation time interval, this will not be captured by the effective process construction. An example given in [28] is the Ornstein-Uhlenbeck process conditioned on its net drift velocity: it stays localized around its potential minimum, until it makes a sudden excursion that furnishes the chosen net drift at time T.

4.3 The case of diffusions

Dynamical large deviation theory applies equally well to diffusion processes as to jump processes [28, 29, 173]. In principle, we could derive the formalism by a continuum limit applied to the conditioned jump processes of the previous section. Indeed, we will use this approach to derive new results for diffusions with boundaries in Chapter 6. Here, we briefly review the theory for diffusions in unbounded domains without reference to the diffusive limit. Thus we consider a d-dimensional diffusion $\mathbf{X}(t)$ evolving in $\mathbb{R}^d$ according to the SDE (1.90)

$$\mathrm{d}\mathbf{X}(t) = \boldsymbol{F}(\mathbf{X}(t)) + \mathsf{B}\,\mathrm{d}\mathbf{W}(t), \tag{4.84}$$

with a constant diffusion matrix $\mathsf{D} = (1/2)\mathsf{B}\mathsf{B}^\top$. For simplicity of moving between stochastic calculus conventions we consider no state dependence of the diffusion matrix, but this is not a necessary limitation of the theory.

A level 2.5 large deviation principle exists, to which contraction can be usefully applied [173, 174]. On the continuum, the empirical flow must be replaced by the empirical current as a partner to the empirical density, because the lattice current, but not the flow or traffic, has a sensible continuum limit. For diffusions, the empirical density is

$$\rho^e_T(\boldsymbol{x}) = \frac{1}{T}\int_0^T \mathrm{d}t\,\delta(\mathbf{X}(t) - \boldsymbol{x}), \tag{4.85}$$

and the empirical current is

$$\mathbf{J}^e_T(\boldsymbol{x}) = \frac{1}{T}\int_0^T \delta(\mathbf{X}(t) - \boldsymbol{x}) \circ \mathrm{d}\mathbf{X}(t) \tag{4.86a}$$

$$= \frac{1}{T}\lim_{\Delta t\to 0}\sum_i \delta\left(\frac{\mathbf{X}(t_i+\Delta t) + \mathbf{X}(t_i)}{2} - \boldsymbol{x}\right)(\mathbf{X}(t_i+\Delta t) - \mathbf{X}(t_i)), \tag{4.86b}$$

where the circle product in the integral indicates the use of the Stratonovich convention. The Stratonvich convention is necessary to make the current properly anti-symmetric under time reversal, and is (as we prove in Chapter 6) what results from the continuum limit of the lattice current.

The level 2.5 large deviation principle is then

$$\mathbb{P}[\rho_T^e = \rho, \mathbf{J}_T^e = \boldsymbol{j}] \asymp e^{-TI[\rho,\boldsymbol{j}]}, \tag{4.87}$$

with the rate function

$$I[\rho,\boldsymbol{j}] = \begin{cases} \frac{1}{4}\int \mathrm{d}\boldsymbol{x}\,(\boldsymbol{j}-\boldsymbol{J}_{\rho,\boldsymbol{F}})^\top(\rho\mathsf{D})^{-1}(\boldsymbol{j}-\boldsymbol{J}_{\rho,\boldsymbol{F}}), & \nabla\cdot\boldsymbol{j}=0,\\ \infty, & \nabla\cdot\boldsymbol{j}\neq 0, \end{cases} \tag{4.88}$$

where

$$\boldsymbol{J}_{\rho,\boldsymbol{F}}(\boldsymbol{x}) = \boldsymbol{F}(\boldsymbol{x})\rho(\boldsymbol{x}) - \mathsf{D}(\boldsymbol{x})\nabla\rho(\boldsymbol{x}). \tag{4.89}$$

(The subscripts on the current $\boldsymbol{J}$ will be notationally convenient in the following.)

Time-additive dynamical observables $A_T = A_T^{\mathrm{occ}} + A_T^{\mathrm{curr}}$ are now defined by

$$A_T^{\mathrm{occ}} = \int \mathrm{d}\boldsymbol{x}\, f(\boldsymbol{x})\rho_T^e(\boldsymbol{x}) = \frac{1}{T}\int_0^T \mathrm{d}t\, f(\mathbf{X}(t)), \tag{4.90a}$$

$$A_T^{\mathrm{curr}} = \int \mathrm{d}\boldsymbol{x}\, \boldsymbol{g}(\boldsymbol{x})\cdot\mathbf{J}_T^e(\boldsymbol{x}) = \frac{1}{T}\int_0^T \boldsymbol{g}(\mathbf{X}(t))\circ\mathrm{d}\mathbf{X}(t). \tag{4.90b}$$

To express the associated rate function and effective process, we consider an alternative to the level 2.5 contraction, based on a direct application of the **Feynman-Kac formula** (see [29, 175] for a pedagogical derivation and historical references). Consider the function

$$u_k(\boldsymbol{x},t) = \left\langle e^{kTA_T} \mid \mathbf{X}(0)=\boldsymbol{x}\right\rangle. \tag{4.91}$$

It gives the SCGF $\lambda(k)$ (which we write in different symbols than $\Lambda(s)$ to distinguish diffusions from jump processes) by integration, logarithm, and scaling,

$$\lambda(k) = \lim_{T\to\infty}\frac{1}{T}\ln\int \mathrm{d}\boldsymbol{x}\, u(\boldsymbol{x},T), \tag{4.92}$$

from which the rate function (if convex) follows from LF transform. The Feynman-Kac formula states that the evolution of u_k follows

$$\partial_t u_k(\boldsymbol{x},t) = \widetilde{\mathcal{L}}_k u_k(\boldsymbol{x},t), \tag{4.93}$$

where

$$\widetilde{\mathcal{L}}_k := \boldsymbol{F} \cdot (\nabla + k\boldsymbol{g}) + (\nabla + k\boldsymbol{g}) \cdot \mathsf{D}(\nabla + k\boldsymbol{g}) + kf \tag{4.94}$$

is the continuum analogue of the tilted (backward generator) $\widetilde{\mathbb{L}}_s^\top$. We can spectrally decompose u_k as

$$u_k(\boldsymbol{x}, t) = \sum_i c_i e^{\lambda_k^{(i)} t} r_k^{(i)}(\boldsymbol{x}), \tag{4.95}$$

where $\lambda_k^{(i)}$ and $r_k^{(i)}$ are the eigenvalues and eigenvectors of $\widetilde{\mathcal{L}}_k$. From (4.92) it follows again that $\lambda(k) = \lambda_k$, the dominant eigenvalue of $\widetilde{\mathcal{L}}_k$, whose corresponding eigenvector we denote r_k.

The generator of the effective process is again related to a generalized Doob-transform of the titled generator,

$$\hat{\mathcal{L}}_k := r_k^{-1} \widetilde{\mathcal{L}}_k r_k - \lambda_k. \tag{4.96}$$

Explicitly, this gives an effective process

$$\mathrm{d}\hat{\mathbf{X}}(t) = \hat{\boldsymbol{F}}_k(\hat{\mathbf{X}}(t)) + \mathsf{B}\,\mathrm{d}\mathbf{W}(t), \tag{4.97}$$

which differs from the original process by the effective force

$$\hat{\boldsymbol{F}}_k := \boldsymbol{F} + 2\mathsf{D}(k\boldsymbol{g} + \nabla \ln r_k). \tag{4.98}$$

The bias parameter k is, as with s in the jump process case, tuned according to $k = I'(a)$, with I the rate function for $A_T = a$. Again in analogy to the jump process case, the steady-state density of the effective process is

$$\hat{\rho}_k^* = \ell_k r_k, \tag{4.99}$$

where ℓ_k is the dominant eigenvector of

$$\widetilde{\mathcal{L}}_k^\dagger := -(\nabla - k\boldsymbol{g}) \cdot \boldsymbol{F} + (\nabla - k\boldsymbol{g}) \cdot \mathsf{D}(\nabla - k\boldsymbol{g}) + kf, \tag{4.100}$$

the dual of $\widetilde{\mathcal{L}}_k$. We impose the normalization

$$\int \mathrm{d}\boldsymbol{x}\, \ell_k(\boldsymbol{x}) = 1, \quad \int \mathrm{d}\boldsymbol{x}\, \ell_k r_k(\boldsymbol{x}) = 1. \tag{4.101}$$

In the next chapter, we return to the simple diffusion conditioned on its net drift, and demonstrate how the use of the spectral large deviation methods described in this chapter allows us to obtain the rate function and effective process advertised in Section 4.1.2.

4.4 Summary of main concepts

Dynamical large deviation theory deals with the exponentially small probabilities of fluctuations in (nonequilibrium) steady states sustained over long observation times T. This is quantified by a large deviation principle (4.12), where a rate function I describes the rate of decay. The scaled cumulant generating function Λ (4.13) is the Legendre-Fenchel (LF) transform of I, and, under appropriate conditions, *vice versa* (Figure 4.3). The relationship between I and Λ is formally similar to that between entropy and free energy density in equilibrium statistical mechanics.

The level 2.5 large deviation principle concerns sustained fluctuations in the empirical probability density P_T^e (4.31) and empirical probability flow C_T^e (4.32). To derive it, one can take a trajectory-statistics view of Markov processes, and compare the path-probability $\mathbb{P}$ of the original process to that of an effective process $\hat{\mathbb{P}}$ under which a given long-time probability density $P_e^T = \hat{P}$ and flow $C_T^e = \hat{C}$ become typical. By applying the contraction principle (4.22) to the level 2.5 large deviation principle, one can derive rate functions for level 1 time-integrated observables A_T (4.50) that are weighted averages of the empirical density and/or flow. This class encompasses important examples such as activity and entropy production. The effective process that makes a chosen value $A_T = a$ of the observable typical in the long-time limit, can be shown to describe in an asymptotically exact sense the trajectories of the original process that generate the fluctuation a.

Concretely, for jump processes we obtain the SCGF of A_T as the dominant eigenvalue of a 'tilted generator' $\widetilde{\mathbb{L}}_s$ for jump processes (4.63), that is constructed from the original generator, the details of the observable, and a bias parameter s. The corresponding right eigenvector is used in constructing the effective process whose rates $\hat{W}_s$ are given by (4.59), and s can be tuned to select a given fluctuation a via $s = I'(a)$. For diffusions, an analogous formalism holds.

Chapter 5

Rare trajectories in multi-state random walks

5.1 Background

In Chapter 4 we introduced the basic elements of dynamical large deviation theory, and described the relationship of the rate function I that quantifies rare events at an exponential time scale, and the scaled cumulant generating function (SCGF) Λ that is its Legendre-Fenchel (LF) dual. In the ideal case, I is a smooth, strictly convex function, and so is Λ. For a multitude of reasons, a model may depart from this ideal case. It is then interesting to understand *why*, both from the point of view of uncovering special dynamical behaviour of the model, and to gain a formal understanding of what conditions allow a large-deviation singularity (of I or Λ) to form.

Large-deviation singularities have been encountered in models of varying complexity, from simple random walks [176–182] to large systems of interacting active particles [167–170]. The large deviation elements of the former class are often exactly solvable, which is useful to assess if the singularity is appearing in some limit, *e.g.* large system size, or has a different origin. For more complex systems, whose large deviation elements must be computed numerically or by advanced simulation techniques, these questions can be more difficult to answer. In this chapter, we focus on non-interacting random walkers and the peculiar dynamical large deviations they can exhibit.

The simplest toy model for probing dynamical large deviations is the asymmetric random walk (ARW), or biased diffusion on the continuum. The exact large deviation elements for the entropy production (1.79) in the ARW were calculated in [144], and followed up in [176, 177], where it was found that an apparent kink emerges in the rate function with diverging asymmetry of the walk. On closer inspection, however, the rate function remains smooth for any finite degree of asymmetry. There are many other examples where a limit in addition to the long-time one produces a singularity: in the small-noise limit, which has been also been studied for the ARW and its continuum counterpart [177], including for periodic potentials [183–185]; when a system-size diverges [179–182]; or a model parameter diverges or vanishes to create time-scale separation, and, in particular, a partitioning of the state space [178–180]. It is generally believed that the SCGF of dynamical observables in compact, irreducible Markov processes must be analytic [183]. But breaking either of these conditions, whether through the use of an additional limit or not, does not mean a singularity will necessarily appear. A particularly simple yet rich example of a singularity in the SCGF, shown to correspond to a dynamical phase transition (DPT) where the character of the associated trajectories changes for different values of the observable [49, 50, 186], was found in the biased diffusion on the infinite line, conditioned on the time spent in a finite interval.

As a continuation of the works on large deviations in the prototypical ARW or biased diffusion, we consider in this chapter the large deviations of either the velocity or the time spent at the origin, of a *multi-state* random walker. Such a particle moves on a linear and homogeneous lattice but with hopping rates depending on an internal state undergoing some independent Markov process. A special case that we will focus on is the run-and-tumble particle from Chapter 2 (or an asymmetric version thereof), for which the tumbling rate ω is anticipated to influence the fluctuation behaviour in possibly peculiar ways. We shall attempt to give an exact solution for the large deviation elements, and to probe the result for unusual large-deviation characteristics, including, in particular, singularities. We will also systematically employ the effective process construction (when valid) to understand the structure of trajectories that generate fluctuations in regimes that we deem interesting in the models we examine.

First, as a warm-up exercise in the use of the spectral method of calculating large deviations that was derived in Chapter 4, we review the calculations of the velocity fluctuations in the ARW and the occupation time DPT in the biased

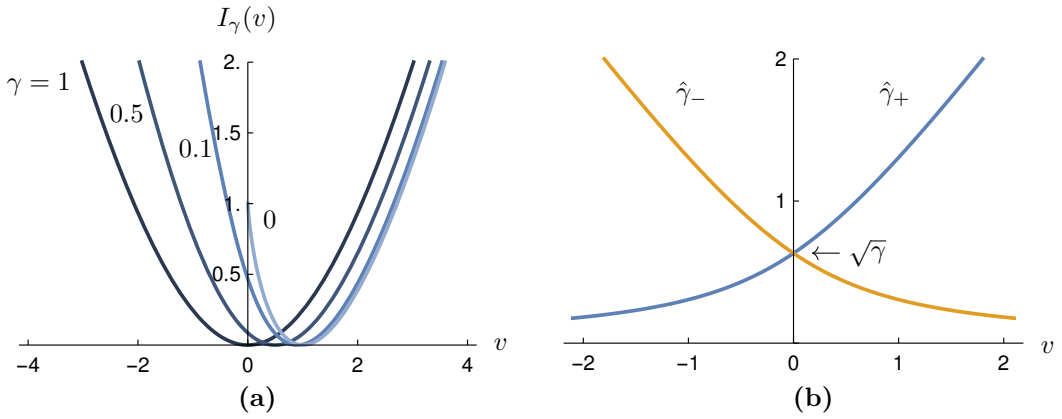

Figure 5.1 *Large deviations of velocity for the ARW. (a) Rate function plotted for $\gamma = 1, 0.5, 0.1$ and 0. (b) Effective forward and backward hopping rates.*

diffusion. Then we introduce the class of multi-state random walkers for which we shall develop methods of obtaining their large deviations for either of these observables.

5.1.1 Large deviations in the asymmetric random walk

We consider long-time velocity fluctuation of the ARW which hops on sites $n = 1, 2, \ldots, L$ (periodic) with rate 1 to the right and γ (≤ 1, say) to the left, giving the master equation

$$\partial_t P(n,t) = P(n-1,t) + \gamma P(n+1,t) - (1+\gamma)P(n,t), \tag{5.1}$$

with $P(n+L,t) = P(n,t)$. The observable V_T is the empirical velocity given by (4.50b) with the weight $g(n \pm 1, n) = \pm 1$. The dominant eigenvalue problem (4.62) that gives the SCGF $\Lambda(s)$ reads in this instance

$$\Lambda(s) R_s(n) = e^s R_s(n+1) + \gamma e^{-s} R_s(n-1) - (1+\gamma) R_s(n), \tag{5.2}$$

with $R_s(n+L) = R_s(n)$. Because the velocity observable is independent of the ring size L, we can without loss of generality put $L = 1$ and conclude

$$\Lambda(s) = e^s + \gamma e^{-s} - (1+\gamma). \tag{5.3}$$

The rate function then follows from the LF transform (4.18) as

$$I_\gamma(v) = 1 + \gamma - 2\sqrt{\gamma + (v/2)^2} - v \ln \left[\frac{1}{\gamma} \left(\sqrt{\gamma + (v/2)^2} - v/2 \right) \right]. \tag{5.4}$$

It satisfies

$$I_\gamma(v) = I_\gamma(-v) - v \ln \gamma. \tag{5.5}$$

which is the Galavotti-Cohen symmetry (4.53) but expressed for velocity rather than entropy production. As shown in Figure 5.1a, as the asymmetry is made total, *i.e.* $\gamma \to 0$, the steepness of the left tail of the rate function diverges, as one intuits from the fact that no negative current can be seen if left hops are impossible. The effective forward and backward hopping rates are $\hat{\gamma}_+ = e^{s^*}$ and $\hat{\gamma}_- = \gamma e^{-s^*}$, where

$$s^* = \ln \left[\frac{1}{\gamma} \left(\sqrt{\gamma + (v/2)^2} + v/2 \right) \right] \tag{5.6}$$

is the saddle-point value in (4.18). This gives

$$\hat{\gamma}_\pm = \sqrt{\gamma + (v/2)^2} \pm v/2. \tag{5.7}$$

Note that the activity parameters (as defined in (1.73)) are not altered between the original and effective process: $\hat{\gamma}_+ \hat{\gamma}_- = 1 \cdot \gamma$. This is a necessary feature when the weight of the flow-like dynamical observable is antisymmetric, $g(x, y) = -g(y, x)$.

Alternatively, we can consider the continuous-space biased diffusion

$$\mathrm{d}X(t) = F \, \mathrm{d}t + \sqrt{2D} \, \mathrm{d}W(t) \tag{5.8}$$

on a ring of circumference L, for which the net drift V_T is a current observable of the form (4.90b) with $g = 1$. Concluding from translational symmetry that the dominant eigenvalue problem for the k-tilted generator (4.94) is solved by $r_k = 1/L$, we find the SCGF to be

$$\lambda_k = k(F + Dk). \tag{5.9}$$

This gives a Gaussian rate function

$$I_F(v) = (v - F)^2/(2D) \tag{5.10}$$

and effective drift

$$\hat{F} = v. \tag{5.11}$$

This is the result that was promised in the example Section 4.1.2 used to motivate the main ideas of dynamical large deviation theory.

Consider also the biased diffusion (5.8) but with the occupation-time observable $A_T(x)$ of the form (4.90a) with the weight $f(x) = \mathbb{1}_{\mathcal{I}}(x)$, the indicator function for the interval $\mathcal{I} = [-a, +a]$ [49, 50, 186]. In contrast to the problem of velocity fluctuations, the ring (a compact space) and infinite line (non-compact) are not interchangeable, as far as large deviations are concerned, because the observable itself is not translation invariant, although the original process is. This opens the possibility of a DPT if we let $L = \infty$. Alternatively, we could consider *e.g.* periodic boundary conditions and expect the same DPT to emerge as $L \to \infty$. In principle, however, we cannot *a priori* exclude the possibility that the long-time limit and large system-size limit do not commute or depends on the boundary conditions of the finite-space model. We consider in any case the infinite line from the start. The tilted generator for the conditioning problem is then

$$\widetilde{\mathcal{L}}_k = F\partial_x + D\partial_x^2 + k\mathbb{1}_{[-a,+a]}(x). \tag{5.12}$$

In [50] the dominant eigenvalue problem for this operator could be mapped to the problem of finding the ground state of a certain quantum particle in a square well. The ground state solution can be represented exactly, but requires the solution of a transcendental equation. The phenomenology is the following. A critical occupation fraction ν_c (conjugate to a critical bias k_c) separates a linear branch of the rate function for occupation fractions $0 < \nu < \nu_c$, and a convex branch for $\nu > \nu_c$. This constitutes a first-order transition because the SCGF, being the free-energy analogue, has a discontinuous first derivative at k_c. In the isomorphic quantum particle problem, the critical well depth k_c separates a bound and non-bound ground state. Similarly, for the classical particle undergoing biased diffusion, if it is conditioned to stay in the interval for a time fraction $\nu > \nu_c$, it localizes around $\mathcal{I}$ for the whole conditioning period T ($\to \infty$). For $\nu < \nu_c$ in contrast, numerical simulation showed that the particle spends a given

fraction of the total time T localized around $\mathcal{I}$, and thereafter follows its natural tendency of drifting off towards infinity. This behaviour is not Markovian, and there is no effective process in the sense of (4.97). (Recall from Section 4.2.3 that the effective process construction at bias k requires strict convexity of the rate function at that point, which does not hold at linear branch of the rate function.) The authors conjectured that one should expect the presence of this DPT for random walks possessing two main qualities. The original process must be transient rather than recurrent, *i.e.* with probability one the particle revisits its starting point only finitely often; or at least it allows transience to emerge upon conditioning on the large deviations if originally it was recurrent. In 1D, recurrence amounts to zero asymptotic velocity. Furthermore, the tilted process generator must allow eigenvalue crossings in the bias parameter s. This cannot be the case for an original equilibrium process, whose tilted generator is necessarily symmetrizable and hence avoids crossings [27].

We introduce now the extension of the ARW to a multi-state random walker on a homogeneous one-dimensional lattice, for which we shall in subsequent sections repeat the above calculations and explore the differences and similarities to the ARW/biased diffusion as a reference case.

5.1.2 Multi-state random walks

A **multi-state random walker** is simply a random walk on a lattice where the waiting-time distribution between jumps, and the direction and length of jumps, depends on an internal state of the walker, a state which undergoes its own evolution, typically by a Markov jump process [77, 187]. This class of random walkers encompasses the continuous-time random walk and persistent random walks, made famous by Montroll and Weiss, and discussed briefly in Section 2.1.1.

We specialize to Markovian multi-state random walks on an infinite linear lattice. When in internal state i, the particle makes a step of Δn sites (which may be a positive or negative number) with rate $\gamma_i(\Delta n)$. The particle switches internal state from i to j with a rate ω_{ji} (with $\omega_{ii} = 0$). Importantly, we take all rates to be independent of the spatial coordinate n (*i.e.*, the process is translationally invariant). The master equation for this class of models reads

$$\partial_t P_i(n) = \sum_k \gamma_i(k)[P_i(n-k) - P_i(n)] + \sum_j [\omega_{ij} P_j(n) - \omega_{ji} P_i(n)] \,. \tag{5.13}$$

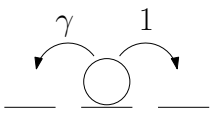

(a) *Asymmetric random walker (*ARW*)*

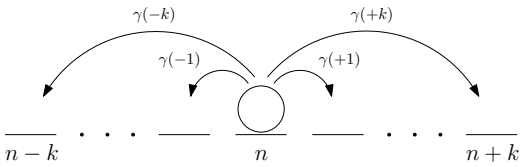

(b) *A multi-step walker*

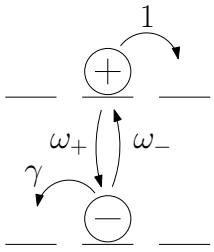

(c) *Asymmetric run-and-tumble particle (*ARTP*)*

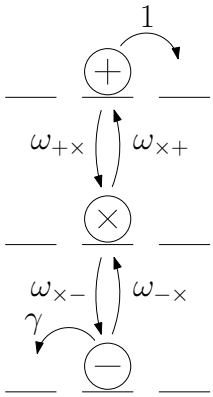

(d) *A three-state model:* RTP *with a refractory state.*

Figure 5.2 *Examples from the class of models described by the master equation* (5.13).

Some examples are illustrated in Figure 5.2.

As in Chapter 2, we consider the generating functions

$$g_i(z,t) := \sum_{n=-\infty}^{\infty} z^n P_i(n,t). \tag{5.14}$$

The generating functions can be inverted by the formula

$$P_i(n) = \frac{1}{2\pi i} \oint_{\partial\mathcal{D}} \frac{dz}{z^{n+1}} g_i(z), \tag{5.15}$$

where $\mathcal{D}$ is the complex unit disk. The evolution of $\boldsymbol{g} := (g_1, \ldots, g_N)^\top$ follows from (5.13) as

$$\partial_t \boldsymbol{g}(z,t) = \mathsf{W}(z)\boldsymbol{g}(z,t). \tag{5.16}$$

Here, the $N \times N$ matrix $\mathsf{W}(z)$ has elements

$$\mathsf{W}_{ii}(z) = \sum_k \gamma_i(k)(z^k - 1) - \sum_j \omega_{ji} \,, \tag{5.17a}$$

$$\mathsf{W}_{ij}(z) = \omega_{ij} \quad (i \neq j)\ . \tag{5.17b}$$

In particular, one simple two-state system we will be interested in is the **asymmetric run-and-tumble particle** (ARTP) that generalizes the RTP master equation (2.9) to

$$\partial_t P_+(n) = P_+(n-1) + \omega_- P_-(n) - (1+\omega_+)P_+(n), \tag{5.18a}$$
$$\partial_t P_-(n) = \gamma P_-(n+1) + \omega_+ P_+(n) - (\gamma+\omega_-)P_-(n), \tag{5.18b}$$

that is

$$\mathsf{W}(z) = \begin{pmatrix} z-1-\omega_+ & \omega_- \\ \omega_+ & \gamma(z^{-1}-1)-\omega_- \end{pmatrix}\ . \tag{5.19}$$

In the degenerate limit $\omega_- = \omega_+ \to \infty$, the ARTP becomes identical to an ARW with left and right rates $\gamma/2$ and $1/2$. If instead $\omega_+ \to 0$ and $\omega_- \to \infty$ the ARTP becomes the above ARW with $\gamma = 0$.

5.2 Velocity fluctuations in a multi-state random walk

Building on the simple example of velocity fluctuations in the ARW, we first demonstrate how, in principle, one would calculate the large deviation elements for the velocity observable of a multi-state random walk described by (5.13). We then focus on the asymmetric RTP, as it is the simplest extension from the ARW and hence the first place to look for new fluctuation phenomena afforded by internal states.

5.2.1 Method of finding the SCGF

The velocity observable V_T is given by (4.50b) with weight function (here called α rather than g)

$$\alpha\left((i, n+k), (i, n)\right) = k \tag{5.20}$$

for each pair of configurations with a nonzero transition rate, $\gamma_i(k) > 0$. Since the observable maintains translation invariance for the problem, the tilted generating function satisfies

$$\partial_t \tilde{\boldsymbol{g}}(z,t;s) = \widetilde{\mathsf{W}}_s(z)\tilde{\boldsymbol{g}}(z,t;s), \tag{5.21}$$

where

$$\widetilde{\mathsf{W}}_{ij}(z;s) = \begin{cases} \displaystyle\sum_k \gamma_i(k)(z^k e^{sk} - 1) - \sum_{k\neq i} \omega_{ki} & \text{if } i = j \\ \omega_{ij} & \text{otherwise} \end{cases}. \tag{5.22}$$

Because velocity fluctuations are identical on the ring and on the infinite line, let us suppose L-periodic boundary conditions, for which in the definition of the generating function we replace z^n with $e^{2\pi i n/L}$, and sum over $n = 0, 1, \ldots, L-1$.

By the same logic used in Section 2.3, the spectrum of $\widetilde{\mathbb{W}}_s$ (dimension $NL \times NL$) is composed of the collection of eigenvalues of $\widetilde{\mathsf{W}}(z)$ (dimension $N \times N$) for $z = 1, e^{2\pi i/L}, \ldots, e^{2(L-1)\pi i/L}$. This is because, in the Fourier basis, $\widetilde{\mathbb{W}}_s$ is block-diagonal with these matrices as the blocks. In particular, the dominant eigenvalue, which coincides with the SCGF Λ_s, is contained within the block $z = 1$, which follows from the argument that this eigenvalue must be independent of L. (In fact, we may without loss of generality suppose $L = 1$.) We must then find the dominant eigenvalue of the matrix

$$\widetilde{\mathsf{W}}(1;s) = \mathsf{W}(e^s). \tag{5.23}$$

It follows from the Perron-Frobenius theorem for finite matrices that, assuming the internal state dynamics is irreducible, $\Lambda(s)$ is simple, and hence does not cross with other eigenvalues as s is varied. Since the matrix elements are differentiable in s and there are no crossings, $\Lambda(s)$ is differentiable, and the Gärtner-Ellis theorem is applicable. There can be no dynamical phase transition.

The asymptotic average velocity $\bar{v}$, for which we will find $I(\bar{v}) = 0$, can be computed from

$$\bar{v} = \sum_i P_i^* \bar{v}_i \,, \tag{5.24}$$

where P_i^* is the steady-state distribution over the internal states i, and $\bar{v}_i$ is the

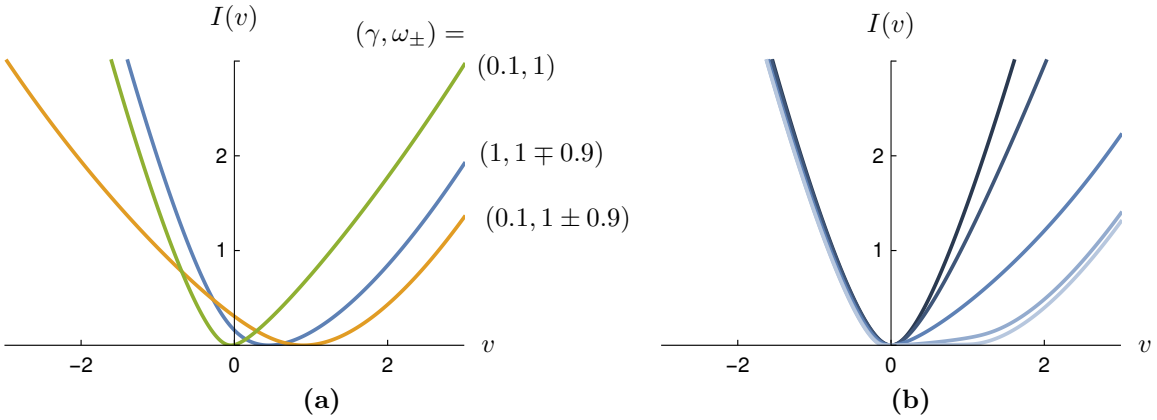

Figure 5.3 *Velocity rate function for the asymmetric RTP. (a) Combinations of symmetric/asymmetric hopping and tumbling. (b) Rates* (5.38) *giving zero limiting velocity;* $\gamma = 0.1$, *and* $\delta = 10^n$, $n = 2, 1, 0, -1, -2$ *from dark to light.*

average velocity of the particle conditioned on being in state i,

$$\bar{v}_i = \sum_k \gamma_i(k) k \ . \tag{5.25}$$

In particular, for the asymmetric RTP, the steady-state condition of the internal dynamics is

$$P_+^* \omega_+ = P_-^* \omega_- \ , \tag{5.26}$$

which yields

$$P_+^* = \frac{\omega_-}{\omega_+ + \omega_-} \ , \quad P_-^* = \frac{\omega_+}{\omega_+ + \omega_-} \ . \tag{5.27}$$

The average velocity is therefore

$$\bar{v}^{\mathrm{RTP}} = P_+^* - \gamma P_-^* = \frac{\omega_- - \gamma \omega_+}{\omega_+ + \omega_-} \ . \tag{5.28}$$

In the following we leave the full generality of the class of walkers we have set out and focus on the tractable case of the asymmetric RTP.

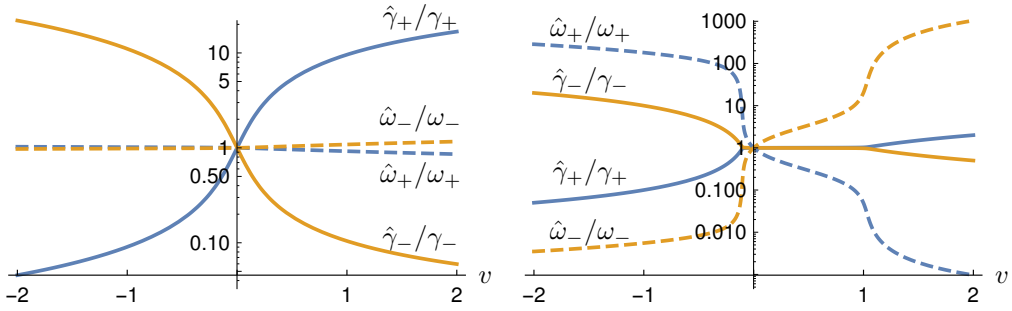

(a) $\gamma = 0.1,\ \delta = 100.$ **(b)** $\gamma = 0.1,\ \delta = 0.01.$

Figure 5.4 *Rates of the effective process normalized by the original rates, plotted on a log-scale versus v. Orange (blue) for left (right), unbroken (dashed) line for hopping (tumbling). Parameter values correspond to the rate function Figure 5.3b, i.e. tumbling rates according to (5.38). See main text for interpretation.*

5.2.2 Velocity fluctuations of the asymmetric RTP

Following the method described above, we find the velocity SCGF $\Lambda(s)$ for the asymmetric RTP as the dominant eigenvalue of the matrix (5.19) with $z = e^s$:

$$\Lambda(s) = \cosh_\gamma(s) - \cosh_\gamma(0) - \omega + \sqrt{\omega^2 - \delta\omega^2 + (\sinh_\gamma(s) - \sinh_\gamma(0) - \delta\omega)^2}, \quad (5.29)$$

where we have defined

$$\cosh_\gamma(x) := \frac{e^x + \gamma e^{-x}}{2}, \quad \sinh_\gamma(x) := \frac{e^x - \gamma e^{-x}}{2}. \quad (5.30)$$

and

$$\omega := \frac{\omega_+ + \omega_-}{2}, \quad \delta\omega := \frac{\omega_+ - \omega_-}{2}. \quad (5.31)$$

The saddle-point value $s^* = I'(v)$ used in the LF transform satisfies

$$v = x + \frac{(x - x_0 - \delta\omega)\sqrt{\gamma + x^2}}{\sqrt{\omega^2 - \delta\omega^2 + (x - x_0 - \delta\omega)^2}}, \quad (5.32)$$

where

$$x = \sinh_\gamma(s^*) \quad \text{and} \quad x_0 = \sinh_\gamma(0)\ . \quad (5.33)$$

Solving (5.32) for x (and therewith s^*) amounts to factorizing a cubic polynomial, which we can always do, but the result is unwieldy. But supposing we have

obtained the solution $x = x(v)$, for example by numerical evaluation of the cubic formula, we then have

$$s^* = \ln\left[\frac{1}{\gamma}\left(\sqrt{\gamma + x(v)^2} - x(v)\right)\right], \tag{5.34}$$

and $I(v) = s^*(v)v - \Lambda(s^*(v))$ is easily written down in terms of $x(v)$.

Next, we solve for the effective process rates. To obtain the dominant *right* eigenvector R_s of $\widetilde{\mathbb{L}}_s = \widetilde{\mathbb{W}}_s^\top$ (*i.e.* the dominant *left* eigenvector of $\widetilde{\mathbb{W}}_s$), we note again that this matrix is block-diagonal in the Fourier basis, and with the dominant eigenvalue lying in the $z = 1$ block,

$$\mathsf{W}^\top(e^s) = \begin{pmatrix} e^s - 1 - \omega_+ & \omega_+ \\ \omega_- & \gamma(e^{-s} - 1) - \omega_- \end{pmatrix}, \tag{5.35}$$

corresponding to the spatially uniform mode. The elements of the right eigenvector are therefore $R_\pm(n) = r_\pm$, where $\boldsymbol{r} = (r_+, r_-)^\top$ is the dominant right eigenvector in the first Fourier block: $\mathsf{W}^\top(e^s)\boldsymbol{r} = \Lambda(s)\boldsymbol{r}$. We find that

$$\begin{pmatrix} r_+ \\ r_- \end{pmatrix} \propto \begin{pmatrix} x(v) - x_0 - \delta\omega + \sqrt{\omega^2 - \delta\omega^2 + (x(v) - x_0 - \delta\omega)^2} \\ \omega - \delta\omega \end{pmatrix}. \tag{5.36}$$

The effective rates then follow as

$$\hat{\gamma}_\pm := \gamma_\pm e^{\pm s^*} = \sqrt{\gamma + x(v)^2} \pm x(v) \tag{5.37a}$$

$$\hat{\omega}_\pm := \omega_\pm \frac{\ell_\mp}{\ell_\pm} = \sqrt{\omega^2 - \delta\omega^2 + (x(v) - x_0 - \delta\omega)^2} \mp (x(v) - x_0 - \delta\omega). \tag{5.37b}$$

We observe again that the activity parameters are not changed by the effective process.

Some special choices of rates warrant a closer investigation.

Zero velocity and time-scale separation

One interesting scenario is where we let the hopping bias and tumbling bias compensate each other such that we have a typical null velocity. For any given γ

this is achieved by

$$\omega_+ = \delta, \quad \omega_- = \gamma\delta, \tag{5.38}$$

where δ is a parameter we are free to vary independently. The particle spends more time in the $-$ state, but there it also hops at a slower rate than in the $+$ state.

As seen in Figure 5.3b where $\gamma = 0.1$, for $\delta \sim 100$, the rate function is nearly symmetric around zero. The effective process Figure 5.4a reveals that, within the range of fluctuations plotted, it is deviations in hopping rates, and not in tumbling rates, that realize atypical velocities.

At the other end with $\delta \sim 0.01$, a qualitative difference between the large deviation tails is apparent. There is an approximate velocity range $-\gamma < v < 1$, where the rate function is almost flat, indicating that all fluctuations in this range are relatively likely to be attained. The presence of a widely fluctuating velocity for random walks with large time-scale separations has been reported on previously [178, 179, 188]. The effective process allows a window onto the mechanism behind this phenomenon. In particular we see from Figure 5.4b that atypical tumbling is responsible for fluctuations in the $-\gamma < v < 1$ range. This is because, with tumbling rates much slower than hopping rates, a large number of hops occurs between tumbles, so that any deviation from typicality in the tumbling rates has a large impact on velocity.

We can check that as $\delta \to 0$ the rate function approaches zero in $-\gamma < v < 1$ with a jump in derivative at the end points. Therefore, the SCGF (5.29) approaches

$$\Lambda(s) = \begin{cases} e^s - 1, & s > 0, \\ \gamma(e^{-s} - 1), & s < 0, \end{cases} \tag{5.39}$$

with a non-analyticity at $s = 0$, so that the rate function approaches

$$I(v) = \begin{cases} v \ln v - v + 1, & v > 1, \\ 0, & -\gamma \leq v \leq 1, \\ -v \ln(-v/\gamma) + v + \gamma, & v < -\gamma. \end{cases} \tag{5.40}$$

We can interpret this as a dynamical phase transition, where $v < -\gamma$ corresponds to the left-moving phase, $v > 1$ to the right-moving phase, and $[-\gamma, 1]$ to a

phase-coexistence regime. We remark that outside the coexistence phase, the rate function is identical to that of either a left-moving random walker with rate γ or a right-moving one with rate 1.

The degenerate RTP

As illustrated in Figure 5.5, if we tune the tumbling rates to

$$\omega_+ = \gamma, \quad \omega_- = 1, \tag{5.41}$$

the generator spectrum exhibits the macroscopic eigenvalue degeneracy that we observed for the symmetric ($\gamma = 1$) RTP in Figure 2.5b. Half (*i.e.* L) eigenvalues coalesce at $-\xi = -(1+\gamma)$, the escape rate found in any configuration, and the other half lie on an oval in the complex plane and exactly correspond to the spectrum of the ARW of Section 5.1.1. For this reason we refer to the ARTP with rates (5.41) as the **degenerate run-and-tumble particle**, or DRTP.

For this choice of rates we can trivially solve (5.32) for the saddle point, using $x_0 + \delta\omega = 0$ to find $x(v) = v/2$. One verifies then that the rate function is *identical* to that of the ARW, *i.e.* to (5.4). For the DRTP the effective rates (5.37) simplify to

$$\hat{\gamma}_\pm = \sqrt{\gamma + (v/2)^2} \pm v/2, \tag{5.42a}$$
$$\hat{\omega}_\pm = \sqrt{\gamma + (v/2)^2} \mp v/2, \tag{5.42b}$$

which shows identical modification of the initial rates 1 and γ as in the effective rates (5.7) of the ARW.

What do we make of this perfect agreement of rate functions, or **large deviation equivalence**, of the ARW and DRTP? It is expected that the large deviation principle itself, and qualitative features of the rate function like convexity, or the presence of DPTs, will show universality, *i.e.* be insensitive to most model details. In contrast, the rate function is expected to be quantitatively different between models. In the next section we explain the large deviation equivalence by the fact that the DRTP, and further multi-state generalizations of it that we shall define, can be thought of as superpositions of multiple ARWs.

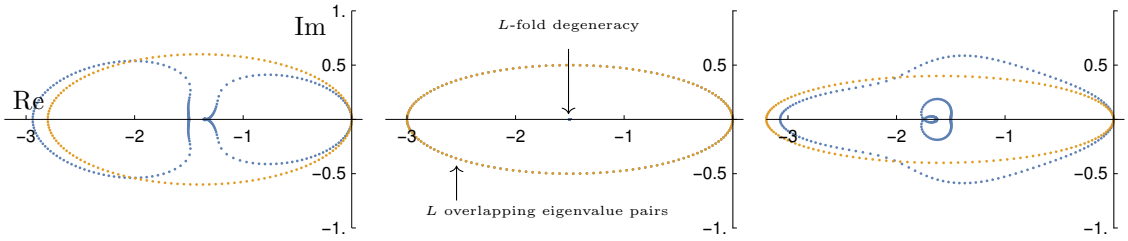

(a) $\gamma = 0.4$ **(b)** $\gamma = 0.5$ **(c)** $\gamma = 0.6$

Figure 5.5 *The spectrum in the complex plane for the ARW (orange) and RTP (blue) with* $\omega_+ = 0.5$, $\omega_- = 1$, $L = 150$, *for three values of* γ. *In (a) and (c) the spectra are distinct; in (c), where the RTP rates satisfy* (5.41), *half the eigenvalues of the RTP coalesce at* $-(1+\gamma)$, *and the rest reproduce the ARW spectrum.*

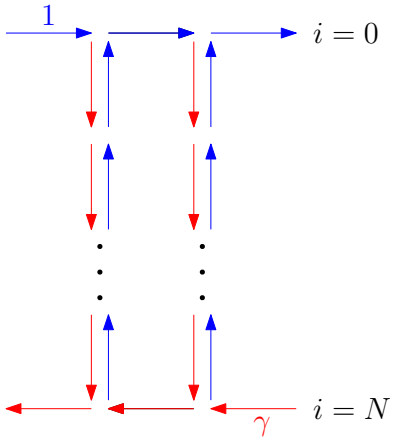

Figure 5.6 *A generalization of the fine-tuned ARW and RTP to multiple 'resting' states. We call this the* N*-ARW, so that the ARW and RTP corresponding to* $N = 0$ *and* $N = 1$.

5.2.3 A probabilistic quasi-particle

Generalizing from the DRTP, consider the multi-state random walk defined by the the transition graph Figure 5.6. There are $N + 1$ internal states, or levels, connected into 'ladders' between two horizontal lanes. Right (left) hops can only be made in level 0, which we also denote by $+$ (level N, also denoted $-$). Up and right transitions occur with rate 1 and down or left transitions with rate γ, which constitutes a special tuning of rates such that the escape rate is $\xi = 1 + \gamma$. We will call this model the N-ARW and note that for $N = 0$ it corresponds to the ARW and for $N = 1$ to the DRTP.

The master equation for the N-ARW is

$$\begin{cases} \partial_t P_0(n) = P_0(n-1) + P_1(n) - (1+\gamma)P_0(n), & \text{(5.43a)} \\ \partial_t P_i(n) = \gamma P_{i-1}(n) + P_{i+1}(n) - (1+\gamma)P_i(n), \quad 0 < i < N, & \text{(5.43b)} \\ \partial_t P_N(n) = \gamma P_N(n+1) + \gamma P_{N-1}(n) - (1+\gamma)P_N(n). & \text{(5.43c)} \end{cases}$$

It is easy to verify that the stationary distribution for the level dynamics is

$$P_i^* = \frac{\gamma^i}{1+\gamma+\gamma^2+\ldots+\gamma^N}. \tag{5.44}$$

The average velocity is therefore

$$\bar{v} = 1 \cdot P_0^* - \gamma \cdot P_N^* = \frac{1-\gamma^{N+1}}{1+\gamma+\gamma^2+\ldots+\gamma^N} = 1-\gamma, \tag{5.45}$$

independently of the number N of levels. As N becomes larger, the walker spends more time transitioning between resting states (levels $1, \ldots, N-1$) rather than making lateral jumps, but it also becomes more biased towards hopping right when a hop does occur. This is seen from the persistence probabilities $P(+ \mid +)$ and $P(- \mid -)$ that the next hop is in the same direction as the previous (calculated in Appendix 5.A):

$$P(+ \mid +) = \frac{1}{1+\gamma P_N^*}, \quad P(- \mid -) = \frac{\gamma}{\gamma + P_0^*}. \tag{5.46}$$

In particular, as $N \to \infty$, $P(+ \mid +) \to 1$ and $P(- \mid -) \to \gamma/(1+\gamma)$. For any large but finite N the increase in persistence and in time spent in the resting states with N balance to keep $\bar{v}$ constant. The $N \to \infty$ carries subtleties that we return to at the end of the section.

Consider now the following ansatz for a solution to (5.43),

$$P_i(n,t) = P_i^* p(n+i,t), \tag{5.47}$$

where $p(n,t)$ evolves by the ARW master equation (5.1). This ansatz requires us to posit a rather particular initial condition, namely $P_i(n,0) = P_i^* p(n+i,0)$, where $p(n,0)$ is any initial distribution for a one-dimensional random walker. This, however, is not a concern because we are ultimately interested in the long-time velocity statistics, which are independent of the initial condition due to ergodicity.

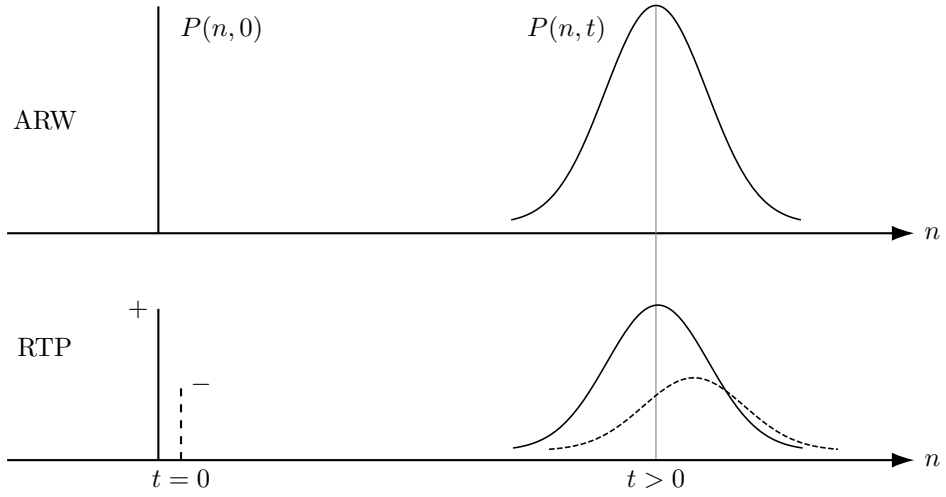

Figure 5.7 *Sketch of the degenerate RTP represented as a pair of offset* ARWs.

We consider first the ansatz for $0 < i < N$. Note that

$$P^*_{i+1} = \gamma P^*_i. \tag{5.48}$$

Then

$$\partial_t[P^*_i p(n+i,t)] = P^*_i[p(n+i-1,t) + \gamma p(n+i+1,t) - (1+\gamma)p(n,t)] \tag{5.49a}$$

$$= \gamma \underbrace{[P^*_{i-1}p(n+i-1,t)]}_{P_{i-1}(n,t)} + \underbrace{[P^*_{i+1}p(n+i+1,t)]}_{P_{i+1}(n,t)} - (1+\gamma)\underbrace{[P^*_i p(n,t)]}_{P_i(n,t)}. \tag{5.49b}$$

This is precisely the master equation (5.43b) once we make the identification (5.47). Now for $i = 0$ we have

$$\partial_t[P^*_0 p(n,t)] = P^*_0[p(n-1,t) + \gamma p(n+1,t) - (1+\gamma)p(n,t)] \tag{5.50a}$$

$$= \underbrace{[P^*_0 p(n-1,t)]}_{P_0(n-1,t)} + \underbrace{[P^*_1 p(n+1,t)]}_{P_1(n,t)} - (1+\gamma)\underbrace{[P^*_0 p(n,t)]}_{P_0(n,t)}, \tag{5.50b}$$

which coincides with (5.43a). A similar derivation holds for $i = N$. Thus (5.47) solves the N-ARW for any initial condition consistent with this form. We can interpret this solution as a probabilistic quasi-particle made up of a superposition of ARWs, such that the quasi-particle itself behaves like an ARW. This idea is sketched in Figure 5.7 for $N = 1$, corresponding to the DRTP.

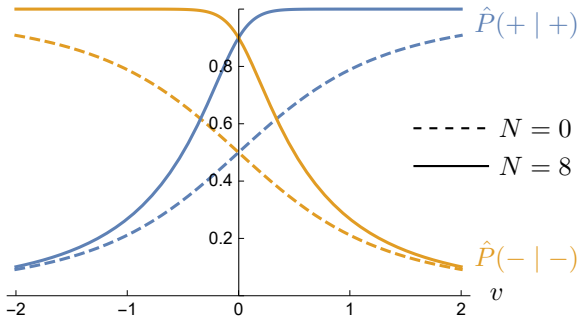

Figure 5.8 *Effective rates for the N-ARW at $\gamma = 0.5$ conditioned on the velocity v.*

For the velocity large deviations of the N-ARW, all we need to note is that $p(vt, t) \asymp e^{-I_\gamma(v)t}$ as derived in Section 5.1.1, and that $p(n, t) \asymp p(n + i, t)$. It then follows that

$$P(vt, t) = \sum_i P_i(vt, t) \asymp e^{-I_\gamma(v)t}, \tag{5.51}$$

and we thus have large deviation equivalence for all (finite) values of N of the N-ARW.

To summarize, the quasi-particle explanation shows that the large deviation equivalence between the N-ARWs is explained by a mapping to the ARW that holds for all time given special initial conditions. For an arbitrary initial condition and finite observation times, the velocity statistics will differ to some degree from the ARW, but limiting our view to the long-time limit allows us to generalize to any initial condition. What makes the N-ARW interesting from a large deviation point of view, is that for different values of N, the trajectories that generate a velocity fluctuation v are qualitatively different even after marginalizing over the internal states, while occurring with identical probability on the exponential scale. We prove this via the effective process.

Following the argument in Section 5.2.2, we conclude that in order to find the effective rates of the velocity-conditioned N-ARW we must find the dominant right

eigenvector of the $(N+1)\times(N+1)$ matrix

$$\mathsf{W}^{\top}(e^s) = \begin{pmatrix} e^s-\xi & \gamma & 0 & & \cdots & 0 \\ 1 & -\xi & \gamma & & & \\ 0 & 1 & -\xi & \gamma & & \vdots \\ \vdots & & & \ddots & & 0 \\ & & & 1 & -\xi & \gamma \\ 0 & & \cdots & 0 & 1 & \gamma e^{-s}-\xi \end{pmatrix}. \tag{5.52}$$

One checks that the dominant eigenvalue is indeed (5.3) with right eigenvector $\boldsymbol{r}$ with elements

$$r_i = (e^s)^i. \tag{5.53}$$

The modification of the original rates to effective rates is then

$$1 \to e^{s^*} = \sqrt{\gamma + (v/2)^2} + v/2, \tag{5.54a}$$

$$\gamma \to \gamma e^{-s^*} = \sqrt{\gamma + (v/2)^2} - v/2, \tag{5.54b}$$

following the colour coding of Figure 5.6. We can rescale the persistence probabilities (5.46) by (5.54) to obtain the effective persistence probabilities plotted in Figure 5.8. These clearly depend on N, telling us that the trajectory ensemble obtaining the fluctuation differs with N.

Finally, we return to the question of $N \to \infty$. The typical relaxation time is expected to be $\tau_{\text{rel}} \sim \gamma^{-N}$. The large deviation results we have calculated are only asymptotically correct for observation times $T \gg \tau_{rel}$, so that we cannot take $N \to \infty$ and meaningfully interpret our derived result. It is clear that in this limit, we separate the upper and lower lanes by an infinite distance, so that we essentially get two distinct processes depending on which lane the walker has a finite distance to in the initial condition, each of which has its own velocity rate function.

In conclusion, the N-ARW serves as an example that internal state structure may not be discernable at the level of the long-time velocity fluctuations, as studied through the rate function, but that the quality of trajectories may still be affected, as studied through the effective process.

5.3 A dynamical phase transition in occupation time

We now consider the multi-state random walk described by (5.13) and provide a novel method of finding the large deviation elements associated with conditioning on the time spent at the origin. We then apply this formula to study the occupation time DPT in the ARW and the asymmetric RTP.

5.3.1 Method of finding the SCGF

Recall that the SCGF is given by

$$\Lambda(s) = \lim_{t\to\infty} \frac{1}{t} \ln Z(t;s) \tag{5.55}$$

with

$$Z(t;s) = \left\langle e^{tsA_t} \right\rangle = \sum_{n,i} \tilde{P}_i(n,t;s), \tag{5.56}$$

where $\tilde{P}_i(n,t;s)$ is the tilted probability evolving by the tilted generator $\widetilde{\mathbb{W}}_s$. If we define the vector $\boldsymbol{Z}(t;s) = (Z_1,\ldots,Z_N)$ with elements

$$Z_i(t;s) := \sum_{n} \tilde{P}_i(n,t;s), \tag{5.57}$$

we find a relationship with the tilted generating function $\tilde{\boldsymbol{g}}$ as

$$\boldsymbol{Z}(t;s) = \tilde{\boldsymbol{g}}(1,t;s), \tag{5.58}$$

and with Z as

$$Z(t;s) = \mathbf{1}\cdot\boldsymbol{Z}(t;s). \tag{5.59}$$

We know the time evolution of $\tilde{\boldsymbol{g}}$, namely

$$\partial_t \tilde{\boldsymbol{g}}(z,t;s) = \mathsf{W}(z)\tilde{\boldsymbol{g}}(z,t;s) + s\tilde{\boldsymbol{p}}(0,t;s) \tag{5.60}$$

where $\tilde{p}_i := \tilde{P}_i$. Furthermore, by the inversion (5.15) of the generating function

$$\tilde{\boldsymbol{p}}(0,t;s) = \frac{1}{2\pi i}\oint_{\partial\mathcal{D}} \frac{\mathrm{d}z'}{z'}\tilde{\boldsymbol{g}}(z',t;s). \tag{5.61}$$

Given (5.55), (5.58) and (5.59), if we can find the long-time asymptotic form of $\tilde{\boldsymbol{g}}$ from (5.60), then we have have the SCGF in a few easy steps. In fact, what we shall do in the following is to turn (5.60) into an equation for $\widetilde{Z}$ in the Laplace-domain. Then we get the SCGF as the dominant singularity in the complex plane of Laplace-transformed $\widetilde{Z}$.

Taking the Laplace transform on the time variable $t \to u$ in (5.60), indicating transformed functions by $\tilde{\boldsymbol{g}} \to \bar{\boldsymbol{g}}$, *etc.*, we get

$$u\bar{\boldsymbol{g}}(z,u;s) - \tilde{\boldsymbol{g}}(z,0;s) = \mathsf{W}(z)\bar{\boldsymbol{g}}(z,u;s) + s\bar{\boldsymbol{p}}(0,u;s), \tag{5.62}$$

Now let us put $z = 1$ and recognize $\bar{\boldsymbol{g}}(1,u;s) = \overline{\boldsymbol{Z}}(u;s)$

$$u\overline{\boldsymbol{Z}}(u;s) - \tilde{\boldsymbol{g}}(1,0;s) = \mathsf{W}(1)\overline{\boldsymbol{Z}}(u;s) + s\bar{\boldsymbol{p}}(0,u;s). \tag{5.63}$$

Further, let us note that $\tilde{g}_i(1,0;s) = \sum_n \bar{P}_i(n,0;s)$. There is no reason the initial condition should depend on s, so we let $\tilde{\boldsymbol{g}}(1,0;s) =: \tilde{\boldsymbol{g}}_0$. Thus

$$[u\mathbb{1} - \mathsf{W}(1)]\overline{\boldsymbol{Z}}(u;s) = \tilde{\boldsymbol{g}}_0 + s\bar{\boldsymbol{p}}(0,u,s). \tag{5.64}$$

We now substitute (5.64) into (5.62) and rearrange to obtain

$$[u\mathbb{1} - \mathsf{W}(z)]\bar{\boldsymbol{g}}(z,u;s) = [u\mathbb{1} - \mathsf{W}(1)]\overline{\boldsymbol{Z}}(u;s). \tag{5.65}$$

We invert the matrix in square brackets on the left and apply $(s/2\pi i)\oint \mathrm{d}z/z$ to both sides of the equation:

$$\frac{s}{2\pi i}\oint_{\partial\mathcal{D}} \frac{\mathrm{d}z}{z}\bar{\boldsymbol{g}}(z,u;s) = \left[\frac{s}{2\pi i}\oint_{\partial\mathcal{D}} \frac{\mathrm{d}z}{z}\left(u\mathbb{1} - \mathsf{W}(z)\right)^{-1}\right]\left[u\mathbb{1} - \mathsf{W}(1)\right]\overline{\boldsymbol{Z}}(u;s) \tag{5.66}$$

Let us define the matrix

$$\mathcal{I}(u) = \frac{1}{2\pi i}\oint_{\partial\mathcal{D}} \frac{\mathrm{d}z}{z}\left(u\mathbb{1} - \mathsf{W}(z)\right)^{-1}. \tag{5.67}$$

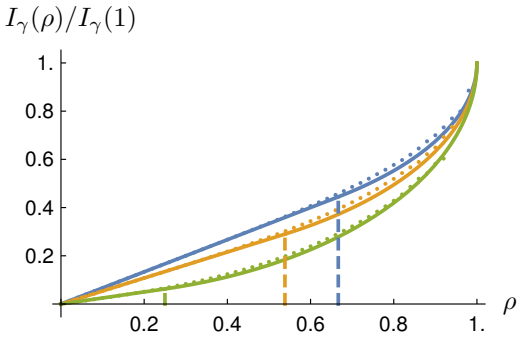

Figure 5.9 *The rate function for origin occupation time in the ARW. The whole lines show exact analytical results, with the vertical dashed lines indicating the phase transition points. Dots show simulation results of about* 5×10^9 *trajectories with duration* $T = 20$*. The values for* γ *used are* $0.2, 0.4, 0.6$ *(blue, yellow, green)*

Using (5.61) and (5.66) we write (5.66) as

$$s\bar{\boldsymbol{p}}(0,u,s) = s\mathcal{I}(u)\,[u\mathbb{1} - \mathsf{W}(1)]\,\overline{\boldsymbol{Z}}(u;s). \tag{5.68}$$

This expression we can now substitute into (5.64) to eliminate $s\bar{\boldsymbol{p}}(0,u,s)$ and obtain an explicit expression for $\overline{\boldsymbol{Z}}(u;s)$. After a few algebraic manipulations:

$$\overline{\boldsymbol{Z}}(u;s) = [u\mathbb{1} - \mathsf{W}(1)]^{-1}\,[\mathbb{1} - s\mathcal{I}(u)]^{-1}\,\tilde{\boldsymbol{g}}_0. \tag{5.69}$$

From this expression, we finally get

$$\overline{Z}(z;s) = \mathbf{1}\cdot[u\mathbb{1} - \mathsf{W}(1)]^{-1}\,[\mathbb{1} - s\mathcal{I}(u)]^{-1}\,\tilde{\boldsymbol{g}}_0. \tag{5.70}$$

From (5.17) we see that $\mathsf{W}(1)$ is the forward generator of the internal state process. Thus its largest eigenvalue is 0, giving $\overline{Z}(z;s)$ a pole at $u = 0$ (and more for negative u) coming from $\det(u\mathbb{1} - \mathsf{W}(1))$. A DPT can arise if there is an additional pole for $u^*(s) > 0$ that crosses $u = 0$ at some finite value of s. We expect this u to be a solution to $\det(\mathbb{1} - s\mathcal{I}(u)) = 0$. It appears difficult to evaluate the (non)existence of such a pole for an arbitrary multi-state random walk of the form (5.17). Instead, we look at two analytically tractable examples: the ARW and the ARTP.

5.3.2 Dynamical phase transition in the ARW

We expect the result of conditioning the ARW on the time spent at the origin to be qualitatively similar to the problem of drifted diffusion conditioned on time spent in an interval, as reviewed in Section 5.1.1. Furthermore, the ARW is the simplest prototype for applying the novel method formula (5.70).

For the ARW, the integral (5.67) is

$$\mathcal{I} = \frac{1}{2\pi i}\oint_{\partial\mathcal{D}} \frac{dz}{z}\,\frac{1}{u-(z+\gamma z^{-1}-(1+\gamma))} = -\frac{1}{2\pi i}\oint_{\partial\mathcal{D}} \frac{dz}{z^2-az+\gamma}, \tag{5.71}$$

with $a = u+1+\gamma$. The poles of the integrand are

$$z_\pm = a/2 \pm \sqrt{(a/2)^2-\gamma}. \tag{5.72}$$

One verifies that $z_+(u=0)=1$ and $\partial_u z_+ > 0$, hence this pole lies outside $\mathcal{D}$ (the unit disk) for $u>0$; $z_-(u=0)=\gamma$, $z_-(u\to\infty)=0$ whilst $\partial_u z_- < 0$, hence this pole lies inside $\mathcal{D}$ for $u>0$ and $\gamma<1$. Using the residue theorem,

$$\mathcal{I} = \frac{1}{z_+-z_-} = \frac{1}{\sqrt{a^2-4\gamma}} = \frac{1}{\sqrt{u(u+2(1+\gamma))+(1-\gamma)^2}}\,. \tag{5.73}$$

Therefore,

$$\overline{Z}(u;s) = \frac{1}{u}\cdot\left[1-\frac{s}{\sqrt{u(u+2(1+\gamma))+(1-\gamma)^2}}\right]^{-1}. \tag{5.74}$$

Only if $s > s^* = 1-\gamma$ does there exist a positive pole, namely

$$u^* = -(1+\gamma)+\sqrt{s^2+4\gamma}\,. \tag{5.75}$$

We therefore conclude

$$\Lambda(s) = \begin{cases} -(1+\gamma)+\sqrt{s^2+4\gamma}, & s>s^*, \\ 0, & s\le s^*. \end{cases} \tag{5.76}$$

Note that in contrast to the version of this problem in continuous space [50], we are able here to obtain an explicit expression for $\Lambda(s)$.

We can see directly that $\Lambda(s)$ is not analytic in s, which means that the Gärtner-Ellis theorem does not apply. Operating on the assumption (to be justified)

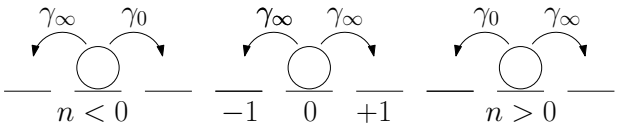

Figure 5.10 *In the ARW occupation-time effective process for $\rho > \rho_c$, jumps toward the origin occur with rates $\gamma_0(\rho)$ and away from the origin with rates $\gamma_\infty(\rho)$.*

that the rate function is convex, we nonetheless obtain the rate function via LF transform. In the restricted range $s \leq s^*$, the maximizer of $s - \Lambda(s)$ is s^*. For $s \geq s^*$, the maximizer is instead

$$s^\dagger = \frac{2\rho\sqrt{\gamma}}{\sqrt{1-\rho^2}}, \tag{5.77}$$

provided that $s^\dagger > s^*$. This condition is equivalent to

$$\rho > \rho_c = \frac{1-\gamma}{1+\gamma}\,. \tag{5.78}$$

The rate function is therefore

$$I_\gamma(\rho) = \begin{cases} (1-\gamma)\rho, & \rho \leq \rho_c, \\ 1+\gamma-2\sqrt{\gamma(1-\rho^2)}, & \rho > \rho_c, \end{cases} \tag{5.79}$$

which is plotted in Figure 5.9. The salient feature is the change from linear to convex shape at ρ_c, which reveals a first-order dynamical phase transition. The correctness of the linear branch of the rate function, and hence convexity, is verified by empirical calculation of the rate function from naive sampling of a large number of simulated trajectories.

We remark that in the case where $\gamma = 0$ the rate function is entirely linear, which follows immediately from the Poisson distribution of leaving the origin, after which a return is impossible. This observation already suggests that the linear part for non-zero γ is due to trajectories that stay close to the origin for the chosen time-fraction before venturing off to infinity.

We next calculate the effective process for in the range of fluctuations where this construction is legitimate, namely $s > s^*$. The dominant left (right) eigenvector $R(n)$ of the tilted forward (backward) generator satisfies

$$\Lambda(s)R(n) = R(n+1) + \gamma R(n-1) - (1+\gamma)R(n) + sR(0)\delta_{n,0}. \tag{5.80}$$

Substituting the value of the SCGF and rearranging,

$$R(n+1) + \gamma R(n-1) - \sqrt{s^2 + 4\gamma}\, R(n) = s\delta_{n,0}. \tag{5.81}$$

The solution by generating function techniques is

$$R(n) = \begin{cases} r^{-n}, & n \geq 0 \\ (\gamma r)^{-|n|}, & n < 0, \end{cases} \tag{5.82}$$

where

$$r = \frac{1}{2\gamma}[\sqrt{s^2 + 4\gamma} - s]\ . \tag{5.83}$$

This leads to the effective rates $\hat{W}$ that are no longer translationally invariant,

$$\hat{W}(n+1, n) = \begin{cases} \frac{1}{2}(\sqrt{s^2 + 4\gamma} + s), & n \geq 0 \\ \frac{1}{2}(\sqrt{s^2 + 4\gamma} - s), & n < 0\ , \end{cases} \tag{5.84a}$$

$$\hat{W}(n, n+1) = \gamma / \hat{W}(n+1, n). \tag{5.84b}$$

Once we substitute the saddle-point value $s^\dagger$ (5.77) the resulting effective process is described by Figure 5.10 with

$$\gamma_0(\rho) = \sqrt{\gamma \frac{1+\rho}{1-\rho}}\ , \quad \gamma_\infty(\rho) = \sqrt{\gamma \frac{1-\rho}{1+\rho}}\ . \tag{5.85a}$$

Since $\gamma_0/\gamma_\infty > 1$, the particle is biased towards the origin: it lives in a linear confining potential that becomes steeper as ρ is increased. Exactly at the transition point ρ_c, $\gamma_0 = 1$ and $\gamma_\infty = \gamma$. The original dynamics has then been modified by mirroring the dynamics for the negative half-lattice to achieve symmetry about the origin.

For $\rho < \rho_c$, since the rate function is not strictly convex, the asymptotic equivalence of the effective process and the conditioned process breaks down, as we can plainly see: attempting to substitute $s = -I'(\rho)$, we find $s = s^* = -(1-\gamma)$ for all $\rho < \rho_c$. This, however, would produce effective rates $\gamma_0(\rho) = 1$ and $\gamma_\infty(\rho) = \gamma$ which always gives a typical occupation ρ_c, and not the chosen $\rho < \rho_c$! Turning instead to direct simulation, we find, in expected agreement with [50], the trajectory structure shown in Figure 5.11. For long simulation times T, the graphs show how the accumulated occupation time at site 0 increases with time

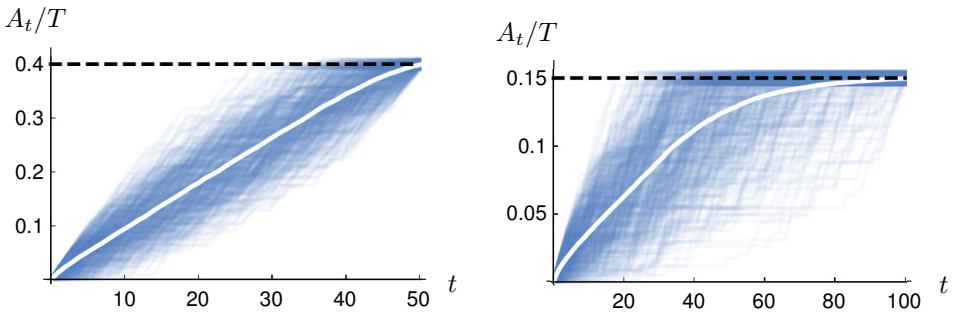

(a) *Time at origin, $\rho > \rho_c$* **(b)** *Time at origin, $\rho < \rho_c$*

Figure 5.11 *The increase in fraction of time A_t/T spent at origin as a function of t, $0 \leq t \leq T$, from simulation of $\sim 10^7$ ARW trajectories with $\gamma = 0.6$. In (a) a subset of 500 trajectories satisfying $\rho = 0.4 \pm 0.05 > \rho_c = 0.25$ at final time $T = 50$ have been selected; in (b) $\rho = 0.15 \pm 0.005 < \rho_c$ and $T = 100$. The white line indicates the average over trajectories. For $\rho > \rho_c$ the approximate linearity of the average shows that the contribution to A_t is evenly distributed throughout; the particle is localized around the origin. For $\rho < \rho_c$, there is a localized period, followed by escape.*

for a large sample of trajectories satisfying the final occupation ρ within some tolerance. Up to a finite time effect, for $\rho > \rho_c$ the contribution is evenly spread through the time interval, resulting in the average occupation increasing linearly (white line). In contrast, for $\rho < \rho_c$ the average increases linearly for about half the simulation time, at which point most of the trajectories have achieved the final occupation. Thus, these trajectories stay localized around the origin for an initial portion of time before escaping off to infinity.

5.3.3 Dynamical phase transition in the ARTP

We consider next the ARTP. With asymmetry in both tumbling and hopping, there is a continuum of parameter values that all lead to zero net velocity, as we found in Section 5.2.2. Our hypothesis is that the occupation DPT will be found if and only if the net velocity is non-zero, whether the asymmetry is created by biased tumbling or hopping.

The matrix $\mathsf{W}(z)$ for the ARTP was given by (5.19) which, for convenience, we will write as

$$\mathsf{W}(z) = \begin{pmatrix} \mu(z) & \omega_+ \\ \omega_- & \nu(z)/z \end{pmatrix} \tag{5.86}$$

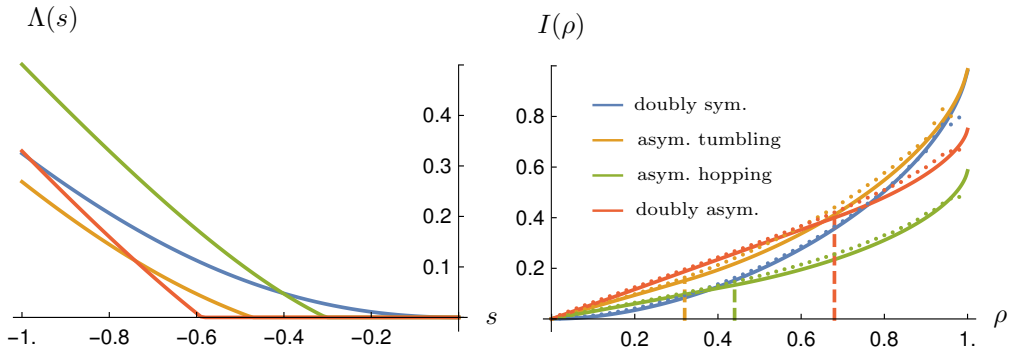

(a) *Various (a)symmetric parameter choices*

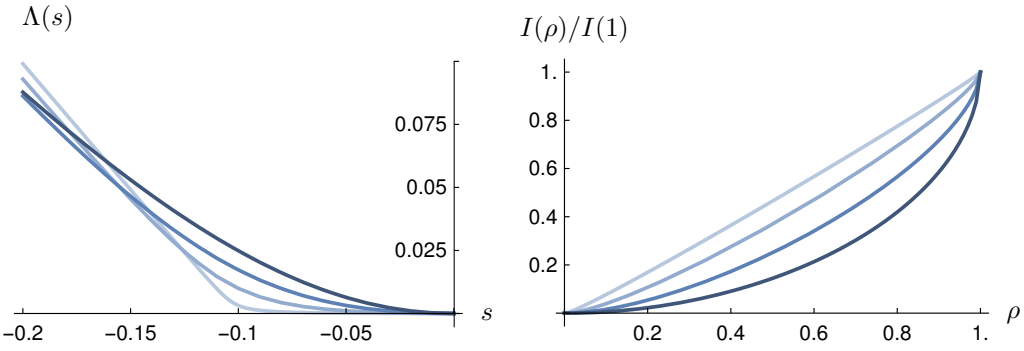

(b) *Zero limiting velocity*

Figure 5.12 *SCGF (left panels) and rate function (right panels) for the RTP occupation problem. The SCGF is non-singular if and only if the limiting velocity is zero. (a) Parameters demonstrate the possible combinations of (a)symmetry* $(\gamma, \omega, \delta\omega = 1, 1, 0;\ 1, 1, 0.5;\ 0.3, 1, 0;\ 0.3, 0.65, -0.45)$*. Dots show simulation results of about* 3×10^9 *trajectories with duration* $T = 25$*. (b) The zero limiting velocity rate rates (5.38) with* $\gamma = 0.1$*, and* $\delta = 10, .5, .1, .01$ *from dark to light line colour.*

with

$$\mu(z) = z - 1 - \omega_+, \tag{5.87a}$$

$$\nu(z) = -z(\gamma + \omega_-) + \gamma. \tag{5.87b}$$

The matrix inverse in the integrand of $\mathcal{I}(u)$ (5.67) is then

$$[uI - \mathsf{W}(z)]^{-1} = \frac{1}{(u - \mu(z))(uz - \nu(z)) - \omega_+\omega_- z} \begin{pmatrix} uz - \nu(z) & \omega_- z \\ \omega_+ z & z(u - \mu(z)) \end{pmatrix}. \tag{5.88}$$

Every element of this matrix has two poles in z given by the zeroes of the quadratic

$$(u-\mu(z))(uz-\nu(z))-\omega_+\omega_- z=-a_-(z-z_+)(z-z_-)\,, \tag{5.89}$$

where

$$z_\pm=\frac{1}{2a_-}\left[a_+a_-+\gamma-\omega_+\omega_-\pm\sqrt{(a_+a_-+\gamma-\omega_+\omega_-)^2-4\gamma a_+a_-}\right], \tag{5.90a}$$

$$a_+=u+1+\omega_+, \tag{5.90b}$$

$$a_-=u+\gamma+\omega_-. \tag{5.90c}$$

One can verify that $z_-\in\mathcal{D}\setminus\partial\mathcal{D}$ (open complex unit disk) and $z_+\notin\mathcal{D}$ for the relevant parameter ranges and $u>0$ (in fact, both roots are real, $z_+>1$, and $1>z_->0$). Then by means of the residue theorem and after some algebraic simplifications we find

$$\mathcal{I}=\frac{1}{a_-(z_+-z_-)}\begin{pmatrix}a_--\frac{\gamma}{z_+} & \omega_-\\ \omega_+ & a_+-z_-\end{pmatrix}. \tag{5.91}$$

Taking into account that $z_\pm>0$ for $u>0$, one can conclude that the positive poles of $\overline{Z}(u,s)$ are given by $\det(\mathbb{1}-s\mathcal{I})=0$, *i.e.*

$$\det\begin{pmatrix}a_-(z_+-z_-)-s(a_--\frac{\gamma}{z_+}) & -s\omega_-\\ -s\omega_+ & a_-(z_+-z_-)-s(a_+-z_-)\end{pmatrix}=0. \tag{5.92}$$

This equation can be solved numerically for the rightmost pole $u^*(s)=\Lambda(s)$. Figure 5.12 shows that the resulting SCGF becomes zero for s larger than some $s^*<0$ in a non-differentiable fashion when the velocity is non-zero. Assuming the validity of obtaining the rate function through LF transform of the SCGF, the rate function develops a linear-convex transition corresponding to the singularity of the SCGF.

We note that the large deviation equivalence for velocity at the parameter values $\omega_+=\gamma$ and $\omega_-=1$ does not extend to the occupation observable. By putting $u=0$ in (5.92) and solving for s, we get $s^*=(1+\gamma)(1-\sqrt{\gamma})$, different from the ARW. Since the SCGFs do not have the same singularity they surely do not coincide.

When we choose rates according to (5.38), producing zero limiting velocity, we

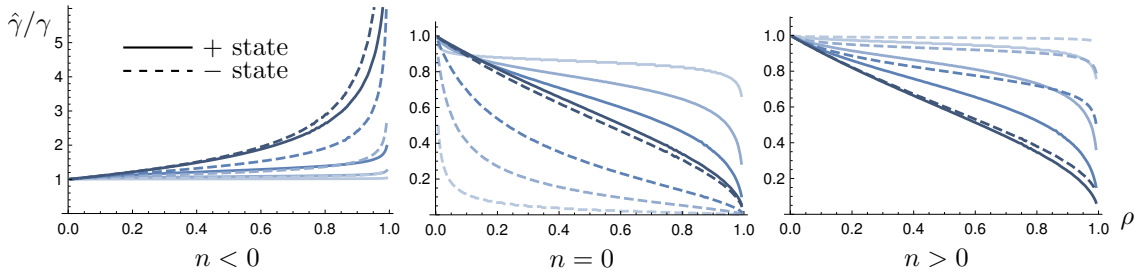

(a) *Effective hopping rates*

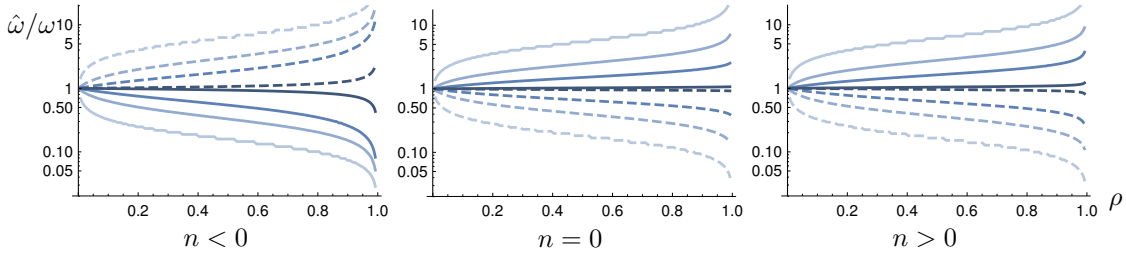

(b) *Effective tumbling rates*

Figure 5.13 *Effective rates corresponding to Figure 5.12b as a function of ρ, normalized by the original rates. (a) shows hopping rates and (b) shows tumbling rates. Whole lines indicate the + state, dashed lines the − state. Note that the tumbling rates are plotted on a vertical log-scale. For interpretation of the graphs, see main text.*

obtain Figure 5.12b. As δ becomes small, the SCGF approaches a singularity at $-\gamma$. Meanwhile, the rate function evolves continuously from convex to linear. As tumble events become rare, the time spent at the origin is dominated by the time the particle sits there before its first exit.

To find the effective process we again seek the dominant right eigenvector $R_\pm(n)$ of $\widetilde{\mathbb{L}}_s$ satisfying

$$\Lambda(s)R_+(n) = R_+(n+1) + \omega_+ R_-(n) - (1 + \omega_+ - s\delta_{n,0})R_+(n) \tag{5.93a}$$

$$\Lambda(s)R_-(n) = \gamma R_-(n-1) + \omega_- R_+(n) - (\gamma + \omega_- - s\delta_{n,0})R_-(n). \tag{5.93b}$$

It was found numerically that $\Lambda(s) > 0$ for s larger than some s^*, and zero below it. We consider the former case, corresponding to the convex branch of the rate function. We reuse the parameters $a_\pm, z_\pm$ of (5.90c), but with $u^* = \Lambda(s)$ substituted for u in their definitions. The generating function form of (5.93) is

$$\begin{pmatrix} z^{-1} - a_+ & \omega_+ \\ \omega_- & \gamma z - a_- \end{pmatrix} \boldsymbol{r}(z) = s\boldsymbol{r}(0)\ . \tag{5.94}$$

Inverting the matrix,

$$\boldsymbol{r}(z) = -\frac{sz}{a_+\gamma(z-\tilde{z}_-)(z-\tilde{z}_+)}\begin{pmatrix} a_- - \gamma z & \omega_+ \\ \omega_- & a_+ - z^{-1} \end{pmatrix}\boldsymbol{r}(0)\ , \tag{5.95}$$

with

$$\tilde{z}_\pm := (a_-/\gamma a_+)z_\pm = 1/z_\mp \tag{5.96}$$

following from $z_+z_- = \gamma a_+/a_-$. Applying the inverse transform,

$$\boldsymbol{r}(n) = sQ(n)\boldsymbol{r}(0)\ , \tag{5.97a}$$

$$Q(n) := -\frac{1}{2\pi i}\oint_{\partial D}\frac{dz}{z^n}\frac{1}{\gamma a_+(z-\tilde{z}_+)(z-\tilde{z}_-)}\begin{pmatrix} a_- - \gamma z & \omega_+ \\ \omega_- & a_+ - z^{-1} \end{pmatrix}. \tag{5.97b}$$

Since $\Lambda(s) > 0$, we have $\tilde{z}_- \in \mathcal{D}\setminus\partial\mathcal{D}$, while $\tilde{z}_+ \notin \mathcal{D}$. For $n = 0$ we get the eigenvalue equation

$$[I - sQ(0)]\boldsymbol{r}(0) = \boldsymbol{0}, \tag{5.98}$$

with $Q(0)^\top = \mathcal{I}|_{u=\Lambda(s)}$ of (5.91). We require a non-trivial solution, which implies that $I - s\mathcal{I}$, whose inverse appears in the dynamical partition function (5.70), is singular at $u = \Lambda(s)$. This indeed follows from the fact this value of u is a pole of $\overline{Z}$ (see (5.92)). We may choose

$$\boldsymbol{r}(0) = \begin{pmatrix} a_-(z_+ - z_-) - s(a_+ - z_-) \\ -s\omega_- \end{pmatrix}. \tag{5.99}$$

For $n \geq 1$ we find instead

$$Q(\pm n) = \frac{(z_\mp)^{\pm n}}{a_-(z_+ - z_-)}\begin{pmatrix} a_- - \frac{\gamma}{z_\mp} & \omega_+ \\ \omega_- & a_+ - z_\mp \end{pmatrix}. \tag{5.100}$$

It is then a matter of simple algebra to find the relevant ratios of eigenvector components, which subsequently produce the effective rates

$$\hat{W}((+,n+1),(+,n)) = \begin{cases} z_- & n > 0 \\ z_-\frac{a_-}{a_- - s}\frac{a_+ - z_+}{a_+ - z_-} & n = 0 \\ z_+ & n < 0 \end{cases} \tag{5.101a}$$

$$\hat{W}((-,n-1),(-,n)) = \begin{cases} \gamma/z_+ & n>0 \\ (\gamma/z_+)\frac{a_- - s}{a_-} & n=0 \\ \gamma/z_- & n<0 \end{cases} \tag{5.101b}$$

$$\hat{W}((-,n),(+,n)) = \begin{cases} \omega_+\omega_- \frac{a_+}{a_-(a_+ - z_+)} & n>0 \\ \omega_+\omega_- \frac{a_+}{(a_- - s)(a_+ - z_-)} & n=0 \\ \omega_+\omega_- \frac{a_+}{a_-(a_+ - z_-)} & n<0 \end{cases} \tag{5.101c}$$

$$\hat{W}((+,n),(-,n)) = \omega_+\omega_-/\hat{W}((-,n),(+,n)). \tag{5.101d}$$

Interestingly, the particle has a special set of rates at the origin. If $\bar{v} = 0$, then the above solution is fully sufficient as the maximizer $s(\rho) \leq s^* = 0$. Figure 5.13 shows the effective rates corresponding to the rates function Figure 5.12b. In the original process the particle hops faster to the right, but spends more time in the left-oriented state. For $n < 0$, the effective process increases both hopping rates, while increasing tumbling frequency into the right-moving state, and decreasing the tumbling frequency out of it. For $n > 0$, all hopping rates are decreased, while tumbles into the left-moving state becomes relatively more favoured. A more remarkable result is that at the origin, the left hopping rates are decreased dramatically, even for small ρ, and the tumbles into the left-moving states are simultaneously increased. Overall, away from the origin the effective process generates a bias towards it, and at the origin the likelihood of being in the left state is increased by an order of magnitude, and its hopping rate decreased by and order of magnitude, effectively trapping it in an inactive state at the origin.

Finally, we investigate by simulation the structure of trajectories in the linear regime of the rate function. The contribution to the occupancy as a function of time is qualitatively the same as for the ARW, Figure 5.11 (and hence the graph is not here reproduced).

In conclusion, our study of the occupation fluctuations in the ARTP supports the hypothesis that transience is necessary for the DPT in occupation times following [50]. In contrast to the ARW, in the ARTP transience is not equivalent to breaking detailed balance, which allows us to disentangle the role of these two properties in the presence of the DPT. Indeed, while the ARTP trivially breaks detailed balance, the DPT was only present when the typical net velocity was non-zero, *i.e.* the process was transient. Further study of the partition function (5.70) may allow this conclusion to be extended to the whole class of multi-state random walks outlined in this Chapter.

5.4 Summary of results

We set out a class of multi-state random walkers on a linear lattice in order to find illustrative examples of distinct large deviation regimes occurring within a single model, and in particular to gain insight into when and how singularities can arise. As dynamical observables we considered the velocity and the time spent at the origin, and gave in both cases a method for finding the dominant spectral elements of the titled generator associated with the large deviation elements. For velocity, we must solve the dominant eigenproblem of a matrix of dimension equal to the number of internal states; for the occupation time, we must find the dominant singularity in the complex plane of a Laplace-transformed dynamical partition function. Both problems were solved exactly in the reference case of the ARW, and we then focussed on the asymmetric RTP (ARTP) which is interesting because of the interplay between hopping asymmetry and tumbling asymmetry.

For velocity fluctuations in the ARTP, we gave an example of a parameter value where the typical velocity is zero, thanks to a balancing of asymmetries in hopping an tumbling, but where the overall time-scale of tumbles can be independently varied. When this time-scale diverges, a flat branch of the rate function emerges, indicating that there is a range of velocity fluctuations that are all of comparable probability at a given time scale (Figure 5.3b). From the effective process rate Figure 5.4 we see that trajectories differ qualitatively between regimes, although the transitions only become sharp as the tumbling time-scale diverges.

We encountered another interesting tuning of parameters in the ARTP that corresponds to the macroscopic eigenvalue crossing of the process' generator, encountered first in Section 2.3 in case of symmetric rates. We were able to understand the origin of this phenomenon, by extending the model to the N-ARW, an $(N+1)$-internal-state walker. It could be described as a 'probabilistic quasiparticle' whose velocity statistics coincides with that of $N+1$ non-interacting, slightly offset ARWs. It transpired that the velocity rate function was independent of N, *i.e.* identical to the ARW. However, N controls the degree of persistence in the walk, so that across all values of N, the trajectories that generate the same velocity with the same probability at the exponential scale, are different. This admittedly contrived, but intriguing, example shows that there may be interesting large deviation phenomena that are invisible in the rate function, but appear in the effective process.

We also investigated for the ARTP the existence of the dynamical phase transition in occupation time reported previously for biased diffusion. Here, across the range of parameters examined we found the DPT to emerge precisely when the typical velocity was non-zero. As in the case of biased diffusion (or the ARW that we solved exactly), there is a linear branch of the rate function, corresponding to non-Markovian behaviour where trajectories stay localized around the origin for a period of time, and then follow their intrinsic bias of escaping to infinity. In the convex branch, the particle remains localized around the origin, but the ARTP has a peculiarity, in comparison to the ARW, that it can make an effective modification to the rates, to make one internal state close to inactive at the origin, in order to keep the particle there for long periods of time.

Appendices for Chapter 5

5.A Marginalization of the N-ARW

In the N-ARW with rates according to Figure 5.6, let us calculate conditional probabilities such as $P(+ \mid +)$, that the next step of the walker is to the right, given that the previous was, and that we start from level 0.

Let $\pi_\tau(+ \mid +)$ (resp. $\pi_\tau(+ \mid -)$) be the probability that starting from level 0 (level N), after τ level transitions without translations the walker ends again in level 0 (level N). Furthermore denote by $P_\uparrow$ ($P_\downarrow$) the probability that the next state transition (whether level or site) is up (down), and by $P_\rightarrow$ ($P_\leftarrow$) the probability that the next transition is a right (left) hop if such a hop is possible:

$$P_\uparrow = \frac{1}{1+\gamma}, \quad P_\downarrow = \frac{\gamma}{1+\gamma}, \tag{5.102a}$$

$$P_\rightarrow = \frac{1}{1+\gamma}, \quad P_\leftarrow = \frac{\gamma}{1+\gamma}. \tag{5.102b}$$

Then we can write

$$P(+ \mid +) = \frac{P_\rightarrow \sum_{\tau=0}^{\infty} \pi_\tau(+ \mid +)}{P_\rightarrow \sum_{\tau=0}^{\infty} \pi_\tau(+ \mid +) + P_\leftarrow \sum_{\tau=0}^{\infty} \pi_\tau(- \mid +)} \tag{5.103}$$

$$= \frac{1}{1+\gamma Q}. \tag{5.104}$$

Here we define

$$Q := \frac{\sum_{\tau=0}^{\infty} \pi_\tau(- \mid +)}{\sum_{\tau=0}^{\infty} \pi_\tau(+ \mid +)}. \tag{5.105}$$

We also have

$$P(- \mid +) = 1 - P(+ \mid +) = \frac{1}{1+(\gamma Q)^{-1}}. \tag{5.106}$$

Similar to (5.103) we have

$$P(+\mid -) = \frac{P_{\rightarrow}\sum_{\tau=0}^{\infty}\pi_\tau(+\mid -)}{P_{\rightarrow}\sum_{\tau=0}^{\infty}\pi_\tau(+\mid -) + P_{\leftarrow}\sum_{\tau=0}^{\infty}\pi_\tau(-\mid -)}, \tag{5.107}$$

which we now seek to express using Q.

Let $c_\tau(+\mid +)$ *etc.* be the number of possible paths starting and ending at level 0 in τ steps without making lateral transitions. Then

$$\pi_\tau(+\mid +) = c_\tau(+\mid +)P_{\downarrow}^{\tau/2}P_{\uparrow}^{\tau/2} = c_\tau(+\mid +)(z^*)^\tau, \tag{5.108}$$

with

$$z^* := \sqrt{P_{\downarrow}P_{\uparrow}} = \frac{\sqrt{\gamma}}{1+\gamma}. \tag{5.109}$$

In (5.108) we have used the fact that in order to start at level 0 and return to it, an equal number of up and down transitions must be made. Next we have

$$\pi_\tau(-\mid +) = c_\tau(-\mid +)P_{\downarrow}^{N}P_{\uparrow}^{\frac{\tau-N}{2}}P_{\downarrow}^{\frac{\tau-N}{2}} \tag{5.110}$$

$$= \left(\frac{P_{\downarrow}}{P_{\uparrow}}\right)^{N/2} c_\tau(-\mid +)(z^*)^\tau, \tag{5.111}$$

from the fact that there must be N more down transitions than up transitions on the whole. Similarly,

$$\pi_\tau(+\mid -) = c_\tau(+\mid -)P_{\uparrow}^{N}P_{\downarrow}^{\frac{\tau-N}{2}}P_{\uparrow}^{\frac{\tau-N}{2}} \tag{5.112a}$$

$$= \left(\frac{P_{\uparrow}}{P_{\downarrow}}\right)^{N/2} c_\tau(+\mid -)(z^*)^\tau \tag{5.112b}$$

$$= \left(\frac{P_{\uparrow}}{P_{\downarrow}}\right)^{N} \pi_\tau(-\mid +), \tag{5.112c}$$

where we used the obvious symmetry $c_\tau(+\mid -) = c_\tau(-\mid +)$. The other symmetry $c_\tau(-\mid -) = c_\tau(+\mid +)$ gives us

$$\pi_\tau(-\mid -) = \pi_\tau(+\mid +). \tag{5.113}$$

Using (5.113) and (5.112) we can express (5.107) as

$$P(+\mid -) = \frac{1}{1 + \frac{P_{\rightarrow}}{P_{\leftarrow}} \left(\frac{P_{\downarrow}}{P_{\uparrow}}\right)^{N} \frac{\sum_{\tau=0}^{\infty} \pi_{\tau}(+|+)}{\sum_{\tau=0}^{\infty} \pi_{\tau}(-|+)}} \tag{5.114}$$

$$= \frac{1}{1 + \gamma^{N+1} Q^{-1}}. \tag{5.115}$$

Then

$$P(-\mid -) = \frac{1}{1 + \gamma^{-(N+1)} Q}. \tag{5.116}$$

We now calculate Q explicitly. Let $c_{\tau}(n)$ be the number of paths on the levels of one lateral site that start at level 0, $c_0(n) = \delta_{n,0}$, and end in level n.

$$\begin{cases} c_{\tau+1}(n) = c_{\tau}(n+1) + c_{\tau}(n-1), \quad 0 < n < N, & \text{(5.117a)} \\ c_{\tau+1}(0) = c_{\tau}(1), & \text{(5.117b)} \\ c_{\tau+1}(N) = c_{\tau}(N-1). & \text{(5.117c)} \end{cases}$$

We introduce the discrete Laplace transform

$$G(z, n) := \sum_{\tau=0}^{\infty} c_{\tau}(n) z^{\tau}, \tag{5.118}$$

which then satisfies

$$\begin{cases} z^{-1} G(z, n) = G(z, n+1) + G(z, n-1), \quad 0 < n < N, & \text{(5.119a)} \\ z^{-1} G(z, 0) - 1 = G(z, 1), & \text{(5.119b)} \\ z^{-1} G(z, N) = G(z, N-1). & \text{(5.119c)} \end{cases}$$

The equations are solved by the ansatz

$$G(z, n) = A(z)\mu(z)^{n} + B(z)\mu(z)^{-n} \tag{5.120}$$

which yields

$$G(z, n) = \frac{\mu^{-(N+1-n)} - \mu^{N+1-n}}{\mu^{-(N+2)} - \mu^{N+2}} \tag{5.121}$$

with

$$\mu(z) = \frac{1}{2z}[1 - \sqrt{1 - 4z^2}]. \tag{5.122}$$

From (5.108) and (5.110) it follows that

$$\sum_{\tau=0}^{\infty} \pi_\tau(+ \mid +) = G(z^*, 0), \tag{5.123}$$

$$\sum_{\tau=0}^{\infty} \pi_\tau(- \mid +) = \gamma^{N/2} G(z^*, N). \tag{5.124}$$

Using $\mu(z^*) = \sqrt{\gamma}$ we have

$$Q = \gamma^N \frac{G(z^*, N)}{G(z^*, 0)} = \frac{1-\gamma}{\gamma^{-N} - \gamma}. \tag{5.125}$$

This can suggestively be written as

$$Q = \frac{\gamma^N}{1 + \gamma + \gamma^2 + \ldots + \gamma^N} = P_N^*, \tag{5.126}$$

the stationary probability of the Nth level.

Chapter 6

Dynamical large deviations in the presence of boundaries

6.1 Background

Diffusion processes with boundaries are used in many application in biophysics [38], *e.g.* the reflective boundary conditions in single-file diffusion describing transport in narrow channels (Section 3.1.1), or partially reflecting or absorbing boundaries for nutrients diffusing within cells, or chemical signalling molecules between bacteria [189]. It is therefore of interest to adapt the dynamical large deviation formalism for diffusions with boundaries, so that fluctuations in observables such as time spent in the vicinity of a boundary, or the particle current in constrained geometries, can be studied. It is also of theoretical interest to understand if the presence of a certain boundary type comes with any general implications for the fluctuation characteristics of a given class of observable.

In this chapter we will be primarily concerned with the large deviations of current-like observables for diffusions with reflective boundaries. Large deviation problems for reflected diffusions have been studied before either in the low-noise limit [190–193] or in the long-time limit but for occupation-type observables [51, 194–201]. We shall derive the boundary conditions that must be imposed on the Donsker-Varadhan spectral problem associated with the large deviation elements of a current-like observable. As we shall see, these are different from the boundary conditions recently found for occupation-like observables [51], and

must be derived in a new way.

With the novel result of how to calculate current large deviations in reflected diffusions, we will be able to study the particle-current fluctuations in the heterogeneous SFD of Chapter 3, which turns out to be exactly solvable. First, however, we review in some detail the mathematics and physical meaning of reflective boundaries.

6.1.1 Introducing boundaries

We consider a diffusion $\mathbf{X}(t)$ in a domain $\Omega \subset \mathbb{R}^d$ which has a boundary $\partial\Omega$ that is smooth, or is a countable union of smooth boundary pieces. In the interior of the domain, the process behaves just like an unbounded diffusion, and is there described by the usual SDE (1.90),

$$\mathrm{d}\mathbf{X}(t) = \boldsymbol{F}(\mathbf{X}(t))\,\mathrm{d}t + \mathsf{B}\,\mathrm{d}\mathbf{W}(t). \tag{6.1}$$

Here and in the following, we let the noise matrix be constant, in order to simplify the exposition, but this is not a fundamental limitation of the methods used or results obtained. The backward and forward generators $\mathcal{L}$ and $\mathcal{L}^\dagger$ are as given for unbounded diffusions in Section 1.3.3, namely

$$\mathcal{L} = \boldsymbol{F}\cdot\nabla + \nabla\cdot\mathsf{D}\nabla, \quad \mathcal{L}^\dagger = -\boldsymbol{F}\cdot\nabla + \nabla\cdot\mathsf{D}\nabla, \tag{6.2}$$

but must now be supplemented with boundary conditions on the domain of functions ϕ and ρ on which they act, in order to account for the boundary behaviour of the process. We recall from Section 1.3.3 that ρ should be interpreted as a possible probability density of the process, and ϕ as some scalar function of the process. In particular, because $\mathcal{L}$ generates the backward Fokker-Planck equation, $\phi(x)$ may be a density value (for some state at some time) but with x referring to the initial state of the distribution.

In the presence of a boundary, the duality relation (1.97) is now defined with an inner product integrating over Ω rather than over all of $\mathbb{R}^d$:

$$\left\langle \mathcal{L}^\dagger\rho, \phi\right\rangle = \left\langle \rho, \mathcal{L}\phi\right\rangle, \quad \left\langle \rho, \phi\right\rangle = \int_\Omega \mathrm{d}\boldsymbol{x}\,\rho(\boldsymbol{x})\phi(\boldsymbol{x}). \tag{6.3}$$

As we apply integration by parts to transition from $\left\langle \mathcal{L}^\dagger\rho, \phi\right\rangle$ to $\left\langle \rho, \mathcal{L}\phi\right\rangle$, we

produce boundary terms that must vanish for the duality to hold, *i.e.* for the generators to be consistently defined in the entire domain Ω: such a prescription constitutes a boundary condition.

Let us perform the calculation explicitly. In higher dimensions, the integration-by-parts scheme follows from a rewriting of the divergence theorem, that for u a scalar field and $\boldsymbol{v}$ a vector field

$$\int_\Omega \mathrm{d}x\, u(\boldsymbol{x})\nabla\cdot\boldsymbol{v}(\boldsymbol{x}) = -\int_{\partial\Omega} \mathrm{d}x\, u(\boldsymbol{x})\boldsymbol{v}(\boldsymbol{x})\cdot\hat{\boldsymbol{n}}(\boldsymbol{x}) - \int_\Omega \mathrm{d}x\, \boldsymbol{v}(\boldsymbol{x})\cdot\nabla u(\boldsymbol{x}), \quad (6.4)$$

where $\hat{\boldsymbol{n}}(\boldsymbol{x})$ is the inward normal vector at point $\boldsymbol{x}\in\partial\Omega$. We recall the notation (4.89) for the probability current,

$$\boldsymbol{J}_{\rho,\boldsymbol{F}}(\boldsymbol{x}) = \boldsymbol{F}(\boldsymbol{x})\rho(\boldsymbol{x}) - \mathsf{D}(\boldsymbol{x})\nabla\rho(\boldsymbol{x}), \quad (6.5)$$

and that

$$\mathcal{L}^\dagger\rho = -\nabla\cdot\boldsymbol{J}_{\boldsymbol{F},\rho}. \quad (6.6)$$

The left-hand side of the duality is then

$$\left\langle \mathcal{L}^\dagger\rho, \phi\right\rangle = \int_\Omega \mathrm{d}\boldsymbol{x}\, (-\nabla\cdot\boldsymbol{J}_{\boldsymbol{F},\rho}(\boldsymbol{x}))\phi(\boldsymbol{x}) \quad (6.7a)$$

$$= \int_\Omega \mathrm{d}\boldsymbol{x}\, \boldsymbol{J}_{\boldsymbol{F},\rho}(\boldsymbol{x})\cdot\nabla\phi(\boldsymbol{x}) + \int_{\partial\Omega} \mathrm{d}\boldsymbol{x}\, \left\{\boldsymbol{J}_{\boldsymbol{F},\rho}(\boldsymbol{x})\cdot\hat{\boldsymbol{n}}(\boldsymbol{x})\right\}\phi(\boldsymbol{x}). \quad (6.7b)$$

We continue with the volume integral:

$$\int_\Omega \mathrm{d}\boldsymbol{x}\, \boldsymbol{J}_{\boldsymbol{F},\rho}(\boldsymbol{x})\cdot\nabla\phi(\boldsymbol{x}) = \int_\Omega \mathrm{d}\boldsymbol{x}\, \left\{\boldsymbol{F}(\boldsymbol{x})\rho(\boldsymbol{x})\cdot\nabla\phi(\boldsymbol{x}) - \mathsf{D}\nabla\rho(\boldsymbol{x})\cdot\nabla\phi(\boldsymbol{x})\right\} \quad (6.8a)$$

$$= \int_\Omega \mathrm{d}\boldsymbol{x}\, \left\{\boldsymbol{F}(\boldsymbol{x})\rho(\boldsymbol{x})\cdot\nabla\phi(\boldsymbol{x}) - \nabla\rho(\boldsymbol{x})\cdot\mathsf{D}\nabla\phi(\boldsymbol{x})\right\} \quad (6.8b)$$

$$= \langle\rho, \mathcal{L}\phi\rangle + \int_{\partial\Omega} \mathrm{d}\boldsymbol{x}\, \rho(\boldsymbol{x})(\hat{\boldsymbol{n}}(\boldsymbol{x})\cdot\mathsf{D}\nabla\phi(\boldsymbol{x})), \quad (6.8c)$$

where we have used the fact that D is a symmetric matrix to write $\mathsf{D}\nabla\rho\cdot\nabla\phi = \nabla\rho\cdot\mathsf{D}\nabla\rho$, and we can recognize the definition of $\mathcal{L}$ after applying again (6.4) to

the second term in (6.8b). Putting the pieces together then,

$$\left\langle \mathcal{L}^\dagger \rho, \phi \right\rangle = \langle \rho, \mathcal{L}\phi \rangle + \int_{\partial\Omega} \mathrm{d}\boldsymbol{x}\, \phi(\boldsymbol{x}) \left\{ \boldsymbol{J}_{\boldsymbol{F},\rho}(\boldsymbol{x}) \cdot \hat{\boldsymbol{n}}(\boldsymbol{x}) \right\} \tag{6.9a}$$

$$+ \int_{\partial\Omega} \mathrm{d}\boldsymbol{x}\, \rho(\boldsymbol{x}) \left\{ \mathsf{D}\nabla\phi(\boldsymbol{x}) \cdot \hat{\boldsymbol{n}}(\boldsymbol{x}) \right\}$$

$$= \langle \rho, \mathcal{L}\phi \rangle + \int_{\partial\Omega} \mathrm{d}\boldsymbol{x}\, \boldsymbol{J}_{\boldsymbol{F},\rho\phi}(\boldsymbol{x}) \cdot \hat{\boldsymbol{n}}(\boldsymbol{x}). \tag{6.9b}$$

Here, the boundary terms must vanish for any ϕ and ρ in the domain of the respective operators: this translates to separate boundary conditions on ρ and ϕ that restrict the domain of the operators $\mathcal{L}^\dagger$ and $\mathcal{L}$ compared to the case without a boundary.

Consider first the special case of $\phi \equiv 1$. The vanishing of the boundary term in (6.9b) then expresses the conservation of total probability:

$$\int_{\partial\Omega} \mathrm{d}\boldsymbol{x}\, \boldsymbol{J}_{\boldsymbol{F},\rho} \cdot \hat{\boldsymbol{n}} = \int_\Omega \mathrm{d}\boldsymbol{x}\, \nabla \cdot \boldsymbol{J}_{\boldsymbol{F},\rho} = \partial_t \int_\Omega \mathrm{d}\boldsymbol{x}\, \rho = 0. \tag{6.10}$$

We will in this chapter primarily be concerned with reflective boundary conditions, in which probability conservation, and indeed the vanishing of the first boundary term in (6.9a) for any ϕ, is guaranteed via

$$\boldsymbol{J}_{\boldsymbol{F},\rho}(\boldsymbol{x}) \cdot \hat{\boldsymbol{n}}(\boldsymbol{x}) = 0 \quad \text{for all} \quad \boldsymbol{x} \in \partial\Omega. \tag{6.11}$$

For the second boundary term, reflective boundary conditions amount to

$$\mathsf{D}\nabla\phi(\boldsymbol{x}) \cdot \hat{\boldsymbol{n}}(\boldsymbol{x}) = 0 \quad \text{for all} \quad \boldsymbol{x} \in \partial\Omega. \tag{6.12}$$

Unlike the current, $\nabla\phi$ does not vanish in the direction normal to the surface, but in the so-called co-normal direction $\mathsf{D}\hat{\boldsymbol{n}}$ [38, 202], as we can see by using $\mathsf{D} = \mathsf{D}^\top$ to write (6.12) as $\nabla\phi \cdot \mathsf{D}\hat{\boldsymbol{n}} = 0$.

As another example of boundary conditions inferred from duality, consider absorption. By definition, densities should vanish on the boundary, $\rho = 0$ on $\partial\Omega$, which then kills the second boundary term in (6.9a). This forces the choice $\phi = 0$ on $\partial\Omega$ to kill the first, which reflects the fact that the actual process density $\rho(\boldsymbol{x}', t' \mid \boldsymbol{x}, t) = 0$ if we start from $\boldsymbol{x} \in \partial\Omega$. For partial absorption–partial reflection we have on the boundary $\nabla\rho \cdot \hat{\boldsymbol{n}} = \alpha\rho$, which implies $\mathsf{D}\nabla\phi \cdot \hat{\boldsymbol{n}} = -\alpha\phi$. Note that the two boundary integrals do not vanish separately in this case.

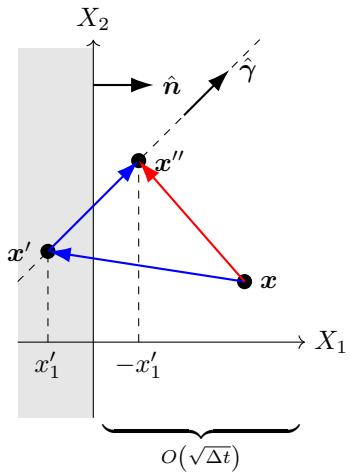

Figure 6.1 *Reflection rule at the boundary to complement the Euler scheme in the bulk. The normal component is mirrored and the particle emerges from the wall in the deterministic direction $\hat{\boldsymbol{\gamma}}$. The wall can with non-negligible probability be reached in one step in one step from a boundary layer of width $O\left(\sqrt{\Delta t}\right)$.*

We will in this chapter primarily be concerned with reflective boundary conditions. Let us therefore think about the subtle issue of what reflected trajectories look like.

6.1.2 Reflected trajectories

How are reflected Brownian trajectories constructed? Since for Brownian trajectories there is no spatial scale on which their variation is sufficiently smooth that an instantaneous velocity is well defined, neither can one define an angle of incidence for the boundary intersection. 'Reflection' for a diffusive particle must therefore mean something different than for a ballistic particle. It is instructive to think about how one would simulate a reflected diffusion based on the Euler scheme (1.89),

$$\mathbf{X}(t+\Delta t) = \mathbf{X}(t) + \boldsymbol{F}(\mathbf{X}(t),t)\Delta t + \mathsf{B}\Delta\mathbf{W}(t). \tag{6.13}$$

There will be layer of width $O\left(\sqrt{\Delta t}\right)$ close to the boundary in which the next increment of the process is likely to put it through the boundary, and outside of its intended domain. We must then devise a boundary rule to put the process back into its domain. Such a prescription is illustrated in Figure 6.1 for a two-dimensional process [38]. If the naive increment takes us from $\boldsymbol{x} \in \Omega$ to $\boldsymbol{x}' \notin \Omega$,

we reflect the component normal to the boundary about the boundary, from x_1' to $-x_1'$ in the figure. We must decide what happens to the components parallel to the boundary surface. In general, we can let the wall push the intruding particle out in a direction $\hat{\boldsymbol{\gamma}}$, placing it at $\boldsymbol{x}''$ with $x_1'' = -x_1'$. The direction $\hat{\boldsymbol{\gamma}}$ should be a property of the wall—*i.e.* part of the model definition—rather than dependent on the transgressing increment itself, as otherwise the reflection depends on an incidence angle that is undefined in the limit infinite steps per time. $\hat{\boldsymbol{\gamma}}$ may vary along with the boundary, though, as long as it can be considered constant within the reach of a single process increment. It is proved by Schuss [38, Thm 2.6.1, p. 61] that as $\Delta t \to 0$, the Euler scheme with the described reflection rule is equivalent to the FPE with reflective boundary condition (6.11) if and only if

$$\hat{\boldsymbol{\gamma}} = \frac{\mathsf{D}\hat{\boldsymbol{n}}}{|\mathsf{D}\hat{\boldsymbol{n}}|}, \tag{6.14}$$

which is referred to as the **co-normal direction**, in contrast to the normal direction $\hat{\boldsymbol{\gamma}} = \hat{\boldsymbol{n}}$. When diffusion is isotropic, the normal and co-normal directions coincide, but when there is spatial bias in diffusion, the co-normal reflection rule is the necessary choice to ensure the bias carries over to the infinitesimally small boundary layer close to $\partial\Omega$.

The limit of this Euler scheme can then be interpreted as a **Skorokhod** SDE, written

$$\mathrm{d}\mathbf{X}(t) = \boldsymbol{F}(\mathbf{X}(t))dt + \mathsf{B}\,\mathrm{d}\mathbf{W}(t) + \hat{\boldsymbol{\gamma}}(\mathbf{X}(t))\,\mathrm{d}L(t), \tag{6.15}$$

where the **local time** $L(t)$ is defined as the time spent in the small boundary layer, scaled by its size [203]:

$$L(t) = \lim_{\epsilon \to 0} \frac{1}{\epsilon} \int_0^t \mathrm{d}t'\, \mathbb{1}[|\mathbf{X}(t') - \partial\Omega| < \epsilon].$$

The local time term can be thought of as a deterministic $O\left(\sqrt{\mathrm{d}t}\right)$ push in the direction $\hat{\boldsymbol{\gamma}}$ effected whenever the particle touches the boundary, compensating the Wiener increment which may otherwise push the process across the boundary.

6.2 Dynamical large deviation theory for reflected diffusions

Let us now consider for reflected diffusions, the large deviation elements associated with a dynamic observable A_T as given by (4.90) with weights f and $\boldsymbol{g}$. Just as in the case without boundaries, we must solve the dominant eigenvalue problems for the k-tilted generators $\widetilde{\mathcal{L}}_k$, and $\widetilde{\mathcal{L}}_k^\dagger$, which we recall were given by

$$\widetilde{\mathcal{L}}_k = \boldsymbol{F}\cdot(\nabla + k\boldsymbol{g}) + (\nabla + k\boldsymbol{g})\cdot \mathsf{D}(\nabla + k\boldsymbol{g}) + kf, \tag{6.16}$$

$$\widetilde{\mathcal{L}}_k^\dagger = -(\nabla - k\boldsymbol{g})\cdot\boldsymbol{F} + (\nabla - k\boldsymbol{g})\cdot \mathsf{D}(\nabla - k\boldsymbol{g}) + kf, \tag{6.17}$$

but now with boundary conditions for the eigenfunctions r_k and ℓ_k on $\partial\Omega$ in some way determined by the reflective boundary of the original process. Clearly, these boundary conditions must be consistent with (6.11) and (6.12) for $k = 0$. In addition to this constraint, the duality relation should also hold for all k.

Is the satisfaction of duality for the tilted generators enough to infer their boundary conditions, by making sure that the boundary terms resulting from integration by parts vanish? In the next section we see that while this strategy works for occupation-like observables, as shown in [51], it does *not* work for current-like observables [5]. For the latter type we then derive the appropriate tilted boundary condition by applying the diffusive limit to a tilted jump process.

6.2.1 Tilted boundary conditions: argument from duality

We repeat the integration-by-parts protocol of Section 6.1.1 for the tilted generators, a calculation which differs only by the need to keep track of a few extra k-dependent terms. The final result is analogous to (6.9):

$$\left\langle \widetilde{\mathcal{L}}_k^\dagger \tilde{\rho}_k, \tilde{\phi}_k \right\rangle = \left\langle \tilde{\rho}_k, \widetilde{\mathcal{L}}_k \tilde{\phi}_k \right\rangle + \int_{\partial\Omega} \mathrm{d}\boldsymbol{x}\, \boldsymbol{J}_{\widetilde{\boldsymbol{F}}_k, \tilde{\phi}_k\tilde{\rho}_k}(\boldsymbol{x})\cdot\hat{\boldsymbol{n}}(\boldsymbol{x}), \tag{6.18}$$

where $\tilde{\rho}_k$ and $\tilde{\phi}_k$ are any functions in the respective domains of $\widetilde{\mathcal{L}}_k^\dagger$ and $\widetilde{\mathcal{L}}_k$, and where we have defined

$$\widetilde{\boldsymbol{F}}_k := \boldsymbol{F} + 2\mathsf{D}(k\boldsymbol{g} + \nabla \ln \tilde{\rho}_k). \tag{6.19}$$

If we substitute for $\tilde{\rho}_k$ and $\tilde{\phi}_k$ the dominant eigenvectors ℓ_k and r_k, then identifying the effective density from (4.99) as $\hat{\rho}_k^* = \ell_k r_k$, and the effective force (4.98) as $\hat{\boldsymbol{F}}_k = \widetilde{\boldsymbol{F}}_k|_{\tilde{\rho}_k = r_k}$, the vanishing of the boundary term in (6.18) expresses the conservation of probability of the effective process:

$$\int_{\partial\Omega} \mathrm{d}\boldsymbol{x}\, \boldsymbol{J}_{\hat{\boldsymbol{F}}_k, \hat{\rho}_k^*}(\boldsymbol{x}) \cdot \hat{\boldsymbol{n}}(\boldsymbol{x}) = 0. \tag{6.20}$$

It is reasonable to suppose that if the original process has reflective boundaries, then so does the effective process. After all, all possible trajectories of the original process are reflected by the same rule, which can be thought of as a deterministic push, as explained in Section 6.1.2. Since every possible trajectory of the effective process is a possible trajectory of the original process, they too must follow the same reflection rule on trajectories, which implies the reflective boundary condition

$$\boldsymbol{J}_{\boldsymbol{F}_k, \ell_k r_k}(\boldsymbol{x}) \cdot \hat{\boldsymbol{n}}(\boldsymbol{x}) = 0 \quad \text{for all} \quad \boldsymbol{x} \in \partial\Omega \tag{6.21}$$

for the dominant eigenvectors in particular, but which also extends to all functions in the respective domains of the tilted generators.

We now attempt to infer from (6.21) separate boundary conditions for ℓ_k and r_k. We can write, for arbitrary constant c,

$$\begin{aligned} \boldsymbol{J}_{\boldsymbol{F}_k, \ell_k r_k} &= (\boldsymbol{F} + 2k\mathsf{D}\boldsymbol{g})\ell_k r_k + \mathsf{D}\ell_k \nabla r_k - \mathsf{D} r_k \nabla \ell_k && \text{(6.22a)} \\ &= [\boldsymbol{F} + 2(1-c)k\mathsf{D}\boldsymbol{g}]\ell_k - \mathsf{D}\nabla\ell_k]\, r_k + \ell_k\, [2ck\mathsf{D}\boldsymbol{g} r_k + \mathsf{D}\nabla r_k]\,. && \text{(6.22b)} \end{aligned}$$

This identity can be separated into the boundary conditions

$$\{[\boldsymbol{F}(\boldsymbol{x}) + 2(1-c)k\mathsf{D}\boldsymbol{g}(\boldsymbol{x})]\ell_k(\boldsymbol{x}) - \mathsf{D}\nabla\ell_k(\boldsymbol{x})\} \cdot \hat{\boldsymbol{n}}(\boldsymbol{x}) = 0, \tag{6.23a}$$

$$\{2ck\mathsf{D}\boldsymbol{g} r_k + \mathsf{D}\nabla r_k\} \cdot \hat{\boldsymbol{n}}(\boldsymbol{x}) = 0, \tag{6.23b}$$

for $\boldsymbol{x} \in \partial\Omega$ and any c. The ambiguity of the undetermined constant c in these conditions arises from the fact that any boundary term in the duality relation that is proportional to $\ell_k r_k$, and that vanishes as $k \to 0$, can be split arbitrarily between the ℓ_k and r_k conditions. We see that if the observable on which we condition the process is only of the occupation-like form, *i.e.* $\boldsymbol{g} \equiv \boldsymbol{0}$, then there is no ambiguity in the boundary conditions. For general or purely current-like dynamical observables, an argument beyond duality is necessary to establish the

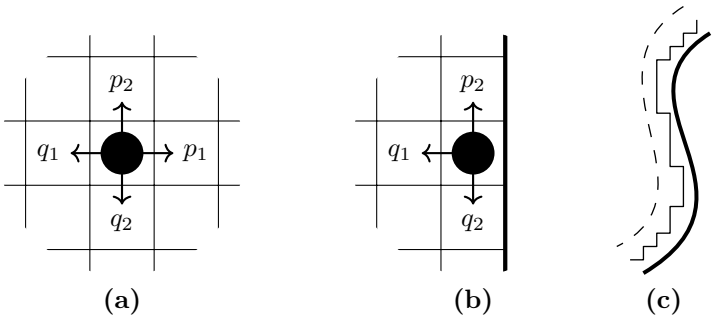

Figure 6.2 *Bulk (a) and boundary (b) configurations of the planar random walk. (c) Illustration of a smooth boundary appearing in the diffusive limit.*

correct tilted boundary conditions.

In the next section we use the diffusive limit applied to a conditioned lattice random walk to derive that the correct value of c is $1/2$. The limit operates similarly to how we derived the reflective boundary conditions for SFDs in Section 3.1.2. In the article [5] an alternative derivation of the tilted boundary conditions due to Johan du Buisson is also given based on the local-time formalism (6.15) and the Feynman-Kac approach (seen in Section 4.3).

6.2.2 Tilted boundary conditions: derivation from the diffusive limit

A strategy to derive the correct boundary conditions on ℓ_k and r_k when conditioning a reflected diffusion on a current-like observable V_T is to consider a jump process $\mathbf{N}(t)$, whose diffusive limit is $\mathbf{X}(t)$, conditioned on a lattice-current-like observable $\mathcal{A}_T$, whose diffusive limit is V_T. Then we can apply the diffusive limit to the spectral elements associated with the conditioning problem on the lattice to find bulk and boundary equations for ℓ_k and r_k.

As in Section 1.3.1, we consider a planar random walk, but with a boundary that tends to some (piecewise) smooth shape $\partial\Omega$ in the diffusive limit. It will be sufficient to consider the boundary only at a position where locally it is planar with, say, $N_1 = 0$; see Figure 6.2. In this setup the non-zero transitions rates are given by

$$W(\boldsymbol{n} + \hat{\boldsymbol{e}}_i, \boldsymbol{n}) = p_i(\boldsymbol{n}), \quad \boldsymbol{n} + \hat{\boldsymbol{e}}_i \in \mathscr{L}, \tag{6.24a}$$

$$W(\boldsymbol{n} - \hat{\boldsymbol{e}}_i, \boldsymbol{n}) = q_i(\boldsymbol{n}), \quad \boldsymbol{n} - \hat{\boldsymbol{e}}_i \in \mathscr{L}, \tag{6.24b}$$

where $\mathscr{L}$ is the set of lattices sites and $\hat{\boldsymbol{e}}_i$ is the single-site translation vector for axis i. If we scale the hopping rates with vanishing lattice constant a as,

$$p_i(\boldsymbol{n}) = \frac{B_i^2}{2a^2} + \frac{F_i(\boldsymbol{x})}{2a} + O(1), \tag{6.25a}$$

$$q_i(\boldsymbol{n}) = \frac{B_i^2}{2a^2} - \frac{F_i(\boldsymbol{x})}{2a} + O(1), \tag{6.25b}$$

we obtain the reflection diffusion with drift $\boldsymbol{F}$ and noise matrix $\mathsf{B} = \mathrm{diag}\{B_1, \ldots, B_d\}$.

Given this diffusive limit setup for the process itself, we next consider how to map the current-like observable from lattice to continuum.

Diffusive limit of the observable

As per (4.50b) a flow-like observable for a jump process is constructed as

$$\mathcal{A}_T = \sum_{\boldsymbol{n},\boldsymbol{n}' \in \mathscr{L}} \alpha(\boldsymbol{n}', \boldsymbol{n}) C_T(\boldsymbol{n}', \boldsymbol{n}), \tag{6.26}$$

with C_T the empirical flow. We choose an antisymmetric α,

$$\alpha(\boldsymbol{n}', \boldsymbol{n}) = -\alpha(\boldsymbol{n}, \boldsymbol{n}') \tag{6.27}$$

and can then write (6.26) as

$$\mathcal{A}_T = \sum_{\boldsymbol{n}} \sum_{i} \alpha(\boldsymbol{n} + \hat{\boldsymbol{e}}_i, \boldsymbol{n}) J_T(\boldsymbol{n} + \hat{\boldsymbol{e}}_i, \boldsymbol{n}) \tag{6.28}$$

with $J_T(\boldsymbol{n}', \boldsymbol{n})$ the empirical lattice current,

$$J_T(\boldsymbol{n}', \boldsymbol{n}) = C_T(\boldsymbol{n}', \boldsymbol{n}) - C_T(\boldsymbol{n}, \boldsymbol{n}'). \tag{6.29}$$

We must show how, in the diffusive limit, the lattice empirical current maps to the continuum counterpart (4.86), and how to relate α to the weight function $\boldsymbol{g}$ in (4.90b).

The lattice empirical current over the $\boldsymbol{n} \to \boldsymbol{n} + \hat{\boldsymbol{e}}_i$ bond is

$$J_T(\boldsymbol{n} + \hat{\boldsymbol{e}}_i, \boldsymbol{n}) = \frac{1}{T} \sum_{t} \left[\delta_{\mathbf{N}(t^-),\boldsymbol{n}} \delta_{\mathbf{N}(t^+),\boldsymbol{n}+\hat{\boldsymbol{e}}_i} - \delta_{\mathbf{N}(t^-),\boldsymbol{n}+\hat{\boldsymbol{e}}_i} \delta_{\mathbf{N}(t^+),\boldsymbol{n}} \right] \tag{6.30a}$$

$$= \frac{1}{T}\sum_t \left[\delta_{\mathbf{N}(t^-),\boldsymbol{n}}\delta_{\mathbf{N}(t^+),\boldsymbol{n}+\hat{\boldsymbol{e}}_i} + \delta_{\mathbf{N}(t^-),\boldsymbol{n}+\hat{\boldsymbol{e}}_i}\delta_{\mathbf{N}(t^+),\boldsymbol{n}}\right] \tag{6.30b}$$
$$\times\,(N_i(t^+) - N_i(t^-)),$$

where the second line follows because $N_i(t^+)$ and $N_i(t^-)$ differ by precisely one step. We now discretize time into points t_j narrowly separated by intervals $\Delta t(a)$, such that the jump process makes at most one jump in each interval for any value of the site separation a. For any such trajectory, the following is an exact identity:

$$\delta_{\mathbf{N}(t_j),n}\delta_{\mathbf{N}(t_j+\Delta t),\boldsymbol{n}+\hat{\boldsymbol{e}}_i} + \delta_{\mathbf{N}(t_j),\boldsymbol{n}+\hat{\boldsymbol{e}}_i}\delta_{\mathbf{N}(t_j+\Delta t),\boldsymbol{n}} = \delta_{\frac{\mathbf{N}(t_j)+\mathbf{N}(t_j+\Delta t)}{2},\boldsymbol{n}+\frac{1}{2}\hat{\boldsymbol{e}}_i}. \tag{6.31}$$

In the diffusive limit we replace $\mathbf{N}(t) = \mathbf{X}(t)/a$, $\delta_{\boldsymbol{n},\boldsymbol{n}'} = \delta(\boldsymbol{x}/a - \boldsymbol{x}'/a)$, and thus

$$J_T(\boldsymbol{n}+\hat{\boldsymbol{e}}_i,\boldsymbol{n}) = \frac{1}{T}\sum_j \delta_{\frac{\mathbf{N}(t_j)+\mathbf{N}(t_j+\Delta t)}{2},\boldsymbol{n}+\frac{1}{2}\hat{\boldsymbol{e}}_i}(N_i(t_j+\Delta t) - N_i(t_j)) \tag{6.32a}$$
$$= \frac{1}{T}\sum_j \delta\left(\frac{\mathbf{X}(t_j+\Delta t)+\mathbf{X}(t_j)}{2} - x\right)(X_i(t_j+\Delta t) - X_i(t_j)) \tag{6.32b}$$
$$\overset{a\to 0}{=} \hat{\boldsymbol{e}}_i\cdot\mathbf{J}_T(\boldsymbol{x}), \tag{6.32c}$$

where $\mathbf{J}_T(\boldsymbol{x})$ was defined in (4.86).

Next, using the fact that α is antisymmetric, we can express it as

$$\alpha(\boldsymbol{n}\pm\hat{\boldsymbol{e}}_i,\boldsymbol{n})/a^d = G(\boldsymbol{x}\pm a\hat{\boldsymbol{e}}_i) - G(\boldsymbol{x}) \tag{6.33a}$$
$$= \pm a g_i(\boldsymbol{x}) + \frac{a^2}{2}\partial_{x_i}g_i(\boldsymbol{x}) + O\left(a^3\right), \tag{6.33b}$$

where G is a smooth function independent of a chosen such that $\partial_{x_i}G = g_i$, with $\boldsymbol{g}$ being the weight in the target continuum observable. (If $\boldsymbol{g}$ cannot be integrated we instead postulate the expansion (6.33b).)

Putting the results together,

$$\mathcal{A}_T/a = \sum_{\boldsymbol{n}}\sum_i \alpha(\boldsymbol{n}+\hat{\boldsymbol{e}}_i,\boldsymbol{n})J(\boldsymbol{n}+\hat{\boldsymbol{e}}_i,\boldsymbol{n})/a \tag{6.34a}$$
$$= \int \frac{\mathrm{d}\boldsymbol{x}}{a^d}\sum_i a^{d+1}g_i(\boldsymbol{x})\hat{\boldsymbol{e}}_i\cdot\mathbf{J}_T(\boldsymbol{x})/a + O(a) \tag{6.34b}$$
$$\overset{a\to 0}{=} V_T. \tag{6.34c}$$

We now condition $\mathbf{N}(t)$ on $\mathcal{A}_T$ and apply the diffusive limit to the associated spectral elements of the tilted generators.

Diffusive limit of the spectral elements

Following (4.66), the (backward) s-tilted generator $\widetilde{\mathbb{L}}_s = \widetilde{\mathbb{W}}_s^\top$ with respect to $\mathcal{A}_T$ is given by

$$\widetilde{\mathbb{L}}_s(\boldsymbol{n}', \boldsymbol{n}) = W(\boldsymbol{n} \mid \boldsymbol{n}') e^{s\alpha(\boldsymbol{n}|\boldsymbol{n}')} - \delta_{\boldsymbol{n},\boldsymbol{n}'} \sum_{\boldsymbol{n}''} W(\boldsymbol{n}'' \mid \boldsymbol{n}), \tag{6.35}$$

with the non-zero transitions rates (6.24).

Motivated by dimensional consideration, we posit that the diffusive scaling of the spectral elements is

$$s = a^d k, \tag{6.36a}$$
$$\Lambda_s = \lambda_k + \mathcal{O}(a), \tag{6.36b}$$
$$L_s(\boldsymbol{n}) = a^d \ell_k(\boldsymbol{x}) + O\left(a^{d+1}\right), \tag{6.36c}$$
$$R_s(\boldsymbol{n}) = a^d r_k(\boldsymbol{x}) + O\left(a^{d+1}\right). \tag{6.36d}$$

To begin, we consider the limit of the right eigenvalue equation,

$$\Lambda_s R_s(\boldsymbol{n}) = \sum_{\boldsymbol{n}'} \widetilde{\mathbb{L}}_s(\boldsymbol{n}, \boldsymbol{n}') R_s(\boldsymbol{n}'). \tag{6.37}$$

For $\boldsymbol{n}$ away from the boundary sites,

$$\Lambda_s R_s(\boldsymbol{n}) = \sum_i \Big[p_i(\boldsymbol{n}) e^{s\,\alpha(\boldsymbol{n}+\hat{\boldsymbol{e}}_i|\boldsymbol{n})} R_s(\boldsymbol{n}+\hat{\boldsymbol{e}}_i) + q_i(\boldsymbol{n}) e^{s\,\alpha(\boldsymbol{n}-\hat{\boldsymbol{e}}_i|\boldsymbol{n})} R_s(\boldsymbol{n}-\hat{\boldsymbol{e}}_i) - (p_i + q_i)(\boldsymbol{n}) R_s(\boldsymbol{n}) \Big]. \tag{6.38}$$

Up to relevant orders in a, and suppressing the function arguments $\boldsymbol{x}$ and $\boldsymbol{n}$,

$$\begin{aligned}\lambda_k r_k = \sum_i \Big[& p_i \left(1 + kag_i + \frac{1}{2}ka^2\partial_{x_i}g_i + k^2a^2g_i^2\right)\left(r_k + a\partial_{x_i}r_k + \frac{1}{2}\partial_{x_i}^2 r_k\right) \\ & + q_i \left(1 - kag_i + \frac{1}{2}k^2a^2\partial_{x_i}g_i + k^2a^2g_i^2\right)\left(r_k - a\partial_{x_i}r_k + \frac{1}{2}\partial_{x_i}^2 r_k\right) \\ & - (p_i + q_i)r_k\Big] \end{aligned} \tag{6.39a}$$

$$\begin{aligned} = \sum_{i=} \Big[& a(p_i - q_i)\left(\partial_{x_i}r_k + kg_i r_k\right) + \frac{a^2}{2}(p_i + q_i)\times \\ & \left(\partial_{x_i}^2 r_k + r_k\partial_{x_i}g_i + 2kg_i\partial_{x_i}r_k + k^2g_i^2 r_k\right)\Big] \end{aligned} \tag{6.39b}$$

$$= \sum_i \left\{F_i(\partial_{x_i} + kg_i)r_k + (\partial_{x_i} + kg_i)\frac{\sigma_i^2}{2}(\partial_{x_i} + kg_i)r_k\right\} \tag{6.39c}$$

$$= \widetilde{\mathcal{L}}_k r_k, \tag{6.39d}$$

with $\widetilde{\mathcal{L}}_k$ as in (4.94). This recovers the spectral equation for r_k in the bulk.

Now let us take $\boldsymbol{n}$ to be a boundary site as in Figure 6.2b. Then

$$\begin{aligned}\Lambda_s R_s(\boldsymbol{n}) = {} & q_1(\boldsymbol{n})e^{s\,\alpha(\boldsymbol{n}-\hat{\boldsymbol{e}}_1|\boldsymbol{n})}R_s(\boldsymbol{n} - \hat{\boldsymbol{e}}_1) - q_1(\boldsymbol{n})R_s(\boldsymbol{n}) \\ & + \sum_{i>1}\Big[p_i(\boldsymbol{n})e^{s\,\alpha(\boldsymbol{n}+\hat{\boldsymbol{e}}_i|\boldsymbol{n})}R_s(\boldsymbol{n} + \hat{\boldsymbol{e}}_i) + q_i(\boldsymbol{n})e^{s\,\alpha(\boldsymbol{n}-\hat{\boldsymbol{e}}_i|\boldsymbol{n})}R_s(\boldsymbol{n} - \hat{\boldsymbol{e}}_i) \\ & - (p_i + q_i)(\boldsymbol{n})R_s(\boldsymbol{n})\Big]. \end{aligned} \tag{6.40}$$

Thus, including all relevant orders,

$$\lambda(k)r_k = q_1\left(1 - kag_1\right)\left(r_k - a\partial_{x_1}r_k\right) - q_1 r_k + O\left(1\right), \tag{6.41}$$

where we have used (6.39) to neglect the sum on the $i > 1$ terms. In fact, the right-hand side of (6.41) is $O\left(1/a\right)$. Substituting q_i with (6.25b), multiplying both sides by a, and taking $a \to 0$, we then arrive at

$$0 = \frac{1}{2}B_1^2\left(\partial_{x_1}r_k + g_1 r_k\right), \tag{6.42}$$

which generalizes, including all other components, to

$$\mathsf{D}(\nabla + k\boldsymbol{g})r_k \cdot \hat{\boldsymbol{n}} = 0. \tag{6.43}$$

Thus we have shown that in (6.23) we must put $c = 1/2$.

Now that the boundary condition on r_k has been established, the boundary condition for ℓ_k follows uniquely from duality. One may also verify that this boundary condition follows from the diffusive limit of the left eigenvalue equation, in a calculation analogous to that of r_k. Furthermore, the duality relation (6.18) is the result of applying the diffusive limit to the trivial identity

$$\sum_{\boldsymbol{n},\boldsymbol{n}'} L_s(\boldsymbol{n})\mathbb{L}_s(\boldsymbol{n},\boldsymbol{n}')R_s(\boldsymbol{n}') = \sum_{\boldsymbol{n},\boldsymbol{n}'} R_s(\boldsymbol{n})\mathbb{L}_s^\top(\boldsymbol{n},\boldsymbol{n}')L_s(\boldsymbol{n}'). \tag{6.44}$$

6.2.3 General consequences of the tilted boundary conditions

By the preceding proof, the tilted boundary conditions are

$$\{\boldsymbol{F}(\boldsymbol{x})\ell_k(\boldsymbol{x}) - \mathsf{D}(\nabla - k\boldsymbol{g})\ell_k(\boldsymbol{x})\} \cdot \hat{\boldsymbol{n}}(\boldsymbol{x}) = 0, \tag{6.45a}$$

$$\mathsf{D}(\nabla + k\boldsymbol{g}(\boldsymbol{x}))r_k(\boldsymbol{x}) \cdot \hat{\boldsymbol{n}}(\boldsymbol{x}) = 0. \tag{6.45b}$$

Since these boundary conditions correspond to (6.23) with $c = 1/2$, we can follow the steps leading to (6.23) in reverse order to conclude that the effective process indeed possesses a reflective boundary. It is striking that the boundary conditions are 'tilted' in the same manner as the tilted generator itself by letting $\nabla \to \nabla + k\boldsymbol{g}$ for r_k and $-\nabla \to -\nabla + k\boldsymbol{g}$ for ℓ_k. Furthermore (6.45b) implies that, on the boundary, the normal component of the effective drift coincides with the original drift:

$$\hat{\boldsymbol{F}}_k(\boldsymbol{x}) \cdot \hat{\boldsymbol{n}}(\boldsymbol{x}) = \boldsymbol{F}(\boldsymbol{x}) \cdot \hat{\boldsymbol{n}}(\boldsymbol{x}) \quad \text{for all} \quad \boldsymbol{x} \in \partial\Omega. \tag{6.46}$$

This situation has been shown for density-like observables [51], and we have now shown that it extends to any dynamical observable for a reflected diffusion. This is not a result with an obvious physical explanation. One proposal for its explanation is that because the effective drift arises due to conspiring diffusive noise, and that infinitesimally close to the boundary in its normal direction the diffusion is dominated by the deterministic reflection rule, this precludes the noise from biasing the drift there.

Finally, we remark that in the special case of an observable satisfying

$$\mathsf{D}\boldsymbol{g}(\boldsymbol{x}) \cdot \hat{\boldsymbol{n}}(\boldsymbol{x}) = 0 \quad \text{for all} \quad \boldsymbol{x} \in \partial\Omega, \tag{6.47}$$

the tilted boundary conditions (6.45) take the same form as the original ones, *i.e.*, (6.11) and (6.12), and are independent of c. The condition (6.47) is a necessary condition for the tilted generators to be symmetrizable, as was discussed in [51].

6.3 Collective current fluctuations in the heterogeneous single-file diffusion

With the results of the previous section, we are now equipped to study the current fluctuations in the heterogeneous single-file diffusion model of Section 3.2. We first consider some related studies of current fluctuations.

6.3.1 Current fluctuations in the ASEP

A large number of studies over two decades have investigated current fluctuations in the ASEP/SSEP/TASEP, for both the open and periodic boundary cases, as comprehensively reviewed by Lazarescu [204]. Typically, one seeks an exact representation of the cumulant generating function at long times (or of the SCGF). This can be obtained exactly using coordinate Bethe-ansatz in the periodic case, or extensions of matrix product methods for open boundaries. Complementing exact results (which may be non-transparent) are limit results such as coarse-graining to a fluctuating hydrodynamic description [205–207], or the restriction to asymptotically large or small currents in finite-size systems [52, 208].

A study by Popkov *et al* [52] is of particular interest to us as it employed the effective process construction to study current fluctuations in the L-site, N-particle ASEP. In the limit of conditioning of asymptotically large currents, the effective potential (4.60) could be derived as

$$V(n_1, \ldots, n_N) = -\sum_{i \neq j} \log \left|\sin(\pi(n_i - n_j)/L)\right|, \tag{6.48}$$

which represents a pairwise repulsion. Intuitively, this repulsive effect decreases the probability that particles get trapped in clusters, and thus contributes to increasing the current. It should be noted that this effect is in addition to the large boost in the base hopping rate by the factor e^s, which may in practice be the dominant effect of conditioning [3]. We are interested to see if the effective

repulsion also appears in the continuum model, and how particle heterogeneity affects the outcome.

6.3.2 Exact current large deviations for the heterogeneous SFD

Recall from Chapter 3 that the heterogeneous single-file diffusion, whose probability density evolves by the set of equations (3.27), could be conceived of as an N-dimensional diffusion $\mathbf{X}(t)$ in a domain $\Omega \subset \mathbb{R}^d$ such that its boundary, which is reflective, is the union of no-crossing hyperplanes: $\partial\Omega = \cup_{i\neq j}\{\boldsymbol{x} \in \mathbb{R}^d : x_i = x_j\}$.

We consider the empirical velocity of particle i, *i.e.* the current in direction i, given by the ith component of the empirical current $\mathbf{J}_T$ integrated over Ω. However, since all particles must have the same net velocity for long averaging periods, all observables of the form (4.90b) with $\boldsymbol{g}$ a constant vector whose components sum to one ($\mathbf{1}\cdot\boldsymbol{g} = 1$) should have the same large deviations. To validate this claim, we keep $\boldsymbol{g}$ arbitrary apart from these constraints, and thus consider the current observable

$$V_T = \boldsymbol{g} \cdot \int_\Omega \mathrm{d}\boldsymbol{x}\, \mathbf{J}_T(\boldsymbol{x})\,. \tag{6.49}$$

To find the dominant eigenvalue λ_k and eigenvector r_k related to this observable, we consider as an ansatz

$$r_k(\boldsymbol{x}) \propto \exp[\boldsymbol{a}\cdot\boldsymbol{x}], \tag{6.50}$$

with $\boldsymbol{a}$ to be determined. This ansatz is motivated by the fact that the dominant eigenvalue 0 for $\mathcal{L}^\dagger$ and $\mathcal{L}$ corresponds to eigenfunctions with an exponential form: the steady-state density (3.28) for the former, and trivially e^0 for the latter.

The normal to each no-crossing hypersurface is $\hat{\boldsymbol{n}} = (1/\sqrt{2})(\hat{\boldsymbol{e}}_i - \hat{\boldsymbol{e}}_j)$, which gives us $\mathbf{1}\cdot\hat{\boldsymbol{n}}(\boldsymbol{x}) = 0$ for all $\boldsymbol{x} \in \partial\Omega$, with $\mathbf{1}$ the only vector with this property (related to the discussion on the inverse FPE method of Section 3.3.2). From the boundary condition (6.45b), we therefore find

$$\mathsf{D}(\boldsymbol{a} + k\boldsymbol{g}) = \alpha\mathbf{1} \tag{6.51}$$

for some constant α. Hence

$$\boldsymbol{a} = \alpha \mathsf{D}^{-1}\mathbf{1} - k\boldsymbol{g}. \tag{6.52}$$

The periodicity (3.27c) requires $\boldsymbol{a} \cdot \mathbf{1} = 0$, so that

$$\alpha = \frac{k\mathbf{1} \cdot \boldsymbol{g}}{\mathbf{1}^\top \mathsf{D}^{-1}\mathbf{1}} = k\overline{D}, \tag{6.53}$$

where we have used the property $\mathbf{1} \cdot \boldsymbol{g} = 1$ and (3.34) for $\overline{D}$. Applying $\mathcal{L}_k$ to r_k, one then finds that r_k is an eigenfunction with eigenvalue

$$\lambda(k) = \overline{D}^{-1}\alpha(\alpha + \bar{v}) = k\bar{v} + k^2\overline{D}. \tag{6.54}$$

By LF transform, we then obtain the rate function

$$I(v) = \frac{(v - \bar{v})^2}{4\overline{D}}, \tag{6.55}$$

which shows that the fluctuations of the current are Gaussian around the stationary velocity $\bar{v}$.

The same eigenvalue (6.54) is obtained by assuming for the left eigenfunction

$$\ell_k \propto \exp[\boldsymbol{b} \cdot \boldsymbol{x}], \tag{6.56}$$

for which we find, in a calculation analogous to the one for r_k,

$$\boldsymbol{b} = \mathsf{D}^{-1}(\boldsymbol{v} + \beta\mathbf{1}) + k\boldsymbol{g}, \tag{6.57}$$

with

$$\beta = -\frac{\mathbf{1}^\top \mathsf{D}^{-1}\boldsymbol{v} + k\mathbf{1} \cdot \boldsymbol{g}}{\mathbf{1}^\top \mathsf{D}^{-1}\mathbf{1}} = -\bar{v} - k\overline{D}. \tag{6.58}$$

Noting that $\boldsymbol{a} + \boldsymbol{b} = \boldsymbol{k}$ we then find that the density of the effective process is

$$\hat{\rho}_k^*(\boldsymbol{x}) = \ell_k(\boldsymbol{x})r_k(\boldsymbol{x}) \propto e^{\boldsymbol{k}\cdot\boldsymbol{x}}, \tag{6.59}$$

that is, it is identical to density of original process for any bias k,

$$\hat{\rho}_k^*(\boldsymbol{x}) = \rho^*(\boldsymbol{x}). \tag{6.60}$$

The effective drift (4.98) works out to

$$\hat{\boldsymbol{F}}_k = \boldsymbol{v} + k\overline{D}\mathbf{1}. \tag{6.61}$$

Thus when we substitute the saddle-point value $k(v) = I'(v) = (v - \bar{v})/(2\overline{D})$,

$$\hat{\boldsymbol{F}}_{k(v)} = \boldsymbol{v} + (v - \bar{v})\mathbf{1}. \tag{6.62}$$

For the particle system to generate an atypical fluctuation of the collective current, each particle generates a fluctuation of equal absolute increase in intrinsic velocity, equal to $\Delta v = v - \bar{v}$ as depicted in Figure 6.3.

In contrast to the current fluctuations in the ASEP [3, 52], there is no effective repulsion between the particles. We would conclude then that this repulsion is a lattice effect that does not survive the diffusive limit. To understand why, we note that jammed configurations form a finite fraction of all possible system configuration in the ASEP, whereas on the continuum, jammed configurations constitute a boundary layer of measure zero relative to the bulk. Therefore, a bias against clustering may not be relevant on the continuum.

It is interesting that the current large deviations of this heterogeneous many-body system are identical to that of a single particle on the ring with parameters $\bar{v}$ and $\bar{D}$. We are reminded of Section 5.2.3, where we also found an example of non-trivially different processes sharing the identical current (*i.e.* velocity) rate function, which we referred to as large deviation equivalence. This single particle is expected to represent the 'centre of mass' of the many-body system, which has to be interpreted with some care given that the particles live on a periodic ring.

Finally, we note that the probability current in the effective process is

$$\boldsymbol{J}_{\hat{\boldsymbol{F}}_k, \hat{\rho}_k^*}(\boldsymbol{x}) = \frac{v}{\bar{v}} \boldsymbol{J}_{\boldsymbol{F}, \rho^*}(\boldsymbol{x}). \tag{6.63}$$

These results are consistent with the fact that the rate function saturates a universal quadratic bound on current fluctuations (an 'uncertainty relation') [36], and are also expected given that the heterogeneous single-file diffusion on a ring, while not satisfying detailed balance directly, does so with respect to a reference frame moving with the collective velocity $\bar{v}$. As a result, the stationary density of the effective process must be equal to the original invariant density, $\hat{\rho}_k^*(\boldsymbol{x}) = \rho^*(\boldsymbol{x})$ [147]. Strictly speaking, however, these general results have not been established for reflected diffusions yet.

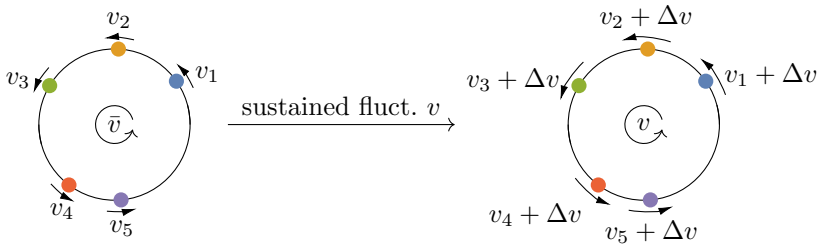

Figure 6.3 *The effective processes representing heterogeneous* SFD *conditioned on an atypical current v, modifies each particles drift by $\Delta v = v - \bar{v}$, where $\bar{v}$ is the typical current around the ring.*

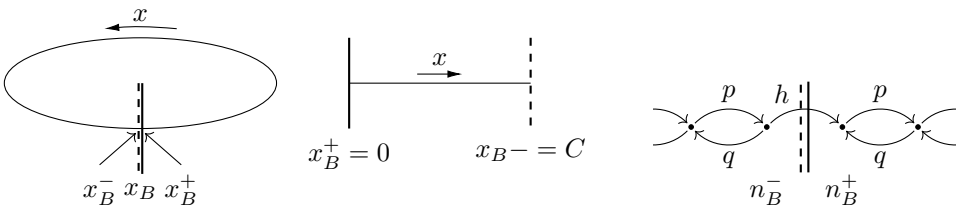

(a) *Semi-permeable barrier on continuous ring*

(b) *Semi-permeable barrier on lattice ring*

Figure 6.4 *(a) Diffusion on a continuous ring with a semi-permeable barrier, which partially reflects from the left (at x_B^-, dashed) and totally reflects from the right (x_B^+). The ring is treated as a line segment with two boundaries. (b) A lattice model that yields the diffusion on the ring with semi-permeable barrier in the diffusive limit.*

In conclusion, the current fluctuations of the heterogeneous SFD are curiously simple, and equivalent to those of a certain single 'effective' particle. To obtain this result, we used for the time the formalism for current large deviations in reflected diffusions derived in the previous section.

6.4 Beyond reflection

As we realized earlier, for reflected diffusions conditioned on a current-like observable, the boundary conditions of the tilted operators $\widetilde{\mathcal{L}}_k$ and $\widetilde{\mathcal{L}}_k^\dagger$ are obtained by replacing $\nabla \to \nabla + k\boldsymbol{g}$ in the boundary conditions for $\mathcal{L}$ to obtain those of $\widetilde{\mathcal{L}}_k$, and $\nabla \to \nabla - k\boldsymbol{g}$ for $\widetilde{\mathcal{L}}_k^\dagger$. We conjecture that this scheme will also prove correct for conditioned diffusions with other types of boundaries. Let us check this for partial reflection, for instance.

To keep the presentation simple, we consider a particle on a one-dimensional ring of circumference C. At the coordinate x_B there is a semi-permeable barrier: it

is partially reflecting from x_B^- and totally reflecting from x_B^+ (see Figure 6.4a). Effectively, the problem can be thought of as a one-dimensional line segment $[x_B^+, x_B^-]$, $x_B^+ = 0, x_B^- = C$, with two boundaries connected such that the particle exiting on the right is put back on the left; alternatively, we can think of an infinite series of such connected segments. The reason for studying a semi-permeable barrier is that we can consider partial reflection while maintaining probability conservation, so we do not need to worry about the large deviations becoming trivial in the long-time limit (*i.e.* no probability remaining in the domain of interest).

We let the rate of passing through the barrier from the left be α. The boundary conditions on the density are then

$$J(x_B^-) \cdot (-\hat{n}(x_B^-)) = \alpha\rho(x_B^-), \tag{6.64a}$$
$$J(x_B^+) \cdot \hat{n}(x_B^+) = \alpha\rho(x_B^-), \tag{6.64b}$$

where the boundary normals are $\hat{n}(x_B^-) = -1$, $\hat{n}(x_B^+) = +1$. The first condition tells us that the current $J(x_B^-) \cdot (-\hat{n}(x_B^-))$ through the barrier, $x_B^- \to x_B^+$, must be equal to the rate of transmission times the probability accumulated on the left of the barrier, $\alpha\rho(x_B^-)$. Similarly, the second condition tells us that the current just past the barrier must also equal $\alpha\rho(x_B^-)$. To derive the boundary conditions on the functions ϕ in the domain of $\mathcal{L}$, we recall that they must make the boundary terms in the duality relation (6.9) vanish:

$$\begin{aligned} 0 &= \phi(x_B^+)\{J(x_B^+)\hat{n}(x_B^+)\} + \phi(x_B^-)\{J(x_B^-)\hat{n}(x_B^-)\} \\ &\quad + \rho(x_B^+)\{D\partial_x\phi(x_B^+)\hat{n}(x_B^+)\} + \rho(x_B^-)\{D\partial_x\phi(x_B^-)\hat{n}(x_B^-)\} \end{aligned} \tag{6.65a}$$
$$\begin{aligned} &= \rho(x_B^+)\{D\partial_x\phi(x_B^+)\hat{n}(x_B^+)\} \\ &\quad + \rho(x_B^-)\{D\partial_x\phi(x_B^-)\hat{n}(x_B^-) + \alpha(\phi(x_B^+) - \phi(x_B^-))\}. \end{aligned} \tag{6.65b}$$

For this to hold independently of ρ (given (6.64)) we require

$$D\partial_x\phi(x_B^-)\hat{n}(x_B^-) = \alpha(\phi(x_B^-) - \phi(x_B^+)), \tag{6.66a}$$
$$D\partial_x\phi(x_B^+)\hat{n}(x_B^+) = 0. \tag{6.66b}$$

We therefore conjecture that the boundary conditions for the dominant eigenvectors of the tilted generators are

$$(F\ell_k - D(\partial_x\ell_k - kg\ell_k))(x_B^-) \cdot \hat{n}(x_B^-) = -\alpha\ell_k(x_B^-), \tag{6.67a}$$

$$(F\ell_k - D(\partial_x \ell_k - kg\ell_k))(x_B^+) \cdot \hat{n}(x_B^+) = \alpha \ell_k(x_B^-). \tag{6.67b}$$

and

$$D\partial_x r_k(x_B^-)\hat{n}(x_B^-) = \alpha(r_k(x_B^-) - r_k(x_B^+)), \tag{6.68a}$$
$$D\partial_x r_k(x_B^+)\hat{n}(x_B^+) = 0. \tag{6.68b}$$

To prove that this is indeed the case, we employ the diffusive limit approach, just as in Section 6.2.2. We start from the lattice process illustrated in Figure 6.4b. In the notation of Section 6.2.2, we have, for example, that the equations for R_s on either side of the barrier is

$$\begin{aligned}\Lambda_s R_s(n_B^-) = &\left[R_s(n_B^- - 1)e^{s\alpha(n_B^- - 1, n_B^-)} - R_s(n_B^-)\right] q(n_B^-) \\ &+ \left[R_s(n_B^+)e^{s\alpha(n_B+, n_B^-)} - R_s(n_B^-)\right] h,\end{aligned} \tag{6.69a}$$
$$\Lambda_s R_s(n_B^+) = \left[R_s(n_B^+ + 1)e^{s\alpha(n_B^+ + 1, n_B^+)} - R_s(n_B^+)\right] p(n_B^+). \tag{6.69b}$$

Performing the diffusive limit using the scaling relations (6.33b), (6.36), and $h = \alpha/a + O(1)$, we do obtain precisely (6.68).

To give the simplest example of the above conditioning problem, let $F \equiv 0$ and $g \equiv 1$, so that we are looking at the velocity fluctuations of an unbiased Brownian particle across a semi-permeable barrier. To obtain the large deviation elements, we must solve the boundary-value problem

$$\begin{cases} \lambda_k r_k(x) = D(\partial_x + k)^2 r_k(x), & 0 < x < C, \quad (6.70a) \\ D(r_k'(C) + k r_k(C)) = \alpha(r_k(0) - r_k(C)), & (6.70b) \\ D(r_k'(0) + k r_k(0)) = 0. & (6.70c) \end{cases}$$

The general solution to (6.70a) and (6.70c) for given λ_k is

$$r_k(x) \propto e^{-kx} \cosh\left(x\sqrt{\frac{\lambda_k}{D}}\right). \tag{6.71}$$

λ_k is then determined by substitution of this solution into (6.70b) to yield

$$C\sqrt{\frac{\lambda_k}{D}} \sinh\left(C\sqrt{\frac{\lambda_k}{D}}\right) + \frac{C\alpha}{D}\cosh\left(C\sqrt{\frac{\lambda_k}{D}}\right) = \frac{C\alpha}{D}e^{Ck}. \tag{6.72}$$

Let $\mu_k := C\sqrt{|\lambda_k|/D}$. For $k \geq 0$ we have $\lambda_k \geq 0$. Consider then that the function

$f_+(\mu) := \mu\sinh(\mu) + (C\alpha/D)\cosh(\mu)$ for $\mu \geq 0$ is monotonically increasing from its minimum at $\mu = 0$. It can only intersect $g(k) := (C\alpha/D)e^{Ck}$ for k such that $f_+(0) \leq g(k)$, *i.e.* for $k \geq 0$. It follows that for $k < 0$, λ_k must be negative. The function $f_-(\mu) := f_+(i\mu) = -\mu\sin(\mu) + (C\alpha/D)\cos(\mu)$ for $\mu \geq 0$ is monotonically decreasing from its maximum at $f_\pm(0)$ until it crosses the μ-axis for the first time somewhere in the interval $(0, \pi/2)$. It therefore intersects $g(k)$ for $k \neq 0$. We thus see that there is real solution λ_k from (6.72).

The effective drift is

$$\hat{F}_k(x) = 2\sqrt{\lambda_k D}\tanh\left(x\sqrt{\frac{\lambda_k}{D}}\right). \tag{6.73}$$

At the left boundary in the line-segment description of the geometry (which we emphasize is totally reflecting from the right), $\hat{F}(0) = 0$, consistent with our general result that the effective drift is not modified at such a boundary. In contrast, at the permeable right boundary, $\hat{F}_k(C) \neq 0$ for $k \neq 0$. For $k > 0$, *i.e.* enhanced velocity, the effective drift is non-negative and increases from $x = 0$ to C. This is physically plausible: once the particle comes close to the boundary it should prefer to stay close to it to have a chance of passing through. For $k < 0$ and lower than typical velocity,(6.73) becomes

$$\hat{F}_k(x) = -2\sqrt{|\lambda_k| D}\tan\left(x\sqrt{\frac{|\lambda_k|}{D}}\right). \tag{6.74}$$

The drift is pointing towards the left boundary, and increases in strength the closer to the right boundary the particle moves. The effective process thus has the qualitative behaviour one might guess from the physics of the problem.

Finally, we mention a completely different approach to modelling impenetrable boundaries. Instead of imposing *e.g.* reflecting boundary conditions, one can condition a process to stay forever within a specified region. The influence of the boundary is then not abrupt, but it is expected to grow stronger the closer to it the process reaches. Such processes have been studied by mathematicians under the name of taboo processes, and are commonly used in financial fields but rarely in statistical physics [209]. Dynamical large deviations in taboo processes could potentially be studied from the level 2.5 perspective: we take a process in an unbounded space, and contract the level 2.5 rate function down to the observable of interest, with the additional constraint the density ρ should vanish outside the bounded region.

Indeed, even for reflective boundaries, contraction from level 2.5 to level 1 should constitute another way to derive the tilted boundary conditions that are the main result of this chapter. We hypothesise that it would be sufficient to restrict the integration domain of the level 2.5 rate function (4.88) to Ω, and add the additional hard constraint that the current satisfies $\boldsymbol{j} \cdot \hat{\boldsymbol{n}} = 0$ on the boundary $\partial\Omega$. We are then supposing rather than deriving that the effective process is also reflecting, but since we now know this is true, this level 2.5 approach should yield correct results. This is left for future investigation.

6.5 Summary of results

The main result of this chapter is the tilted boundary conditions (6.45) that must be imposed on the spectral problem associated with the large deviations of general dynamical observables (4.90), and in particular currents, of reflected diffusions. We obtained this result by applying the diffusive limit to a spatial discretization of the reflected diffusion as a jump process. A general consequence of the tilted boundary conditions is that the effective process describing how the large deviations arise is also a reflected diffusion, and at the boundary must have the same drift normal to it as in the original process.

As an application of these novel results, we considered the large deviations of the particle current in the heterogenous single-file diffusion. We found that the long-time fluctuations of the net velocity around the ring for this many-body system are identical to those of a single particle with the averaged drift (3.33) and diffusivity (3.34) that featured in the steady state solution of the model. In contrast to the homogeneous lattice version of the problem, *i.e.* the ASEP, there are no effective repulsive forces between the particles as they achieve the fluctuation; each particle modifies its drift to a different constant value to furnish the specified common net velocity. This example is a rare instance of exactly solvable large deviations in an interacting N-body system, and to my knowledge the first solved case of current fluctuations of a reflected diffusion in the literature.

Based on the pattern of how the tilted boundary conditions and generators relate to the original ones, we conjectured a scheme for inferring tilted boundary conditions for other boundary types. This pattern was verified for partially reflected diffusions, with the example of a one-dimensional unbiased diffusion across a semi-permeable membrane. Here, we saw that the effective drift can be

modified normal to the boundary, in contrast to at a totally reflecting boundary.

The formalism here developed is expected to be usefully applied to a variety of physically relevant models. Of particular interest would to find an example of a dynamical phase transition whose existence depends in an essential way on the presence of the boundary. We also expect that the methods used to derive (6.45)—the diffusive limit, and the local-time + Feynman-Kac approach also presented in [5]—can be usefully employed in the future, and can be complemented by a level 2.5 contraction approach, that we have left for future investigation.

Conclusions

In the beginning of this thesis I set out two themes relating to the long-time statistics of nonequilibrium Markov process: the first, regarding the description of a nonequilibrium steady state and the process of relaxation by which it is attained; the second, the rare fluctuations in steady states observed over long times, as quantified by dynamical large deviation theory. I have explored these themes by seeking exact results mainly for two concrete models, both of which can be seen as extensions of the paradigmatic and exactly solvable ASEP, which comprises particles hopping on a one-dimensional lattice under volume-exclusion. The first extension was the ring-lattice run-and-tumble model, where particles stochastically alter their persistent direction of hopping, and the second was the heterogeneous single-file diffusion, where particles have distinct but spatially constant drift and diffusion parameters on the continuous ring. Several connections appeared between the two models and themes that I will highlight below in this final discussion of the main results.

First, I solved exactly the RTP model for one and for two particles in Chapter 2, in the sense of diagonalizing the process generator. For one particle, this was an easy exercise in linear algebra and Fourier analysis; for two particles, it was found to be a laborious and subtle undertaking, resulting in polynomial equations (2.72) for two complex numbers z_1, z_2 whose solutions implicitly determine the spectrum and eigenvectors. In both cases, the spectrum depended in an interesting way on the model parameter ω, the tumbling rate, and transitioned from real to complex via eigenvalue crossings (Figure 2.5 and Figure 2.7). In particular, at $\omega = 1$ a macroscopic eigenvalue crossing involving an $O(1)$ fraction of all eigenvalues appeared, and at an 'exceptional' value $\omega^* \sim 1/L$ (inverse ring size) there was a crossing of the spectral gap.

The consequence of the spectral gap eigenvalue crossing (occurring once for one particle, and twice for two) was a non-analytic minimum in the relaxation time.

For one particle, we could explain why a minimum should exist, reasoning that when the particle typically runs $O(1)$ times round the ring per tumble, the uncertainty of its whereabouts should grow the fastest. It would be interesting to understand how ubiquitous relaxation singularities are across the breadth of physically relevant nonequilibrium Markov processes. The logical place to look would be jump processes with a continuous parameter that interpolates between equilibrium and nonequilibrium conditions, as the spectrum will generically transition from real to complex with such a parameter.

The meaning of the macroscopic eigenvalue crossing only became clear in Chapter 5, when I studied the large deviations in velocity of a single asymmetric RTP. The half of the eigenvalues not participating in the crossing became identical to an asymmetric random walker (ARW), and I could show that the ARTP, at least at long times, behaves like a certain superposition of ARWs—a 'probabilistic quasiparticle' (Figure 5.7). This could even be generalized to an 'N-ARW'. While the latter is admittedly a contrived example, it serves to make the interesting point, that the presence of internal states can be invisible to the rate function describing the rarity of fluctuations, yet leave a clear mark on the effective process describing the character of trajectories that produce a given fluctuation. Furthermore, the way I stumbled upon this example suggests that a fruitful way of exploring simple Markov processes is to look at the entire spectrum in the complex plane (*e.g.* numerically) versus a continuous parameter, in the search of patterns. Indeed, recent general bounds on the spectra of stochastic matrices seems to have been discovered in this way [210].

In Chapter 5 I also used the ARW and ARTP conditioned on time spent at the origin to demonstrate that the dynamical phase transition in occupation time for the biased diffusion on the infinite line [50] is robust to modelling details, and seems to appear under the condition that the typical net velocity is non-zero. The method I introduced to calculate the large deviation elements was to obtain the dynamical partition function Z from the 'tilted' generating function of the conditioning problem, and then to seek the scaled cumulant generating function (SCGF) as the dominant pole of the Laplace transform in time of Z. In particular, this yielded the compact expression (5.70) in the case of multi-state random walkers conditioned on time at the origin. This approach has since proven useful in other models [211].

Turning our attention to the heterogeneous SFD of Chapter 3, I used an exponential ansatz to solve the stationary Fokker-Planck equations of the

model exactly, yielding (3.42). Importantly, the normalization constant of the probability density of the N-particle positions could be calculated in closed form for arbitrary particle disorder, and even explicitly marginalized over any subset of particles. From the probability current, one obtains the net particle current $\bar{v}$ around the ring, which has the simple form (3.33) of a weighted sum of the individual particle drifts, where the weights depend on the whole set of diffusivities. From this expression, one can conclude that the current is biased towards the drift of the least diffusive particles; this was explained as an inter-particle ratchet effect.

Noting the similarity to the above solution of a many-filament ratchet model [44], I set out to understand what special property makes these models solvable—after all, they are disordered, interacting, N-particle NESSs! By considering a rather abstract model of a d-dimensional 'tube' containing overdamped, spherical particles interacting via volume-exclusion, it appeared that 'quasi-one-dimensionality' was key—*i.e.* that no particle is able to overtake all others—because this situation forces a common net velocity in the long-time limit. I reached this conclusion by analysing the irreversible drift that is the part of the drift without which a process would satisfy detailed balance. In this context, I proposed an 'inverse' approach to solving high-dimensional Fokker-Planck equations: solve (3.90) for the irreversible drift $\boldsymbol{u}$ as a function of the drift and diffusion matrix, *e.g.* by an ansatz, then find which drifts and diffusion matrices are compatible with the solution, as demanded by the potential condition (3.91). In particular for the tube model with constant drift and diffusion, the ansatz that irreversible drift is a constant vector in (periodic) phase space is correct, which implies the existence of a constantly moving frame of reference with respect to which the model respects detailed balance. Looking for completely different diffusions that have this property, using the inverse approach, could potentially open up a new class of exactly solvable nonequilibrium processes.

At the end of Chapter 3, I made a connection with Chapter 2 based on the continuous-space, thermal RTPs considered in [102] for $N = 2$ following my work on the lattice problem. On the lattice, it was difficult to extract from the two-particle solution in the relative coordinate, an ansatz for an N-particle solution. Generalizing from [102], I could in the continuum setting generate a plausible N-particle ansatz for the stationary distribution, which is based on merging the exponential ansatz that solves the heterogeneous SFD, with a vector accounting for the discrete orientation states of particles, (3.127). The plausibility of this

ansatz is based on the observation that at any point in time, the thermal SFD looks like a heterogeneous SFD with a disorder set by the particle orientation. As explained in that section, the difficulty is finding the appropriate ansatz for the structure of the 'wave vectors' $\boldsymbol{k}$. This leaves an exact N-particle elusive, for now. A suggestion for how to proceed, would be to simulate the distribution of a few, *e.g.* 3, RTPs on the continuum *without* thermal noise, *i.e.* with ballistic motion and stochastic tumbling. If one can understand the structure of 'delta-spikes' in the distribution, *i.e.* if they contain $\delta(x_i - x_j)$, $\delta(x_i - 2x_j + x_k)$ or other patterns, that may guide the ansatz in the more analytically favourable thermal setting, as we expect each delta spike to be replaced with an exponential $\exp(\boldsymbol{k} \cdot \boldsymbol{x})$.

In the last chapter, Chapter 6, in order to analyse the large deviations in the heterogeneous SFD, I had to derive the correct boundary conditions for the tilted operators $\tilde{\mathcal{L}}_k$ and $\tilde{\mathcal{L}}_k{}^\dagger$ associated with a current-like observable in a reflected diffusion. I pursued a general answer to this question, not limited to single-file diffusion. The approach I adopted was based on the diffusive limit of a corresponding lattice problem which furnished the result (6.45). From these tilted boundary conditions followed the fact that the corresponding effective process is also a reflected diffusion, and that the effective drift is not modified normal to the boundary. I gave a physical explanation of these facts based on analysis of the mechanics of reflection for Brownian trajectories.

The rate function and effective process for the current fluctuations in the heterogeneous SFD could then be calculated exactly. It transpired that the large deviations were identical to those of a single diffusive particle with intrinsic drift $\bar{v}$ and $\overline{D}$, being the parameters that featured in the steady-state current. Each of the N particles modified its drift by the same amount $\Delta v = v - \bar{v}$ to achieve the fluctuation v. This is in interesting contrast to the lattice ASEP, where there emerges also effective repulsive forces between the particles in the effective process.

An alternative derivation of the tilted boundary conditions (6.45) was presented in the paper [5] based on the local-time formalism and Feynman-Kac formula. Another approach, which would also be an important theoretical advancement, is to find how the level 2.5 large deviation principle should be expressed for a reflected diffusion. Then (6.45) should emerge in some way from the contraction principle.

In general, extending the dynamical large deviation theory to processes with

every kind of boundary condition should be a worthwhile endeavour, both from the perspective of completeness of the theory but also to enable new interesting examples. Eq. (6.45) already suggests a pattern of tilted boundary conditions that I confirmed for partially reflected diffusion. A radically different case is absorption, where ergodicity of the process is broken, leading to triviality of the large deviation principle unless the absorption is controlled. Very recently, Monthus showed how to use the level 2.5 large deviation rate function to study fluctuations in absorbing jump processes conditioned on staying alive over the observation time window [212]. In a forthcoming work, I will show a completely different result, on how to use the level 2.5 large deviation principle to study the trajectories that lead to absorption in some chosen time, or through some chosen state. The trick is to first extend the absorbing process into an ergodic process, apply conditioning to it, and then map the effective process back to an 'effective absorption process'.

In conclusion, seeking exact results to minimal models within the mathematical framework of nonequilibrium Markov processes is conducive to discovering novel nonequilibrium phenomena, ascertaining their logical connection to the way reversibility is broken, and to guide the further development of mathematical structure also valid for nonequilibrium systems of greater complexity.

Bibliography

[1] E. Mallmin, R. A. Blythe, M. R. Evans. Exact spectral solution of two interacting run-and-tumble particles on a ring lattice. *J. Stat. Mech. Theor. Exper.* 013204 (2019)

[2] E. Mallmin, R. A. Blythe, M. R. Evans. A comparison of dynamical fluctuations of biased diffusion and run-and-tumble dynamics in one dimension. *J. Phys. A: Math. Theor.* **52**, 42 (2019)

[3] F. Cagnetta, E. Mallmin. Efficiency of one-dimensional active transport conditioned on motility. *Phys. Rev. E* **101**, 022130 (2020)

[4] E. Mallmin, R. A. Blythe, M. R. Evans. Inter-particle ratchet effect determines global current of heterogeneous particles diffusing in confinement. *J. Stat. Mech.* 013209 (2021)

[5] E. Mallmin, J. du Buisson, H. Touchette. Large deviations of currents in diffusions with reflective boundaries. *J. Phys: A: Math. Theor.* **54**, 295001 (2021)

[6] N. G. van Kampen. *Stochastic Processes in Physics and Chemistry.* Elsevier B.V., third edition (2007)

[7] R. Zwanzig. *Nonequilibrium statistical mechanics.* Oxford University Press (2001)

[8] J. Uffink. *Philosophy of Physics Part B*, chapter Compendium of the foundations of classical statistical physics, 923–1074. North-Holland (2007)

[9] H. Touchette. The large deviation approach to statistical mechanics. *Phys. Rep.* **478**, 1 (2009)

[10] T. Chou, K. Mallick, R. K. P. Zia. Non-equilibrium statistical mechanics: from a paradigmatic model to biological transport. *Rep. Prog. Phys.* **74**, 116601 (2011)

[11] R. Livi, P. Politi. *Nonequilibrium Statistical Physics: A Modern Perspective.* Cambridge University Press (2017)

[12] P. L. Krapivsky, S. Redner, E. Ben-Naim. *A Kinetic View of Statistical Physics*. Cambridge University Press (2010)

[13] R. A. Blythe, M. R. Evans. Nonequilibrium steady states of matrix-product form: a solver's guide. *J. Phys. A: Math. Theor.* **40**, R333 (2007)

[14] C. Gardiner. *Stochastic Methods: A Handbook for the Natural and Social Sciences*. Springer Verlag, fourth edition (2009)

[15] G. R. Grimmett, D. R. Stirzaker. *Probability and Random Processes*. Oxford U. P., 4 edition (2020)

[16] F. P. Kelly. *Reversibility and Stochastic Networks*. Wiley (1979)

[17] O. Golinelli, K. Mallick. The asymmetric simple exclusion process: an integrable model for non-equilibrium statistical mechanics. *J. Phys. A: Math. Gen.* **39**, 12679 (2006)

[18] B. Derrida, M. R. Evans, V. Hakim, V. Pasquier. Exact solution of a 1D asymmetric simple exclusion model using a matrix product formulation. *J. Phys. A* **26**, 1493 (1993)

[19] B. Derrida. An exactly soluble non-equilibrium system: The asymmetric simple exclusion process. *Phys. Rep.* **301**, 65 (1998)

[20] A. G. Thompson, J. Tailleur, M. E. Cates, R. A. Blythe. Lattice models of nonequilibrium bacterial dynamics. *J. Stat. Mech.* P02029 (2011)

[21] H. C. Berg. *E. coli in Motion*. Springer (2004)

[22] C. Bechinger, R. D. Leonardo, H. Löwen, C. Reichhardt, G. Volpe, G. Volpe. Active particles in complex and crowded environments. *Rev. Mod. Phys.* **88**, 046006 (2016)

[23] E. Fodor, C. Marchetti. The statistical physics of active matter: From self-catalytic colloids to living cells. *Physica A* **504**, 106 (2018)

[24] J. Tailleur, M. E. Cates. Statistical Mechanics of Interacting Run-and-Tumble Bacteria. *Phys. Rev. Lett.* **100**, 218103 (2008)

[25] M. E. Cates, J. Tailleur. Motility-Induced Phase Separation. *Annu. Rev. condens. Matter Phys.* **6**, 219 (2015)

[26] A. Ryabov. *Stochastic Dynamics and Energetics of Biomolecular systems*. Springer Theses. Springer (2015)

[27] R. L. Jack, P. Sollich. Large Deviations and Ensembles of Trajectories in Stochastic Models. *Prog. Theor. Phys.* **184**, 304 (2010)

[28] R. Chetrite, H. Touchette. Nonequilibrium Markov Processes Conditioned on Large Deviations. *Ann. Henri Poincaré* **16**, 2005 (2015)

[29] H. Touchette. Introduction to dynamical large deviations of Markov processes. *Physica A: Stat. Mech. & App.* **504**, 5 (2018)

[30] A. Dembo, O. Zeitouni. *Large Deviations Techniques and Applications.* Springer, New York, 2nd edition (1998)

[31] C. Monthus. Non-equilibrium steady states: maximization of the Shannon entropy associated with the distribution of dynamical trajectories in the presence of constraints. *J. Stat. Mech.* P03008 (2011)

[32] H. Touchette, R. J. Harris. *Nonequilibrium Statistical Physics of Small Systems*, chapter 11. Large Deviation Approach to Nonequilibrium Systems, 335. Wiley-VCH (2013)

[33] R. J. Harris, G. M. Schütz. Fluctuation theorems for stochastic dynamics. *J. Stat. Mech.* P07020 (2007)

[34] U. Seifert. Stochastic thermodynamics, fluctuation theorems and molecular machines. *Rep. Prog. Phys.* **75** (2012)

[35] R. Klages, W. Just, C. Jarzynski (Editors) *Nonequilibrium Statistical Physics of Small Systems.* Wiley-VCH (2013)

[36] T. R. Gingrich, J. M. Horowitz, N. Perunov, J. L. England. Dissipation Bounds All Steady-State Current Fluctuations. *Phys. Rev. Lett.* **116**, 12601 (2016)

[37] U. Seifert. From stochastic thermodynamics to stochastic inference. *Annu. Rev. Condens. Matter Phys.* **10**, 171 (2019)

[38] Z. Schuss. *Brownian Dynamics at Boundaries and Interfaces*, volume 186 of *Applied Mathematical Sciences.* Springer, New York (2013)

[39] A. B. Slowman, M. R. Evans, R. A. Blythe. Jamming and Attraction of Interacting Run-and-Tumble Random Walkers. *Phys. Rev. Lett.* **116**, 218101 (2016)

[40] M. Karbach, G. Müller. Introduction to the Bethe ansatz I. *arXiv:9809162* (1998)

[41] M. R. Evans. Bose-Einstein condensation in disordered exclusion models and relation to traffic flow. *Europhys. Lett.* **36**, 13 (1996)

[42] J. Krug, P. Ferrari. Phase transitions in driven diffusive systems with random rates. *J. Phys. A: Math. Gen.* **2**, L465 (1996)

[43] M. R. Evans. Exact steady states of disordered hopping particle models with parallel and ordered sequential dynamics. *J. Phys. A: Math. Gen.* **30**, 5669 (1997)

[44] A. J. Wood, R. A. Blythe, M. R. Evans. Solvable model of a many-filament Brownian ratchet. *Phys. Rev. E* **100**, 042122 (2019)

[45] R. Graham, H. Haken. Generalized Thermodynamic Potential for Markoff Systems in Detailed Balance far from Thermal Equilibrium. *Z. Physik* **243**, 289 (1971)

[46] C. Maes, K. Netočný. Canonical structure of dynamical fluctuations in mesoscopic nonequilibrium steady states. *Euro. Phys. Lett.* **82**, 30003 (2008)

[47] R. Chetrite, H. Touchette. Variational and optimal control representations of conditioned and driven processes. *J. Stat. Mech.* P12001 (2015)

[48] A. C. Barato, R. Chetrite. A Formal View on Level 2.5 Large Deviations. *J. Stat. Phys.* **160**, 1154 (2015)

[49] P. Tsobgni Nyawo, H. Touchette. A minimal model of dynamical phase transition. *Europhys. Lett.* **116**, 50009 (2016)

[50] P. Tsobgni Nyawo, H. Touchette. Dynamical phase transition in drifted Brownian motion. *Phys. Rev. E* **98**, 052103 (2018)

[51] J. du Buisson, H. Touchette. Dynamical large deviations of reflected diffusions. *Phys. Rev. E* **102**, 012148 (2020)

[52] V. Popkov, G. M. Schütz, D. Simon. ASEP on a ring conditioned on enhanced flux. *J. Stat. Mech.* P10007 (2010)

[53] H. Tasaki. Two theorems that relate discrete stochastic processes to microscopic mechanics. *arXiv:0706.1032* (2007)

[54] G. F. Mazenko. *Nonequilibrium statistical mechanics* (2006)

[55] M. Margaliot, L. Grüne, T. Kriecherbauer. Entrainment in the master equation. *R. Soc. open sci.* **5**, 172157 (2018)

[56] L. F. Cugliandolo. Dynamics of glassy systems. *Les Houches lecture notes* arxiv:cond–mat/0210312 (2002)

[57] J. Lee. Derivation of Markov processes that violate detailed balance. *Phys. Rev. E* **97**, 032110 (2018)

[58] J. O'Byrne, Y. Kafri, J. Tailleur, F. van Wijland. Time-(ir)reversibility in active matter; from micro to macro. *arXiv:2104.03030* (2021)

[59] M. F. Weber, E. Frey. Master equations and the theory of stachastic path integrals. *Rep. Prog. Phys.* **80** (2017)

[60] S. Redner. *A guide to first-passage processes.* Cambridge U. P. (2001)

[61] E. Seneta. *Non-negative Matrices and Markov Chains.* Springer, second edition (1981)

[62] H. Haken. *Synergetics: An Introduction.* Springer, 3rd edition (1983)

[63] A. N. Kolmogorov. Zur Theorie der Markoffschen Ketten. *Math. Ann.* **112**, 155 (1936)

[64] R. K. P. Zia, B. Schmittmann. Probability currents as principal characteristics in the statistical mechanics of non-equilibrium steady states. *J. Stat. Mech.* (2007)

[65] C. Battle, C. P. Broedersz, N. Fakhri, V. F. Geyer, J. Howard, C. F. Schmidt, F. C. MacKintosh. Broken detailed balance at mesoscopic scales in active biological systems. *Science* **352**, 6285 (2016)

[66] J. P. Garrahan, R. L. Jack, V. Lecomte, E. Pitard, K. van Duijvendijk, F. van Wijland. First-order dynamical phase transitions in models of glasses: an approach based on ensembles of histories. *J. Phys. A: Math. Theor.* **42**, 075007 (2009)

[67] M. Baiesi, C. Maes, B. Wynants. Fluctuations and response of nonequilibrium states. *Phys. Rev. Lett.* **103**, 010602 (2009)

[68] U. Basu, C. Maes. Nonequilibrium response and frenesy. *J. Phys.: Conf. Ser.* **638**, 012001 (2015)

[69] C. Maes. Frenesy: Time-symmetric dynamical activity in nonequilibria. *Phys. Rep.* **850**, 1 (2020)

[70] C. Maes, K. Netočný, B. Wynants. Monotonicity of the dynamical activity. *J. Phys. A: Math. Theor.* 455001 (2012)

[71] G. Haag. *Modelling with the Master equation.* Springer

[72] C. Maes. *Non-Dissipative Effects in Nonequilibrium Systems.* Springer Verlag (2018)

[73] T. Tomé, M. J. de Oliveira. Stochastic approach to equilibrium and nonequilibrium thermodynamics. *Phys. Rev. E.* (2015)

[74] J. Schnakenberg. Network theory of microscopic and macroscopic behavior of master equation systems. *Rev. Mod. Phys* **48** (1976)

[75] C. Maes, K. Netočný. Heat Bounds and the Blowtorch Theorem. *Ann. Henri Poincaré* **14**, 1193 (2013)

[76] M. Baiesi, C. Maes. Life efficiency does not always increase with the dissipation rate. *J. Phys. Comm.* **2**, 4 (2018)

[77] G. H. Weiss. *Aspects and applications of the random walk.* North-Holland (1994)

[78] J. Masoliver, K. Lindenberg, G. H. Weiss. A continuous-time generalization of the persistent random walk. *Physica A* **157**, 891 (1989)

[79] M. Boguñá, J. M. Porrà, J. Masoliver. Persistent random walk model for transport through thin slabs. *Phys. Rev. E* **59**, 6517 (1999)

[80] M. Miri, H. Stark. Persistent random walk in a honeycomb structure: light transport in foams. *Phys. Rev. E* **68**, 031102 (2003)

[81] H. Wu, B.-L. Li, T. A. Springer, W. H. Neill. Modelling animal movement as a persistent random walk in two dimensions. *Ecological Modelling* **132**, 115 (2000)

[82] S. Fujita, Y. Okamura. Theory of polymer conformation based on the correlated walk model. *J. Chem. Phys.* **72**, 3993 (1980)

[83] D. Bhat, M. Gopalakrishnan. Memory, bias, and correlations in bidirectional transport of molecular-motor-driven cargoes. *Phys. Rev. E* **88**, 042702 (2013)

[84] M. J. Schnitzer. Theory of continuum random walks and application to chemotaxis. *Phys. Rev. E* **48**, 4 (1993)

[85] L. Angelani. Confined run-and-tumble swimmers in one dimension. *J. Phys. A: Math. Theor,* **50**, 325601 (2017)

[86] A. Dhar, A. Kundu, S. N. Majumdar, S. Sabhapandit, G. Schehr. Run-and-tumble particle in one-dimensional confining potential: Steady state, relaxation and first passage properties. *Phys. Rev. E* **99**, 032132 (2019)

[87] T. Demaerel, C. Maes. Active processes in one dimension. *Phys. Rev. E* **97**, 032604 (2018)

[88] K. Malakar, V. Jemseena, A. Kundu, K. V. Kumar, S. Sabhapandit, S. N. Majumdar, S. Redner, A. Dhar. Steady state, relaxation and first-passage properties of a run-and-tumble particle in one dimension. *J. Stat. Mech.* 043215 (2018)

[89] P. Pietzonka, U. Seifert. Entropy production of active particles and for particles in active baths. *J. Phys. A* **51**, 01LT01 (2018)

[90] M. R. Evans, S. N. Majumdar. Run and tumble particle under resetting: a renewal approach. *J. Phys. A: Math. Theor.* **51**, 475003 (2018)

[91] J. Tailleur, M. E. Cates. Sedimentation, trapping, and rectification of dilute bacteria. *EPL* **86**, 60002 (2009)

[92] D. Escaff, R. Toral, C. V. den Broeck, K. Lindenberg. A continuous-time persistent random walk model for flocking. *Chaos* **28**, 075507 (2018)

[93] R. Soto, R. Golestanian. Run-and-tumble dynamics in a crowded environment: persistent exclusion process for swimmers. *Phys. Rev. E* **89**, 012706 (2014)

[94] A. B. Slowman, M. R. Evans, R. A. Blythe. Exact solution of two interacting run-and-tumble random walkers with finite tumble duration. *J. Phys. A* **50**, 375601 (2017)

[95] G. H. Weiss. Some applications of persistent random walks and the telegrapher's equation. *Physica A* **311**, 381 (2002)

[96] S. Muhuri, I. Pagonabarranga. Collective vesicle transport on biofilaments carried by competing molecular motors. *Euro. Phys. Lett.* **84**, 58009 (2006)

[97] P. Diaconis, S. Holmes, R. M. Neal. Analysis of a Nonreversible Markov Chain Sampler. *The Annals of Applied Probability* **10**, 3 (2000)

[98] T. Kato. *Perturbation theory for linear operators.* Springer (1966)

[99] W. D. Heiss. The physics of exceptional points. *J. Phys. A: Math. Theor.* **45**, 444016 (2012)

[100] E. Brattain. *The Completeness of the Bethe Ansatz for the Asymmetric Simple Exclusion Process.* Ph.D. thesis, University of California (2016)

[101] O. Golinelli, K. Mallick. Spectral degeneracies in the totally asymmetric exclusion process. *J. Stat. Phys.* **120**, 779 (2005)

[102] A. Das, A. Dhar, A. Kundu. Gap statistics of two interacting run and tumble particles in one dimension. *J . Phys. A: Math. Theor.* **53**, 345003 (2020)

[103] A. L. Hodgkin, R. D. Keynes. The potassium permeability of a giant nerve fibre. *J. Physiol.* **128**, 61 (1955)

[104] K. Hahn, J. Kärger, V. Kukla. Single-file diffusion observation. *Phys. Rev. Lett.* **76**, 15 (1996)

[105] J. Kärger, D. M. Ruthven, D. N. Theodorou. *Diffusion in nanoporous materials.* Wiley (2012)

[106] T. E. Harris. Diffusion with "Collisions" between Particles. *J. App. Prob.* **2**, 323 (1965)

[107] C. Rödenbeck, J. Kärger, K. Hahn. Calculating exact propagators in single-file systems via the reflection principle. *Phys. Rev. E* **57**, 4 (1998)

[108] L. Lizana, T. Ambjörnsson. Single-File Diffusion in a Box. *Phys. Rev. Lett.* **100**, 200601 (2008)

[109] A. Ryabov, P. Chvosta. Single-file diffusion of externally driven particles. *Phys. Rev. E* **83**, 020106(R) (2011)

[110] D. Kumar. Diffusion of interacting particles in one dimension. *Phys. Rev. E* **78**, 021133 (2008)

[111] D. Dhar. An exactly solvable solved model for interfacial growth. *Phase Transit.* **9**, 51 (1987)

[112] C. King, F. Y. Wu (Editors). *Exactly Soluble models in statistical mechanics*, volume 13 of *Series on Advances in Statistical Mechanics*. World Scientific (1996)

[113] C. Aslangul. Single-file diffusion with random diffusion constants. *J. Phys. A: Math. Gen.* **33**, 851 (2000)

[114] T. Ambjörnsson, L. Lizana, M. A. Lomholt, R. J. Silbey. Single-file dynamics with different diffusion constants. *J. Chem. Phys.* **129**, 185106 (2008)

[115] P. Gonçalves, M. Jara. Scaling Limits of a Tagged Particle in the Exclusion Process with Variable Diffusion Coefficient. *J. Stat. Phys.* **132**, 1135 (2008)

[116] A. Miron, D. Mukamel, H. A. Posch. Phase transition in a 1D driven tracer model. *J. Stat. Mech.* 063216 (2020)

[117] J. Civindi, D. Mukamel, H. A. Posch. Driven tracer with absolute negative mobility. *J. Phys. A: Math. Theor.* 085001 (2018)

[118] I. Lobaskin, M. R. Evans. Driven tracers in a one-dimensional periodic hard-core lattice gas. *J. Stat. Mech.* 053202 (2020)

[119] M. S. Miguel, S. Chaturvedi. Limit Cycles and Detailed balance in Fokker-Planck Equations. *Z. Physik B - Cond. Mat.* **40**, 167 (1980)

[120] G. Q. Cai, Y. K. Lin. On exact stationary solutions of equivalent non-linear stochastic systems. *Int. J. Non-Linear Mechanics* **23**, 4 (1988)

[121] M. O. Magnasco. Forced Thermal Ratchets. *Phys. Rev. Lett.* **71**, 10 (1993)

[122] C. R. Doering, W. Horsthemke, J. Riordan. Nonequilibrium Fluctuation-Induced Transport. *Phys. Rev. Lett.* **72**, 19 (1994)

[123] C. J. Olson, C. Reichhardt, B. Jankó, F. Nori. Collective Interaction-Driven Ratchet for Transporting Flux Quanta. *Rhys. Rev. Lett.* **87**, 17 (2001)

[124] I. Derényi, T. Vicsek. Cooperative Transport of Brownian Particles. *Phys. Rev. Lett.* **75**, 3 (1995)

[125] J. V. d. V. Clécio C. de Souza Silva, M. Morelle, V. V. Moshchalkov. Controlled multiple reversals of a ratchet effect. *Nature* **440** (2006)

[126] C. J. O. Reichhardt, C. Reichhardt. Ratchet Effects in Active Matter Systems Matter Systems. *Annu. Rev. Consens. Matter Phys.* **8**, 51 (2017)

[127] M. D. Donsker, S. R. S. Varadhan. Asymptotic evaluation of certain Markov process expectation for large time, I. *Commun. Pre Appl. Math* **28**, 1 (1975)

[128] M. D. Donsker, S. R. S. Varadhan. Asymptotic evaluation of certain Markov process expectation for large time, II. *Commun. Pre Appl. Math* **28**, 279 (1975)

[129] M. D. Donsker, S. R. S. Varadhan. Asymptotic evaluation of certain Markov process expectation for large time, III. *Commun. Pre Appl. Math* **29**, 389 (1976)

[130] M. I. Freidlin, A. D. Wentzell. *Random Perturbations of Dynamical Systems*. Springer-Verlag (New York), 2 edition (1998)

[131] R. S. Ellis. *Entropy, Large Deviations, and Statistical Mechanics*. Springer (2006)

[132] R. P. Feynman, A. R. Hibbs. *Quantum mechanics and path integrals*. McGraw Hill Book Comp. (New York) (1965)

[133] M. Kac. On distributions of certain Weiner functionals. *Trans. Am. Math. Soc.* **65**, 1 (1949)

[134] D. Ruelle. *Thermodynamic Formalism*. Addison-Wesley (Reading, Mass.) (1978)

[135] V. Lecomte, C. Appert-Rolland, F. van Wijland. Thermodynamic formalism and large deviation functions in continuous time Markov dynamics. *C. R. Physique* **8**, 609 (2007)

[136] C. Monthus. Revisiting the Ruelle thermodynamic formalism for Markov trajectories with application to the glassy phase of random trap models. *J. Stat. Mech.* 063301 (2021)

[137] E. T. Jaynes. Macroscopic prediction. In H. Haken (Editor) *Complex Systems — Operational Approaches*, p. 254. Springer-Verlag, Berlin (1985)

[138] R. Dewar. Information theory explanation of the fluctuation theorem, maximum entropy production and self-organized criticality in non-equilibrium stationary states. *J. Phys. A: Math. Gen.* **36**, 631 (2003)

[139] P. D. Dixit, J. Wagoner, C. Weistuch, S. Pressé, K. Ghosh, K. A. Dill. Perspective: Maximum caliber is a general variational principle for dynamical systems. *J. Chem. Phys.* **148**, 010901 (2018)

[140] G. E. Crooks. Parth-ensemble averages in systems driven far from equilibrium. *Phys. Rev. E* **61**, 3 (2000)

[141] R. Kubo, M. Toda, N. Hashitsume. *Statistical Physics II*. Springer-Verlag Berling Heidelberg, second edition (1998)

[142] G. Gallavotti, E. G. D. Cohen. Dynamical Ensembles in Nonequilibrium Statistical Mechanics. *Phys. Rev. Lett.* **74** (1995)

[143] J. Kurchan. Fluctuation theorem for stochastic dynamics. *J. Phys. A* **31**, 3719 (1998)

[144] J. L. Lebowitz, H. Spohn. A Gallavotti-Cohen-Type Symmetry in the Large Deviation Functional for Stochastic Dynamics. *J. Stat. Phys.* **95**, 333 (1999)

[145] C. Jarzynski. Nonequilibrium Equality for Free Energy Differences. *Phys. Rev. Lett.* **78** (1997)

[146] P. Pietzonka, A. C. Barato, U. Seifert. Universal bounds on current fluctuations. *Phys. Rev. E* **93**, 052145 (2016)

[147] C. Nardini, H. Touchette. Process interpretation of current entropic bounds. *Eur. Phys. J. B* **91**, 16 (2018)

[148] D. Simon. Construction of a coordinate Bethe ansatz for the asymmetric simple exclusion process with open boundaries. *J. Stat. Mech.* P07017 (2009)

[149] R. J. Harris, V. Popkov, G. M. Schütz. Dynamics of Instantaneous Condensation in the ZRP Conditioned on an Atypical Current. *Entropy* **15**, 5065 (2013)

[150] O. Hirschberg, D. Mukamel, G. M. Schütz. Density profiles, dynamics, and condensation in the ZRP conditioned on an atypical current. *J. Stat. Mech* P11023 (2015)

[151] J. P. Garrahan, R. L. Jack, V. Lecomte, E. Pitard, K. van Duijvendijk, F. van Wijland. Dynamical First-Order Phase Transition in Kinetically Constrained Models of Glasses. *Phys. Rev. Lett.* **98**, 195702 (2007)

[152] P. Torkaman, F. H. Jafarpour. Effective stochastic generators for conditioned dynamics at an atypical reaction-diffusion current. *Phys. Rev. E* **92**, 062104 (2015)

[153] P. Torkaman, F. H. Jafarpour. Effective dynamics in an asymmetric death-branching process. *J. Stat. Mech.* 083206 (2017)

[154] P. Torkaman, F. H. Jafarpour. Stochastic modeling of gene expression: application of ensembles of trajectories. *Phys. Biol.* **16**, 066010 (2019)

[155] S. Whitelam. Multi-point nonequilibrium umrella sampling and associated fluctuation relations. *J. Stat. Mech.* 063211 (2018)

[156] M. Bause, T. Wittenstein, K. Kremer, T. Bereau. Microscopic reweighting for nonequilibrium steady-state dynamics. *Phys. Rev. E* **100**, 060103(R) (2019)

[157] A. Guyader, H. Touchette. Efficient Large Deviation Estimation Based on Importance Sampling. *J. Stat. Phys.* **181**, 551 (2020)

[158] R. M. L. Evans. Rules for transition rates in nonequilibrium steady states. *Phys. Rev. Lett.* **92**, 15 (2004)

[159] R. M. L. Evans. Detailed balance has a counterpart in non-equilibrium steady states. *J. Phys. A: Math. Gen.* **38**, 2 (2005)

[160] R. M. L. Evans. Statistical physics of shear flow: a non-equilibrium problem. *Contemp. Phys.* **51**, 5 (2010)

[161] H. Touchette. Legendre-Fenchel transforms in a nutshell (2005). URL https://appliedmaths.sun.ac.za/~htouchette/archive/notes/lfth2.pdf

[162] M. D. Donsker, S. R. S. Varadhan. Asymptotic evaluation of certain Markov process expectation for large time, IV. *Commun. Pre Appl. Math* **36**, 183 (1986)

[163] T. M. Cover, J. A. Thomas. *Elements of Information Theory.* Wiley Interscience, second edition (2006)

[164] G. Kishore, A. Kundu. Local time of an Ornstein–Uhlenbeck particle. *J. Stat. Mech.* 033218 (2021)

[165] T. Agranov, P. L. Krapivsky, B. Meerson. Occupation-time statistics of a gas of interacting diffusing particles. *Phys. Rev. E* **99**, 052102 (2019)

[166] J. Dolezal, R. L. Jack. Long-ranged correlations in large deviations of local clustering. *Phys. Rev. E* **103**, 052132 (2021)

[167] F. Cagnetta, F. Corberi, G. Gonneli, A. Suma. Large Fluctuations and Dynamic Phase Transition in a System of Self-Propelled Particles. *Phys. Rev. Lett.* **119**, 158002 (2017)

[168] T. Nemoto, Étienne. Fodor, M. E. Cates, robert L. Jack, J. Tailleur. Optimizing active work: Dynamical phase transitions, collective motion, and jamming. *Phys. Rev. E* (2019)

[169] E. Fodor, T. Nemoto, S. Vaikuntanathan. Dissipation controls transport and phase transitions in active fluids: mobility, diffusion and biased ensembles. *New. J. Phys.* **22**, 013052 (2020)

[170] Y.-E. Keta, E. Fodor, F. van Wijland, M. E. Cates, R. L. Jack. Collective motion in large deviations of active particles. *Phys. Rev. E* **103**, 022603 (2021)

[171] R. Chetrite, H. Touchette. Nonequilibrium Microcanonical and Canonical Ensembles and Their Equivalence. *Phys. Rev. Lett.* **111**, 120601 (2013)

[172] H. Touchette. Equivalence and Nonequivalence of Ensembles: Thermodynamic, Macrostate, and Measure Levels. *J. Stat. Phys.* **159**, 987 (2015)

[173] C. Maes, K. K. Netočný, B. Wynants. Steady state statistics of driven diffusions. *Physica A* **387**, 2675 (2008)

[174] J. Hoppenau, D. Nickelsen, A. Engel. Level 2 and level 2.5 large deviations functionals for systems with and without detailed balance. *New J. Phys.* **18**, 083010 (2016)

[175] S. N. Majumdar. Brownian functionals in physics and computer science. *Curr. Sci.* **89**, 12 (2005)

[176] J. Mehl, T. Speck, U. Seifert. Large deviation function fo entropy production in driven one-dimensional systems. *Phys. Rev. E* **78**, 011123 (2008)

[177] T. Speck, A. Engel, U. Seifert. The large deviation function for entropy production: the optimal trajectory and the role of fluctuations. *J. Stat. Mech.* P12001 (2012)

[178] P. Pietzonka, K. Kleinbeck, U. Seifert. Extreme fluctuations of active Brownian motion. *New J. Phys* **18**, 052001 (2016)

[179] S. Whitelam. Large deviations in the presence of cooperativity and slow dynamics. *Phys. Rev. E* **97**, 062109 (2018)

[180] F. Coghi, J. Morand, H. Touchette. Large deviations of random walks on random graphs. *Phys. Rev. E* **99**, 022137 (2019)

[181] S. Whitelam, D. Jacobson. Varied phenomenology of models displaying dynamical large-deviation singularities. *Phys. Rev. E* **103**, 032152 (2021)

[182] S. Vaikuntanathan, T. R. Gingrich, P. L. Geissler. Dynamic phase transitions in simple driven kinetic networks. *Phys. Rev. E* 062108 (2014)

[183] P. Tsobgni Nyawo, H. Touchette. Large deviations of the current for driven periodic diffusions. *Phys. Rev. E* **94**, 032101 (2016)

[184] K. Proesmans, B. Derrida. Large-deviation theory for a Brownian particle on a ring: a WKB approach. *J. Stat. Mech.* 023201 (2019)

[185] N. Tizón-Escamilla, vivien Lecomte, E. Bertin. Effective driven dynamics for one-dimensional conditioned Langevin processes in the weak-noise limit. *J. Stat. Mech.* 013201 (2019)

[186] P. Tsobgni Nyawo. *Driven nonequilibrium systems modeled with Markov processes.* Ph.D. thesis, Faculty of Sciences at Stellenbosch University (2017)

[187] J. Masoliver, K. Lindenberg. Continuous time persistent random walk: a review and some generalizations. *Eur. Phys. J. B* **90**, 107 (2017)

[188] G. Gradenigo, A. Sarracino, A. Puglisi, H. Touchette. Fluctuation relations without uniform large deviations. *J. Phys. A: Math. Theor.* **46**, 335002 (2013)

[189] A. Trovato, F. Seno, M. Zanardo, S. Alberghini, A. Tondello, A. Squartini. Quorum vs. diffusion sensing: a quantitative analysis of therelevance of absorbing or reflecting boundaries. *FEMS Microbiol. Lett.* **352**, 198 (2014)

[190] P. Dupuis. Large deviations analysis of reflected diffusions and constrained stochastic approximation algorithms in convex sets. *Stochastics* **21**, 63 (1987)

[191] S. J. Sheu. A large deviation principle of reflecting diffusions. *Taiwanese J. Math.* **2**, 2511 (1998)

[192] K. Majewski. Large deviations of the steady-state distribution of reflected processes with applications to queueing systems. *Queueing Systems* **29**, 351 (1998)

[193] I. A. Ignatyuk, V. A. Malyshev, V. V. Scherbakov. Boundary effects in large deviation problems. *Russ. Math. Surveys* **49**, 41 (1994)

[194] D. S. Grebenkov. Residence times and other functionals of reflected Brownian motion. *Phys. Rev. E* **76**, 041139 (2007)

[195] M. Forde, R. Kumar, H. Zhang. Large deviations for the boundary local time of doubly reflected Brownian motion. *Stat. Prob. Lett.* **96**, 262 (2015)

[196] V. R. Fatalov. Brownian motion on $[0, \infty)$ with linear drift, reflected at zero: Exact asymptotics for ergodic means. *Sbornik: Math.* **208**, 1014 (2017)

[197] R. G. Pinsky. On the Convergence of Diffusion Processes Conditioned to Remain in a Bounded Region for Large Time to Limiting Positive Recurrent Diffusion Processes. *Ann. Prob.* **13**, 363 (1985)

[198] R. Pinsky. The I-function for diffusion processes with boundaries. *Ann. Prob.* **13**, 676 (1985)

[199] R. Pinsky. On evaluating the Donsker-Varadhan I-function. *Ann. Prob.* **13**, 342 (1985)

[200] A. Budhiraja, P. Dupuis. Large deviations for the emprirical measures of reflecting Brownian motion and related constrained processes in $\mathbb{R}_+$. *Elect. J. Prob.* **8**, 1 (2003)

[201] J. Dolezal, R. L. Jack. Large deviations and optimal control forces for hard particles in one dimension. *J. Stat. Mech.* 123208 (2019)

[202] M. Freidlin. *Functional Integration and Partial Differential Equations*, volume 109 of *Annals of Mathematics Studies*. Princeton University Press, Princeton (1985)

[203] D. S. Grebenkov. Probability distribution of the boundary local time of reflected Brownian motion in Euclidean domains. *Phys. Rev. E* **100**, 062110 (2019)

[204] A. Lazarescu. The physicist's companion to current fluctuations: one-dimensional bulk-driven lattice gases. *J. Phys. A: Math. Theor.* **48**, 503001 (2015)

[205] L. Bertini, A. D. Sole, D. Gabrielli, G. Jona-Lasinio, C. Landim. Microscopic fluctuation theory for stationary non–equilibrium states. *J. Stat. Phys.* **107**, 3/4 (2002)

[206] B. Derrida. Non-equilibrium steady states: fluctuations and large deviations of the density and of the current. *J. Stat. Mech.* P07023 (2007)

[207] B. Derrida, T. Sadhu. Large deviations conditioned on large deviations II: fluctuating hydrodynamics. *J. Stat. Phys.* **177**, 151 (2019)

[208] V. Belitsky, G. M. Schütz. Microscopic structure of shocks and antishocks in the ASEP conditioned on low current. *J. Stat. Phys.* **152**, 93 (2013)

[209] A. Mazzolo. Sweetest taboo processes. *J. Stat. Mech.* 073204 (2018)

[210] M. Uhl, U. Seifert. Affinity-dependent bound on the spectrum of stochastic matrices. *J. Phys. A: Math. Theor.* **52**, 40 (2019)

[211] B. Houchmandzadeh. Large deviation of long time average for a stochastic process: an alternative method. *J. Phys. A: Math. Theor.* **53**, 095004 (2020)

[212] C. Monthus. Large deviations for metastable states of Markov processes with absorbing states with applications to population models in stable or randomly switching environment. *arXiv:2107.05354v1* (2021)